Mechanical behavior of bio-cemented soils

Tong Yu

THESE DE DOCTORAT

NNT : 2022UPAST094

Mechanical behavior of bio-cemented soils

Comportement mécanique des sols bio-cimentés

Thèse de doctorat de l'université Paris-Saclay

École doctorale n° 579 : sciences mécaniques et énergétiques, matériaux et géosciences (SMEMaG)
Spécialité de doctorat : Génie Civil
Graduate School : Sciences de l'ingénierie et des systèmes. Référent : CentraleSupélec

Thèse préparée dans la unité de recherche **LMPS** (Université Paris-Saclay, CentraleSupélec, ENS Paris-Saclay, CNRS), sous la direction de **Jean-Marie FLEUREAU**, professeur, la co-direction de **Hanène SOULI**, Maîtresse de Conférence, HDR

Thèse soutenue à Paris-Saclay, le 6 juillet 2022, par

Tong YU

Composition du Jury

Yu-Jun CUI Professeur, Université Gustave Eiffel, Ecole des Ponts-ParisTech	Président
Mahdia HATTAB Professeure, Université de Lorraine	Rapportrice & examinatrice
Said TAIBI Professeur, Université de Normandie-Le Havre	Rapporteur & examinateur
Annette ESNAULT-FILET Cheffe de projet, Solétanche-Bachy	Examinatrice
Xin WEI Professeure associée, Xi'an Jiaotong University, Chine	Examinatrice
Katia BICALHO Professeure, Universidade Federal de Espirito Santo, Vitoria, Brésil	Examinatrice
Jean-Marie FLEUREAU Professeur, CentraleSupélec	Directeur de thèse
Hanène SOULI Maîtresse de Conférence, HDR, Université de Lyon, CentraleLyon-ENISE	Co-directrice de thèse

Acknowledgements

Doctoral journey is like a lovely movement in the symphony of life. Notes go up and down, fast and slow, interspersed with pauses. It brings lively and cheerful moments mixed with wanderings and difficulties.

Along the way, above all, I would like to express my greatest appreciation to my supervisor, Dr. Jean-Marie Fleureau. He is a kind and gentle man, with witty conversation and profound wisdom in the eyes. His comprehensive knowledge, rich experience, patient inspiration, kindly guidance and generous support affect me deeply in spheres of work and life.

I would like to express sincere thanks to my co-supervisor Hanène Souli for providing constructive suggestions and interesting ideas. I would like also to thank Fernando Lopez-Caballero, Filipa Lopes, Denis Aubry and Yoan Péchaud, who gave precious opinions for improving the work and witnessed the development of the subject.

I would like to express my heartful gratitude to all the jury members, Katia Bicalho, Annette Esnault-Filet, Mahdia Hattab, Xin Wei, Yu-Jun Cui, Said Taïbi, for their professional dedication and valuable advice.

I would like to acknowledge the funding from Chinese Scholarship Council.

I would like to thank Solétanche-Bachy for providing materials, and Brice Desvages for his technical support.

Special thanks to all my friends and colleagues from LMPS, who have helped and accompanied me during my adventure.

At last but not least, I would like to thank my family, for their unconditional love and forever support.

TABLE OF CONTENTS

LIST OF FIGURES

LIST OF TABLES

List of symbols & abbreviations

Symbols

C_c	Curvature coefficient
C_u	Uniformity coefficient
d_{50}	Mean diameter (mm)
n	Porosity
D_r	Relative density
D_{max}	Maximum density
D_{min}	Minimum density
$D_{r,c}$	Relative density after consolidation
$D_{r,f}$	Relative density after compression
ρ_d	Dry density (g/cm^3)
$\rho_{d,f}$	ρ_d after consolidation (g/cm^3)
$\rho_{d,c}$	ρ_d after compression (g/cm^3)
e	Void ratio
e_{max}	Maximum void ratio
e_{min}	Minimum void ratio
e_c	Void ratio after consolidation
e_f	Final void ratio
e_{if}	Interfine void ratio
e_s	Intergranular void ratio
q	Deviator stress (kPa)
q_{max}	Maximum deviator stress (kPa)
$q_{max,norm}$	Normalized maximum deviator stress (kPa)
q_0	y-intercept in [p'-q plane] (kPa)
p'	Effective stress (kPa)
M	Slope of the failure lines
M_{UT}	M value of untreated specimen
M_T	M value of treated specimen
ϕ	Friction angle (°)
ϕ_{UT}	Friction angle of untreated specimens (°)
ϕ_T	Friction angle of treated specimens (°)
c	Cohesion (kPa)
σ_c	Confining pressure (kPa)
σ_c'	Effective confining pressure (kPa)
σ_d	Applied cyclic deviator stress (kPa)
ε_1	Axial strain (%)
ε_v	Volumetric strain (%)
$\varepsilon_{v,c}$	ε_v during consolidation (%)
$\varepsilon_{v,f}$	ε_v during compression (%)
$\delta\varepsilon_1$	Axial strain amplitude (%)
Δu	Pore pressure increment (kPa)

r_u	Excess pore pressure
OD_{425}	Optical density at 600 nm wavelength
OD_{600}	Optical density at 600 nm wavelength

Abbreviations

Bacterial solution	BS
Cementation solution	CS
Consolidated drained	CD
Consolidated undrained	CU
Critical state line	CSL
Cyclic stress ratio	*CSR*
Difference between the real $CaCO_3$ content and the $CaCO_3$ content limit	$\Delta CaCO_3$
Fines content	*FC*
Heavily treated	HT
Lightly treated	LT
Moderately treated	MT
Mercury intrusion porosimetry	MIP
Microbial induced calcium carbonate precipitation method	MICP
Number of cycles to liquefaction	N_L
Oxygen transfer rate	OTR
Pore volume	PV
Scanning electron microscope	SEM
Sum of squared errors	*SSE*
Transitional fine content	*TFC*
Treated	T
Untreated	UT
X-Ray diffraction	XRD

Abstract

Microbial induced calcium carbonate precipitation (MICP) is one of the most promising bio-mediated methods with little carbon footprint. It plays various roles in geotechnical engineering applications, such as ground improvement, crack repair, etc. Many studies explored the mechanical properties of MICP-treated soils, but mainly in the case of poorly graded sands with very fine grains (< 1 mm), and often in a qualitative rather than quantitative way. The present study was carried out on a series of quartz sand mixtures with grain diameters up to 5 mm, various fine contents *FC* (i.e., percentages of grains smaller than 1 mm) and uniformity coefficients C_u. Bio-physico-chemical tests were performed to characterize two types of bacteria (DSM 33 from Leibniz Institute, and SB from Solétanche-Bachy) and define the treatment protocol, while many monotonic drained (CD) and cyclic undrained (CU) triaxial tests were done on untreated and MICP-treated specimens to assess the effect of the treatment on the mechanical properties of soils, notably for small calcium carbonate contents. Additional optical & electronic microscopy observations, X-ray diffraction and mercury intrusion porosimetry tests helped interpret the results.

Among the two studied bacteria, the DSM33 features a longer lifetime whereas SB presents a faster reaction rate and higher efficiency. Results of mechanical tests show that MICP treatment with SB bacteria enhances the resistance of sand specimens to both monotonic and cyclic solicitations, the enhancement increasing with the cementation level. Under monotonic loading, treated soils exhibit a significant increase in peak strength compared to untreated ones, and a dilative behavior. The improvement is mainly attributed to an increase in effective cohesion, and, to a lesser extent, to an increase in grain surface roughness and bulk density. Under cyclic loading, the effects of both density and cementation on liquefaction resistance are important. For the coarsest sands (*FC* = 0-20%), the cyclic resistance of heavily treated specimens is comparable to that of untreated dense specimens, but their mechanical behavior is different. For soils with *FC* larger than 40%, the effect of cementation is predominant, and even the lightly treated samples resist better than dense samples. For these soils, the influence of a small percentage of $CaCO_3$ seems to be more important in cyclic tests than in monotonic ones. It is interesting to note that complete cementation of a sample is not necessary to improve its properties, but small lumps of cemented soils inside the sample are enough.

In both cases, the relation between the enhancement of the mechanical properties and the deposited calcium carbonate content (C_{CaCO3}) is complex, characterized by a minimum value of C_{CaCO3} below which its effect is not visible. This "minimum value" of C_{CaCO3} increases when *FC* decreases, from 2 to 7% for monotonic tests, and 1 to 9% for cyclic tests. Above the "minimum value", the properties (e.g., the monotonic normalized peak strength, $q_{max,T}/q_{UT}$, or the cyclic stress deviator leading to liquefaction in 100 cycles, N_{L100}) increase linearly with C_{CaCO3}. Regarding the influence of grain size distribution, the mean diameter d_{50} always plays an important part, as well as C_u in monotonic tests, and *FC* in cyclic tests. Microscope observations

confirm the interplay of several mechanisms that can explain the effect of MICP treatment on the mechanical properties of the soil through the increase in cohesion (bridging), surface roughness (coating) and density (pore-filling). The SEM images and XRD patterns show that the main morphology of the formed $CaCO_3$ crystals is calcite, with a small amount of vaterite. According to the results of mercury intrusion porosimetry, the coarser the sand grains, the larger the pores, the smaller the total pore volume in treated specimens.

Résumé

La précipitation de carbonate de calcium induite par des microbes (MICP) est l'une des méthodes les plus prometteuses avec une faible empreinte carbone. Elle a différentes applications en géotechnique, telles que l'amélioration des sols, la réparation des fissures, etc. De nombreuses études ont exploré les propriétés mécaniques des sols traités par MICP, mais principalement dans le cas de sables à granulométrie étroite et à grains très fins (< 1 mm), et souvent de manière qualitative plutôt que quantitative. La présente étude a été réalisée sur plusieurs mélanges de sable de quartz avec des diamètres de grains jusqu'à 5 mm. Des tests bio-physico-chimiques ont été faits pour caractériser les bactéries utilisées et définir le protocole expérimental, tandis que de nombreux essais triaxiaux monotones drainés, et cycliques non drainés ont été effectués sur des échantillons non traités et traités par MICP pour évaluer l'effet du traitement sur les propriétés mécaniques du sol, notamment pour les faibles teneurs en carbonate de calcium. Des observations complémentaires de microscopie optique et MEB, des tests de diffraction des rayons X et de porosimétrie au mercure ont aidé à interpréter les résultats.

Parmi les deux bactéries étudiées, la DSM33 (de Leibniz Institute) présente une durée de vie plus longue alors que la SB (de Solétanche-Bachy) présente une vitesse de réaction plus rapide et une efficacité plus élevée. Les résultats des tests mécaniques ont montré que le traitement MICP améliorait sensiblement la résistance des échantillons de sable aux sollicitations monotones et cycliques, l'amélioration augmentant avec le niveau de cimentation. Sous chargement monotone, les sols traités présentent une augmentation de la résistance maximale et un comportement dilatant. L'amélioration est principalement attribuée à une augmentation de la cohésion effective et, dans une moindre mesure, à l'augmentation de la rugosité des grains ou de la densité. Sous chargement cyclique, les effets de la densité et de la cimentation sont importants, avec un rôle prépondérant de la cimentation dans les sols les plus fins et une importance plus grande de la densité dans les sols plus grossiers. Pour les sols fins, l'effet d'un faible pourcentage de $CaCO_3$ semble être plus important dans les essais cycliques que dans les essais monotones. Il est intéressant de noter que la cimentation complète d'un échantillon n'est pas nécessaire pour améliorer ses propriétés, mais que de petits morceaux de sol cimenté à l'intérieur de l'échantillon suffisent.

Dans les deux cas, la relation entre l'amélioration des propriétés mécaniques et la teneur en carbonate de calcium déposé (C_{CaCO3}) est complexe, caractérisée par une valeur minimale de C_{CaCO3} en dessous de laquelle son effet n'est pas visible. Cette « valeur minimale » de C_{CaCO3} augmente lorsque le pourcentage de fines (< 1 mm) diminue. Au-dessus de la "valeur minimale", les propriétés (par exemple, la résistance maximale normalisée ou le déviateur de contrainte cyclique conduisant à la liquéfaction en 100 cycles) augmentent linéairement avec C_{CaCO3}. En ce qui concerne l'influence de la distribution granulométrique, le diamètre moyen d_{50} joue toujours un rôle important, de même que le coefficient d'uniformité dans les essais monotones et

la teneur en fines dans les essais cycliques. Les observations au microscope confirment l'existence de plusieurs mécanismes pouvant expliquer l'effet du traitement MICP sur les propriétés mécaniques du sol à travers l'augmentation de la cohésion (pontage), de la rugosité de surface (revêtement) et de la densité (remplissage des pores). Les images MEB et les diagrammes DRX montrent que les cristaux de $CaCO_3$ formés sont principalement de la calcite, avec un peu de vatérite. Selon les résultats de la porosimétrie, plus les grains de sable sont grossiers, plus les pores sont gros, plus le volume poreux total des échantillons traités est petit.

General introduction

In the last 15 years, bio-mediated and bio-inspired methods have gained more and more attention and start to burgeon in the field of geotechnical engineering. These multi-disciplinary methods take advantage of microbial metabolic processes and provide a low-carbon and sustainable solution to geotechnical problems. Microbial induced calcite precipitation (MICP) is one of the most popular bio-mediated methods, which can enhance engineering properties of soil via producing and accruing calcium carbonate precipitates. This method has been tried to solve various geotechnical problems, including liquefaction mitigation, seepage of dams, stabilization of slopes, crack repair, dust control, etc. However, very often, the existing results on the mechanical properties of treated sands only concern specific sands, i.e., silica sands with grains smaller than 1 mm, mean diameters smaller than 0.7 mm and uniformity coefficients C_u smaller than 2, such as Ottawa 50-70 and Ottawa 20-30 sands. Moreover, studies on the cyclic behavior of treated specimens are still rare, compared to studies on monotonic behavior. In addition, more quantitative results on the mechanical behavior of treated sands are needed before their use can be generalized.

The general goal of our study is to enhance the development of the MICP method, which is of prime importance, through examining the possibility to use other sands (mainly other grain size distributions), analyzing, and summarizing both qualitative and quantitative results regarding the mechanical properties of treated specimens.

Hence, the specific objectives of this study are,

- to understand MICP process and to compare the characteristics of two kinds of bacteria in MICP treatment
- to explore the effect of various parameters (such as injection mode, injection speed, etc.) on the efficiency of MICP treatment
- to establish MICP treatment protocols using sands with relatively larger grains and different grain size distributions.
- to study the monotonic mechanical behavior of soils treated with small amounts of $CaCO_3$, and to analyze the effect of various parameters by comparison with results on untreated soils.
- to study the cyclic behavior (i.e., liquefaction) of MICP-treated soils, and to analyze the effect of various parameters, also by comparing the results with those on untreated soils.

This thesis comprises 7 chapters. Chapter 1 presents the literature review regarding two main aspects of the previous MICP studies, the optimization of the MICP protocol and the mechanical properties of the treated specimens. This chapter is based on two published papers synthetizing the microbiological, physicochemical and mechanical studies. The literature review is completed on specific points in the

following chapters in order to compare and analyze the obtained results. Chapter 2 introduces the materials and the methods used in the whole thesis. For example, the characteristics of the soil grains, soil mixtures and the process for the preparation of sand specimens are given. The experimental methods, in terms of bacteria, MICP protocol and mechanical tests, are presented at the same time. Chapter 3 to chapter 6 present the experimental results. Chapter 3 shows the results concerning bacterial metabolism and MICP process and protocol. Chapter 4 focuses on the results of monotonic triaxial tests on untreated and treated loose sand specimens. Typical stress-strain behavior, friction angle, cohesion, void ratio evolution and effect of parameters (confining pressure, $CaCO_3$ content, grain size distribution) are discussed. Extra evidence through characterization of treated specimens, using optical & SEM images, X-ray diffraction and mercury intrusion pore measurement, are also provided. Chapter 5 shows the cyclic behavior of untreated specimens, while chapter 6 focuses on the cyclic properties of treated specimens. In both cases, the analysis includes typical stress strain behavior, excess pore pressure generation mode and related modified Seed model, deformation characteristics and the effect of some key parameters such as soil density, cementation level, grain size distribution, etc.). Chapter 7 integrates the main conclusions of the whole thesis and the recommendations for future studies.

2 annexes present the collection of equations and results of all the cyclic tests in terms of pore pressure generation and axial displacement accumulation.

Chapter 1 Literature review

1.1 Introduction

In this chapter, the literature review is presented with a brief introduction on liquefaction and two detailed reviews on the microbial induced calcium carbonate precipitation (MICP) method. In the Liquefaction part (§1.2), the concept, influence factors, some results and mitigation methods are presented. The review on MICP-treatment method, based on two published papers, is presented from two perspectives. Details of the two review articles as follows,

Review 1: This is an Accepted Manuscript of an article named "Optimizing protocols for microbial induced calcite precipitation (MICP) for soil improvement-a review" published by Taylor & Francis in journal of "European Journal of Environmental and Civil Engineering" on 23, April 2020, available online:

https://doi.org/10.1080/19648189.2020.1755370.

Review 2: This is an Accepted Manuscript of an article named "Review on engineering properties of MICP-treated soils" published in journal of "Geomechanics and Engineering", vol. 27, No. 1 (2021) 13-30, available online:

https://www.tandfonline.com/doi/full/10.1080/19648189.2020.1755370.

The first one is the optimization of the protocols, such as the parameters affecting bacterial activity & soil properties, the used cementation solutions and injection modes. A suitable range of some parameters is given. The other is on the mechanical properties of MICP-treated sands. In this part, the sands used by different researchers and many mechanical results (unconfined compressive strength, results of CD and CU triaxial tests, cohesion and friction angle, shear wave velocity, permeability, etc.) are shown as a function of the deposited calcium carbonate content in the treated specimens. Qualitative and quantitative results are synthesized and summarized.

1.2 Liquefaction

Liquefaction usually happens in loose, near-surface and water-saturated sediments in the presence of cyclic loading (often caused by earthquakes). The solid soil then behaves as a liquid, which can lead to severe damages in infrastructures (like roads, buildings, roads, bridges, dams, embarkments, etc) and even threaten human lives. Related cases can be found in many places, such as 5100 homes destroyed in Nihonkai-Chubu (Japan, 1983), massive devastation and loss of human lives in Niigata-ken Chuetsu earthquake (Japan, 2004), Wenchuan earthquake (China, 2008) and Chile Earthquake (2010), etc.

For the last fifty years, many studies had been carried out on liquefaction of various soils (Seed & Idriss, 1971; Ladd, 1974; Seed, Idriss & Arango, 1983; Lade & Yamamuro, 1997; Yamamuro & Lade, 1998; Polito & Martin II, 2001; Adalier et al. 2003; Xenaki & Athanasopoulos, 2008). To determine the occurrence of liquefaction,

two criteria, based on excess pore pressure (Seed & Lee, 1966) and large axial strains (Ishihara, 1993) are widely used. Three failure modes are captured in various sand studies, i.e. flow liquefaction, cyclic mobility, axial strain accumulation (Chiaro et al., 2012; Pan et al., 2022). Factors affecting liquefaction of soils include factors related to the nature and state of the soil (grain size distribution, density, plasticity, etc.), factors concerning loading conditions (form of dynamic waves, frequency of oscillation, duration of oscillation, intensity of the load, etc.), factors concerning test conditions (preparation method, size of the specimen, etc.), factors related to the stress state of the soil (stress history, initial stress, etc.), etc. (Seed & Idriss, 1970; Yilmaz et al., 2008).

Though there have been many studies on the effect of grain size distribution on the cyclic resistance of clean sands or silty sands, the conclusion is still controversial (Gobbi et al., 2021; Monkul et al., 2021). The most studied factors for studying grain size distribution include fine content (*FC*), uniformity coefficient (C_u) or curvature coefficient (C_c), or mean grain size (d_{50}). Some researchers also intended to use new parameters to better understand the behavior. For instance, (Monkul et al., 2021) combined the C_u of the sand and the C_u of the silt with its *FC*. As an example of the conclusions about the effect of the grading on the resistance to liquefaction, different researchers highlighted (1) a decrease of the liquefaction resistance with an increasing amount of fines up to a typical fine content and an increase afterwards (Papadopoulou & Tika, 2008) (2) a decrease of the liquefaction resistance with an increasing fine content (Lade & Yamamuro, 1997; Yilmaz et al., 2008) or (3) an increase of resistance with an increasing fine content up to a typical fine content and a decrease afterwards (Gobbi et al., 2021), (4) an increase in the resistance to liquefaction with C_u up to a relative density of 40-50% and a decrease afterwards (Vaid et al., 1990). The discrepancies among various studies might be owing to the different experimental conditions, e.g., the parameters chosen as the initial state of the soil (same void ratio versus same relative density).

For liquefaction mitigation, traditional methods include densification, pre-mixing, drainage, injection of cement, etc., which might affect the surrounding environment and cause massive carbon emission. Hence, some alternative techniques have emerged, such as injecting colloidal silica, bio-cementation & bio-gas generation, etc.

Optimizing protocols for microbial induced calcite precipitation (MICP) for soil improvement – A Review

Tong YU[1], Hanène SOULI[2], Yoan PECHAUD[3], Jean-Marie FLEUREAU[1]*

[1] Laboratoire de mécanique des Sols, Structures et Matériaux, CNRS UMR 8579, Université Paris Saclay, Centrale-Supélec, 8-10 Rue Joliot Curie, 91190 Gif-sur-Yvette, France –
e-mail: jean-marie.fleureau@ecp.fr; tong.yu@centralesupelec.fr

[2] Laboratoire de Tribologie et Dynamique des Systèmes, CNRS UMR 5513,
Ecole Nationale d'Ingénieurs de Saint Etienne, 58 rue Jean Parot, 42023 Saint Etienne Cedex, France –
e-mail: hanene.souli@enise.fr

[3] Laboratoire Géomatériaux et Environnement, Université de Paris-Est – Marne-la-Vallée, 77454 Marne-la-Vallée Cedex 2, France –
e-mail: yuan.pechaud@u-pem.fr

* Corresponding author

Abstract

With the fast-developing bioengineering techniques in recent decades, researchers have started to try to apply bio-techniques to geotechnical engineering. Microbial induced calcite precipitation (MICP) has known a mushroom growth, due to its sustainability and feasibility. In order to achieve lower cost, higher efficiency and higher operational feasibility, many studies have been carried out to optimize the protocols. It is crucial to synthesize the existing literature to give a synthetic summary of the optimized conditions in the various protocols. This article assembled, analyzed and summarized the results of studies on the optimization of protocols in state-of-the-art literature. The main factors incorporating biological, physical, chemical and operational aspects, were presented in this article. It can provide a clear insight in how these factors are acting on the process. Up-to-date instructions on the selection of parameters can inspire further studies.

Key words

MICP, soil improvement, optimization of protocol, efficiency, influence factors

1. Introduction

Biotechnology (including environmental microorganisms, related products-

enzymes, biosensors…) has been extensively used in depollution, detection and monitoring of the environment, which has resulted in tremendous advance in soil science and soil remediation. As for geotechnical applications, the majority of traditional soil improvement techniques consume substantial amounts of energy in producing materials and on-site operation, which also gives rise to potential danger (toxic chemicals, massive carbon dioxide emissions) to the environment. Producing concrete accounts for the major source of man-made global CO_2 emission (around 6 %) (Achal & Mukherjee, 2015). For expanding applications and sustainable concerns, researchers have started to find sustainable biogenic alternatives for ground improvement with minimal carbon footprint (Chang et al., 2016; Ashraf et al., 2017).

Microbial induced calcite precipitation (MICP), commonly realized by injecting ureolytic bacteria and reagents (urea and Ca^{2+}), makes use of bioactivity to cement sand by precipitating calcium carbonates (Al Qabany et al. , 2012). This technique has been used to enhance mechanical properties of soil by taking advantage of the energy-conserving microbial metabolic processes, which can remarkably reduce carbon footprint compared to other traditional techniques. It has gained more and more attention from researchers and companies in the last ten years (Whiffin et al., 2007; De Jong et al., 2013). Lots of research have been carried out using this technique, the majority of which at the laboratory scale, in columns (several centimeters to meters) (Qabany & Soga, 2013; Zhao et al., 2014; Mirmohammad Sadeghi et al., 2015; Rowshanbakht et al., 2016). A few researchers carried out large-scale in-situ tests (Gomez et al., 2015, 2017; van Paassen et al., 2010; Esnault Filet et al., 2019); some others set up comprehensive models (Barkouki et al., 2011; Fauriel & Laloui, 2012; Gai & Sánchez, 2019; Mahanty et al., 2014) or carried out microscopic visualization of the fabric of cemented soils (Li et al., 2017; Terzis & Laloui, 2019). This research on MICP in geotechnical field mainly concerned the following aspects: 1) exploring the mechanisms to optimize the effectiveness of soil bio-cementation through the study of different factors, 2) measuring the properties (especially the mechanical properties) of bio-cemented soils. Though there are still unsolved problems, results from these studies give a comprehensive view of the process and of the resulting soil properties from the microscopic scale (a few micrometers) to the macroscopic scale (thousands of meters).

MICP has shown a huge potential in geotechnical applications (Ivanov & Chu, 2008; De Jong et al., 2013; Achal & Mukherjee, 2015), such as liquefaction mitigation (Montoya et al., 2013), suffusion control (Sibille et al., 2015; Jiang et al., 2017), crack repair (Choi et al., 2017; Son et al., 2018), dust reduction, stabilization of dams, slopes, and offshore structures (Cheng et al., 2014; Salifu et al., 2016), etc. It is worth noting that there are still problems regarding this technique for future applications. For instance, the left ammonium produced by urea hydrolysis might bring about the pollution of subsurface environment. In a long-term study, the ammonia volatilization can also lower the pH in the liquid and cause dissolution of a portion of the precipitated calcite (Gat et al., 2017). Hence there are still barriers for using MICP in real practical works.

Attempts have been made to optimize the effectiveness of MICP process under

various conditions. For instance, Al Qavany et al. (2012) investigated the injection mode and cementation reagent concentration. Soon et al. (2014) studied the influence of bacteria concentration, cementation reagent concentration, treatment duration and reagent flow pressure. Among these studies, monitoring and evaluation of MICP often includes biological analyses (bacterial concentration through optical density measurements), physical analyses (temperature), chemical analyses (pH, concentrations of urea and calcium, ammonium, $CaCO_3$ content…) and geotechnical analyses (strength, stiffness, porosity, permeability…) (Martinez et al., 2013).

In consideration of the huge potential and the high feasibility of MICP method in the field of soil improvement, it is of great significance to give a clear view of the whole cementation process, especially for geotechnicians, and to try to establish a practical protocol that can be scaled-up to real site applications. The previous reviews were mainly focused on the description of MICP method, on the comparison of the effectiveness of MICP method with other soil-improving methods, and on the engineering properties of MICP-treated soils and potential applications in various fields. Because it is unpractical to draw conclusions among different strains of bacteria, this article is focused on the results of different studies aiming to optimize the protocols mainly based on the widely used strain called *Sporosarcina pasteurii*. In this review, results obtained by researchers are presented, analyzed, summarized and compared. At the end of the article, some helpful suggestions and reference values for designing experiments are given. It aims to help prospective researchers to choose their own parameters in the framework of their own studies.

2. MICP process and μ-organisms involved

MICP is an ubiquitous natural phenomenon (Stocks-Fischer et al., 1999) that occurs with a wide range of microbial species in various environments (soils, oceans, freshwaters, saline lakes etc.) (Hammes et al., 2003; Wei et al., 2015). There are three groups of microorganisms that can be involved in the precipitation of calcium carbonate. One group is that of photosynthetic microorganisms (such as cyanobacteria and microalgae), which is photoautotrophic. The other two are heterotrophic, and are related to sulphate cycle (sulphate-reducing bacteria) and nitrogen cycle (such as nitrate reducing bacteria and ureolytic bacteria), separately (De Muynck et al., 2010; Al-Salloum et al., 2017).

Urea is an important organic nitrogen carrier, and large quantities of urea are released in the environment through urine and biodegradation. In soil and water environments, urease (urea aminohydrolase E.C.3.5.1.5) produced by bacteria, fungi, plants and animals, plays an important role in global nitrogen cycle through urea hydrolysis (Kafarski & Talma, 2018). Urea hydrolysis, catalyzed by urease, which releases ammonium and carbonate ions in the environment, is a rapid process compared to urea degradation without urease (10^{14} times) and the reaction can be controlled easily. With the presence of Ca^{2+} ions, calcium carbonate can be formed. To date, one of the most commonly used systems of MICP is based on the urea hydrolysis

catalyzed by ureolytic bacteria that can produce urease. Fig. 1 gives out a schematic representation of the processes involved in MICP. During the process, urea is degraded, the pH of the ambient environment increases due to the production of ammonia, which favors calcite formation on the surface of particles as well as at particle contacts in the presence of calcium ions. The role of bacteria can be described as follows, i) it produces urease by hydrolyzing urea, ii) it increases pH by generating alkalinity, iii) it provides nucleation sites to produce precipitation (van Paassen, 2009). Chemical equations are as follows,

$$CO(NH_2)_2 + 2H_2O \xrightarrow{\text{urease}} 2NH_4^+ + CO_3^{2-}$$

$$Ca^{2+} + CO_3^{2-} \leftrightarrow CaCO_3 \downarrow$$

Sporosarcina pasteurii (*S. pasteurii*, also known as *Bacillus pasteurii*, *B. pasteurii*) is extensively used as model microorganism in MICP, due to its high urease activity (giving a high efficiency in MICP process), high adaptability to the ambient environment with no pathogenicity. *S. pasteurii* is a gram-positive, aerobic, alkalophilic bacteria (De Jong et al., 2006; Zhao et al., 2014), classified as risk group 1 (unlike to cause human disease)(Venda Oliveira et al., 2015). It is either round, rod-like or spiral, and its cell diameter is usually in the range of 0.5-3 μm. Thus the free passage of this bacteria is inhibited usually when pore throat is smaller than 0.4 μm (De Jong et al., 2006). Bacteria used in MICP studies is either bought from companies or isolated locally from water, soils or sludge samples (Omoregie et al., 2017). For type strains, such as ATCC 11859, the growth condition is cultivated aerobically (inadequate oxygen limits growth) at ambient temperature (optimal temperature is around 30°C) in a pH range from 6 to 9. Early stationary phase can be achieved after around 40 hours cultivation.

To carry out MICP, injection of bacteria solution and injection of chemical reagents are needed. As for bacterial injection, bio-augmentation method (addition of pre-grown microbial cultures) and bio-stimulation method (addition of nutrients to stimulate the growth of specific indigenous bacteria) are used by researchers to enhance the performance of bacteria. In most lab-based studies, bio-augmentation is always used by injecting bacteria into artificially prepared soils. For field trials, Gomez et al. (2018) have already completed a successful trial of a 12 m bio-stimulation treatment in the field. Although there are few studies about bio-stimulation at field scale, it is an effective method that uses indigenous bacteria, which lowers the ecological risk and the cost of cultivation and transportation.

For injecting cementation solution, commercial chemical reagents (urea and Ca^{2+} ions) are used. For sustainable, environmental and cost-effective consideration, researchers used alternatives to replace pure chemical reagents in specific regions. According to Danjo & Kawasaki (2016), urea available in coastal regions, resulting for instance of biodegradation of dead fish as well as urine from animals, can be used as carbon source. In a limited-resource-region like Sahel in Sahara desert (Bernardi, 2012), urea from urine and calcium possibly from bones and milk are used to produce bricks together with sand and soil bacteria as building material. Using urine is under debate

because of the related sanitary problems (water pollution, health risk). Chemical reagents (like calcium chloride, calcium acetate) are used for calcium source. Cheng et al. (2014) successfully used seawater as calcium source. Liang et al. (Liang et al., 2019) proposed to use kitchen waste (oyster shells, scallop shells and eggshells) instead of pure reagents. Though these usages of waste are promising, attention should be paid to the problems like sanitary problems or secondary pollution.

In recent years, some researchers started to use enzymes directly instead of bacterial solutions to achieve the process of bio-cementation. Some studies indicate that the growing cells give better results in enhancing soil properties than dead and resting cells (Chou et al., 2011). However, many aspects related to this no-cell method should be considered, like high cost, relatively sensitive enzymes compared to live cells, etc.

3. Factors influencing the fabrication of bio-cemented soils

In order to better understand the mechanisms and maximizing the efficiency of MICP, a large amount of experiments has been designed considering various factors that influence the cementing process. In Fig. 1, comprehensive factors involved in different steps of the process were given. In short, these factors can be summarized as i) factors related to bacteria and cementation solution (strain source and type, nutrient, cell concentration, oxygen availability, aqueous environment, pH, temperature), ii) factors related to soil (size distribution, density, saturation degree), iii) factors related to the fabrication of bio-cemented soils (injection rate and mode, retention time, number of cycles). Since urea hydrolysis is not notably inhibited by the concentration of ammonium within the range of mostly used concentrations of cementation solution in various studies (Lauchnor et al., 2015), the ammonium concentration does not appear as a main factor in this review. In this part, only the major factors in each aspect were chosen to clarify their effects on MICP.

3.1 Factors influence microbial activity

Controlling biological activity provides a way to control the timing, rate and spatial distribution of chemical reactions (De Jong et al., 2010). Obtaining the maximum biomass and enzyme activity and fixing the bacteria at the desired place are vital to assure the final success of MICP.

3.1.1 Bacteria concentration

Usually, the late exponential phase (early steady phase, when the number of bacteria becomes stable) of bacteria growth is adopted by most researchers. Hindered by organic matters and continuously formed precipitates, it is unpractical to monitor the number of bacteria during MICP reactions in porous medium. Knowing the input

number of bacteria in the system is necessary. OD_{600} is the optical density of the biomass measured at 600 nm wavelength using ultraviolet-visible spectrophotometer. The OD_{600} of the bacteria solution is usually used to characterize the input biomass in MICP studies. Sometimes, the value of OD_{600} is converted into cells/mL by the following equation for *S. pasteurii* (Okwadha & Li, 2010),

$$C_{(\text{cells.mL}^{-1})} = 8.59 \times 10^7 \times (\text{OD}_{600})^{1.3627}$$

Some authors also use other microbiological methods to quantify bacteria concentration, like the plate count method, using cfu/mL (colony forming units per mL) to represent bacteria concentration (Soon et al., 2014).

Van Paassen (2009) used an initial OD_{600} = 1.583 to achieve cementation of a 5 m column. Mirmohammad Sadeghi et al. (2015) used four OD_{600} values (0.75, 1.5, 2.5, and 4) to conduct experiments. A huge difference was seen between 0.75 and 1.5 and small differences between 1.5, 2.5 and 4. Therefore, these authors recommended a value of 1.5 for large-scale applications. Zhao et al. (2014) used OD_{600} ranging from 0.3 to 1.5 (0.3, 0.6, 0.9, 1.2, 1.5), and observed increases in unconfined compression strength (UCS), from 100% (0.44 MPa) for 0.3 to 300% for 0.6, 337% for 0.9, 424% for 1.2 and 478% for 1.5. Okwadha & Li (2010) used several concentrations of bacteria (10^6-10^8 cells/mL) and found that the 10^8 cells/mL concentration was optimal, with a 30% $CaCO_3$ increment.

During the cementation process, a greater influence on the efficiency of MICP was seen when increasing the amount of cells (8.5×10^6, 7.5×10^7, 2.3×10^8) rather than the initial concentration of urea (333 mM and 666 mM) (Okwadha & Li, 2010). This means that injecting more bacteria to increase the rate of ureolysis is more efficient than providing more urea to the system during MICP. Similar results were obtained by Mirmohammad Sadeghi et al. (2015). Nonetheless, a high concentration of bacteria (OD_{600} over 2) does not provide a significant improvement compared to a relatively lower concentration.

3.1.2 Urease and its activity

Enzyme content is not always proportional to biomass (Whiffin, 2004). Bacteria will release their enzymes when confronted with depletion of nutrients (van Paassen, 2009) and diluted in saline solution (9 g/L NaCl) (Harkes et al., 2010). Therefore, biomass concentration is not the appropriate parameter to quantify urease activity. Thus, to achieve repeatability, urease activity must be controlled before injection. It is obvious that, with a higher urease activity, more precipitation can be obtained if other conditions are favorable. In the majority of the studies, urease activity is always measured and calculated according to Whiffin's method before injection (Whiffin, 2004). Urease activity is equal to the slope of the conductivity change according to time in the first five minutes of measurement. And the specific urease activity is calculated as follows,

$$specific\ urease\ activity = \frac{urease\ activity(mM\ urease\ hydrolysed.min^{-1})}{biomass(OD_{600})}$$

A certain amount of biomass can provide sufficient urease for MICP process. Zhao et al. (2014), using a bacteria solution with OD_{600} = 0.6, concluded that a urease activity equal to 5.5 mM hydrolyzed urea/min/OD_{600} was efficient. Al Qabany et al. (2012), using a bacteria solution with OD_{600} ranging from 0.8-1.2, found that this guaranteed a high urease activity (5-20 mM urea/h).

Urease activity drops quickly (from 90 mM urea/h in the first 24 hours to 30 mM urea/h between 24 and 48 h), possibly because of the increasing amount of precipitation and the reduction of bacteria and pore space (Whiffin et al., 2007). Van Paassen (2009) found that urease activity dropped to less than 5 mM urea/h (for an initial OD_{600} = 1.583, without nutrients injection) after 20 days due to hydraulic constraints (encapsulation of bacteria in small pore spaces or generated precipitation, smaller available volume of cementation solution) and starvation (less biomass). A re-injection of bacteria can help to maintain the activity for another 20 days. After 6-8 steps of injection, a drop in the pH of the effluent (from 9 to 8) was observed, indicating a decreasing activity of bacteria. Feng & Montoya (2016) also re-injected a small dose of bacteria suspension (2 mL) to maintain urease activity. Urease activity can also influence the crystal type and shape of $CaCO_3$. Van Paassen prepared MICP samples for XRD and SEM analysis. Results showed that, for urease activity increasing from 9 to 36 mM urea/h, vaterite content increased from 5 to 90 %. With urease activity higher than 30 mM urea/h or lower than 10 mM urea/h, spherical crystals of vaterite or rhomboidal crystals of calcite were formed separately (van Paassen, 2009). However, there is much more that needs to be understood of this aspect.

3.1.3 pH and temperature

pH and temperature have a direct bearing on the growth and urease activity of the bacteria. *S. pasteurii* is sensitive to pH and temperature during the cementation process as some studies have shown (Kim et al., 2018; Sun et al., 2019). pH and temperature also have impacts on the equilibria of dissolution and precipitation during MICP process. Here we mainly talk about the influence of microbial activity caused by these parameters.

pH has a crucial biochemical effect on the activity of urease produced by *S. pasteurii* (Whiffin, 2004). Optimal pH for bacteria and urease activity are not the same. For cultivation of the bacteria, the optimal pH is around 9, while the optimum pH for urease activity is usually near neutral for *S. pasteurii* (Mobley, 1995). According to Whiffin (2004), pH in the range of 6.25 to 7.7 gives a urease activity higher than 40 mM urea/min and the maximum (around 43 mM urea/min) occurs around pH=7. Cheng et al. (2014) found that pH lower than 3.5 and higher than 9.5 is adverse to the cementation process. The experimental results of Omoregie et al. (2017) showed that the pH range 7.5-8 was the optimal one for the urease activity of five *S. pasteurii strains.* During MICP process, Stocks-Fischer et al. (1999) determined that MICP starts at pH = 8.3 and its rate increases up to pH 9. Kim et al. (2018) studied the effect of the pH (in the range of 6-10) of an urea-$CaCl_2$ solution and found that pH=7 was the optimal condition for biocementation.

Temperature affects microbial growth and urease activity. Bahmani et al. (2017) studied the urease activity of *S. pasteurii* at different temperatures (10, 15, 21, 35, 50, 60 and 80°C), and found that urease activity increased with temperature up to an optimum temperature of 60°C. During the process of cultivation of bacteria, the optimal temperature for different strains of *S. pasteurii* to reach the maximum specific urease activity is 25°C or 30°C, e.g. for DSMZ 33 the optimal temperature is 30°C (Omoregie et al., 2017). Cheng et al. (2014) found that increasing temperature could increase the production of calcite; however, the strength was smaller than that obtained at room temperature. For the cementation of relatively coarse materials (1-3 mm), a moderate temperature of 20°C was optimal (Mahawish et al., 2018). In Sun et al. (2019) study, 30°C resulted in the highest rate of $CaCO_3$ precipitation. Kim et al. (2018) studied the influence of temperatures between 20 and 50°C and found that 20, 25, 30℃ were the optimal temperatures for different strains of *S. pasteurii*.

3.2 Soil characteristics

Soil characteristics, such as density, grading, saturation, have a vital impact on bio-treatment efficiency. Studying soils with different characteristics are beneficial to understand the use of MICP in various sites. Soil samples preparation should consider the aim of the research. Studying the effect of soil characteristics makes the protocol more feasible and efficient in varying conditions of geological sites. Some of these parameters are considered below.

3.2.1 Soil density

Density of sand has a great impact on its mechanical behavior. The density state is also characterized by the relative density D_r, calculated by:

$$D_r(\%) = \frac{e_{max} - e}{e_{max} - e_{min}}\%$$

where e_{max}, e_{min} represent the standardized maximum and minimum void ratios, and e the actual void ratio of the sand. For similar MICP treatments, increasing density (40%, 70%, 80%) resulted in a reduction of $CaCO_3$ production and an increase in strength (Rowshanbakht et al., 2016). Bahmani et al. (2017) conducted a series of experiments with various soil densities (1.86, 1.93, 2.11, 2.23, 2.36 gr/cm^3, corresponding to relative densities of 0%, 17%, 56%, 78%, 100%). Results indicated that the treated soil sample with a density of 2.11 gr/cm^3 had the highest value of stiffness and compressive strength. It shows that the highest density does not necessarily lead to the highest strength. Rowshanbakht et al. (2016) used poorly graded sandy silica (D_{max}=0.4 mm, C_u=1.46, C_c=0.83, D_{50}=0.2 mm) with no shape description, Bahmani et al. (2017) used poorly graded angular to sub-angular quartz grains (D_{max}=1 mm, C_u=2.2 , C_c=0.77 , D_{50}=0.18 mm). Both of them used ASTM Standards. The results obtained by Rowshanbakht et al. (2016) and Bahmani et al. (2017) are conflicting, maybe because Bahmani used a sand with a higher fines content

(20% < 0.1 mm) whereas, in the study of Rowshanbakht et al., the fines content (< 0.1 mm) was 1%. When the relative density increases from 56% to higher values, the smaller pore throats inhibited the transport of bacteria, thereby decreasing the efficiency of MICP.

Gao et al. (2019) used Ottawa sand (ASTM poorly graded round quartz sand), with grain sizes ranging from 0.2-0.5 mm, and a mean size of 0.36 mm. For loose (D_r = 30%) and medium dense (D_r = 50%) sands, a slight bio-treatment gave a strength improvement comparable to, or exceeding, that of untreated dense sand (D_r = 90%) (Gao et al., 2019). Xiao et al. (2019) applied cyclic loadings to MICP-treated calcareous sand (angular, with no fines, D_{10}=0.19 mm, D_{50}=0.38 mm) and untreated sand with different relative densities (10%, 50%, 80%) and different magnitudes of bio-cementation. Comparing treated and untreated sands, with the same increment in dry unit weight, they showed that treated sand samples had gained a larger increase in cyclic resistance, which indicates that the MICP treatment method is more efficient in promoting cyclic resistance of calcareous sand than densification.

3.2.2 Particle size

Many studies have been carried out using sands (e.g. Ottawa silica sand, Fontainebleau sand) with grain diameters smaller than 2 mm (Hamdan et al., 2013; Zhao et al., 2014; O'Donnell & Kavazanjian, 2015; Choi et al., 2016; Gao et al., 2019). Under the consideration of free passage of bacteria, as well as limit of injectability in-situ, very fine grains are usually not used. For example, De Jong et al. (2006) used Ottawa 50-70 sand to represent loose natural deposit, which is sufficient for the bacteria in the size range of 1-3 μm. Bahmani et al. (2017) used a soil with a particle size ranged between 50 and 400 μm, which was sufficient for the transportation of bacteria. Hataf & Jamali (2018) tried to determine the maximum fine content (i.e. a clay with low plasticity) that did not influence the effect of MICP. For that, a fine-grained soil (100 % finer than 75 μm, 25.6 % finer than 2 μm) and a coarse-grained soil (0.4 mm - 5 mm) were mixed at different percentages, and consolidated drained direct shear tests were carried out before and after the MICP treatment. Results showed that the higher the fine content is, the lower the strength increase due to MICP. A fine content up to 20 % did not affect the efficiency of MICP. Few studies include larger grains in soil preparation. However, in the study of Mahawish et al. (2018), Pakenham Blue Metal (Old Basalt) coarse grain (2.36-16 mm) and relatively fine grains (0.075-9.5 mm) were mixed at different percentages to conduct column cementation experiments. As a result, in comparison with other groups of materials, materials with 25% fine grains resulted in a better distribution of $CaCO_3$ and a relatively higher value of unconfined compressive strength.

3.2.3 Saturation degree

In the literature, it has been proved that a decrease in the saturation degree (by

a few percents) can dramatically increase the effect of MICP on small strain stiffness (He et al., 2014) during undrained loading, with a marked increase in cyclic resistance. He et al. (2014) used a denitrifying bacteria (i.e., that produces N_2 gas) to lower the saturation degree (100 %-87.5%) in undrained soil samples (100 or 140 mm long, Φ=50 or 70 mm, D_r = 9-10%). They used Ottawa sand (round poorly-graded quartz sand) with 0.4 mm mean diameter. As a result, a considerable increase in undrained liquefaction resistance and a substantial reduction in pore water pressure were observed after MICP treatment, compared to saturated samples. The authors concluded that gas bubbles acted as pressure buffer to abate the increasing pore water pressure and thus enhanced liquefaction resistance. As the gas was produced, MICP concentration increased due to the decreasing liquid volume, which might also lift the efficiency of precipitation and enhance liquefaction resistance. Cheng et al. (2013) achieved different saturation degrees in a MICP-treated soil column (160 mm long, Φ=55mm) by using a vacuum pump to control the volume of solution remaining in the sample. It came out that, for a certain amount of $CaCO_3$ produced, a higher strength was obtained with a decrease in the saturation degree (from 100% to 80%, 40% and 20%). To obtain similar strength, MICP-treated samples with a 20 % degree of saturation needed around 1/3 $CaCO_3$ content with respect to MICP-treated saturated samples. Fig. 2 shows that $CaCO_3$ bonds mainly occurred at soil particle contact because of the restricted meniscus- shaped distribution of MICP solution on the basis of unsaturated soil mechanics theory (Cheng & Cord-Ruwisch, 2012) in the sample of 20 % degree of saturation. This means that the efficiently distributed $CaCO_3$ bonds gave a significant strength enhancement for a smaller quantity of calcium carbonate produced. By contrast, in the fully saturated MICP-treated sample, most of the $CaCO_3$ bonds were located on the surface of the soil particles.

3.3 Cementation solution

In the MICP protocols, the cementation solution (CS) certainly provides the basic chemicals for MICP process (as urea and Ca^{2+} source). Sometimes, it also includes components like pH stabilizer ($NaHCO_3$), a carbon source or nutrients (nutrient broth, yeast) to maintain the bacteria. Concentration of CS refers to the concentration of urea and Ca^{2+} in the CS. It is an important parameter when designing a MICP protocol (De Jong et al., 2013). Many authors have conducted laboratory experiments by applying different concentrations of CS (either equimolar or non-equimolar concentrations of urea and Ca^{2+}, usually < 2 M) to different soils, and tried to find out the optimal concentration for their experimental conditions.

3.3.1 Equimolar CS

Many researchers have used CS with equimolar urea and Ca^{2+} to conduct experiments. Lee et al. (2012) concluded that the MICP process was improved with an increasing concentration of CS up to 0.5 M, whereas the improvement was less

important for the concentration of 1 M. De Muynck et al. (2010) concluded from their study that 0.425 M was the upper limit dosage for the improvement of MICP. Higher dosage had an inhibiting effect. Zhao et al. (2014) came to the conclusion that, for concentrations ranging from 0.25-0.5 M, the unconfined compression strength (UCS) increased 10 times compared to a 2-times increase from 0.5 M to 1.5 M. Al Qabany et al. (2012) compared two series of SEM images of treated samples with 0.5 M and 0.25 M CS, with the same injection rate. Thicker, larger and more heterogeneous distribution of precipitation crystals were produced by using 0.5 M CS. They also found that a higher concentration (1 M) could change the calcite precipitation pattern. New calcite precipitates preferentially on existing crystals instead of forming nucleation in new sites, which gives bigger crystals. These bigger crystals occupy the pore space and hamper the metabolic process of bacteria when the soil is relatively fine, resulting in higher risks of partial clogging and presenting an inhibiting effect on MICP. Reasons for the inhibiting effect of higher CS concentration can be attributed to the enzyme amount that gives a limited urea hydrolysis rate, which influences the MICP efficiency (Whiffin, 2004). Mahawish et al. (2018) successfully used higher concentrations of CS (1 M) to cement coarse materials (1-3 mm) that require larger size and amount of precipitates to attain good results.

3.3.2 Non-equimolar CS

Some authors tried to improve MICP effects by using non-equimolar CS. Mahawish et al. (2018) found that non-equimolar CS (e.g., 0.5 M urea and 0.25 M Ca) promised higher amount, larger crystals and more homogenous distribution of $CaCO_3$, and also larger compressive strength, while using much higher concentration solutions (2.0 M urea, 1.0 M Ca or 1.5 M urea, 1.5 M Ca^{2+}) produced a larger amount of $CaCO_3$, but a lower compressive strength (Mahawish et al., 2018). Increasing only the urea concentration of the CS can also increase the efficiency of MICP. However, if the urea content in the CS is increasing more than the amount that is sufficient for precipitation process, the efficiency stops to grow. Only increasing the Ca^{2+} concentration of the CS from 0.025 M to 0. 25 M can provide more than 100 % of the amount of $CaCO_3$ (Okwadha & Li, 2010).

3.4 Injection mode and rates

3.4.1 Injection methods

Injection methods are quite different from one study to another. The main injection methods are presented below,

1. Mixing before injection

Mixing the bacteria and CS before injection gives rise to an instant reaction, producing $CaCO_3$ precipitation and bacteria flocculation immediately. This injection method is appropriate for the treatment of coarse materials (van Paassen, 2009) that

need higher reaction rates and larger amounts of precipitates. And it is also used in surface stabilization, because it only needs to cement the soil to a limited depth. Because this method needs less injection time, it makes the process easier and reduces cost in real works. In recent studies, this method has been improved to prevent the occurrence of an immediate reaction by prolonging the lag period of the reaction. It has been applied successfully to lab column experiments, either by lowering concentration of bacteria and adjusting the initial pH of the mixture to pH 4 (Cheng et al., 2019), or by refrigerating the bacteria and CS at low temperature (4°C) before mixing (Xiao et al., 2019).

2. Percolation

This method is easy to perform and suitable for stabilization of the soil surface. A limited depth can be reached by using this method. Cheng & Cord-Ruwisch (2012) achieved the treatment down to 1 m depth with a reasonable degree of homogeneity by using the percolation method.

3. Two-phase injection (by first injecting the bacterial cell solution followed by the CS)

This method is expected to prevent clogging and give a more homogeneous distribution of $CaCO_3$ crystals (Whiffin et al., 2007). It is widely used by many researchers.

3.4.2 Retention time

The time intervals during the different phases of a test must be long enough to ensure sufficient reaction process, but not too long to guarantee substantial bacterial activity. Usually there are two retention times that are used during the MICP process, one between the injection of bacteria and the injection of the CS, and the other one after the injection of the CS to allow cementation to occur.

After injection of bacteria, a retention time is needed before injecting the CS, so that the bacteria in the column will have time to distribute and fix on the surface of the soil. Retention time for bacteria solution should be decided by the results of preliminary experiments. When the injection concentration of bacteria is low, a longer retention time will be needed for the bacteria to grow to a certain amount (i.e. providing a sufficient urease activity of 5-20 mM/h) in the column.

Retention time after injection of the CS requires the accomplishment of cementation process. It depends on the reaction time of the chemicals and can be estimated according to the concentration of the CS. Al Qabany et al. (2012) found that either a 1 M CS with 24 h retention time, or a 0.5 M CS with 12 h retention time, or a 0.25 M CS with 6 h retention time, representing the same CS content injected, were equivalent to obtain high efficiency of the MICP process. These three concentrations of CS with corresponding retention times can all give a significantly large efficiency (over 80 %, and up to 100 % injected chemicals precipitating as $CaCO_3$) in producing $CaCO_3$.

3.4.3 Injection rate

Injection rate plays an important role in the distribution of bacteria and precipitates, thus influences the homogeneity of the treatment. Dynamic interactions among the rate of urea hydrolysis, retention time and the flow rate of CS need to be considered to achieve homogeneity and required strength. Pulse injection (i.e. injecting a certain amount of CS into the soil and giving a rest time for the reactions) has been proved to be more efficient than continuous injection (Al Qabany et al., 2012). Many studies used this injection-retention process repetitively for MICP treatment.

For strengthening soil surface, injection is usually realized by surface percolation. For ground improvement, Whiffin et al. (2007) used 0.35 L/h (for a column 5 m long, Φ = 66 mm), Mortensen et al. (2011) used 10 ml/min (column: 100/50 mm long, Φ = 50 mm), Cheng et al. (2013) used 1 L/h (column: 160 mm long, Φ = 55 mm). They all obtained good cementation results in their samples of various sizes (<1 mm) with the mentioned injection rates. To make the results more clear, seepage velocity (the velocity through the bulk of the porous medium) is calculated using the following equation to unify the units, v=Q/A, where v is the seepage velocity (m/day), Q is the total volume flowing through the corresponding cross-sectional area per time unit m^3/day, A is the cross-section area of the flow m^2. The results are 2.5 m/day, 7.3 m/day and 10.1 m/day for Whiffin et al. (2007), Mortensen et al. (2011) and Cheng et al. (2013), respectively. Whiffin (2007) concluded that relatively low flow rates (< 10 m/day) were desirable. However, if the urea hydrolysis is quite fast, to prevent clogging near the inlet, a higher injection rate is expected to deliver precipitates to further locations.

3.4.4 Numbers of injections

Feng & Montoya (2016) defined the cementation level by the mass percentage of precipitate: a value below 1.5% represents light cementation, a value between 1.5 and 3.5% represents moderate cementation and above 3.5% represents heavy cementation. They achieved these different levels of cementation by injecting a solution (333 mM urea, 374 mM NH_4Cl, 50 mM $CaCl_2$) around 10 times, 20 times and 40 times for light, moderate and heavy cementation of samples (145 mm long, Φ = 72 mm). In practice, it should be noted that more times of injections might cause higher risks of clogging, and also increase costs of operation. In the next study, Feng & Montoya (2017) found that, for a similar cementation content, the samples behaved differently under cyclic loading, indicating that this parameter alone (for a given concentration of reagents) is not sufficient to choose the number of injections to characterize the cementation level. Another parameter is necessary, such as the shear wave velocity derived from bender elements measurements. Montoya et al. (2013) set target shear wave velocities of 300 m/s, 650 m/s and 1200 m/s to represent light, moderate and heavy cemented samples respectively. This is a range of values going from soil-like behavior to rock-like behavior.

3.4.5 Injection of fixation solution

The adsorption rate of the input biomass on the pore surface and the movement of bacterial cells in pores affect MICP efficiency and homogeneity. Factors of transportation and adsorption of bacteria on the soil have been studied a lot, including physiological characters of microorganisms (size, surface charge, hydrophobicity…), physical and chemical properties of pore water (pH, salinity, etc.) and properties of the porous medium itself (pH, water content, mineral composition, texture and particle size distribution, etc.) (Abu-Ashour et al., 1994).

Whiffin et al. (2007) achieved the consolidation of a 5 m column by injecting a 50 mM $CaCl_2$ solution to immobilize the bacteria after bacterial injection. Harkes et al. (2010) compared the injection of different compositions of the fixation solution (50 mM $CaCl_2$ solution, deionized water, fresh surface water, 9 g/L NaCl solution and cementation fluid), right after the injection of the bacterial suspension or maintained for 2 hours before injection of the cementation solution. The size of the soil column was 6.6 cm in diameter and 18 cm in length. Results showed that transportation of bacteria was enhanced, i.e. large amounts of bacteria were removed from the soil, when injecting a fixation fluid with low ionic strength (deionized water or fresh surface water). On the contrary, with the injection of a high ionic strength solution (50 mM $CaCl_2$, NaCl solution and cementation solution), adsorption of bacteria on the soil was enhanced. The aim of injecting a fixation solution is to enhance adsorption of bacteria and to distribute bacteria evenly in a desired way. It can both mobilize (enhance transport) or immobilize (enhance absorption) the bacteria in the soil. This could be partly explained by the classical Derjaguin-Landau-Verwey-Overbeek (DLVO) theory, i.e. that the stability of colloids (bacteria are bio-colloids) depends on the electrostatic repulsive forces (caused by the electrical double layer) and attractive van der Waals forces. High concentration of fixation solution will provide a high ionic strength, which compresses the electrical double layer and lowers the repulsive electrostatic force. At that time, the attractive forces (Van Der Waals forces) are the primary forces, resulting in enhancement of adsorption and adhesion of bacteria to the porous media (Adamczyk & Weroński, 1999; Okwadha & Li, 2010). Chu et al. (2014) injected fixation solutions with different valences (Ca^{2+}, Fe^{3+}, Al^{3+}) before injecting bacteria (isolated from tropical beach sand, representative of genus *Bacillus*). The adsorption of bacteria is obviously enhanced by injecting different fixation solutions (20-30 % increment), compared to only injecting water. The increasing effect among the three fixation solutions is similar. The authors suggested that the increase in the number of positively charged sites on soil surface enhanced adsorption, in spite of the strength of the bonds. It is known that iron is essential to microbial metabolism. While the interaction between the bacteria and the ferric ions was not taking into account by the authors. In Mortensen's study (2011), similar size (D_{50}=0.12 mm) of quartz sand and sand rich in iron oxide treated by the same MICP process obtained similar shear wave velocity increase. The results showed that the presence of iron oxide might have little influence to MICP process. For another biocementation system using ion-reducing bacteria, ferric ions can be reduced to ferrous ions and precipitates like undissolved ferrous

compound are generated (Ivanov & Chu, 2008).

The above-mentioned results show that using a fixation solution can help to enhance the efficiency of MICP. Considering the different bacteria strains used and the various soil environments, preliminary experiments are required to obtain better results.

4. Conclusion and future expectation

The optimization of the MICP protocol is of much concern to promote efficiency, economize reagents and simplify operations. In the light of all the results summarized from various research teams, the following conclusions can be drawn,

- For the cultivation of *S. pasteurii*, under the conditions of a pH equal to 9 and an ambient temperature equal to 30°C, a large quantity of biomass can be obtained. And for the cementation process, a pH ranging from 7-8, and a temperature around 25±5°C are optimal conditions for high urease activity and precipitate production.
- A wide range of values of concentration of bacteria (corresponding to OD_{600} between 0.1 and 4) has been successfully used in various studies. A concentration range of OD_{600} value from 0.6-1.5, which promises a urease activity value over 5 mM urea/h, can yield a reasonable amount of cementation. It has been proved to be efficient in samples scaling from several tens of centimeters to several meters.
- To achieve a more homogeneous bacterial distribution and enhancing bacteria adsorption, a pre-designed fixation solution can be used.
- In real applications, the soil is imposed, and the treatment must be adapted to the soil. Loose and medium dense soils can behave like a dense soil after treatment. Less than 20 % of fine particles (< 75 μm) in 0.4 - 5 mm soils and less than 25 % medium-fine grains (75 μm – 9.5 mm) in 2.36 - 16 mm soils were found to have no influence on bio-treatment.
- When the soil is not saturated, the bio-cementation method can give a more efficient precipitation distribution by precipitating mainly at particle contacts, which promises a larger gain in strength with a lighter treatment.
- To find an appropriate concentration that can be used in the field, beside the soil characteristics, not only efficiency (higher conversion ratio) but also cost balance (injection operation, CS and bacteria concentration) should be taken into account. Low concentration (0.2 M) of CS solution may give high efficiency in using reagent but it needs more injection times, which sounds not cost-effective for large scale use. A concentration of 0.5 M can give a high efficiency of the calcification process and requires less injection times. For bio-cementation of soils with a relatively high content of large size grains, concentration can be raised up to 1 M to improve efficiency.
- Factors of injection depend on the value of the above parameters, and also the site and expected mechanical properties. In practice, reducing the number of injections can be more feasible and reduce significantly the cost.

This article discussed the factors separately to understand the effect of each factor. It should be noted that MICP is a comprehensive process affected by the combined effects of all these factors. For establishing a high-efficiency and low-cost protocol, it is hard to give a unified solution in the variety of possible conditions. Nevertheless, the above indications can help to choose values for designing experiments. All the parameters and their interactions should be taken into account and it seems necessary to carry out preliminary tests to choose specific values for operational conditions and purposes.

Acknowledgements

The authors would like to thank the support of China Scholarship Council (CSC). We are also grateful for assistance from Solétanche-Bachy.

Review on engineering properties of MICP-treated soils

Tong Yu[1a], Hanène Souli[2b], Yoan Pechaud[3b] and Jean-Marie Fleureau*[1]

[1] *Laboratoire de mécanique des Sols, Structures et Matériaux, CNRS UMR 8579, Université Paris Saclay, CentraleSupélec,*
8-10 Rue Joliot Curie, 91190 Gif-sur-Yvette, France
[2] *Laboratoire de Tribologie et Dynamique des Systèmes, CNRS UMR 5513, Ecole Nationale d'Ingénieurs de Saint Etienne,*
58 rue Jean Parot, 42023 Saint Etienne Cedex, France
[3] *Laboratoire Géomatériaux et Environnement, Université Gustave Eiffel,*
77454 Marne-la-Vallée Cedex 2, France

(Received keep as blank , Revised keep as blank , Accepted keep as blank)

Abstract. Microbial induced calcium carbonate precipitation (MICP), a sustainable and effective soil improvement method, has experienced a burgeoning development in recent years. It is a bio-mediated method that uses the metabolic process of bacteria to cause $CaCO_3$ precipitation in the pore space of the soil. This technique has a large potential in the geotechnical engineering field to enhance soil properties, including mitigation of liquefaction, control of suffusion, etc. Multi-scale studies, from microstructure investigations (microscopic imaging and related rising techniques at micron-scale), to macroscopic tests (lab-based physical, chemical and mechanical tests from centimeter to meter), to in-situ trials (kilometers), have been done to study the mechanisms and efficiency of MICP. In this article, results obtained in recent years from various testing methods (conventional tests including unconfined compression tests, triaxial and oedometric tests, centrifuge tests, shear wave velocity and permeability measurements, as well as microscopic imaging) were selected, presented, analyzed and summarized, in order to be used as reference for future studies. Though results obtained in various studies are rather scattered, owning to the different experimental conditions, general conclusions can be given: when the $CaCO_3$ content (CCC) increases, the unconfined compression strength increases (up to 1.4 MPa for CCC=5%) as well as the shear wave velocity (more than 1-fold increase in V_s for each 1% $CaCO_3$ precipitated), and the permeability decr eases (with a drop limited to less than 3 orders of magnitude). Concerning the mechanical behavior of MICP treated soil, an increase in the peak properties, an indefinite increase in friction angle and a large increase in cohesion were obtained. When the soil was subjected to cyclic/dynamic loadings, lower pore pressure generation, reduced strains, and increasing number of cycles to reach liquefaction were concluded. It is important to note that the formation of $CaCO_3$ results in an increase in the dry density of the samples, which adds to the bonding of particles and may play a major part in the improvement of the mechanical properties of soil, such as peak maximum deviator, resistance to liquefaction, etc.

---

*Corresponding author, Professor, E-mail: jean-marie.fleureau@centralesupelec.fr
[a] Ph.D. Student, E-mail: tong.yu@centralesupelec.fr
[b] E-mail: Hanène Souli, associate professor, hanene.souli@enise.fr; Yoan Pechaud, associate professor, yoan.pechaud@u-pem.fr

Keywords: MICP; biocementation; engineering properties; microstructures

1. Introduction

Microbial induced calcium carbonate precipitation (MICP) is a novel, sustainable, cost-competitive soil improvement technique with a low-CO_2 emission (Røyne *et al*. 2019). It has known a great development in the past decade, in the exploration of protocols (Yu *et al*. 2020), engineering properties and up-scaling applications. The process of MICP is schematically shown in Fig. 1. The method benefits from the metabolic process of microorganisms, such as *Sporosarcina pasteurii* (*S. pasteurii*), a ubiquitous, non-toxic and effective strain often used in practice. This strain can produce an enzyme – urease – that enhances the hydrolysis process of urea. Ammonium and carbonate ions are produced. With the presence of Ca^{2+} ions, the resulting crystals of $CaCO_3$ can precipitate on the surface and in the pore throats of soil grains, which in return improves the soil engineering properties by forming bonds between soil particles and increasing their surface roughness. These properties include physical, conduction, mechanical properties, and chemical composition (Dejong *et al*. 2013).

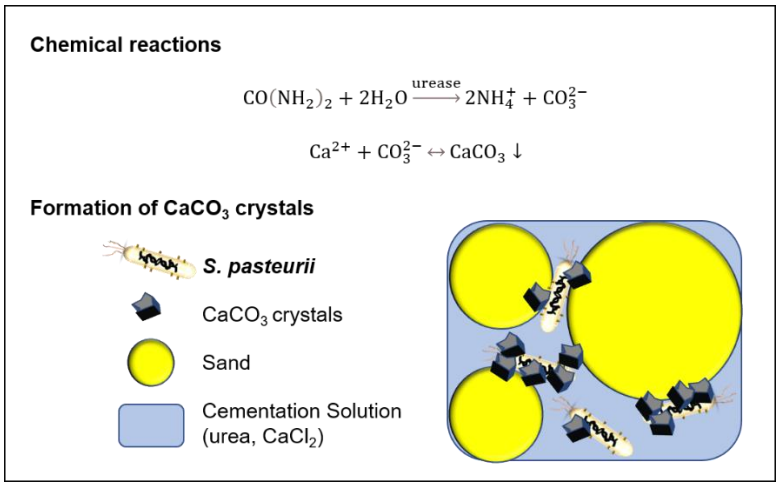

Fig. 1 Schematic diagram of MICP process

MICP is promising in many geotechnical engineering fields, as summarized in some existing review articles (Ivanov and Chu 2008, Dejong *et al*. 2010). Studies of MICP, related to liquefaction mitigation (Montoya *et al*. 2012, Wu 2015, Xiao *et al*. 2018), stability and erosion control of slopes, dams and coastal area (Jang *et al*. 2017, Do *et al.* 2019, Haouzi *et al.* 2019, Imran *et al.* 2019), wind erosion and dust control (Bahmani *et al*. 2017, Li *et al*. 2018), crack repair in concrete and mortar (Choi *et al*. 2017, Son *et al*. 2018), etc., have proved the effectiveness of this method. It can also be a good choice if the local soil is not suitable for conventional treatment methods like injecting cement or chemicals. Due to these prospective applications, researchers have carried out multi-scale studies using different testing methods to study the mechanisms and efficiency of MICP, from microscopic analyses to macroscopic tests and in-situ trials. Results of lab-based tests on MICP-treated soils highlight the enhanced soil behavior under either monotonic or dynamic loading.

Meanwhile, microscopic studies give a more thorough knowledge of the role of microbes and $CaCO_3$ crystals in the MICP process.

In the past reviews concerning MICP method, processes, and applications, comparison among different soil improvement methods were well summarized (e.g. Ivanov and Chu 2008, Dejong *et al*. 2010, Wang *et al.* 2017). Recently, a review by Choi *et al.* (2020) brought out very interesting quantitative data about microscopic and macroscopic properties of MICP-treated soils. However, in terms of engineering properties of MICP-treated soils, there is still a need for analysis and synthesis of the fast-growing experimental results for the future development of MICP technique. The objective of the present review is therefore to analyze critically the behavior of MICP-treated soils under monotonic and dynamic loadings. Some crucial engineering properties such as unconfined compression strength, compressibility coefficient, friction angle, cohesion, shear wave velocity and permeability are discussed precisely and incisively, and presented as a function of $CaCO_3$ content. Results from microscopic studies are also provided to better understand the micro-mechanisms that are of great significance to improve the efficiency of the method and engineering behavior of MICP-treated soils. At the end of the article, some interesting and useful conclusions and expectations are provided for future reference.

2. Testing methods and mechanical properties of bio-cemented soils

In this section, engineering properties of bio-cemented soil were summarized and analyzed on the base of various tests, including monotonic/cyclic loading tests and measurements of shear wave velocity and permeability.

2.1 Unconfined compression tests

Unconfined compression test is a simple and fast way to measure the strength of soil samples. Unconfined compression strength (UCS) is widely used for rapid comparison of the strength of MICP-treated samples that are fabricated using different protocols. Fig. 2(a) shows the change in UCS as a function of the percentage of deposited calcium carbonate for various sands of the literature. The median diameter of the grains (d_{50}) used in these studies, as well as the uniformity coefficient C_u, are reported in Fig. 2(b) as an indication of the grain size distributions. There is a large scatter in the values of UCS for a given percentage of carbonate.

The change in UCS in saturated specimens depends on several parameters, e.g. (i) the percentage of carbonate, (ii) the repartition of the $CaCO_3$ crystals in the porous medium, (iii) the adhesion of the crystals on particles. In granular soils, the standardized minimum and maximum void ratios mainly depend on the uniformity coefficient and grain shape (Biarez and Hicher 1994). This means that, under similar conditions of uniformity coefficients, relative densities, and grain shapes, the void ratio of the soil remains constant, independently of the size of the grains. Therefore, the percentage of calcium carbonate necessary to obtain a similar filling of the voids is independent of the size of the grains and should therefore produce a similar effect on the unconfined compression strength. Fig. 2 confirms this assumption as, for the same carbonate content, the UCS of the coarse sand of Gomez and Dejong (2017) are very high whereas those of the aggregates of Mahawish *et al*. (2018) are very low. The reason is probably different repartitions of the crystals in the soil.

Another parameter that must be taken into account is the saturation of the tested specimens. Unsaturation results in the existence of a suction within the soil and leads to an increase in strength

due to capillary and adsorption phenomena (e.g. Taibi *et al*. 2008). In fine sands, this capillary effect may be very important and affect the results as it is impossible to separate the role of cementation from that of saturation. In most of UCS tests, the degree of saturation can be assumed to be lower than 1 but, unfortunately, this parameter is never mentioned in the papers, and this contributes to the scatter of the results.

Concerning the influence of the uniformity coefficient C_u, it is well established that the standardized minimum and maximum void ratios decrease when C_u increases from 1 to 10, and remain more or less constant afterwards. As a consequence, for a given relative density (and grain shape factor), the soil will be denser if C_u is larger. For most of the tested soils, the relative density is high enough (larger than 50%, mostly around 80-90%), so that this parameter plays a limited part. It appears in Fig. 2(a) that the soils with the highest uniformity coefficient (i.e. the sand S4 of Cheng *et al*. (2017), the sand (b) of Gomez and Dejong (2017), that of Cui *et al*. (2017) and the sand (c) of Terzis and Laloui (2019) are predominantly located above the main bulk of samples. For the other soils, the value of C_u seldom exceeds 2. This observation is consistent with the remarks of several researchers (e.g. Martinez and Dejong 2009, Terzis and Laloui 2019) who noted that, at a given calcium carbonate percentage, the densest specimens featured the highest UCS because they had a larger number of contact points between particles where the crystals could form. In fact, the spreading of the grading curves (characterized by C_u) seems to be much more important than the maximum size of the grains.

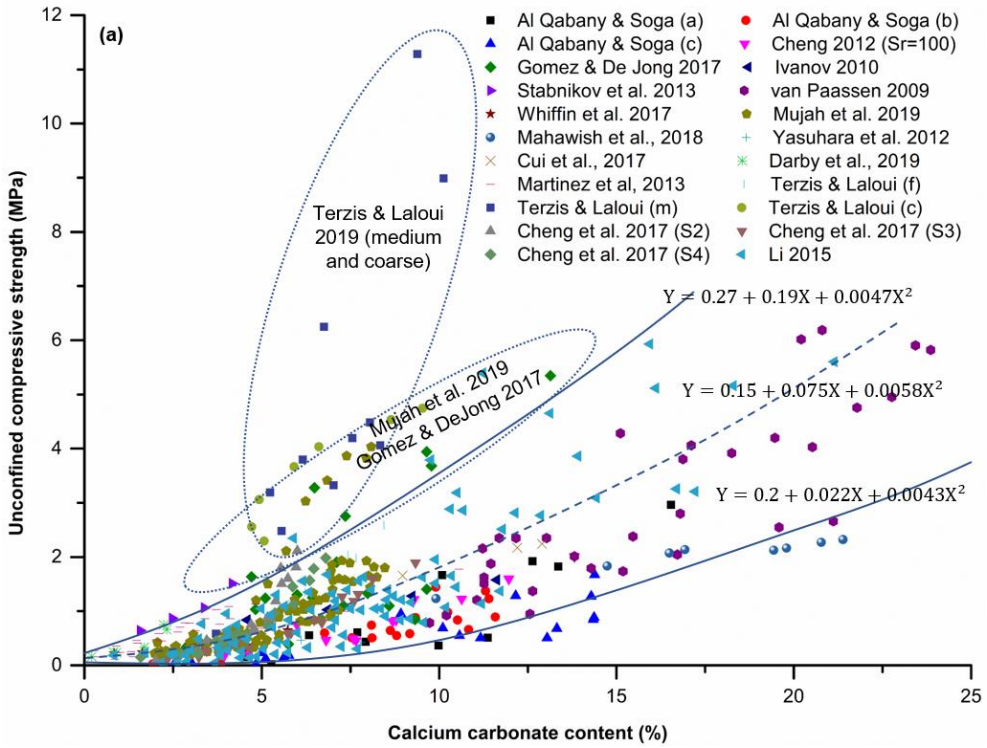

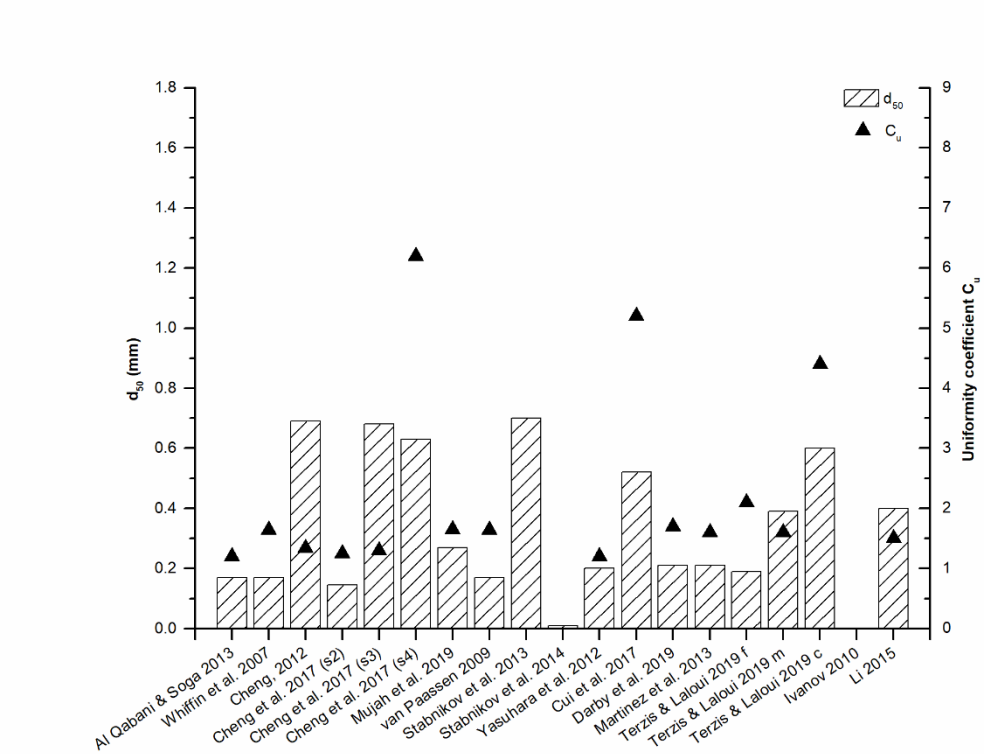

Fig. 2 (a) Unconfined compressive strength as a function of calcium carbonate content for various papers of the literature; (b) Medium diameter d_{50} and uniformity coefficient C_u for the different soils reported above.

Considering now all the points of Fig. 2(a), it appears that most points are comprised between the two continuous curves with parabolic shapes, with a mean value represented by the dashed line. Note that, up to 8% of calcium carbonate content, the experimental points are located equally on both sides of the dashed line whereas, for larger $CaCO_3$ contents, the points are predominantly between the dashed line and the lowest line, and even below the latter. However, three family of results are mostly out of the previous range: those of Gomez and Dejong (2017), Mujah *et al*. (2019) and Terzis and Laloui (2019), surrounded by ellipses in Fig. 2(a). The information present in the papers does not allow to understand or explain the origin of these large differences. Obviously, the strength of the soil, for a given percentage of carbonate, will be higher if the crystals are located at the contact points between particles rather than on the surface of particles but nothing, in the papers, confirms this assumption. The different protocols used, the activity of bacteria, etc. may explain the large scatter of the results. In the range of calcium carbonate percentages used in practice (i.e. smaller than 5%), the curve shows that one can expect an unconfined compression strength comprised between 0 and 1.4 MPa (e.g. for 5%, 0.7 MPa ± 0.7 MPa).

2.2 Shear wave velocity

Shear waves are very small-strain elastic waves propagating in materials, in which particle displacement is perpendicular to the direction of propagation (Dejong *et al*. 2010). The shear wave

velocity V_s is an effective stress parameter that can be a direct measure of the stiffness of the material (Hussien and Karray 2016). In an isotropic soil, it is related to the shear modulus G_{max} (which is defined as the ratio of shear stress to shear strain) by the following relation: $G_{max} = \rho V_s^2$, where ρ is the soil density. The measurement of V_s is a nondestructive and real-time method, widely-used in the lab and in the field to estimate the elastic properties of soil (Ahmadi and Akbari Paydar 2014). For example, it can be used, together with the National Earthquake Hazards Reduction Program (NEHRP) site classification, to predict the susceptibility of a soil to liquefaction (Weil *et al*. 2012). Measurement of shear wave velocity is carried out by conventional experiments using resonant column, bender elements or piezoelectric ring-actuators in the laboratory, and by seismic cone penetration tests (SCPT) and surface waves in-situ (Weil *et al*. 2012; Hussien and Karray 2016). V_s is mainly influenced by particle-particle stiffness that depends on cementation level as well as soil density, confining pressure and degree of saturation. It can be used to monitor the cementation process during MICP (Martinez *et al*. 2013; Dejong *et al*. 2014; Lin *et al*. 2016) and ensure that cementation level is sufficient to satisfy engineering application requirements. Feng and Montoya (2017) compared the cyclic behavior (strains and excess pore pressures) of two specimens (with similar $CaCO_3$ content, V_s = 425 and 676 m/s, respectively). The observed difference in cyclic resistance indicated that V_s was a more reliable indicator of the effect of MICP treatment on mechanical behavior than the $CaCO_3$ percentage. V_s measurement is also used in some studies to monitor the degradation of cementation of MICP during loading (breakage of particle-particle contacts in soil causes V_s to decrease) (Montoya and Dejong 2015; Feng and Montoya 2017).

Fig. 3 shows the change in the normalized shear wave velocity, i.e. the value of V_s after MICP-treatment divided by the initial V_s of the untreated soil, as a function of the $CaCO_3$ content. The normalized V_s values are scattered, which is caused by the various distributions of $CaCO_3$ resulting from the different used MICP protocols. Most of the points are located above the 1:1 line, meaning that every 1% of $CaCO_3$ produced can result in more than 1-fold increase in V_s. The points for relatively coarse sand (Ottawa 20-30) are located in the upper part of the graph. Similar results can also be derived from O'Donnell *et al*. (2017): for the same MICP treatment, the final increment of V_s for Huntington beach soil (relatively fine soil) was smaller than that of Ottawa 20-30 sand. This can possibly be attributed to the fact that the coarsest sand (Ottawa 20-30 sand) has less particle-particle contacts than the finest sands (Ottawa 50-70 and Huntington beach sand), which means that it needs less $CaCO_3$ to increase the bulk properties (V_s values). It should be noted that O'Donnell used denitrifying bacteria that produced gas in the pore space, and we do not know from the text whether shear wave velocities were measured before or after the saturation process in the triaxial cell, so it is not possible to know if the results are influenced by the saturation degree.

The effect of relative density on normalized shear wave velocity is not clear. Martinez *et al*. (2013) and Dejong *et al*. (2014) tested samples with relatively high relative densities (Table 1), and the points are distributed all over the graph without preference, which means that, surprisingly, relative density might be not very important for the development of V_s during MICP. Concerning the effect of confining pressure, there are very few available results and it is difficult to derive a definite conclusion. In Fig. 3, the results of Lin *et al*. (2016) show that, for similar increase in $CaCO_3$ content, the increments of normalized V_s are similar regardless of confining pressure (Table 1). This is perhaps due to the relatively close confining pressures they used.

There is a large scatter in the results shown in Fig. 3. According to Weil *et al*. (2012), for the same $CaCO_3$ content, the precipitation of $CaCO_3$ at the particle-particle contacts results in higher strength or stiffness increase than when $CaCO_3$ is deposited in the pore fluid or on exposed particle surfaces. Most of the results of Gomez and Dejong (2017) and Gomez *et al*. (2018) are located below

the others, maybe because many $CaCO_3$ crystals precipitated on the soil surface, as shown in the SEM images of Gomez and Dejong (2017), and inhomogeneous distribution of $CaCO_3$ was observed in the tank specimens of Gomez *et al*. (2018). Their results are interesting these researchers used a different protocol by stimulating native microorganisms in the soil rather than directly injecting well-prepared bacteria solutions as in the other studies. Their results are quite helpful as a reference for practical use in-situ, because using indigenous bacteria can avoid potential ecological impacts that may result from introducing non-native bacteria species and save the cost (laboratory cultivation and transportation). There are also inefficient MICP precipitation cases, as reported in Weil *et al*. (2012), Montoya *et al*. (2013) and Feng and Montoya (2017). The inefficient cases of Weil *et al*. and Feng and Montoya might be due to different precipitation patterns or distributions of $CaCO_3$. For Montoya *et al*. (2013), the plug formed by uneven MICP treatment in the outlet of the sample led to inflated $CaCO_3$ content but low shear wave velocity. Some points of Martinez *et al*. (2013) in the lower and right part of the figure were also due to a plug of calcium carbonate near the inlet of the cell.

Table 1 Parameters of the shear wave velocity tests in the literature

Reference	Bacteria	Sand	d_{50} (mm)	Relative density	C_u	Confining pressure (kPa)
(Weil *et al*. 2012)	*S. pasteurii*	Ottawa 50-70	0.12	40-60	1.4	100
		Ottawa 20-30	0.7		1.17	
(Martinez *et al*. 2013)	*S. pasteurii*	Ottawa 50-70	0.21	78-100	1.4	100
(Montoya *et al*. 2013)	*S. pasteurii*	Ottawa 50-70	0.22	40	1.4	-
(Dejong *et al*. 2014)	*S. pasteurii*	Ottawa 50-70	0.21	84	1.4	-
(Lin *et al*. 2016)	*S. pasteurii*	Ottawa 50-70	0.33	41	1.43	25, 50, 100
		Ottawa 20-30	0.71	39	1.17	
(Montoya and Dejong 2015)	*S. pasteurii*	Ottawa 50-70	0.22	31-45	1.4	100
(Feng and Montoya 2017)	*S. pasteurii*	Ottawa 50-70	0.22	38	1.4	100
(O'Donnell *et al*. 2017)	Denitrifying bacteria	Ottawa 20-30	*0.85	21-51	-	3
		Huntington beach sand	0.55	67	-	
(Gomez and Dejong 2017)	Native soil microorganism	SM	*0.15	50-65	2.3	60, 100
		SP	*0.97-1.59		6.6-10.1	
			*0.26		7.7	
			*1.95		1.6	
		SP-SC	*0.38-0.51		4.4-7.3	
		SP-SM	*0.21-0.28		3.2-3.6	
(Gomez *et al*. 2018)	Native soil microorganism	Concrete sand	-	-	-	-
		Monterey sand	-	-	-	-

* values inferred from the context - values not given in the text

In some studies, linear relationships between V_s and $CaCO_3$ content were established (Al Qabany *et al*. 2011, Weil *et al*. 2012, Martinez *et al*. 2013, Dejong *et al*. 2014), but with such limitations that these relations can only be used in relation with their own MICP process. In fact, it is quite hard but helpful to give a relationship that can be generally used. As Weil *et al*. (2012) suggested, parameters reflecting soil characteristics (size, particle-particle contact stress) and possible spatial distribution of $CaCO_3$ can help establish an advanced relationship.

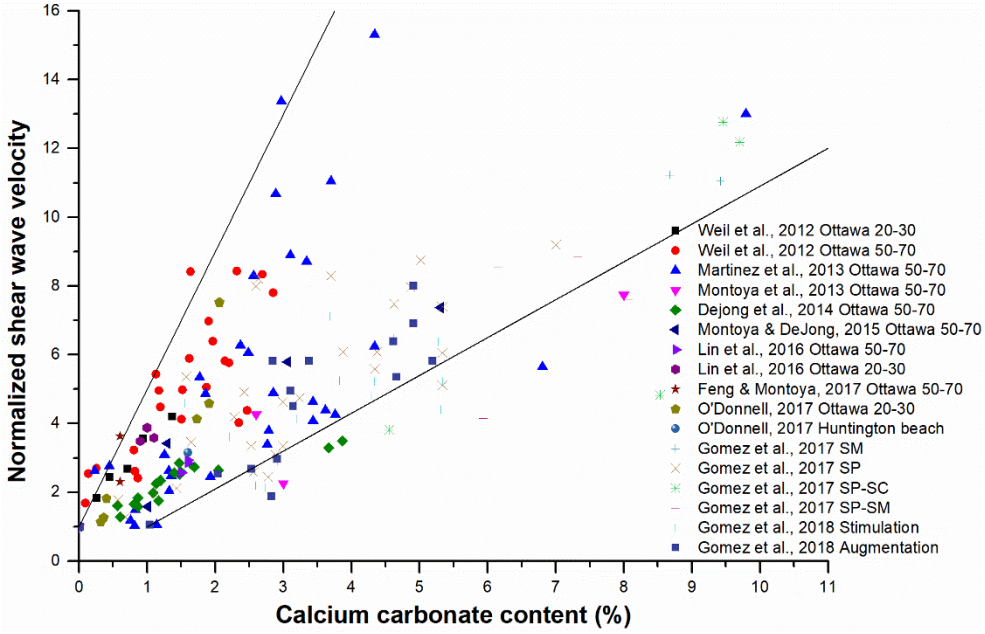

Fig. 3 Normalized shear wave velocity as a function of calcium carbonate content from various articles

2.3 Oedometric consolidation tests

Oedometric tests allow to measure the compressibility of a soil under nil transversal strain conditions. When the change in void ratio is plotted as a function of the axial stress (in logarithmic scale) on a loading path, the oedometric curve features two segments of straight lines: for stresses lower than the preconsolidation stress, the behavior is reversible and the slope of the line is called the "swelling coefficient C_s"; for stresses larger than the preconsolidation stress, the behavior is irreversible and the slope is called the "compressibility coefficient C_c".

To the authors' knowledge, there are few available studies using oedometric tests. Results of Cardoso *et al*. (2016) (using uniformly graded 0.075-0.425 mm sand) showed limited increase in swelling coefficient C_s (0.009-0.013) and nearly unchanged compressibility coefficient C_c (0.057-0.058). Cardoso *et al*. explained that the changes in the elastic behavior of the MICP-treated soil could be attributed to bond breakage during loading. These non-obvious effects were owning to the treatment process under nil vertical stress. Results of Cardoso *et al*. (2018) showed that elastoplastic coefficient C_c increased and elastic value C_s remained unchanged, either when using only sand (uniformly graded 0.4-2 mm sand) or the same sand mixed with 26 % kaolin. Values of C_c for the

sand mixed with distilled water or MICP-treated were 0.044 and 0.089, respectively. Values of C_c for the sand-kaolin mixtures mixed with distilled water, cementation solution only, and MICP-treated were 0.075, 0.145 and 0.127, respectively. The decrease of compressibility of MICP-treated samples was possibly due to the small amount of $CaCO_3$ and bond breakage during loading (Cardoso *et al*. 2016, 2018). Unfortunately, the $CaCO_3$ contents of the specimens were not provided. For sand with kaolin, osmotic consolidation (i.e. sensitivity to pH and ionic strength of clay) played a more significant role than MICP treatment in increasing C_s. For future study of MICP-treated sand with clay, chemical effects should be taken into consideration.

In the confined compression tests of Lin *et al*. 2016 on Ottawa 50-70 sand, using triaxial system, C_c was equal to 0.024 for untreated specimen, and 0.009 for MICP-treated specimen (2.6 % $CaCO_3$). In the case of the tests on Ottawa 20-30 sand, C_c was equal to 0.019 for untreated specimen, and 0.009 for MICP-treated specimen (1.6 % $CaCO_3$). MICP-treated specimens featured a lower compressibility compared to untreated soil. As expected, compressibility decreases with increasing cementation level. The same conclusion was reached by Xiao *et al*. (2021) who also observed that, in the case of Fujian silica sands (C_u=1-10, d_{50}=0.4-0.95 mm, d_{max}=1 mm), cementation breaking occurred at about 30 kPa while particle breaking occurred around 3 MPa. The particle breaking stress can be lower in the case of calcareous sands.

2.4 Triaxial tests

2.4.1 Consolidated drained tests

Isotropically Consolidated Drained (ICD) triaxial tests are considered as one of the best ways to estimate the behavior of a granular soil and derive its constitutive law. Usually, the results of the tests are plotted in the Mohr-Coulomb coordinate system [σ_n, τ] and two parameters are derived from the linear failure criterion: the friction angle ϕ corresponding to the slope of the failure criterion, and the intersection of the failure criterion with the vertical axis that is called cohesion (c). The same parameters may also be derived from the loading paths plotted in the [p, q] coordinate system. Here, the slope of the failure criterion is called M, which is related to ϕ.

Analysis of the results found in the literature was carried out to highlight the change in failure criterion and maximum volumetric changes (contractancy and dilatancy) due to MICP treatment. Unfortunately, very few tests could be re-interpreted for different reasons: (i) the absence of the original stress-strain curves and volumetric strain versus axial strain curves in the papers; in many papers, the only available results are the failure criteria, but often without information about what these criteria represent (peak values or residual values), (ii) the fact that several investigators performed tests under a single confining stress (e.g. Waller, 2011), (iii) the use of unfounded assumptions to interpret the results of the tests; for instance, some researchers (e.g. Gao *et al*. 2019) assumed that the failure criterion was represented by the line that links the origin to the (maximum) deviator stress (i.e. that the soil cohesion was nil, whatever the MICP treatment), which results in very high and unrealistic values of the friction angle. In addition, the conditions of saturation of the samples are seldom indicated in the papers. For all these reasons, the analysis of the effect of MICP treatment on the failure criterion is very difficult to carry out seriously and is based only on the results of a small number of research groups. The results are plotted in Figs. 4(a)-(l) for 6 soils and various treatments. The median diameter of the grains (d_{50}) and the uniformity coefficient of the soil (C_u) are indicated in the captions. In some cases where several treatments were done (e.g. Feng and Montoya 2016), one treatment corresponds to a range of several percentages of $CaCO_3$ deposited in the soil, for instance for highly cemented specimens, to percentages ranging from 4.3-5.3, which

may introduce some scatter in the results. Note that the results of Li (2015) (Figs. 4(c)-(d)) were obtained for two confining stresses only, which is hardly enough to plot a reliable failure criterion. It must be pointed out that, in all of the cases, the analysis of the effect of MICP treatment on the Critical State Line (CSL) could not be carried out due to the lack or uncertainty of data.

As observed in soils cemented with cement or lime, Fig. 4 (a)-(l) shows that MICP-cementation has little or no effect on residual values: when the bonds formed by the cement between the particles are broken, the behavior is that of the original (uncemented) material. In general, when there is a difference between the residual values of treated and untreated soils, this difference is due to the fact that the tests were stopped too soon, before reaching the real residual value. Therefore, the only observed effect of MICP is an increase in the peak properties.

Based on the results of the different researchers, the cohesion of the treated specimens was plotted in Fig. 5 as a function of formed calcite content. As observed in the case of UCS, the cohesions vary largely from one test to another, and the regression coefficient R^2 is low (0.69). However, these results show a definite increase in cohesion with calcite content, reaching several hundreds of kPa in the results of Terzis and Laloui (2019) and Gowtaman (2021) for $CaCO_3$ contents larger than 20%. The same analysis was attempted in the case of friction angles but the scatter is much more important and the regression coefficient R^2 does not exceed 0.2, meaning that there is no correlation between the two parameters. In fact, a few researchers (e.g. Feng and Montoya 2016, Cui et al. 2021) observed a decrease in friction angle when the calcite content increased, while most others highlighted an increase in friction angle, for instance, from 33-35° to 49-51° for Terzis and Laloui (2019), from 40° to 50° for Esnault-Filet *et al*. (2019) in the case of Fontainebleau sand (d_{50} = 0.21 mm, C_u = 1.5). Interesting results were published by Montoya and Dejong (2015) who carried out drained tests on Ottawa 50-70 sand at a confining stress of 100 kPa on different loading paths (axial compression, constant p and radial extension). Unfortunately, the results of the tests are too scattered to derive a definite conclusion on the effect of stress path.

Another effect of MICP treatment that is often cited in the papers is the large dilative behavior of MICP-treated soils. It should be mentioned here that this parameter is often difficult to estimate precisely as, in most of the papers, the tests are carried out to relatively small maximum axial strains (12 to 15%) and without anti-friction devices, which often does not allow dilation to fully develop (this is noted NS in the figures). In addition, this parameter is highly dependent on relative density, whose value is not always mentioned in the papers. Figs. 4(b)-(l) show the maximum contractancy and maximum dilatancy for the different tests analyzed here as a function of the effective confining stress. In practically all the tests, the contractive behavior is similar between untreated and treated specimens. Concerning the dilative behavior, the results are rather dispersed and depend on the level of cementation and confining stress. Globally, dilatancy does not seem to decrease when the confining stress increases, nor to increase with the level of cementation. For instance, in the results of Lin (2016) on Ottawa 50-70 sand, or Terzis and Laloui (2019) on fine sand, the dilation strains are of the same order of magnitude for untreated and treated specimens, even lower for treated specimens in the second case. In the other studies, the values may be close for some confining stresses, and different for others. It should be pointed out also that, in the case of heavily bio-cemented soils, failure occurring at the peak is not homogeneous and features a failure surface, making it more difficult to measure correctly the volumetric strains. Therefore, concerning the aspect of dilative behavior, the conclusion is not clear and more tests are necessary.

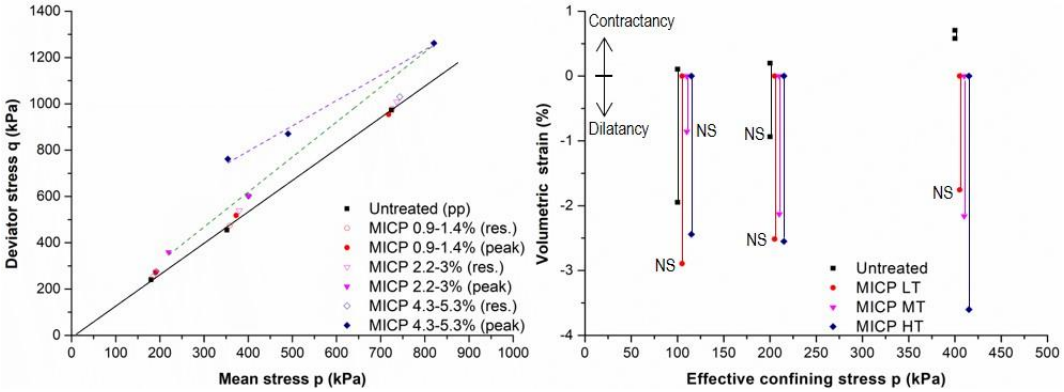

(a) & (b) Feng and Montoya (2016) on fine sand (d_{50} = 0.22 mm, C_u = 1.4)

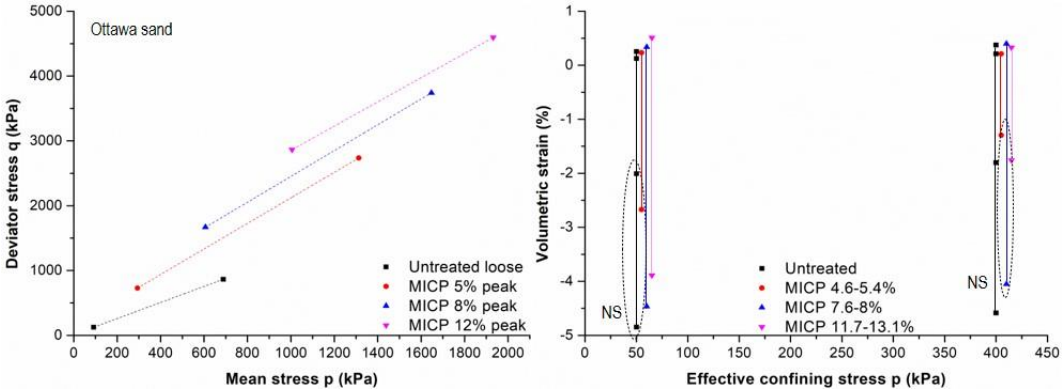

(c) & (d) Li (2015) on medium Ottawa sand (d_{50} = 0.4 mm, C_u = 1.5)

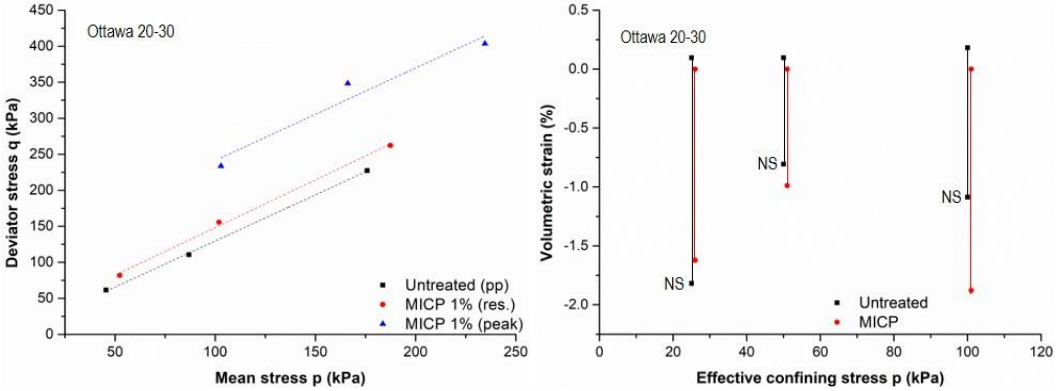

(e) & (f) Lin (2016) on Ottawa 20-30 sand (d_{50} = 0.71 mm, C_u = 1.2)

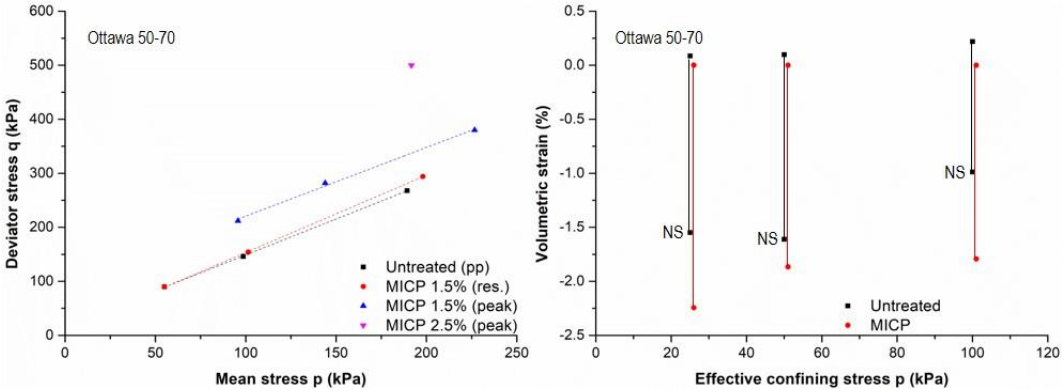

(g) & (h) Lin (2016) on Ottawa 50-70 sand (d_{50} = 0.33 mm, C_u = 1.2)

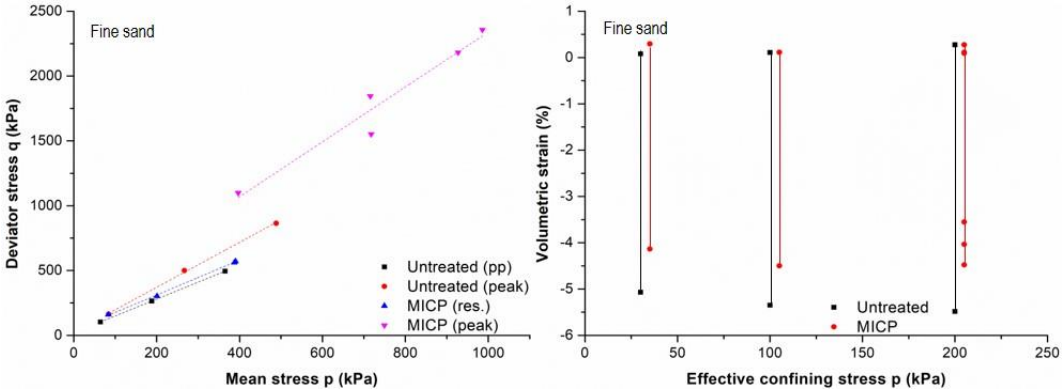

(i) & (j) Terzis and Laloui (2019) on fine sand (d_{50} = 0.19 mm, C_u = 2.1)

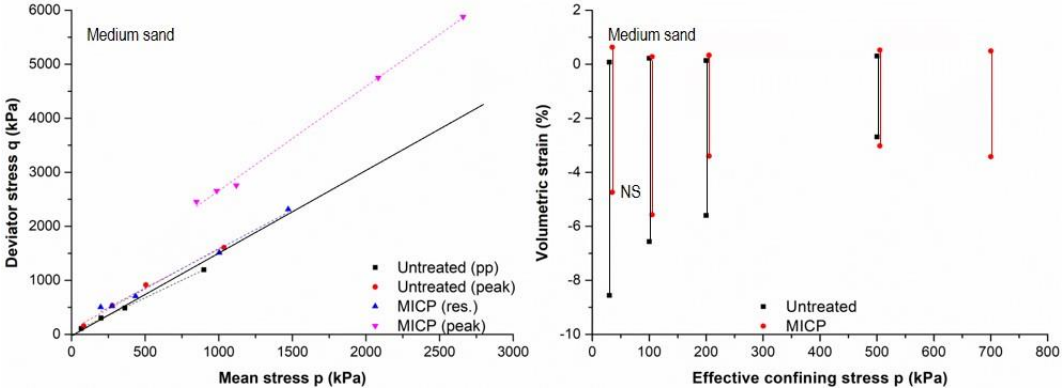

(k) & (l) Terzis and Laloui (2019) on medium sand (d_{50} = 0.39 mm, C_u = 1.6)

Fig. 4 Reinterpretation of the results of the literature [pp: perfect plasticity, peak: maximum strength; res.: residual strength after peak]

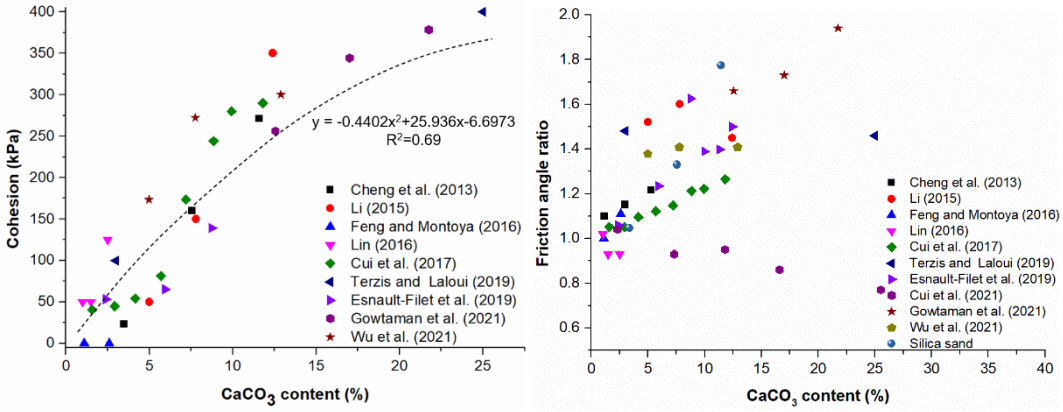

(a) (b)

Fig. 5 Synthesis of CD triaxial tests: (a) cohesion and (b) friction angle ratio as a function of formed $CaCO_3$ content

2.4.2 Consolidated undrained monotonic triaxial tests

The behavior of MICP treated specimens on *Isotropically Consolidated Undrained* (ICU) triaxial paths can be derived from that of the samples on ICD triaxial tests: the changes in volumetric strains will result in changes in pore pressure, which will affect the strength of the soil through the effect of the effective stresses. The few results available in the literature are often difficult to re-interpret because of a lack of precise data. Montoya and Dejong (2015) performed tests on untreated and treated samples of Ottawa 50-70 sand (d_{50} = 0.22 mm, C_u = 1.4, $D_R \cong$ 40%) under one confining stress. To interpret their results, they considered that the cohesion was unchanged by the treatment and that the increase in strength was due to an increase in the peak friction angle. However, in the case of CU tests, the failure criterion can also be defined with reasonable accuracy by the stress path when the sample reaches perfect plasticity, as shown for instance by O'Donnell *et al*. (2017).

Re-interpretation of the results of Montoya and Dejong (2015), using this method, led to the data of Table 2 that show an increase in cohesion with the treatment, and the invariance of the friction angle. O'Donnell *et al*. (2017) carried out tests on undisturbed and MICP-treated (1% $CaCO_3$) Ottawa 20-30 sand (d_{50} = 0.7 mm, C_u = 1.2, D_R = 45%) and obtained the same friction angle and an increase in cohesion of 37 kPa. Hataf and Jamali (2018) studied the effect of MICP treatment on binary mixtures of sand (d_{50} = 1.3 mm, C_u = 2.4) and clay (100% < 75 µm, d_{50} = 6 µm, C_u > 10). They concluded that the treatment resulted in no change of friction angle and cohesion for clay contents larger than 30%, and a large increase in cohesion for clay contents of 10 and 20%. However, these results are difficult to interpret as the untreated remolded clay featured an unexpected cohesion of nearly 50 kPa. Globally, the conclusions of these studies seem qualitatively consistent with those of the CD triaxial tests, but there is a dire need for more results to confirm the conclusions.

2.4.3 Consolidated undrained cyclic triaxial tests

Undrained cyclic triaxial tests on saturated MICP treated soils, in which the samples are subjected to compression-extension solicitations under controlled conditions of stress deviator, all show the same trend of result:

- A slower increase in pore pressure and axial strain in treated samples, compared to untreated soils.
- A larger number of cycles necessary to reach liquefaction for the same value of the cyclic stress ratio (CSR), which is equal to the ratio of the half cyclic deviator stress to the effective consolidation stress (i.e. $q_c/2\sigma'_3$).

Table 2 Reinterpretation of the results of Montoya & DeJong (2015)

MICP treatment: $CaCO_3$ content		0	1%	-	1.3%	3.1%	5.3%
V_s (m/s)		190	300	450	650	1100	1400
Interpretation of Montoya and Dejong (2015)	c (kPa)	0	0	0	0	0	0
	ϕ (°)	33	33.6	37.4	39.2	41.5	43.7
Re-interpretation of the results	c (kPa)	0	10	35	55	85	95
	ϕ (°)	31.7	30.3	31.1	31.1	31.1	31.1

- value not given in the text

As a consequence, the classical liquefaction curves that represent the relation between the CSR and the number of cycles leading to liquefaction (N_L) are shifted to the right or upward (i.e. to higher number of cycles or cyclic deviator stress) when the soil is cemented by MICP, all the more so as the $CaCO_3$ content is higher. Of course, these curves depend on other factors like the type and grading of the soil, the relative density of the samples, etc. The latter is especially important as the mass of formed $CaCO_3$ is taken into account in the dry mass of the sample, which leads to an increase in its relative density. For example, in a standard sand (e.g. e_{max}=0.84; e_{min}=0.55) the formation of 9% $CaCO_3$ increases the relative density from 30% to more than 80%, and the initially "loose" sand may become finally a "dense" sand.

Riveros and Sadrekarimi (2020) concluded from their tests on fine Fraser river sand that MICP-treatment led to a change of the failure mechanism, from liquefaction failure in the untreated sand to cyclic mobility in the MICP-treated samples. To try to compare the results obtained by different researchers in the literature, the vertical shift of the liquefaction curves was plotted in Fig. 6 as the normalized CSR (CSR_{norm}), i.e. the ratio of the CSR for the treated soil to that for the untreated soil for two numbers of cycles: (a) for N_L = 10 cycles, and (b) for N_L = 100 cycles. Several conclusions can be drawn from Fig. 6:

- There is a large scatter in the results, even if the relative densities are similar, so that it is difficult to draw a quantitative conclusion;
- The effect of MICP is more important when the initial relative density of the soil is lower;
- For the same initial relative density, the normalized CSR_{norm} increases with the $CaCO_3$ content (Fig. 6c). For instance, for N_L = 10 cycles: for a very light treatment (0.7% of $CaCO_3$), the effect of the treatment is hardly visible ($CSR_{norm} \cong$ 1.1 to 1.2); for a light treatment (1.2% of $CaCO_3$), CSR_{norm} is equal to 1.5; for a medium treatment (2.5% of $CaCO_3$), CSR_{norm} is equal to 2.5; and for heavily treated specimens (5% of $CaCO_3$), the normalized CSR reach 2.7 to 3.5.

Of course, all these conclusions are based on a very small number of results and should be controlled and confirmed by additional tests, especially as the information about the materials, the tests, the $CaCO_3$ content, etc. is often incomplete, sometimes missing.

Porcino (2011) performed simple shear tests on untreated and MICP-treated specimens of sand

and observed that, for untreated samples, the pressure build-up was similar to that obtained during triaxial tests whereas, for treated specimens, the pressure build-up was much slower in the simple shear tests than in the triaxial tests. Lee et al. (2020), using a dynamic shear test device with Ottawa F65 sand, found that the presence of even low levels of cementation could significantly alter the cyclic resistance of sands subjected to CSRs of 0.1 and 0.2 with approximately one order of magnitude increase in the number of cycles required to trigger liquefaction. However, post-triggering shear strain accumulation was not significantly affected at these low levels of cementation.

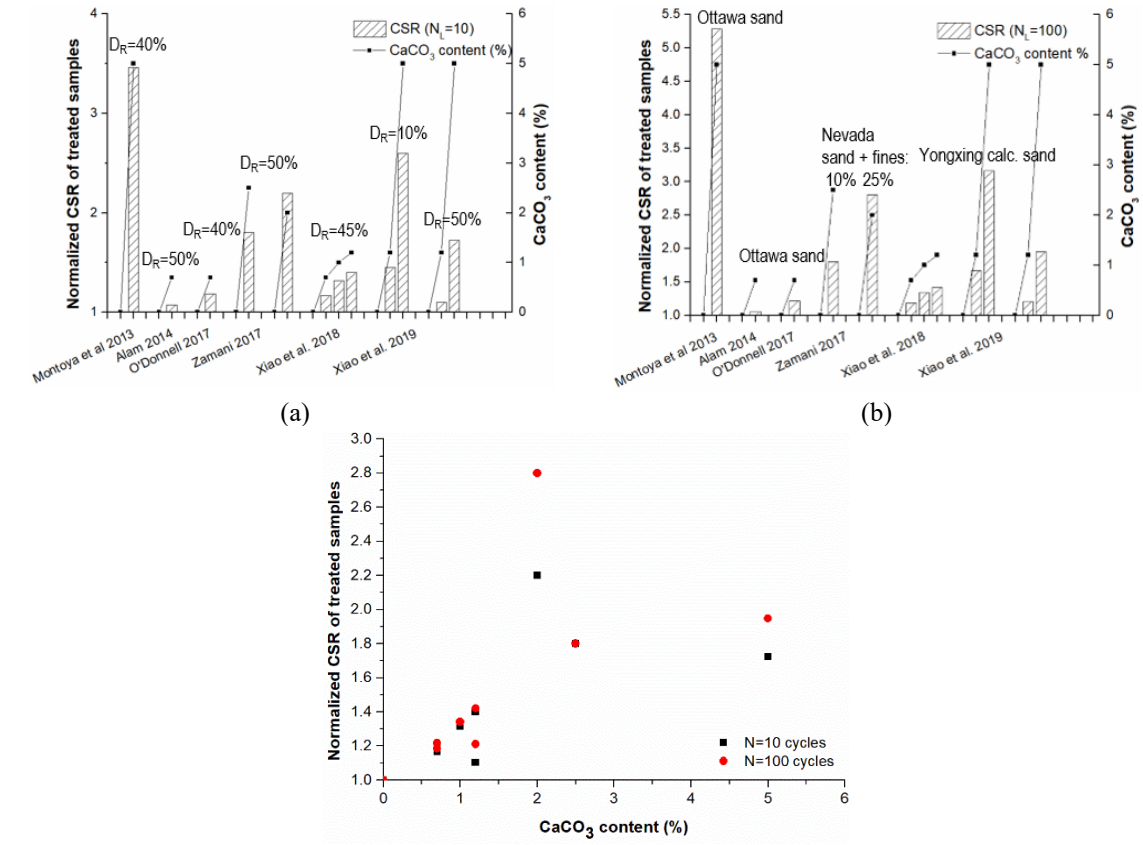

Fig. 6 Ratio of CSR of treated soils to CSR of untreated soils and corresponding $CaCO_3$ contents (a) for a number of 10 cycles leading to liquefaction, (b) for a number of 100 cycles leading to liquefaction, (c) as a function of the $CaCO_3$ percentage for relative densities ranging from 40-50%

2.5 Centrifuge tests

As shown in the previous paragraph, MICP can effectively mitigate liquefaction by reducing excess pore pressure and deformation. Centrifuge tests on loose (D_R=40%) untreated and moderately MICP-treated Ottawa 50-70 sand subjected to a series of shaking events with increasing shaking amplitudes were carried out by Montoya *et al*. (2012). The level of shaking is characterized by the

maximum acceleration a_{max} at the base of the model. The pore pressure parameter r_u that represents the ratio of the excess pore pressure to the vertical effective stress, is often used to characterize the effect of treatment on the increased resistance to liquefaction. For the results of free-field soil response, MICP-treated sample showed a marked reduction in the generation of excess pore pressure at both low (a_{max} = 0.3 g) and high (a_{max} = 0.7 g) levels of shaking, but a longer time was needed to dissipate the excess pore pressure due to the reduced permeability caused by $CaCO_3$ precipitation (refer to § 2.6): in the first case (a_{max} = 0.3 g), r_u ranged from 0.15-0.2 from depth to surface for MICP-treated samples, compared to r_u = 0.4-1.0 for untreated samples whereas, in the second case (a_{max} = 0.7 g), r_u ranged from 0.3-0.4 from depth to surface for MICP-treated samples, compared to r_u = 0.7-1.0 for untreated samples. When untreated, the soil below the structure experienced similar generation of excess pore pressure, with values of r_u = 0.25-1.0 from depth to surface at low shaking levels (a_{max}= 0.3 g), and r_u = 0.6-1.0 from depth to surface at high shaking levels (a_{max}= 0.7 g). MICP-treated soil generated very little excess pore pressure at both low and high levels of shaking. Smaller deformations in the sand beneath the structure were also seen in the MICP-treated sample, with average vertical strains equal to 8.4 % at 5 m depth, and 24 % at the surface, for the untreated sample, compared to values of 2 % and 9 % for the MICP-treated sample.

In the following study of Montoya *et al*. (2013), centrifuge tests on MICP-treated samples with different cementation levels (lightly cemented with a target shear wave velocity V_s = 350 m/s, moderately cemented with V_s = 660 m/s, heavily cemented with V_s = 1200 m/s) were conducted using the same sand and the same centrifuge model, and the results were compared to those on loose (D_R = 40%) and dense (D_R = 85%) untreated sands. The behavior of the loose sand obtained from centrifuge tests showed a soil-to-rock-transition with increasing cementation level. As observed by many researchers, the resistance of the dense untreated sand to dynamic loading was markedly enhanced by comparison with the loosely untreated sand, with an evidence of lower values of r_u. All degrees of MICP-treated samples featured a lower r_u value (well below 1.0) at both shaking levels, which demonstrates the increased ability to resist dynamic loading. When subjected to a series of ground motions, at first, the trend of increments in shaking-induced settlements and their magnitudes in MICP-treated samples were similar to those of dense untreated sand. After a certain amount of degradation of cementation was achieved, the settlements of MICP-treated samples showed an increase, similarly to loosely untreated sand. But the settlement values were still smaller than those for the loose untreated sand, which indicates an improvement in resistance to cyclic loading. Darby (2019) also applied repeated shakings to centrifuge models of untreated and MICP-treated Ottawa sand (DR = 38 and 53%) with low (0.8%), moderate (1.4%) and high (2.2%) $CaCO_3$ contents. Results showed that moderately and heavily MICP-treated sand needed larger peak base accelerations (PBAs) to trigger liquefaction than untreated loose and medium sands, with values of 0.17g, 0.45g, 0.06g and 0.12g, respectively. For lightly cemented sand, the PBA to trigger liquefaction was between those of untreated loose and medium-dense sands: The higher the cementation level, the higher the PBAs to trigger liquefaction.

Interestingly, higher maximum surface accelerations values were obtained by Montoya *et al*. (2012) in MICP-treated samples compared to loosely untreated sand under high (0.7 g) shaking dynamic loading. Zhang *et al*. (2020) also found that surface accelerations of MICP-treated calcareous sand in shaking table tests were amplified. Of course, these results are related to the higher stiffness of treated soil. The undesirable higher surface motions need to be considered when applying MICP methods in-situ.

The conclusion of these tests is that MICP-treated specimens need higher accelerations to trigger

liquefaction, and that the treatment can help reducing excess pore pressure and settlements, which can help them to resist cyclic loadings. The conclusions of centrifuge tests are highly consistent with those of undrained cyclic triaxial tests, but they are also based on a very small number of tests and remain mostly qualitative.

3. Hydraulic properties of MICP-treated soils

Permeability (k) is a crucial geotechnical parameter to describe fluid flow in soil. It reflects how easily the fluid is able to pass through the pores. In soil columns, permeability is usually measured by constant head tests (for coarse grained soil) or falling head tests (for fine grained soil). Fig. 7 shows the change in normalized permeability, i.e. the ratio of permeability after MICP treatment to its initial value before treatment, as a function of the carbonate content deposited in the soil, and Table 3 indicates the parameters of the permeability tests in the literature.

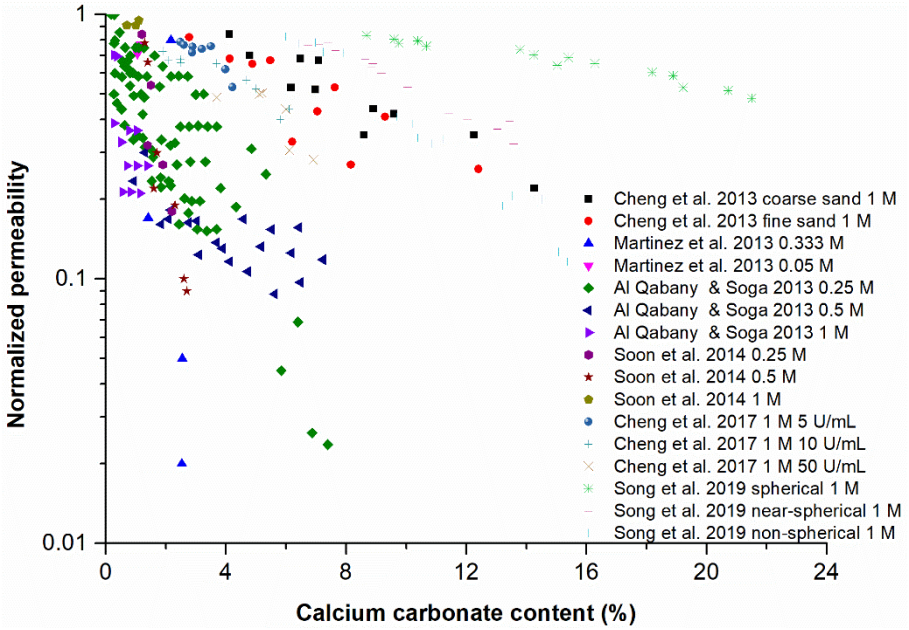

Fig. 7 Normalized permeability as a function of calcium carbonate content from various articles

Table 3 Parameters of permeability tests in the literature

Reference	Sand	d_{50} (mm)	C_u	D_R (%)	Porosity	Bacteria
(Cheng *et al.* 2013)	Fine sand	0.205	1.57	-	0.39	*Bacillus sphaericus*
	Coarse sand	0.7	1.39			
(Martinez *et al.* 2013)	Ottawa 50-70	0.21	1.4	78-100	0.34-0.38	*S. pasteurii*
(Al Qabany and	Grade D silica	0.165	-	20-100	0.585-0.907	*S. pasteurii*

Soga 2013)	sand					
(Soon *et al*. 2014)	Tropical residual soil (silt)	<0.05	-	90	-	*Bacillus megaterium*
(Cheng *et al*. 2017)	SP		1.65	95	0.4915	*Bacillus sphaericus*
(Song *et al*. 2019)	Artificial silica Intact Ottawa Crushed Ottawa	*0.21	-	-	0.385-0.401	*S. pasteurii*

* values inferred from the context - values not given in the text

After MICP treatment, the permeability of the soil is usually changed. In most cases, permeability is reduced by less than 1 order to 2 orders of magnitude. For example, in the study of Yasuhara *et al*. (2012), the k values dropped from 4×10^{-4} m/s to 10^{-6} - 10^{-7} m/s. The treatments of Eryürük *et al*. (2015) reduced k from 8.4×10^{-3} - 4.1×10^{-5} m/s to 9.9×10^{-6} - 2.1×10^{-8} m/s. The results of Wen *et al*. (2019) indicated that the permeability was reduced from 1.4×10^{-3} m/s to 1×10^{-5} m/s after four treatment injections. A marked reduction was seen during the first treatment, followed by gradual reduction. On the other hand, the k values experienced only one, or less than one, order of reduction (from 10^{-7} to 10^{-8} m/s) in the study of Safavizadeh *et al*. (2017). In some cases, permeability stayed almost unchanged. Whiffin (2004) observed a minor decrease of 2-14 % of the porosity and almost unchanged permeability. Jiang and Soga (2017) found that MICP-treated sand-gravel mixed soil showed a limited reduction of k after treatment, the increase in cementation concentration having only a slight effect on the reduction of k.

As reported in El-Latief *et al*. (2015) suspension-based fine grouts (cement grouts, cement-bentonite grouts and clay grouts) decrease the permeability of about 3-5 orders of magnitude, and chemical grouts (acrylamide grout, NMA grout) reduce permeability of about 6-8 orders of magnitude. An advantage of MICP-treatment is that soils can retain a relatively high permeability compared to other grouting methods. For example, higher permeability can reduce the failure risk of a foundation (such as that of hydraulic structures) by lowering the uplift of pore water pressure, which in turn lowers the cost of construction and installation of a drainage system in-situ (Cheng *et al*. 2013). And it also permits additional treatment in terms of engineering requirements.

In Fig. 7, the general trend is that permeability decreases as the $CaCO_3$ content increases. Loss of permeability in MICP-treated soil is caused by (i) reduction of porosity, due to the occupation of the space by forming $CaCO_3$ crystals (Martinez *et al*. 2013), (ii) plugging by the forming crystals in pore space or pore throats (Stocks-Fischer *et al*. 1999), (iii) bio-clogging by the biomass or related metabolic products (Ivanov and Chu 2008, Al Qabany and Soga 2013, Farah *et al*. 2016). These different causes are very difficult to discriminate in the test results. The reduction of porosity is seldom measured or mentioned in the papers. In Fig. 7, the points are very scattered and, for the same calcium carbonate content, there are large differences in the degree of reduction. This phenomenon is caused by the initial pore characteristics of the soil and precipitation patterns of $CaCO_3$ in the pore spaces due to the different treatment protocols. Al Qabany and Soga (2013) studied the effect of the concentration of the cementation solution on the reduction of permeability. At high concentrations (1M), permeability experienced a sharp drop once the $CaCO_3$ started to precipitate because it produced large crystals that plugged locally the samples. At low concentrations (0.25 M), permeability declined more gradually and the points were more scattered. In that case, the deposition of $CaCO_3$ crystals was more progressive and homogenous, and the decrease in

permeability was negligible (Dejong *et al*. 2010). Concerning the effect of relative density, the normalized permeability decreased faster in denser soils (D_R > 70%) than in looser soils (D_R < 60%) (Al Qabany and Soga 2013). In MICP-treated soils with relative densities of 85, 90 and 95%, the normalized permeability was reduced to 0.46, 0.39, 0.26, respectively (Soon *et al*. 2013). But in Fig. 7, we cannot conclude on the effect of relative density, because of the difference in the MICP treatments. Regarding the influence of particle morphology (Song *et al*. 2019), spherical particles led to larger $CaCO_3$ contents and lower permeability reduction than non-spherical and angular particles after the same MICP treatment. In the test on spherical particles, $CaCO_3$ crystals distributed uniformly and were generated continuously on the particle surface probably because of the even adhesion of bacteria. And the reduction of permeability caused by occupation of $CaCO_3$ was not obvious. For non-spherical and angular particles, $CaCO_3$ crystals were located only on some parts of soil surface due to the roughness of soil particles. These $CaCO_3$ crystals progressively occupied slim slot-shaped pore spaces formed by irregular particles, thus decreasing permeability.

4. Microscopic studies

In addition to these relatively macro-scale studies, it is vital to understand more about the molecular-level chemical and biological processes (Li *et al*. 2017, Wang *et al*. 2017), in order to improve $CaCO_3$ repartition in the soil and to apply this technique to real works with various requirements. Common techniques used in various references of MICP studies include scanning electron microscopy (SEM) (Dejong *et al*. 2006; van Paassen 2009; Cheng *et al*. 2013; Soon *et al*. 2013; Choi *et al*. 2017; Simatupang and Okamura 2017; Liang *et al*. 2019;Choi *et al.* 2019), X-ray diffraction (XRD) (Sarda *et al*. 2009; Ghosh *et al*. 2019; Omoregie *et al*. 2019), Fourier-transform infrared (FT-IR) spectroscopy (Dhami *et al*. 2013; Cardoso *et al*. 2018), confocal and Raman spectroscopy (Nehrke and Nouet 2011; Connolly *et al*. 2013; Dhami *et al*. 2013), μ-CT (Dadda *et al.* 2017; Terzis and Laloui 2019), etc.

Evidence obtained from microscopic studies shows that bacteria serve as nucleation sites (Gat *et al*. 2014; Ghosh *et al*. 2019) and influence the $CaCO_3$ crystals formation. Dhami *et al*. (2013) shed light on the process of bacteria providing nucleation sites for $CaCO_3$ precipitation by capturing bacterial imprints on the surface of $CaCO_3$ crystals. Results of Ghosh *et al*. (2019) gave direct evidence that nanometer-sized $CaCO_3$ crystals deposited on the cell surface of *S. pasteurii*. They clarified the nucleation sites provided by bacteria and the likely nucleation routes using field emission scanning electron microscopy (FESEM) with Energy Dispersive X-Ray Spectroscopy (EDS), and high resolution transmission electron microscopy (TEM). Using XRD tests, van Paassen *et al*. (2009) concluded that vaterite and calcite are the dominant crystals at high and low urea hydrolysis rates, respectively.

Metabolic products secreted by bacteria also affect precipitation, e.g. by trapping calcium ions or as a result of specific proteins that influence precipitation (Kawaguchi and Decho 2002). Schultze-Lam *et al*. (1992) showed that the proteinaceous S-layer (part of the cell envelope composed by proteins) plays a part in the mineralization process. Ercole *et al*. (2012) found that both exopolysaccharides (EPS, natural high-molecular-weight polymers composed of sugar residues that are secreted by microorganisms) and capsular polysaccharides (CPS, polysaccharides layers that are part of the outer envelope of a bacterial cell) isolated from different calcifying bacteria could take part in the precipitation process by serving as nucleation sites as well as playing a direct role in

$CaCO_3$ formation. Dhami *et al*. (2013) concluded that EPS can specifically combine with Ca^{2+} and induce $CaCO_3$ precipitation. Specific functional groups on EPS influence the extent and types of precipitation (crystals or amorphous organominerals) (Decho 2010). Nevertheless, there is still much unknown about the precise role of the S-layer and EPS in the process of MICP. Knowledge about these mechanisms could be quite interesting to optimize the use of bacteria.

Microscopic images (e.g. SEM with EDS) contributed to the visualization of microstructures of MICP treated soil (i.e. distributions of $CaCO_3$ and the determination of the characteristics of $CaCO_3$ crystals), which are quite important to explain the differences in macroscopic engineering properties. For example, Cheng *et al*. (2013) presented images of MICP-treated sand at 100% and 20% degree of saturation. In the images of saturated samples, $CaCO_3$ crystals were distributed not only at particle contacts, but also on particle surface and in pore fluids. By contrast, at 20% of saturation, $CaCO_3$ mainly precipitated at particle contacts, which resulted in relatively higher UCS values and lower $CaCO_3$ contents. Soon *et al*. (2014) proved that the $CaCO_3$ produced by MICP formed on the soil particles as well as at particle contacts, and highlighted the bonds between soil particles in SEM images. Images of Lin *et al*. (2016) showed that $CaCO_3$ crystals contributed to contact cementing and matrix supporting between soil particles, which helped increase strength and stiffness in MICP-treated soils.

Characteristics of $CaCO_3$ crystals are important for improving engineering properties. Dadda *et al*. (2017) used synchrotron X-ray tomography combined with computed 3D images to study the microstructure (volume fraction and specific area of $CaCO_3$) and physical properties (permeability, effective diffusion) of MICP-treated soil. They concluded that the average thickness of the $CaCO_3$e layer was 6-7 μm. Their 3D images also showed that the specific surface area increases slightly when the volume fraction of $CaCO_3$ is less than 10%, and it decreases slightly when the $CaCO_3$ volume is larger than 10% owning to the new created particle contacts. Wang *et al*. (2019) and Marzin *et al*. (2020) observed the whole process of MICP and the evolution of $CaCO_3$ by using a transparent microfluidic chip combined with an optical microscope. Terzis and Laloui (2019) used time-lapse video microscopy and X-ray micro-computed tomography (μ-CT) combined with 3D volume reconstruction to characterize qualitatively the number, sizes, orientations and purity of $CaCO_3$. They found that a medium-grained sand gained larger $CaCO_3$ crystals and more homogeneous distribution of precipitations compared to the fine-grained Itterbeck sand. Another crucial finding is that the average mass of bonds does not necessarily yield the expected mechanical response, because the mechanical behaviour is also related to the intrinsic properties of the soils and the fabric of bio-cemented soil.

5. Conclusions and future expectations

Based on the above analysis, the following conclusions can be drawn:

- UCS increases with increasing $CaCO_3$ content. In the range of calcium carbonate percentages used in practice (i.e. smaller than 5%), the results show that one can expect an UCS up to 1.4 MPa (e.g. for 5%, 0.7 MPa ± 0.7 MPa). For a given $CaCO_3$ percentage, the densest specimens, and the specimens with the more widespread grain size distribution, feature the highest UCS.
- When subjected to monotonic loadings, MICP-treated soils show an increase in the peak properties, an indefinite increase in friction angle and a large increase in cohesion with the $CaCO_3$

content. Concerning the dilative behavior, the results are rather dispersed and depend on the level of cementation and confining stress.

- When subjected to cyclic/dynamic loadings (triaxial, simple shear or centrifuge tests), marked enhancement can be seen in lowering the pore pressure generation, reducing the strains, decreasing peak base acceleration (to trigger liquefaction) and number of cycles to reach liquefaction in MICP-treated soil. The effect of MICP is more important for 10 cycles than for 100 cycles, and when the initial relative density of the soil is lower. For the same initial relative density, the normalized CSR_{norm} increases with the $CaCO_3$ content. MICP-treated soils feature a progressive soil to rock transition for an increasing cementation level.
- Similarly, the shear wave velocity V_s increases with increasing cementation level ($CaCO_3$ content) but, as for the other properties, this increase highly depends on where $CaCO_3$ crystals precipitate: if precipitation takes place at particle-particle contacts, the increase in V_s is important. Growing $CaCO_3$ crystals on the soil particle surface is less efficient but may eventually enhance properties as well. In most cases, for every 1% $CaCO_3$ precipitated, more than 1-fold V_s increment can be expected.
- In most cases, the drop in permeability due to MICP treatment remains limited to less than 1 to 3 orders of magnitude. Normalized permeability decreases with increasing $CaCO_3$ content. The decrease is larger when the cementation solution is more concentrated, and in more angular soils.
- The data of the literature (normalized UCS, V_s, and especially k values) are very scattered, which is caused by using various materials (soils, strains of bacteria) and MICP protocols. Incorporating parameters that reflect soil characteristics (e.g. size, particle-particle contact), possible spatial distribution of $CaCO_3$, etc., could help establish advanced relationships between $CaCO_3$ content and UCS/V_s/k.
- The formation of calcium carbonate results in an increase in the dry density of the samples that may play a major part in the improvement of the soil properties, such as peak maximum deviator, resistance to liquefaction, etc. Many researchers have pointed out that the enhancement of soil properties by MICP cementation was equivalent to an increase in density, but it is not clear whether they speak of the real density increase or of the bonding of particles. This important phenomenon must be taken into account in the analyses.

Though abundant conclusions can be drawn, there is still much work left for further studies. The previous conclusions are based on too few tests and the data of the tests are often partial or missing. This technique still needs to progress in the way of lowering cost, maximizing efficiency and adapting to goals. A few suggestions for future studies are listed below,

- MICP-treatment of soils with different compositions: Most of the existing studies use quartz sands. Because the soils to be used in-situ during construction are imposed, the studies should include different soils.
- The grain size range and grading of effective MICP treatment considering in-situ injection: The lower boundary size of grains (in order not to inhibit the transport of bacteria in the pore space) was discussed in (Dejong *et al*. 2010). On the other hand, most studies have been carried out on fine sands with limited size range (usually less than 1 mm), as shown in Fig. 2(b), Table 1 and Table 3. Very few studies explore extended grain range and relatively larger grains that are important for engineering use.

- The optimal protocols for various soils: For different soils, the varying physical characteristics might influence the efficiency of the treatment. Thus, it is essential to establish a comprehensive protocol for the application of MICP method to various soils, which will benefit its practical use in real works.
- The performance of MICP-treated soil on various loading paths: In the literature, very few studies have been carried out on the effect of loading paths and crucial parameters such as confining pressure, cyclic frequency, waveform, overconsolidation degree, etc. In most papers, shearing results are presented whereas, in terms of real applications, various environmental loadings could be met. Hence, mechanical behavior of MICP-treated soil should be explored more thoroughly.
- The role of EPS during MICP process: Microscopic studies have shown the role of EPS during MICP process, such as helping the formation of $CaCO_3$ and taking part in crystal formation. But other effects of EPS are almost unknown. It would be quite interesting to study the precise role of EPS to understand more about the basic microscopic mechanisms to optimize the MICP technique.

Acknowledgments

The authors would like to thank the financial support of China Scholarship Council (CSC) and the assistance of Solétanche-Bachy.

Chapter 2 Soil, bacteria and experimental methods

2.1 Introduction

The objective of the research is mainly to study the optimal way to consolidate real works, such as dams and slopes, when they are considered as not strong enough to withstand additional loads or earthquakes of increasing intensities. These infrastructures are made of very different grain size distributions according to their location and the materials available in-situ. However, most past studies were done with relatively fine sands (< 1 mm) and very few with coarser materials. In this thesis, we used a series of quartz sand mixtures, through mixing the coarse grains (1-5 mm) with various percentages (i.e., 0, 20, 40, 60 and 100%) of fine grains (< 1mm), and we examined the effect of grain size distribution on the efficiency of bio-treatment.

The object of this chapter is (1) to give an overall description of the characteristics of the soil used; (2) to show the methods related to the exploration of bacterial metabolism and MICP process; and (3) to introduce the preparation methods of untreated and treated specimens, and the procedures of the mechanical tests throughout the study.

Knowing well the physical property of the sand is the base for further analysis of the mechanical behavior. To know the morphology and minerology of the soil grains, optical microscopy observations and X-Ray diffraction (XRD) tests were done. Then, some physical properties of the soil mixtures used in this study, such as grain size distribution, standardized maximum and minimum densities, intergranular and interfine void ratios, as well as transitional fine content are presented and analyzed.

As for the bacteria, the experimental methods concern two kinds of bacteria (DSM33 and SB). For the DSM33 bacteria, the methods include cultivation and growth of the bacteria, oxygen limit determination and preparation of bacterial solution. For the SB bacteria, the methods include the preparation of bacterial solution and bacterial activity monitoring. MICP trials were carried out to compare the two bacterial solutions.

In the last section, the experimental methods concern the preparation of soil specimens, MICP treatment protocol, mechanical test procedures (for monotonic consolidated drained triaxial tests and cyclic consolidated undrained triaxial tests) and characterization of treated specimens.

2.2 Soil

2.2.1 Methods for characterizing the soil grains

The soil used throughout this study is a quartz sand that was chosen because it contained very little $CaCO_3$. The sand, coming from the "Mer de Glace" glacier, was

taken in the Arve River in Chamonix, and sieved to different grain size distributions. Morphology and mineralogy of the sand grains were captured by light microscopy and X-Ray diffraction (XRD) test, as shown in Fig. 2.1.

We can clearly see the large range of particle diameters in the sand. According to the XRD result (Fig.2.1 (b)), the main mineral type is quartz. There are also minerals belonging to feldspar, such as albite and plagioclases. A small fraction of clay minerals, like kaolinite and illite, can be found as well. The vitreous luster and translucence of quartz and feldspar can also be seen in Fig 2.1 (a). The reflective surface and some light spots (metal luster and submetallic luster) might be minerals such as pyrite and goethite.

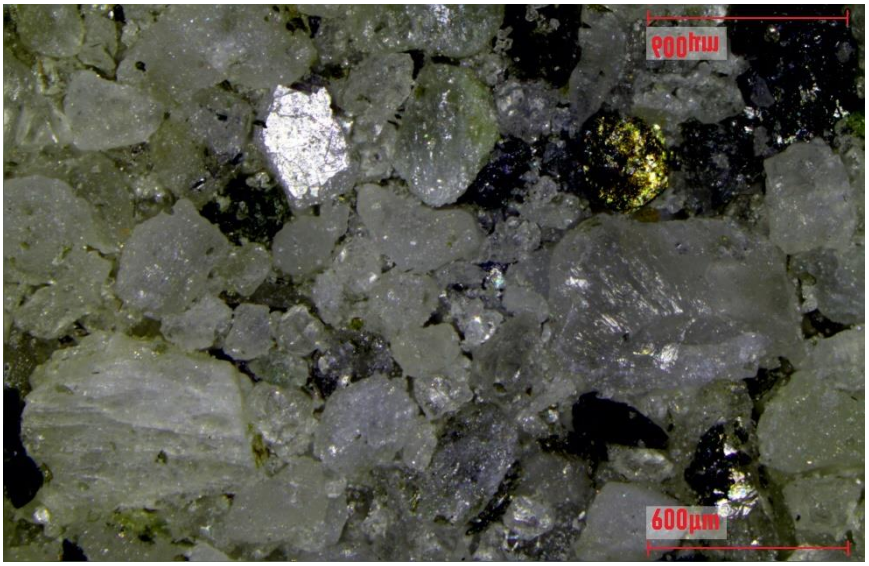

(a) Images of sands at the magnification of 31×

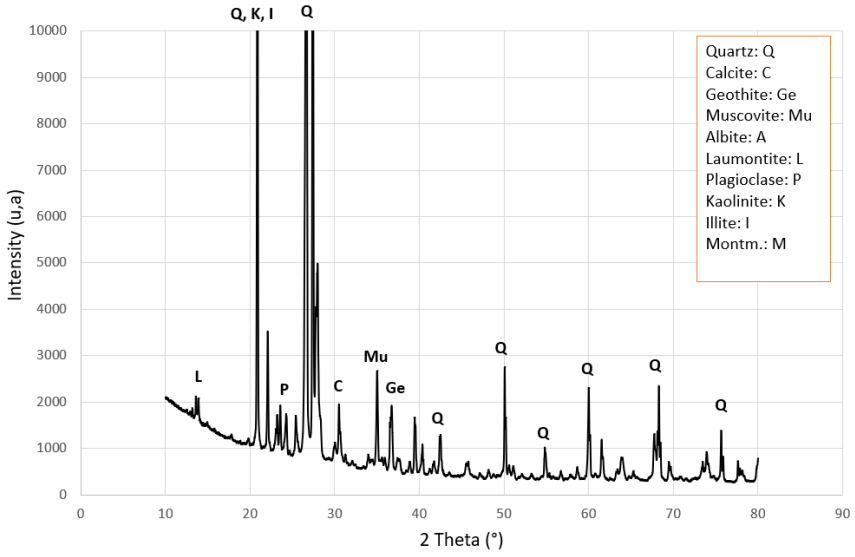

(b) XRD result

Fig. 2.1 Images of the sand grains (a) and result of X-ray diffraction (b)

2.2.2 Preparation of the different mixtures

To obtain various grain size distributions, the original sand was separated into two fractions:

- The "coarse" grains with grain size ranging from 1 to 5 mm
- The "fine" grains with grain size smaller than 1 mm

Then, the fine grains were remixed with the coarse grains at different percentages (or "fine contents, *FC*"), equal to 0, 20, 40, 60 and 100% of fines. The different materials thus obtained are called MS6.x, where x represents the percentage of fines (e.g., MS6.0 for the coarsest soil, MS6.40 for the soil containing 40% of fines, MS6.100 for the finest soil).

(1) Grain size distribution

To carry out this operation, the oven-dried original soil was sieved using an automatic sieving machine and a series of sieves of various diameters (5, 4, 3.15, 2.5, 2, 1.6, 1, 0.71, 0.5, 0.315, 0.16, 0.08 and < 0.08 mm sieves). Soil grains larger than 5 mm were removed. To characterize the grain size distribution of the different soils, the Coefficient of uniformity (C_u) and coefficient of curvature (C_c) were calculated,

$$C_c = \frac{d_{30}^2}{d_{60} \times d_{10}}$$

$$C_u = \frac{d_{60}}{d_{10}}$$

Fig. 2.2 (a) shows the grain size distribution curves of the mixtures with various fine contents, and the comparison with the limits of the potentially and most liquefiable sands (Tsuchida & Hayashi, 1972). Fig. 2.2 (b) shows the comparison between the d_{50} and C_u of our sands and those of the sands used in previous studies. Table 2.1 indicates a few characteristics of our sands. An important feature of these curves is the percentage of grains smaller than 80 µm that plays an important part in the efficiency of the MICP-treatment in spite of its small values.

Table 2.1 Physical properties of the used mixtures

Name of the soil	*FC* (%)	d_{10} (mm)	d_{30} (mm)	d_{50} (mm)	d_{90} (mm)	< 80 µm %	C_u	C_c	e_{min}	e_{max}
MS6.0	0	1.14	1.41	1.71	2.69	0	1.7	0.9	0.608	0.838
MS6.20	20	0.53	1.17	1.51	2.54	0.5	3.2	1.5	0.530	0.753
MS6.40	40	0.33	0.69	1.23	2.41	1.0	4.4	1.0	0.521	0.721
MS6.60	60	0.25	0.53	0.77	1.80	1.6	4.0	1.1	0.485	0.717
MS6.100	100	0.18	0.37	0.53	0.86	2.6	3.3	1.3	0.549	0.829

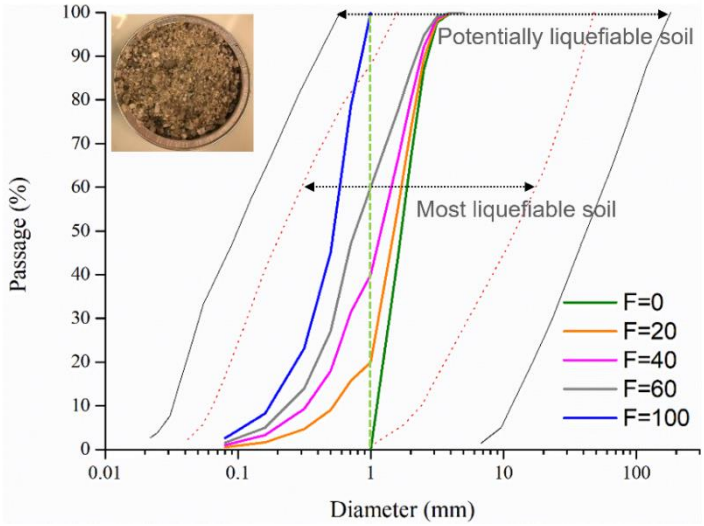

(a) Grain size distribution and limits of liquefiable soils (Tsuchida & Hayashi, 1972)

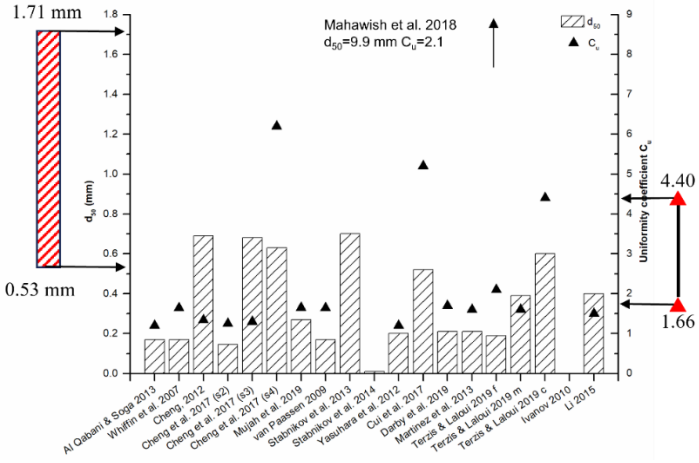

(b) Comparison of d_{50} and C_u with those of sands in the literature

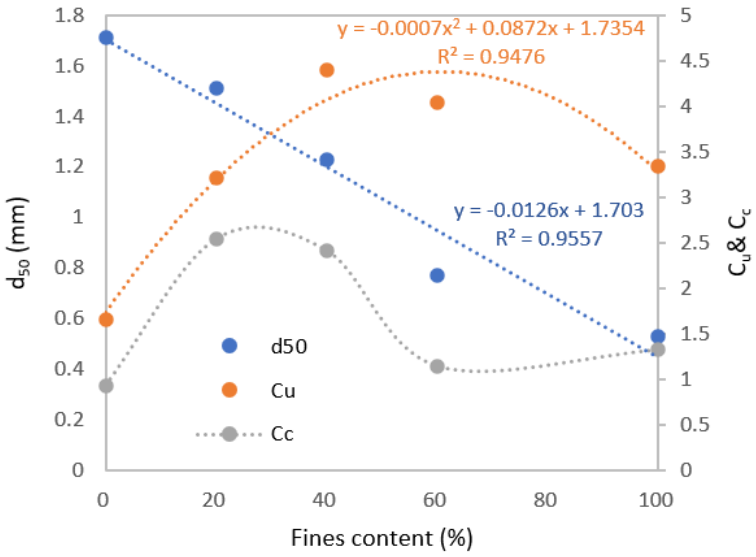

(c) d_{50}, C_u & C_c change with fines content

Fig. 2.2 (a) Grain size distribution of the sands; (b) comparison between the d_{50} and C_u of the used sands and those from the literature; (c) d_{50}, C_u & C_c change with fines content

In Fig. 2.2 (a), we can see that all the sands are in the size range of most liquefiable soils. In most cases, the d_{50} of the sands used in previous studies was less than 0.7 mm, whereas the d_{50} of the sands used in this study is between 0.53 and 1.71 mm (Fig. 2.2 (b)). It should be noted that the d_{50} of the finest sand (MS6.100) in this study is already comparable to, or even larger than, the d_{50} of the "coarse" sands used in other studies. The C_u of the sands in most previous studies were in the range from 1-2. In this study, the C_u are larger (between 3 and 4.5), except for MS6.0 (1.7). MS6.0, MS6.20 and MS6.100 are poorly (uniformly) graded sands ($C_u < 4$), while MS6.40 and MS6.60 are well graded sands ($4 < C_u < 6$, $1 < C_c < 3$). In Fig. 2.2 (c), we observe that the mean diameter of the sand decreases linearly with increasing fine content. When *FC < 50%*, the C_u increase with the fine content. When *FC > 50%,* a reverse trend is seen. There is no clear relationship between C_c and *FC*.

(2) Standardized maximum and minimum void ratios and correlations

The maximum density (D_{max}) and minimum density (D_{min}) of the different sands were measured according to the standard test methods ASTM D4253 and ASTM D4254. To give more details, the minimum density (D_{min}) of the sand is measured by depositing the sand carefully into an empty rigid mold (15.24 cm in diameter and 15.5 cm in height) layer by layer. D_{min} is calculated as the mass of sand divided by the volume of the mold. The measurement is repeated 6 times, and the D_{min} is the average value of the six measurements. The maximum density (D_{max}) is measured using the same rigid mold, which is fixed on a vibratory table with a heavy cap (approximately 25 kg) on the top. The whole system is vibrated for 20 min under a standard acceleration. The settlement is calculated by the average of the measurements at 8 different points well-distributed around the cap. The maximum void ratio (e_{max}) and minimum void ratio (e_{min}) are calculated as follows,

$$e = \frac{2.7}{D} - 1$$

where e and D represent the void ratio and density of the sand, respectively, and 2.7 g/cm^3 is the specific gravity of the sand.

Fig. 2.3 shows the e_{max} and e_{min} void ratios. The two parameters decrease when the fine content increases to around 50%, then increase with the fine content.

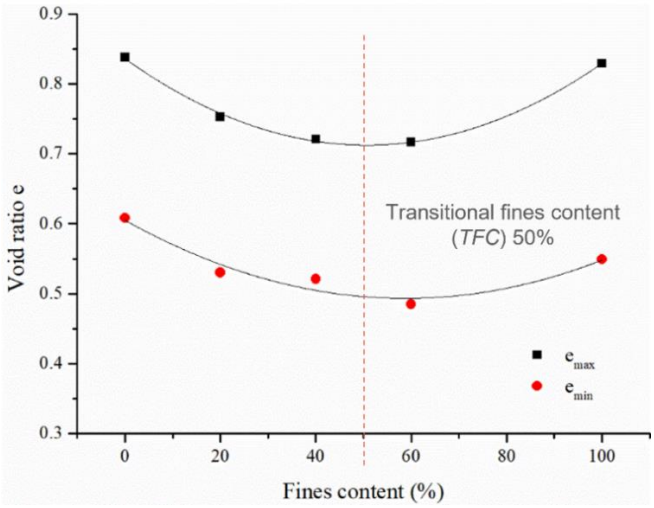

Fig. 2.3 Maximum and minimum void ratio of sands with various fines content

Fig. 2.4 shows the results of the comparison between the measured e_{max} and e_{min} and the corresponding values e_{max} & e_{min} deduced from the correlations of (Biarez & Hicher, 1994) and (Poulos, 1988). In general, the e_{max} & e_{min} values deduced from the correlations of Biarez & Hicher correspond better with the measured e_{max} & e_{min} values than the values obtained from Poulos. Usually, the measured e_{min} values are larger than the e_{min} values from the correlations (Fig. 2.4 (c) & (e)), and the measured e_{max} values are smaller than the e_{max} values from the correlations (Fig. 2.4 (d) & (f)). For MS6.100, the difference between the measured and correlation values is obvious, whilst the others show much less difference.

(3) Intergranular and Interfine void ratios, Transitional fine content

When dealing with binary mixtures, it is interesting to consider the "*intergranular void ratio* (e_s)" and the "*interfine void ratio* (e_{if})". The intergranular void ratio is the void ratio of the coarsest fraction, without taking into account the fines. The interfine void ratio is the void ratio of the fine fraction, without taking into account the coarsest grains. Both parameters are derived from the following equations (Thevanayagam, 1998),

$$e_s = \frac{e+FC}{1-FC} \quad \text{and} \quad e_{if} = \frac{e}{FC}$$

Their values for the different mixtures are plotted in Table 2.2.

Table 2.2 Intergranular and Interfine void ratios of the used sand

Name of the soil	*FC* (%)	Intergranular e_s	Interfine e_{if}
MS6.0	0	0.769	-
MS6.20	20	1.108	3.430
MS6.40	40	1.768	1.653
MS6.60	60	3.119	1.079
MS6.100	100	-	0.745

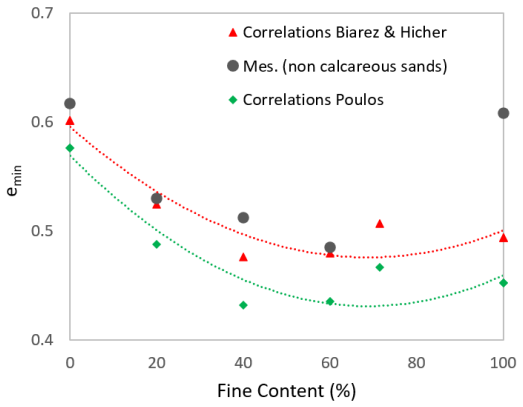

(a) e_{min} versus FC

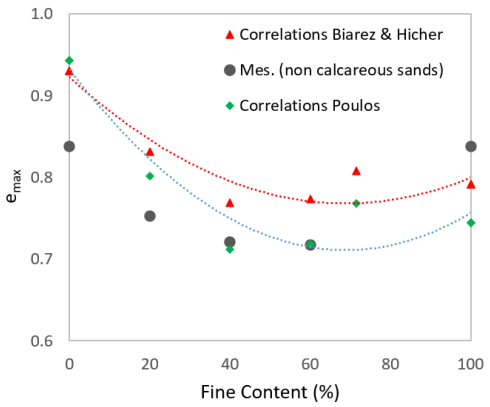

(b) e_{max} versus FC

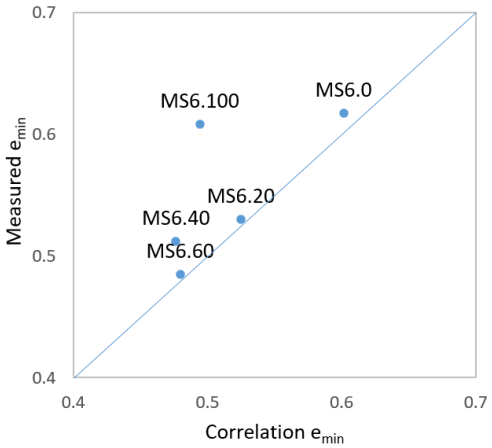

(c) Measured e_{min} versus B & H e_{min}

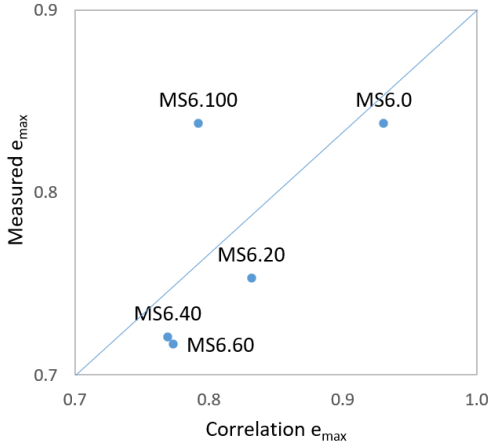

(d) Measured e_{max} versus B & H e_{max}

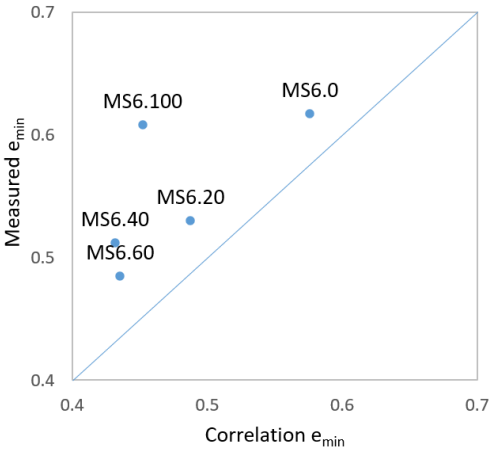

(e) Measured e_{min} versus P e_{min}

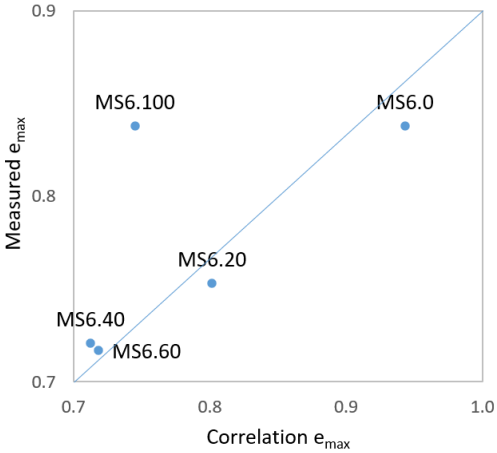

(f) Measured e_{max} versus P e_{max}

Fig. 2.4 Relations between measured void ratios and void ratios derived from correlations: (a) & (b) measured e_{min} & e_{max} and e_{min} & e_{max} derived from the correlations versus FC; (c) & (d) measured e_{min} & e_{max} versus e_{min} & e_{max} deduced from Biarez & Hicher (B & H), 1994; (e) & (f) measured e_{min} & e_{max} versus e_{min} & e_{max} deduced from Poulos (P), 1988

Another important parameter of mixtures is the "*Transitional fine content*" (*TFC*), which is the fine content for which the behavior of the soil passes from a coarse particles-driven behavior to a fine particles-driven behavior. When *FC* is lower than the *TFC*, the coarse fraction is the supporting skeleton, and the increase in the percentage of fines practically does not change the intergranular void ratio, as the fines only fill the voids between the larger balls. At the same time, the voids are progressively replaced by the finest grains, leading to a decrease in bulk void ratio. When the fine percentage reaches a "maximum" value (the *TFC*) corresponding to the maximum diameter of the free fines, the fines fill the voids between the coarse structure and their increase leads to an increase in the intergranular void ratio. Above the *TFC*, the picture is that of a matrix of fine grains with dispersed coarse grains. The stresses are then supported by the fine grains.

In the case of our coarse and fine fractions, the transitional fines content (*TFC*) derived from a simple volume measurement is around 50%. The TFC also represents the minimum of the [e_{min} and e_{max} vs. *FC*] curves, as well as the maximum of the [C_u vs. *FC*] curve in Fig. 2.2 (c).

In Fig. 2.5, the measured e_{max} & e_{min} values are plotted in the diagram of (Biarez & Hicher, 1994). According to Fig. 2.4 (a) & (b) the shape of the sands can be classified as sub-angular sand, except in the case of MS6.100 (angular). This is more or less in agreement with the photo of the sand in Fig. 2.1 (a).

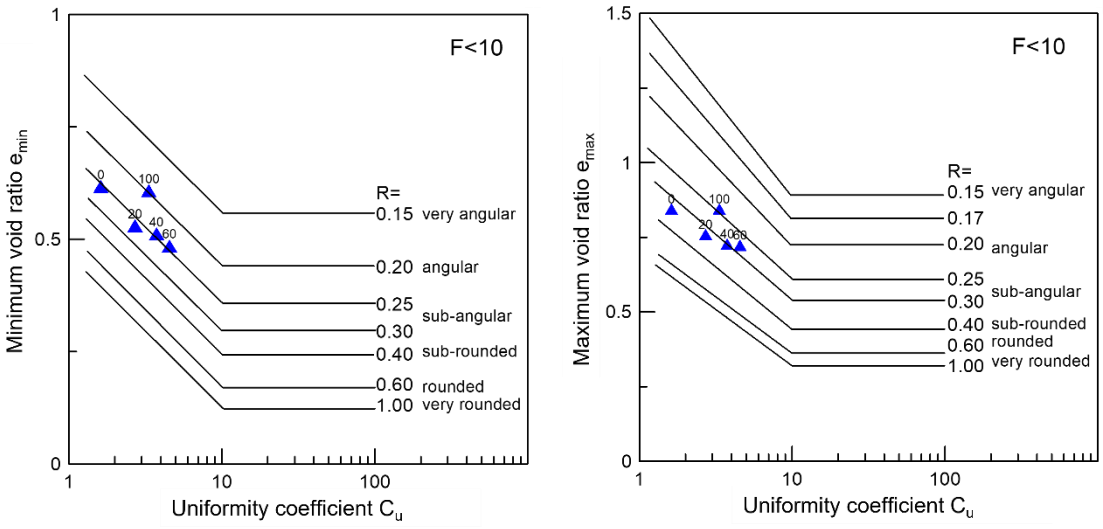

(a) e_{min} versus C_u (b) e_{max} versus C_u

Fig. 2.5 Relationships between measured e_{min} & e_{max} and C_u

(4) Internal stability of the sand mixtures

In the case of mixtures of different soils, it is essential to assess the internal stability of the soil, i.e. the possibility of having migration of fine grains between the coarse grains (suffusion). Two internal stability criteria based on grain size distribution curve, those of Kenney and Lau (Kenney & Lau, 1985, 1986) and Burenkova (Burenkova, 1993), were used for analyzing the internal stability of the

sands. The results are shown in Table 2.3. According to the (Kenney & Lau, 1985, 1986) criterion, all the sands are stable. When using the (Burenkova, 1993) criterion, MS6.20 and MS6.100 are unstable, while MS6.0, MS6.40 and MS6.60 are stable.

Table 2.3 Internal stability of the sands

Sands	Fines content (%)	Criteria	
		(Kenney & Lau, 1985, 1986)	(Burenkova, 1993)
MS6.0	0	Stable	Stable
MS6.20	20	Stable	Unstable
MS6.40	40	Stable	Stable
MS6.60	60	Stable	Stable
MS6.100	100	Stable	Unstable

2.3 Bacteria

According to the literature review, *Sporosarcina pasteurii* (*S. pasteurii*), a widely used non-pathogen bacteria with high efficiency in urea hydrolysis, was chosen as the used strain. Two kinds of bacterial solution were prepared, DSM33 (fresh bacterial solution) and SB (freeze-dried bacterial solution). The use of DSM33 implies to grow the bacteria under very strict conditions, which is a time- and energy-consuming process. The use of SB bacteria, on the other hand, is considerably easier and better suited for a work in which the main objective is to study the mechanical properties of MICP-treated soils.

2.3.1 Determination of physical, chemical and biological parameters

A SenTix® 940 (WTW) electrode was used to measure the *pH*. A 3430 (WTW) multimeter connected with an optical IDS dissolved oxygen sensor (FDO® 925, WTW) and IDS digital conductivity cells (TetraCon® 925, WTW) was used for measuring dissolved oxygen (*DO*) and conductivity.

Biomass determination (OD_{600})

To characterize the biomass of the bacteria, a commonly used parameter is the OD_{600} value, which is the optical density of the bacterial solution at 600 nm wavelength using UV spectrophotometer. The target solution is diluted to an OD_{600} value lower than 0.8 and pipetted into a transparent 4-mL cuvette. The final OD_{600} value is the OD_{600} value of the solution in the cuvette multiplied by the dilution ratio.

Urease activity and specific urease activity

The urease activity characterizes the capacity of the bacteria to produce the enzyme called urease, i.e., the enzyme able to hydrolyze urea. To measure the urease activity, a 1.1 M urea solution is made by dissolving 1 M urea into 900 mL of distilled water. A vial with 27 mL of urea solution (kept at around 20°C) is placed on a

magnetic stirrer and the solution is mixed up all the time. Then 3 mL of bacterial solution are added into the vial, the conductivity of the mixed solution is measured at intervals of 1 minute during the first 6 minutes. The corresponding urease activity (mM/min), representing the quantity of urea hydrolyzed (mM) per minute, is calculated according to (Whiffin, 2004). The specific urease activity, representing the quantity of urea hydrolyzed (mM) per minute by unit biomass (OD_{600} = 1), is then calculated as follows,

$$Specific\ urease\ activity\ (mM/min/OD) = \frac{Urease\ activity\ (mM/min)}{Biomass\ (OD_{600})}$$

Ammonium concentration

The ammonium concentration is determined using a modified Nessler method as described in (Whiffin, 2004). To measure the ammonium concentration, the samples are filtered through a 0.22 filter to remove the biomass. The resulting supernatant is transferred into a clean tube and stored at 4°C prior to analysis. Samples are diluted to be in range of 0-0.5 mM. Then 2 mL of diluted sample are added to a cuvette and well-mixed with 100 µL of Nessler reagent (Merck, Germany). After 1 min, the OD_{425} value (i.e., the optical density at 425 nm wavelength) of the sample is then read in the UV spectrophotometer. The ammonium concentration can be calculated on the basis of the standard curve. Fig. 2.6 shows the standard curve of ammonium concentration (NH_4^+, mM) vs. OD_{425}. A linear relationship is established between the absorbance and the corresponding ammonium concentration (0-0.5 mM).

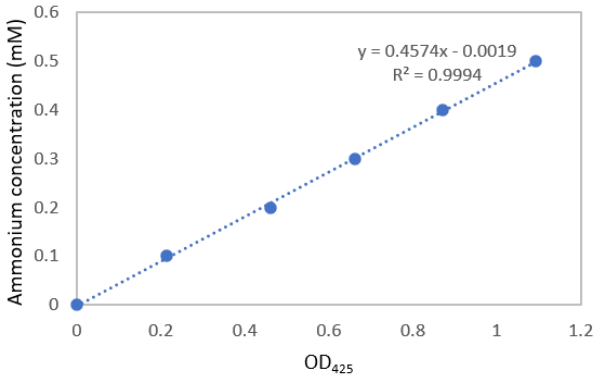

Fig.2.6 standard curve of ammonium concentration (mM) vs. OD_{425}

$CaCO_3$ content

$CaCO_3$ content measurement is carried out in accordance with the standard NF P 94-048 using a Dietrich-Frühling calcimeter. The method consists in dissolving the sample in hydrochloric acid and measuring the volume of the generated CO_2 gas. The calcium carbonate content is calculated with the following equation,

$$CaCO_3\ (\%) = \frac{120 \times V_{CO_2}}{m \times (\theta_b + 273)}$$

where m represents the dry mass of the sample (g), V_{CO_2} the volume of CO_2 collected (mL), and θ_b the room temperature in degrees Celsius (℃).

2.3.2 Bacterial solution of DSM33

The strain of DSM33 was purchased from Leibniz Institute, DSMZ-German Collection of Microorganisms and Cell Cultures. The recommended culture medium refers to the NH4-YE medium (ATCC 1376), containing 20 g/L yeast extract, 10 g/L NH_4Cl, 0.13 M Tris buffer (pH = 9). The DSM33 is activated, then inoculated onto a fresh growth medium with 1/100 (V/V), and grown at 30°C in a bottle placed on a rotary shaker. Several bottles of live cultures are kept as backups.

(1) Biomass, urease activity and specific urease activity in DSM33 culture

To draw the growth curve (Biomass vs. culture time), 2 mL of DSM33 culture (at pH = 7 and pH = 9) are taken out at intervals of 2 hours to measure the biomass (OD_{600}). The urease activity and specific urease activity of the culture at pH = 9 are also measured at various culture times.

(2) Oxygen limit

Two mL of bacteria solution are inoculated into 100 mL of liquid medium in a sealed 200-mL beaker with a dissolved oxygen probe and a conductivity probe. The dissolved oxygen quantity (mg/L) and conductivity (mS/cm) are noted every hour for 6 hours. After 6 hours, the data are collected every 20 minutes. The beaker is agitated with a magnetic stirrer during the test for uniform distribution of oxygen, nutrient and bacteria.

To compare the biomass (OD_{600}) and specific urease activity of the culture in a closed bottle at various culture times. Four bottles of the culture are opened at 14 h, 24 h, 25 h and 37 h culture time to measure the OD_{600} and specific urease activity.

(3) Protocol for making the bacterial solution of DSM33 for MICP treatment

The bacterial solution is harvested after 24 h cultivation at 30°C and centrifuged at 4000g for 20 minutes. Supernatant is replaced with 3 g/L NaCl solution (in Cristaline® water) to a target OD_{600} value (around 1.0). The fresh bacterial solution of DSM33 is ready to be used within 2 weeks and kept below 4°C.

2.3.3 Bacterial solution of SB

The ready-to-use freeze-dried bacteria powder of *S. pasteurii*, provided by Solétanche Bachy, was prepared by directly adding the bacteria powder to the saline solution (3 g/L of NaCl dissolved into Cristaline® water) to a target OD_{600}. For a thorough rehydration, the bacterial suspension is well mixed for at least 20 minutes using a magnetic stirrer.

Evolution of biomass, urease activity and specific urease activity with time after the preparation of the bacterial solution are monitored in SB solution at similar OD_{600} (around 1.3) at room temperature (around 20°C).

2.3.4 MICP tests in solution

MICP trials are conducted by mixing equal volumes of bacterial solution (100 mL) and cementation solution (100 mL). For bacterial solution (BS), both kinds of bacteria, DSM33 and SB, at OD_{600} equal to 1.1-1.2, were tested for comparison. Cementation solution (CS) is made by dissolving 1.4 mole $CaCl_2$ and 1.4 mole urea in 1 L tap water. The pH, conductivity and ammonium concentration in the mixing solution are measured every hour for 5 h. The reagents were purchased from VWR® or Fisher Scientific®.

2.4 Experimental methods for studying the mechanical behavior of sand specimens

2.4.1 Preparation of untreated soil specimens

All the untreated soil samples were prepared directly on the base of the triaxial cell. A hollow cylinder rubber membrane (with 0.8 mm thickness for soils with less than 40% fines, 0.5 mm for soils with 40% fines or more) is fixed with rubber rings at one end, then a porous stone or a metal disc with holes is inserted into the membrane down to the pedestal to hold the sand. A rigid split mold with an inner diameter of 10 cm and a length of 17.5 cm is placed around the membrane. The other side of the membrane is folded to wrap up the top of the mold. Then a vacuum pump is connected to the split mold to force the membrane to stick to the inner wall of the mold. The moist tamping method was used to compact the untreated samples to the chosen density. To achieve the desired density, 5 layers of moist sand are compacted one after the other to fill the mold, with control of the mass and final height of each layer. The relative densities (D_r) of loose and dense samples for monotonic and cyclic triaxial tests were equal to 0.3 and 0.9, respectively.

2.4.2 Establishing the MICP protocol and preparation of treated specimens

(1) Sand column preparation

Before treatment, the samples were prepared in PVC molds. Schematic diagram of the mold is shown in Fig. 2.7. PVC molds used for preparing bio-cemented soils are made of two bases with rubber rings and flow channels placed at the two ends and a hollow cylinder in the middle, sealed with four cap screws. For monotonic triaxial tests, the size of the sample is 3.3 cm in diameter and 6.7 cm in length. For cyclic triaxial tests, larger samples (9.5 cm in diameter and 17 cm in length) are used. Moist tamping method is used to compact the samples to a relative density of 0.3. For the

small molds, 3 layers of sand are used. For the large molds, 5 layers of sand are prepared. A plastic filter is placed at both ends of the specimen.

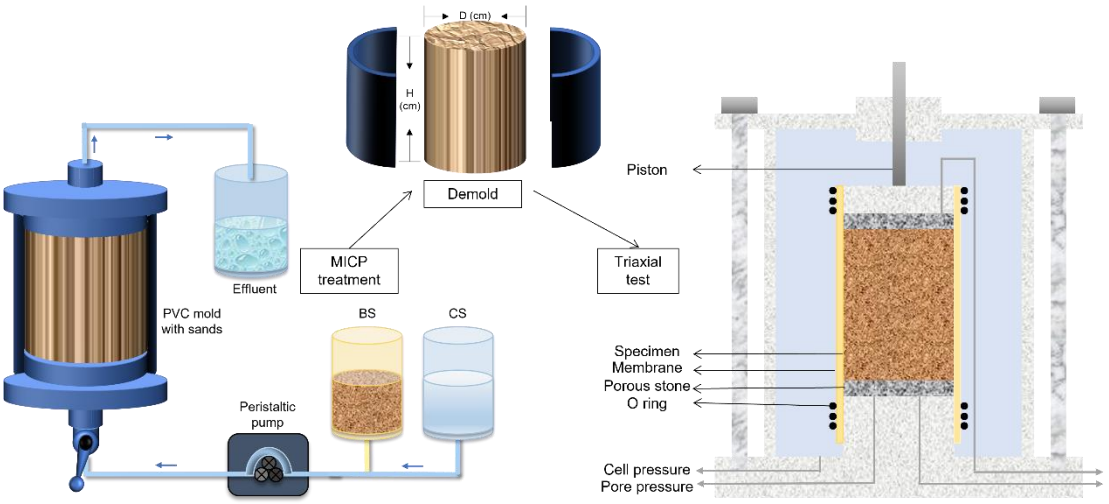

Fig. 2.7 Schematic diagram of MICP treatment and triaxial tests

(2) Exploration of MICP protocols

After preliminary efficiency tests (see Chapter 3), the SB bacteria were finally used for MICP treatment. The OD_{600} of the bacterial solution (BS) is around 3. The cementation solution (CS) is made of 1.4 M equimolar urea and $CaCl_2$ dissolved in tap water.

Different protocols (as follows) were tried in large sand specimens. Based on the preliminary studies, 1.5 pore volume (PV) for BS and 1.2 PV for CS are sufficient to achieve the breakthrough in the sand column. Generally, fines have a positive effect on bacterial adsorption. Hence the following protocol was first tried in the sands having a small or medium fine content (MS6.0, MS6.40), then applied to a sand with more fines (MS6.100).

Generally, MICP treatment is done by

(1) injecting 1.5 PV of BS followed by a rest period of 1 hour

(2) injecting 1.2 PV of CS followed by a rest period of 1 day

The protocols used in different tests are shown in Table 2.4. The changing parameters include the used sand, the injection rate of CS and the injection sequence (1BS followed by 1 or 2 CS).

Table 2.4 Protocols used in different tests

Name of the test	Sand used	Injection rate of CS (mL/min)	Injection sequence	
T1	MS6.40	50	1BS	1CS / 1CS
T2	MS6.40	25	1BS	1CS
T3	MS6.0	50		
T4	MS6.0	25		
T5	MS6.100	25		

(3) Preparation of bio-cemented soil specimens:

Fig. 2.7 shows a schematic diagram of MICP treatment. One cycle of MICP treatment is done by injecting 1.5-1.6 pore volume (PV) of BS, followed by 1.1-1.3 pore volume of CS using a peristaltic pump. For the big molds, the injection rates of BS and CS are around 50 mL/min and 30 mL/min. For the small molds, the injection rates of BS and CS are around 6-7 mL/min and 3-4 mL/min. The Darcy velocity of injection adopted for the big specimens is similar to that for the small specimens. Treatment processes are repeated, the number of cycles of treatment depending on the soil used and the desired cementation level.

The bio-treatment processes are monitored by measuring,

1) the initial optical density (OD_{600}) of the BS, the initial conductivity of the BS and CS
2) the injection rate and volume of BS and CS,
3) the optical density and conductivity of the effluent

After bio-treatment, 1.5 PV of tap water is injected to flush out the remaining chemicals. Sometimes, the bottom of the specimens is blocked. Sometimes, salt remains in the specimen, which might pose problems in the following mechanical test and treated specimen characterization.

The samples in the PVC molds are pushed out using pressure and transferred to the triaxial cell. Sometimes the sample sticks to the mold and needs a rather high pressure to push it out, which might partly damage the specimen, especially when it is lightly-treated.

2.4.3 Monotonic consolidated drained triaxial tests

Consolidated drained (CD) triaxial tests are carried out according to the AFNOR standard. The monotonic triaxial testing program includes a saturation stage, the control of saturation, a consolidation stage and a shearing stage.

Saturation stage

After sample installation, the soil samples are pre-saturated using a reservoir placed 1.5 m above the sample under a water head of approximately 15 kPa for a few

hours, with 35 kPa cell pressure (using automatic pressure controller). Then, another automatic pressure-volume controller is connected to regulate the inner pressure of the sample. Cell pressure and back pressure are increased linearly to target pressures controlled by computer, maintaining an almost constant difference of 20 kPa between confining and back pressures. Then, the *B*-value ($B = \Delta u/\Delta\sigma_3$) is measured to control the saturation degree. If the *B*-value is insufficient (< 0.95), an extra saturation stage is applied.

Consolidation stage

The samples are isotropically consolidated under different effective confining pressures (100, 200, 300 kPa). The consolidation process is maintained until the volume change of the sample is no longer significant.

Shearing stage

Shearing is applied gradually to ensure full drainage of the sample. In our study, the speed of the loading frame ranges from 0.035-0.05 mm/min, corresponding to shearing rates ranging from 0.020-0.028%/min for the large samples and 0.058-0.083%/min for the small samples. The controlled parameters are the confining stress and pore pressure, and the measured parameters are the axial displacement, the axial force and the volume change.

2.4.4 Cyclic consolidated undrained triaxial tests

The cyclic consolidated undrained (CU) triaxial test program includes a saturation stage, the control of saturation, a consolidation stage and a cyclic shearing stage. The saturation and consolidation stages are the same as for monotonic triaxial tests. The only difference is that specimens are consolidated under 100 kPa effective confining stress only.

During the cyclic shearing stage, triangle wave forces are applied at frequencies of 0.1 and 0.5 Hz using a hydraulic (MTS) loading frame. The controlled parameters of these tests are the confining stress and the applied force, and the measured parameters are the axial displacement and the pore pressure. The bulk volume of the sample remains constant. Two kinds of process are applied.

(1) One-stage loading

In the case of untreated samples or a few lightly-treated samples, only one cyclic stress ratio (*CSR*, i.e., the ratio of the half cyclic deviator to the effective confining stress) is applied in each test and the test continues until liquefaction occurs. Generally, at least 3 tests are carried out to obtain the change in stress ratio as a function of the number of cycles to liquefaction.

(2) Multi-stage loading

Fig. 2.8 shows the schematic diagram of the cyclic loading procedure in the case of multi-stage loadings. For untreated dense samples and most treated samples,

firstly, a *CSR* of 0.25 is applied with 300 cycles of loadings. If the sample does not liquefy, the first loading is followed by 100 more cycles with a 0.05 increment in *CSR*. The process goes on with, each time, 100 more cycles and an increase in the *CSR* of 0.05 until liquefaction happens. If liquefaction does not happen when the *CSR* reaches 0.5, the specimen is considered as non-liquefiable (which is very seldom).

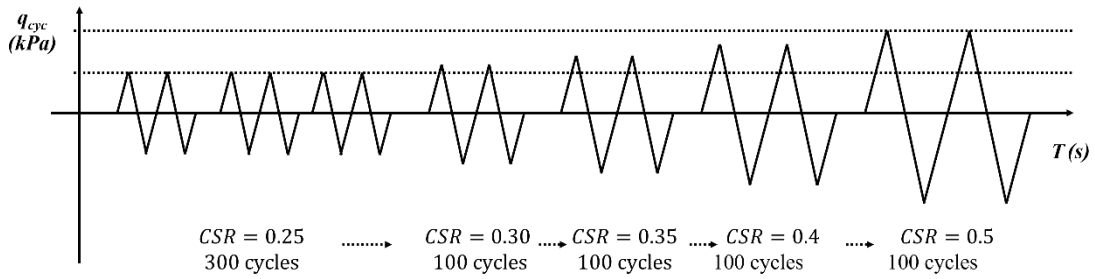

Fig. 2.8 Schematic diagram of cyclic loading mode

2.4.5 Characterization of MICP-treated specimens

After the cyclic tests, soil specimens are collected and oven-dried. The $CaCO_3$ content is measured 3 times with 2 g of oven-dried treated sand, using the hydrochloric acid (§ 2.3.1). The final $CaCO_3$ content is the mean value of the three measurements. Another bulk measurement of $CaCO_3$ Content is derived from the increase in the dry mass of the specimen after drying, but this value may be affected by the presence of un-reacted and un-flushed chemicals in the sample, for instance when bio-clogging occurs during the preparation.

Images of treated specimens are captured using optical microscope and scanning electron microscope (SEM) to see the position and crystal form of $CaCO_3$. XRD tests are also carried out on treated specimen to confirm the crystal type of $CaCO_3$. Mercury intrusion porosimetry (MIP) tests are done to show the size and volume of the pores in the treated specimens. Both SEM observations and MIP measurements are made on oven-dried specimens.

Chapter 3 Bacteria performance and physicochemical process of MICP treatment

3.1 Introduction

Sporosarcina pasteurii (*S.pasteurii*), a gram-positive, bio-safe, and ubiquitous ureolytic bacteria strain with high urease activity, is used in this study. The object of this chapter is to better understand the bacterial metabolism, to know about the changing parameters during MICP reactions, to study the influence of different parameters on the MICP efficiency and to establish the MICP protocol used in the preparation of samples for the mechanical tests.

For the sake of a better understanding of the mechanisms and systematic study, crucial parameters related to bacteria and cementation processes are analyzed. Two kinds of bacterial solution are used, the DSM33 bacterial solution and the SB bacterial solution. The DSM33 bacterial solution is made of freshly cultured bacteria before each use. Hence, studies on DSM33 concern bacterial growth (biomass obtained), urease activity evolution, oxygen limit and preservation. The SB bacterial solution is made of rehydrated freeze-dried bacteria. Thus, related studies concern the viability after rehydration, the evolution of biomass and urease activity. MICP tests are conducted by (1) mixing one kind of bacterial solution with the cementation solution, (2) test in sand columns. The pH, conductivity and ammonium concentration are monitored for comparison.

To study the efficiency of MICP treatment and establish the protocol to prepare treated soil specimens for mechanical tests, the influence of several parameters (injection mode, injection rate of cementation solution, etc.) is analyzed and corresponding efficiency is presented.

3.2 Results and discussions

3.2.1 Performance of DSM33 bacterial solution

(1) Growth curve and urease activity

Bacteria growth and regulatory enzyme activity are important for using the strain. As indicated in Chapter 2, the optical density at a wavelength of 600 nm (OD_{600}) is used to characterize the biomass, and the urease activity represents the ability of the bacteria to hydrolyze urea through producing urease. Fig. 3.1 shows (a) the growth curves of the bacteria at *pH* = 7 and 9 and the specific urease activity in the stable phase, and (b) the urease activity and specific urease activity as a function of the

biomass (at *pH* = 9).

In Fig. 3.1 (a), we can see simultaneous growth of the bacteria in these two cultures. The period from 0-6 hours is the lag phase, in which cellular metabolism is accelerating to prepare for the later growth. In this stage, cell size increases while biomass remains stable. After 6 hours, the exponential phase starts, and we can observe a maximum rate of cell division and an exponential increase of biomass. After 20 hours, due to nutrients depletion and toxic metabolites accumulation, the rate of reproduction decreases. The stationary phase begins with a balanced rate of cell growth and death. The biomass remains stable for hours and begins to decline.

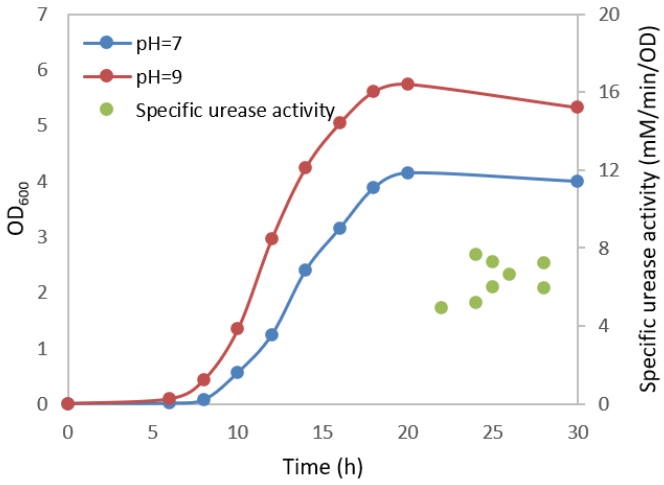

(a) Growth curve of the bacteria at pH=7&9 and specific urease activity at stable phase

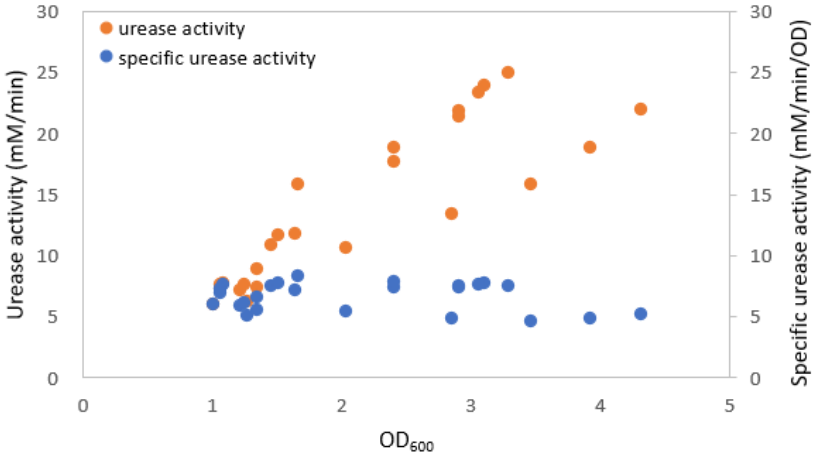

(b) Urease activity and specific urease activity as a function of biomass (at pH=9)

Fig. 3.1 (a) Growth curve of bacteria DSM33 at different pH, and specific urease activity in the stable phase; (b) urease activity (mM/min) and specific urease activity (mM/min/OD) as a function of biomass (pH=9)

If we compare the two cultures at *pH* 7 and 9 (Fig. 3.1 (a)), the second one (*pH* = 9) seems to be more appropriate to grow DSM33: the biomass increases faster than at

pH = 7, and more biomass is obtained after 20 hours of culture.

In Fig. 3.1 (b) shows points from 5 subcultures, we can see an increasing trend of urease activity with increasing OD_{600} although the points are scattered. The scatter is normal because enzymatic activity is not often the same. The corresponding specific urease activity of DSM33 bacterial solution is stable, within the range of 5-8 mM/min/OD. This result is consistent with that of (Liu et al., 2020).

The harvest time of DSM33 is chosen right after reaching the stable phase to get the maximum biomass with similar specific urease activity, between 22 and 28 hours. Several tests of bacterial solutions harvested between two times were made and showed that the specific urease activity value is repeatable within the range from 5-8 mM/min/OD (green points in Fig. 3.1 (a)). From 20-30 h, even after depletion of the nutrients, the specific urease activity remains unchanged at 30°C.

(2) Oxygen limit

As an obligate aerobic strain (Skorupa et al., 2019), oxygen availability is quite important for the growth of *S. pasteurii*. Thus, it is an indispensable parameter to know the applicability conditions of this strain. During the culture process, we observed the inhibition of bacterial growth under closed culture conditions. Hence, we conducted experiments to see the rate of depletion of oxygen. The protocol is presented in section 2.2.2. Fig. 3.2 shows the evolution of dissolved oxygen (mg/L) and conductivity (mS/cm) during the culture of the bacteria and the corresponding oxygen transfer rate. The oxygen transfer rate (OTR) during culture can be used to identify oxygen limitation (Lapierre et al., 2020). In this study, the OTR (mmol/L/h) is simply defined as the change of molar concentration of dissolved oxygen in the culture in unit time.

As a whole, the dissolved oxygen quantity decreases with increasing culture time, the oxygen transfer rate increases with the bacterial activity (biomass) and decreases rapidly with oxygen depletion. In Fig. 3.2 (a), from 0 – 5 hours, there is a steady decrease in dissolved oxygen quantity and a stable conductivity of the bacterial culture. From 5 h - 6.5 hours, due to the exponential phase of the bacteria growth, the dissolved oxygen in the system decreases rapidly and a steady increase in conductivity occurs. After 7 hours, there is hardly any dissolved oxygen in the culture while the conductivity still increases a bit, maybe due to the continuous metabolic activity. Fig. 3.2 (b) shows that, in the first several hours, the OTR remains unchanged (around 20 mmol/L/h). A rapid increase in OTR follows, to reach a maximum (90 mmol/L/h) at 6 hours. Then a rapid decrease in OTR down to 0 is seen due to oxygen depletion.

In an oxygen-depleted environment, after some time, the biomass decreases, and the specific urease activity remains unchanged. The OD_{600} is equal to 1.265 (14 h), 1.074 (24 h), 1.001 (25 h) and 1.055 (37 h). The corresponding specific urease activity is 5.16, 7.67, 5.99 and 6.92 mM/min/OD. The OD_{600} decreases because of the death of the bacteria, but the specific urease activity values is still in the range from 5-8 mM/min/OD.

(3) Preservation of DSM bacterial solution

The bacterial solution is prepared according to the protocol described in section 2.2.2 and kept at 4°C. The *pH* value of the bacterial solution is stable within 14 days (around 7.5-8). The biomass, whose initial OD_{600} value is equal to 1.17 decreases a bit (1.03) after 3 days and is reduced to nearly half (0.6) after 14 days. However, the specific urease activity of the bacteria decreases little, i.e., decreases to 88% of its value after 3 days and 77% after 2 weeks.

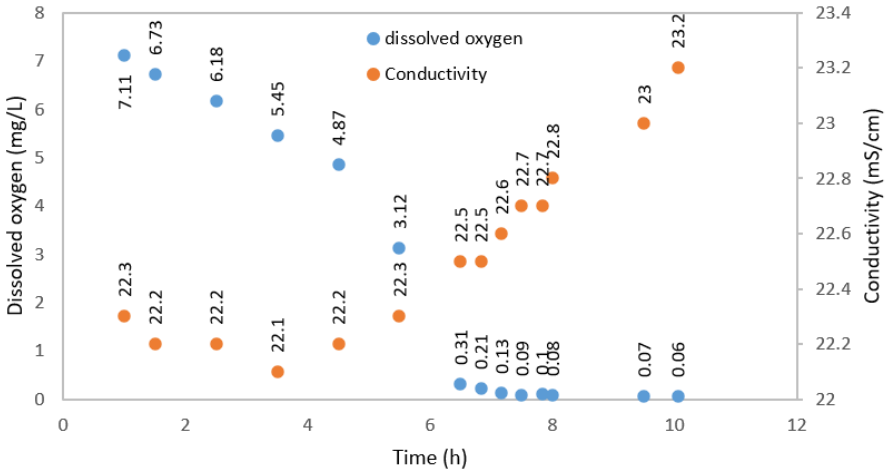

(a) Dissolved oxygen (mg/L) and conductivity (mS/cm) vs. culture time (h)

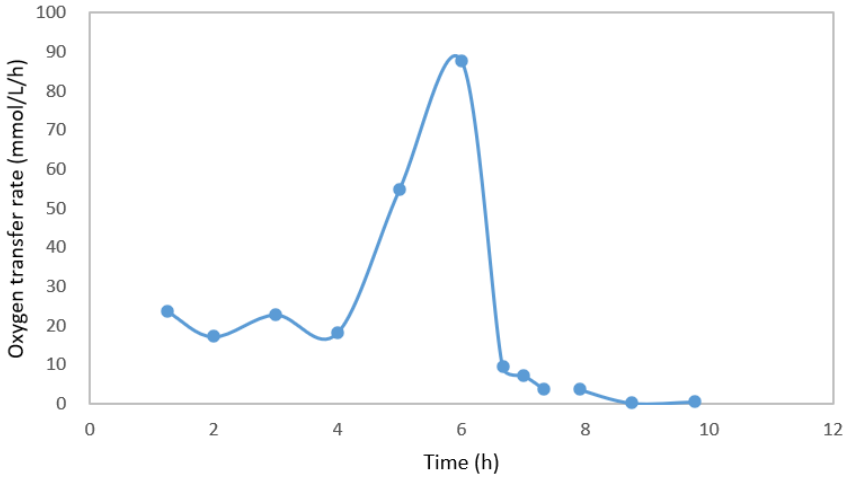

(b) Oxygen transfer rate (mmol/L/h) vs. time (h)

Fig. 3.2 (a) Dissolved oxygen (mg/L) and conductivity (mS/cm) vs. culture time (h); (b) Oxygen transfer rate (mmol/L/h) vs. time (h)

3.2.2 Performance of SB bacterial solution

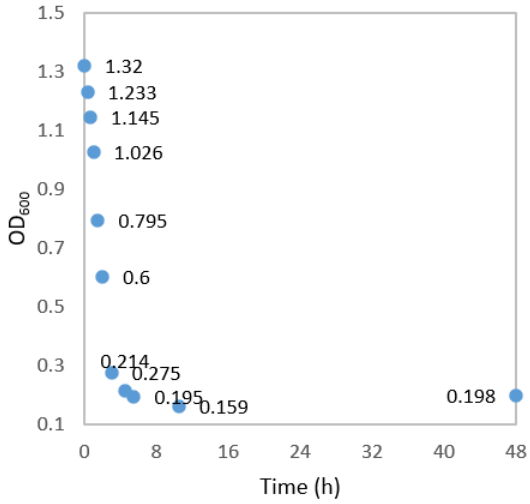

(a) OD_{600} vs. Time (h)

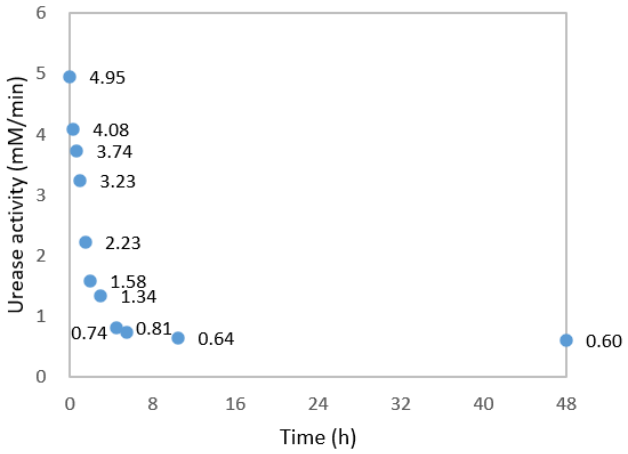

(b) Urease activity (mM/min) vs. Time (h)

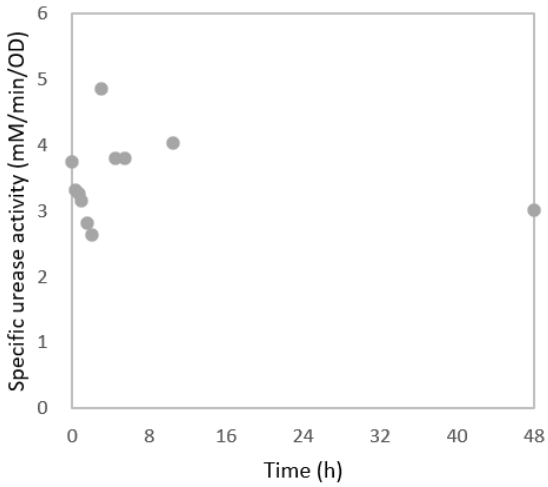

(c) Specific urease activity (mM/min/OD) vs. Time (h)

Fig. 3.3 (a) *OD_{600}*, (b) urease activity (mM/min) and (c) specific urease activity (mM/min/OD) of SB bacterial solution as a function of time (h)

Freeze-drying (lyophilization) process is one of the best and well-established methods to preserve bacterial culture for archiving and long-term use, usually 1-3 years. In real projects, it presents great benefit because of its simple and quick preparation process. Freeze-dried bacteria powder (*S. pasteurii*) is provided by Solétanche Bachy. Rehydration of the bacteria to make SB bacterial solution is done according to the protocol described in section 2.2.3. Fig. 3.3 shows the evolution of the OD_{600}, urease activity (mM/min) and specific urease activity (mM/min/OD) of SB bacterial solution as a function of time.

Keeping the bacterial solution at ambient temperature (around 20°C) can dramatically decrease the viability of the cells, but it has little effect on the specific urease activity of surviving bacteria. As shown in Fig. 3.3 (a), the biomass of the SB bacterial solution decreases rapidly in the first 3 hours (from 1.3 to 0.3) and decreases more slowly afterwards (from 0.3 to 0.2 in 45 hours). Similar trend is seen in the evolution of urease activity shown in Fig. 3.3 (b). The urease activity decreases from 5.3 to 1.34 mM/min in the first 3 hours and decreases slightly afterwards (to 0.6 mM/min). The specific urease activity seems unchanged (3-4 mM/min/OD) for 0-12 hours. The drop in biomass and urease activity are due to the death of the bacteria. The stable specific urease activity is probably due to the fact that the surviving bacteria remain active. Therefore, SB bacterial solution needs to be used as soon as possible after preparation.

It is inevitable to see cell death during the use of the bacterial solution. However, efforts should be made to minimize the deaths. Moreover, when the stability and viability of the bacterial solution drop quickly, improving, for instance the lyophilization protocol or subsequent maintenance (e.g., adding nutrients), can be tried to prolong the activity of the rehydrated freeze-dried bacteria.

3.2.3 MICP tests in solution (without soil)

To compare the two kinds of bacterial solution and to better understand the MICP process, MICP trials are made by mixing equal-volume bacterial solution (OD_{600} = 1.1-1.2) and cementation solution (1.4 M). Fig. 3.4 shows the evolution of *pH*, conductivity (mS/cm) and ammonium concentration (mM) as a function of the reaction time (h). As mentioned in Chapter 2, an increase in conductivity and ammonium concentration shows the activity of the bacteria in hydrolyzing urea.

Fig. 3.4 (a) shows that the pH is lower in DSM33 solution than in SB solution. *S. pasteurii* is an alkaliphile bacteria. Low pH hinders MICP reactions and, as a consequence, SB bacterial solution gets better results in MICP tests than DSM33 bacterial solution. Fig. 3.4 (a) shows that, with MICP going on, there is an increase (with decreasing slope) in conductivity and ammonium concentration. The decreasing slope is due to a loss of biomass (meaning a decrease in urease activity) and a decrease in chemical concentration (decrease in reaction rate) in the system with time. Theoretically, 100 % hydrolyzed urea can produce 1400 mM ammonium for the concentration of the cementation solution used in this section. For both bacteria, less

than one third of this quantity (200 mM and 350 mM) is achieved. The low efficiency may be due to the low pH (5.6) of the cementation solution, resulting in the low pH of the mixed solution, shown in Fig. 3.4 (b). During the first 2 hours, the higher hydrolysis rate of urea can cause an increase in pH that compensates a bit the low initial pH. After 2 hours, the rate of urea hydrolysis is reduced, the pH drops and remains around 6.5. We can see that the conductivity and ammonium concentration of SB bacteria are higher than those of DSM33. This is probably because of the higher resistance of the SB bacterial solution to low *pH*. As shown in the previous section, the urease activity of SB bacterial solution decreases rapidly in the first 5 hours. Hence, the better performance of the SB bacterial solution might also be caused by the fact that adding cementation solution provides nutrients (urea) that maintain the bacterial activity.

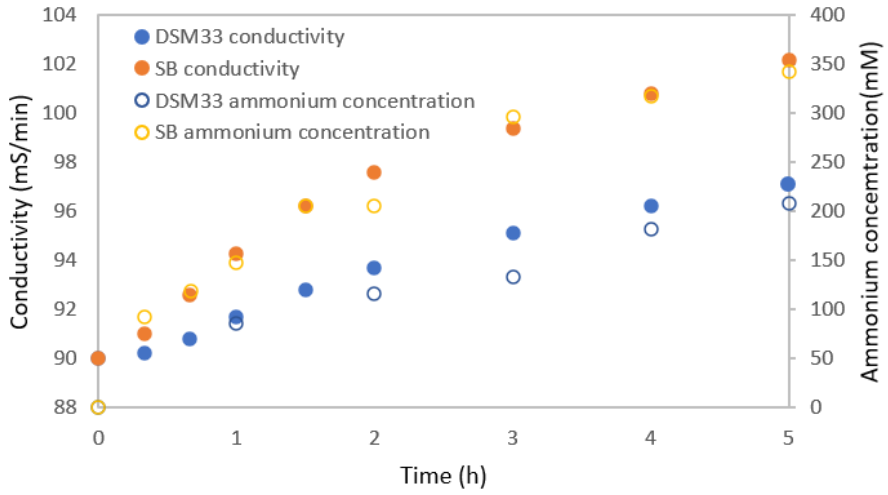

(a) Conductivity (mS/cm) & ammonium concentration (mM) vs. Time (h)

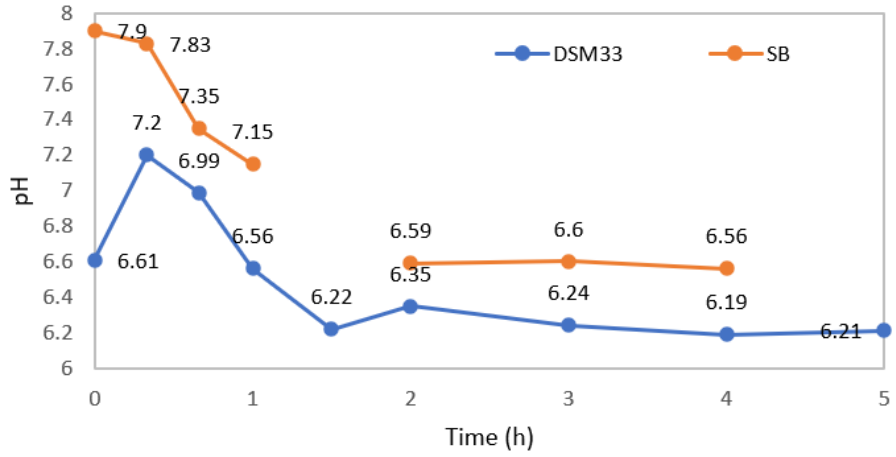

(b) pH vs. Time (h)

Fig. 3.4 Results of MICP tests using DSM33 and SB bacterial solution: (a) Conductivity (mS/cm) & ammonium concentration (mM) vs. Time (h); (b) pH vs. Time (h)

Because of the better behavior of the SB bacterial solution and the much simpler preparation process, the subsequent MICP tests were carried out using the SB bacterial solution (OD_{600} = 1.3) mixed with cementation solution (*pH* around 7.5). The ammonium concentration, conductivity and efficiency are shown in Fig. 3.5 as a function of the reaction time. The efficiency is calculated by dividing the real chemical concentration (i.e, the hydrolyzed urea) by the concentration used in the reaction (applied urea concentration). At this time, the *pH* of the mixed solution remains equal to 7 - 8 during the reaction. We can see that a nearly 100% efficiency is obtained after only 3.5 hours (Fig. 3.5 (b)). Fig 3.5 (a) shows that the conductivity and ammonium concentration increase rapidly, then become stable. The quite large increase in efficiency is probably due to the higher pH of the cementation solution.

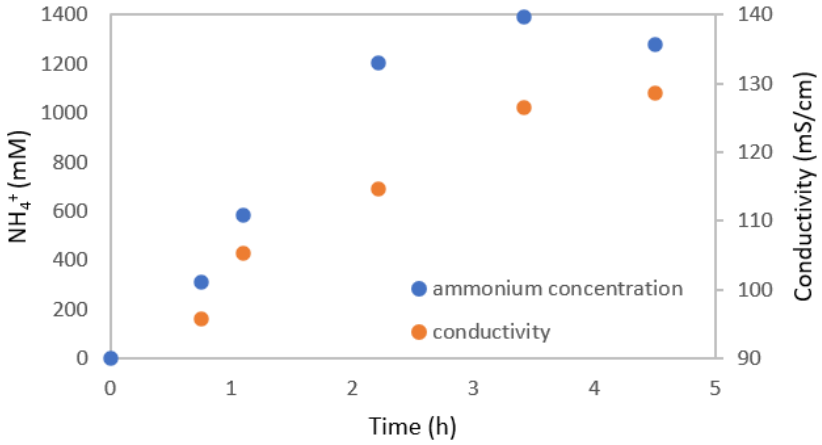

(a) Conductivity (mS/cm) & ammonium concentration (mM) vs. Time (h)

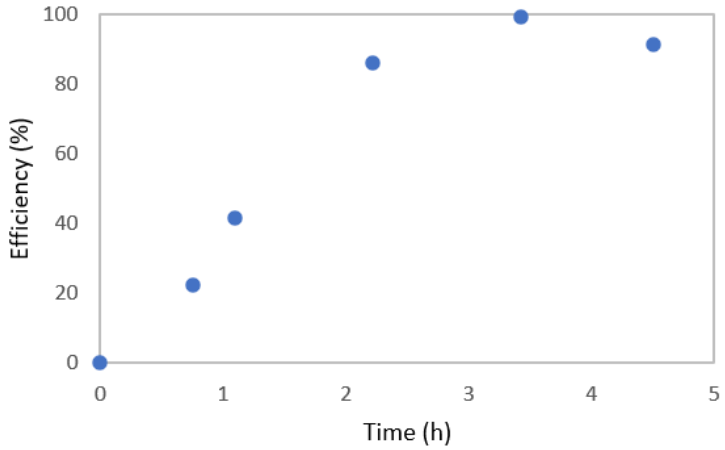

(b) Urease activity (mM/min) vs. Time (h)

Fig. 3.5 Results of MICP trials using SB bacterial solution: (a) Conductivity (mS/cm) & ammonium concentration (mM) vs. Time (h); (b) Urease activity (mM/min) vs. Time (h)

Based on the previous result showing that the conductivity in the mixed solution increases continuously when reaction goes on, Fig.3.6 shows the synthesis of results

of 6 mixing tests, i.e., the efficiency vs. the increase in conductivity (mS/cm). We can see that conductivity increases linearly (R^2 = 0.98) with efficiency (i.e., the hydrolyzed urea ratio). For a conductivity increase of 10 mS/cm, one can expect around 20% of hydrolyzed urea. This result can provide a simple and fast way to estimate the quantity of hydrolyzed urea in the solution.

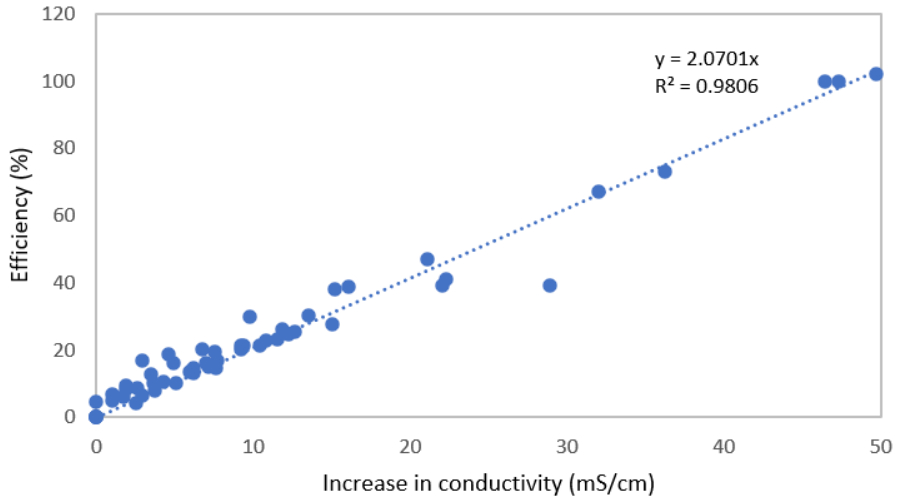

Fig. 3.6 Efficiency (%) vs. increase in conductivity in the mixed solution (mS/cm)

3.2.4 MICP tests in soil columns

Because large amounts of bacterial solution are required for the preparation of MICP-treated soil columns, SB bacteria were chosen for the following mechanical tests. Different protocols were tested to establish the final protocol of MICP treatment. For all the tests, there are some unchanged parameters:

- The retention time of the bacterial solution (BS) remains equal to 1 hour,
- The retention time of the cementation solution (CS) is equal to 1 day,
- The OD_{600} of BS is around 3,
- The concentration of CS is equal to 1.4 M,
- The injection rate of BS is equal to 50 mL/min.

Table 3.1 Protocol used in different tests and results of efficiency

Name of the test	Sand used	Injection rate of CS (mL/min)	Injection mode		Efficiency (%)
T1	MS6.40	50	1BS	1CS	50
				1CS	12
T2	MS6.40	25	1BS	1CS	76
T3	MS6.0	50			32
T4	MS6.0	25			65
T5	MS6.100	25			91

Table 3.1 shows the various conditions in each test, including the sand fraction used, the injection rate of CS, the injection mode (1 BS followed by 1 CS or 2 CS) and the corresponding efficiency. In the following part, we will discuss how these various conditions affect the efficiency of MICP treatment:

(1) Effect of injection mode

In the case of T1, after injecting 1 BS, the first injection of CS gives 50% efficiency while the second injection of CS gives only 12% additional efficiency. This can be explained by the fact that some of the bacteria become nucleation sites for $CaCO_3$ crystal growth and make no contribution to the following MICP reactions. Continuous bacterial death and decrease in urease activity shown in section 3.2.2 can also be part of the reason. Hence, 1 BS followed by 1 CS seems better for increasing the overall efficiency and shortening the time for MICP treatment.

(2) Effect of injection speed of CS

Comparing T1 and T2, in the MS6.40 sand, when the injection rate of CS is reduced from 50 to 25 mL/min, the efficiency obviously increases by half (from 50% to 76%). It is likely that this is due to the fact that the lower injection rate of CS favors the stay of the bacteria and MICP reaction in the specimen. If we compare T3 and T4, in the MS6.0 sand, the efficiency doubles after decreasing the injection speed of CS. It might be because the lower quantity of fines in the soil matrix makes it harder for the bacteria to initially get adsorbed on the grains, while a lower injection speed favors adsorption.

(3) Effect of the soil used

Comparing the result of T2, T4 and T5, we observe that the efficiency increases with increasing fines content in the sand matrix. Fines helps the adsorption of the bacteria on the sand particles, and the largest efficiency is seen in the sand with more fines.

(4) Other considerations

Because the cycle of treatment differs for various cementation levels, when more than 1 cycle of treatment is needed, we find that the efficiency of MICP treatment in the first cycle is less than in the following cycles. The adsorption of the bacteria in the first cycle is less than in the following cycles. This is probably due to the fact that, in the second cycle of treatment and the following ones, when injecting the BS, there is already a much higher ionic strength and many more cations in the pore space due to the chemicals left after the last cycle of treatment. This can enhance the adsorption of the negatively charged bacteria on the grains in the following cycles. Further improvement to enhance the efficiency of the first cycle could be to use a BS with a relatively larger NaCl concentration (9 g/L instead of 3 g/L), or to pre-inject cations in the sand specimen. However, this can little improve the overall effect of multi-cycle treatments and complicates a bit the MICP process.

The efficiency of the MICP treatment in soil columns hardly reaches 100% of what is obtained in mixed solutions tests. On one hand, the lower efficiency in sand specimen compared to mixed solution is probably due to the unevenly distributed bacteria in the pore space. Bacteria can use only the chemicals nearby. On the other hand, small pore sizes, compared to free solution, restrict the contact area between bacteria and chemicals, which can also restrict the reactions.

Based on these results, the injection mode of 1 BS followed by 1 CS, and 25 mL/min for CS injection rate were chosen for the final MICP protocol.

DSM33 bacterial solution was also tested in MICP treatment of soil columns. Based on the results shown in sections 3.2.1 and 3.2.2, the two kinds of bacterial solutions can give similar specific urease activity, which is similar to, or stronger than, what is found in the literature. Table 3.2 shows the differences between DSM33 and SB bacterial solutions. We can see that the advantages of DSM33 include the longer preservation time after preparing the bacterial solution and the relatively stable rate of MICP reactions for longer time treatments. The advantages of using SB include the much simpler preparation process and the faster rate of MICP treatment.

Table 3.2 Differences between DSM33 and SB bacterial solutions

	DSM 33	SB
Preparation of bacterial solution	Very complicated	Simple
Preservation	4°C, for 2 weeks	Bacteria must be prepared right before use
Urease activity	Remains constant at 30°C	Decreases fast at 20°C
MICP reaction rate in mixed solutions	slower	faster
MICP efficiency in soil columns when injecting 1 BS followed by 3 days injection of CS	Stable MICP efficiency with each injection of CS within the 3 days	High efficiency during the 1st day of injection of CS, much reduced efficiency on the 2nd day

3.3 Conclusions

For DSM 33,

- A *pH* of 9 is more appropriate for culture.
- Urease activity increases with biomass.
- Specific urease activity remains stable as a function of biomass, i.e., in the range of 5 - 8 mM/min/OD.
- Bacterial solution can be harvested after 22-28 hours of culture.
- Insufficient oxygen prevents the bacterial growth.

- In a closed system, the dissolved oxygen in the bacterial solution decreases with increasing culture time.
- Oxygen transfer rate increases with the bacterial activity (biomass) and decreases rapidly due to oxygen depletion.

For SB,

- Must be used right after preparation. When using SB, the following MICP treatment should be started within 1 h.
- At ambient temperature (around 20°C), a dramatic decrease in the viability and urease activity of the cells can be seen in the first 6 hours. Afterwards, the two values remain stable for 2 days. However, the specific urease activity of the surviving bacteria is little affected (3 - 4 mM/min/OD).
- 100% of MICP efficiency can be achieved using SB bacterial solution after 3.5 hours.

Comparing the two bacteria,

- The two kinds of bacteria can give enough specific urease activity for MICP treatment.
- SB shows faster MICP reaction rate than DSM33 in MICP tests (mixed cementation solution with the two bacterial solutions).
- The advantages of DSM33 include the longer preservation after the preparation of the bacterial solution and the relatively stable rate of MICP reactions for longer time treatment.
- The advantages of using SB include the much simpler preparation process and the faster rate of MICP treatment.

For establishing MICP protocol in treating soil columns, SB bacteria were used. The effects of the injection mode, injection speed of cementation solution, soil used and some other considerations on the efficiency of MICP are discussed. The injection mode of 1 BS followed by 1 CS and 25 mL/min for CS injection rate is chosen for the final MICP protocol.

Chapter 4 Monotonic mechanical behavior of untreated and MICP-treated soils

4.1 Introduction

The object of this chapter is to study the mechanical behavior of untreated and MICP-treated soils under monotonic loading. For MICP-treated specimens, the major concern is the effect of relatively small $CaCO_3$ contents, i.e., less than 10%, compared to contents as high as 30% in the literature. Sands with different grain size distributions (Chapter 2), i.e., soils with relatively large particles and various fine contents (0, 20, 40, 60, and 100%), were used to carry out consolidated drained triaxial tests under various (100 kPa, 200 kPa and 300 kPa) confining pressures. In this study, the "fines" refer to particles smaller than 1 mm.

To interpret the mechanical behavior of MICP-treated soil specimens, the mechanical behavior of untreated soil specimens is first analyzed (§4.2). Discussions include typical stress-strain behavior, effect of confining pressure, failure criterion, critical state, etc. Then the shearing parameters, i.e., friction angle and cohesion, are analyzed with respect to grain size distribution and mean grain size.

In §4.3, to evaluate the effects of cementation on monotonic behavior of treated specimens, the stress-strain characteristics are presented, for various cementation levels (i.e., light treatment, moderate treatment, and heavy treatment) and various confining pressures (100, 200, 300 kPa). Failure criterion is used to analyze friction angle and cohesion. The effect of $CaCO_3$ content and void ratio is also highlighted. Both qualitative and quantitative results on the mechanical properties of MICP-treated soils are given. Paragraph 4.4 provides extra evidence on the distribution and morphology of $CaCO_3$ crystals, i.e., microscopy and X-ray diffraction results on the MICP-treated sands.

4.2 Monotonic response of untreated soils

4.2.1 Stress strain behavior of untreated soils

Untreated loose samples are prepared at a relative density (D_r) of 30%. Therefore, a strain hardening failure mode and a contractive strain behavior are expected. An increase in soil strength and contractive behavior with increasing confining pressure is also anticipated.

The conditions and the main parameters of the triaxial tests are indicated in Table 4.1. The results of the tests are shown in Fig. 4.1 in the [ε_1, q] and [ε_1, ε_v] coordinate systems. Fig 4.2 presents the void ratios after consolidation (e_c) and the final void ratios (e_f) of the untreated specimens.

Table 4.1 Conditions of the consolidated drained monotonic triaxial tests on untreated sands

Soil	Name of the test	Fines content (%)	Confining pressure (kPa)	e_c	e_f	$D_{r,c}$ (%)	$D_{r,f}$ (%)	$\rho_{d,c}$ (%)	$\rho_{d,f}$ (%)	$\varepsilon_{v,c}$ (%)	$\varepsilon_{v,f}$ (%)
MS6.0	CD100UT	0	100	0.744	0.778	41	26	1.548	1.519	0.48	-1.93
	CD200UT	0	200	0.733	0.753	46	37	1.558	1.540	1.35	-1.15
	CD300UT	0	300	0.701	0.707	60	57	1.587	1.582	1.69	-0.35
MS6.20	CD100UT	20	100	0.654	0.644	45	49	1.633	1.642	0.70	0.59
	CD200UT	20	200	0.644	0.613	49	63	1.642	1.674	1.53	1.86
	CD300UT	20	300	0.642	0.586	50	75	1.644	1.702	2.37	3.43
MS6.40	CD100UT	40	100	0.587	0.569	67	76	1.701	1.721	0.45	1.17
	CD200UT	40	200	0.577	0.560	72	80	1.712	1.731	1.04	1.08
	CD300UT	40	300	0.586	0.558	67	82	1.702	1.733	0.87	1.80
MS6.60	CD100UT	60	100	0.608	0.608	47	47	1.680	1.680	0.42	1.88
	CD200UT	60	200	0.616	0.578	43	60	1.670	1.711	0.61	2.36
	CD300UT	60	300	0.600	0.559	51	68	1.688	1.732	1.64	2.57
MS6.100	CD100UT	100	100	0.695	0.696	48	48	1.593	1.592	0.33	-0.01
	CD200UT	100	200	0.734	0.689	34	50	1.557	1.599	1.01	2.62
	CD300UT	100	300	0.708	0.696	43	48	1.580	1.592	1.39	0.73

Note: CD: consolidated drained triaxial test; UT: untreated specimen; e_c: e after consolidation, e_f: final void ratio; $D_{r,c}$: D_r after consolidation, $D_{r,f}$: D_r after compression; $\rho_{d,f}$: ρ_d after consolidation, $\rho_{d,c}$: ρ_d after compression; $\varepsilon_{v,c}$: ε_v during consolidation, $\varepsilon_{v,f}$: ε_v during compression

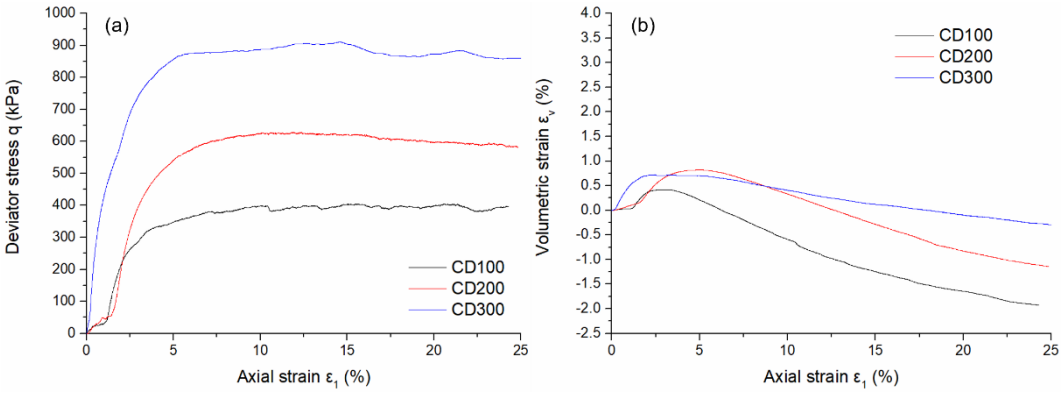

(a) & (b) Stress-strain and volumetric behavior of untreated MS6.0

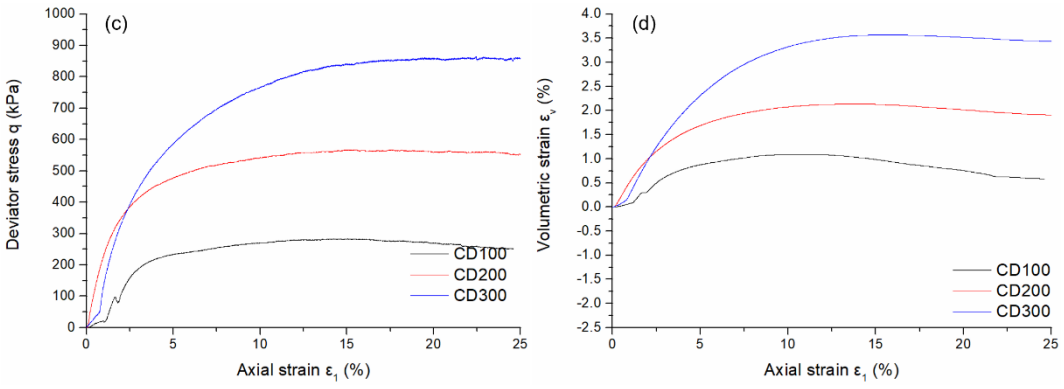

(c) & (d) Stress-strain and volumetric behavior of untreated MS6.20

Fig. 4.1 Stress-strain and volumetric behavior of untreated samples in monotonic CD triaxial tests under 100, 200, 300 kPa confining pressures

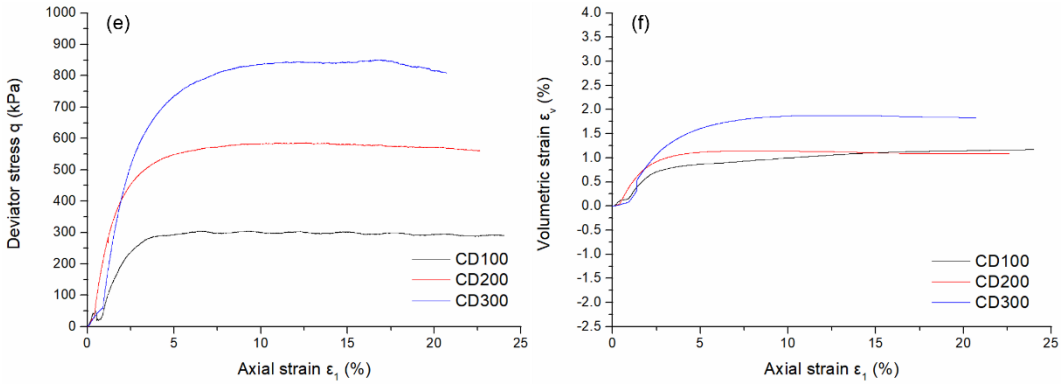

(e) & (f) Stress-strain and volumetric behavior of untreated MS6.40

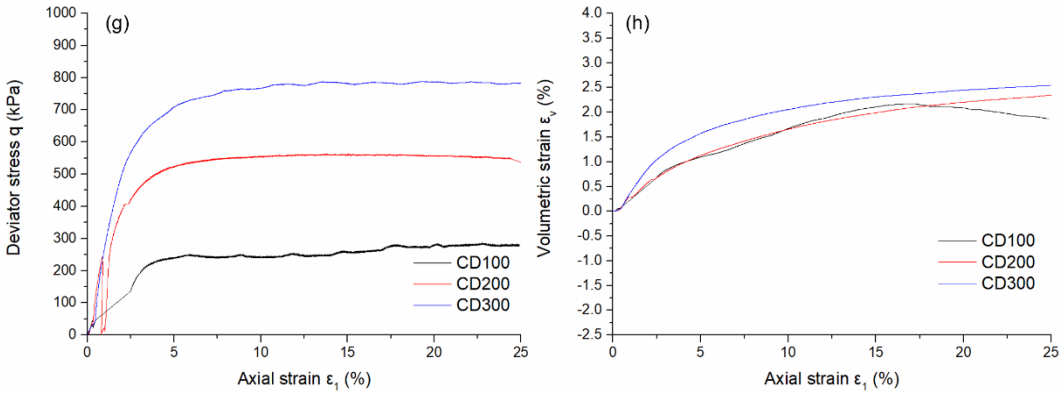

(g) & (h) Stress-strain and volumetric behavior of untreated MS6.60

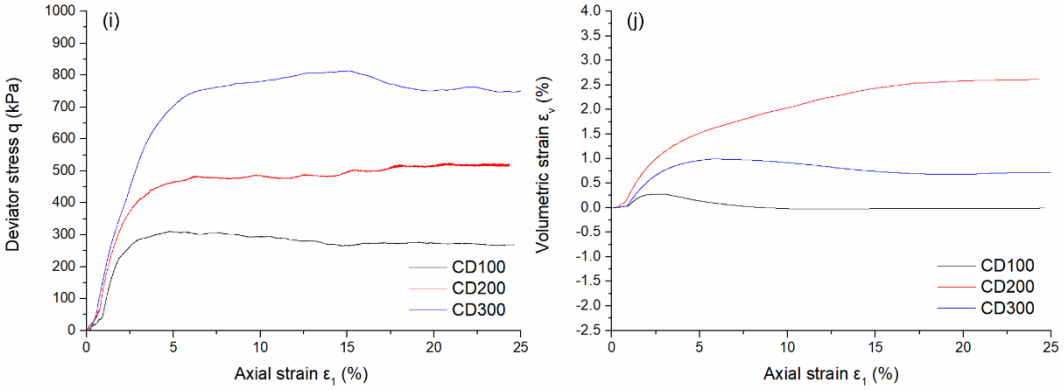

(i) & (j) Stress-strain and volumetric behavior of untreated MS6.100

Fig. 4.1 (continued) Stress-strain and volumetric behavior of untreated samples in monotonic CD triaxial tests under 100, 200, 300 kPa confining pressures

As expected, consolidation decreases the void ratio of the soil specimens. After consolidation, in most cases, the initial D_r of 30% increases to $D_{r,c}$ = 35-50% (Table 4.1). In Fig. 4.2 (a), most of the e_c of the untreated specimens are located around or above the midpoints of e_{max} and e_{min}, corresponding to $D_{r,c}$ = 50%. In the case of MS6.0, some of the points are even below the middle point of e_{max} and e_{min}, maybe because the coarsest sand MS6.0 is more sensitive to confining stress. After compression (Table 4.1 and Fig. 4.2 (b)), for the soils with fines (MS6.20-100), the void ratios of the soil specimens decrease a bit ($e_f < e_c$). For MS6.0, the void ratio increases ($e_f > e_c$).

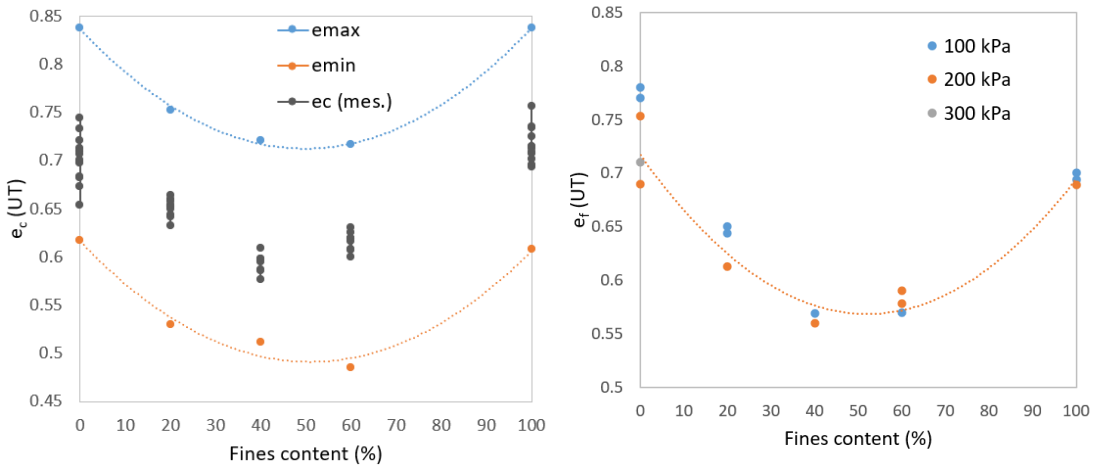

(a) e_c vs. *FC* (%) (b) e_f vs. *FC* (%)

Fig.4.2 (a) Void ratios after consolidation (e_c) and (b) final void ratios (e_f) of untreated specimens

Fig. 4.1 shows that, for the different soils, a strain hardening mechanism results in a continuous increase in strength leading to a steady state, i.e., the absence of peak as it is expected of relatively loose soils. In addition, as expected, the strength of the sands increases with the confining pressure.

For the volumetric strain behavior shown in Fig. 4.1 in the $[\varepsilon_1\text{-}\varepsilon_v]$ planes, only the samples of MS6.0 dilate, while all the other samples contract. This is consistent with the change in void ratio before and after compression. The obvious dilation of MS6.0 is probably owing to the strong interlocking and rearrangement of relatively larger soil particles. The dilation of MS6.0 decreases when the confining pressure increases. For the other samples, contractive behavior increases with increasing confining pressure. For increasing confining pressures, the volumetric strain evolves along three different ways:

(1) first contraction (1-2%) followed by a small dilation (less than 0.5% approximately), then steady state, e.g., in MS6.20_CD100, MS6.20_CD200, MS6.60_CD100, MS6.100_CD100, MS6.100_CD200,

(2) contraction followed by steady state, e.g., in MS6.20_CD300, MS6.40_CD200, MS6.40_CD300,

(3) contraction all the way, e.g., in MS6.60_CD200, MS6.60_CD300 and MS6.100_CD300.

4.2.2 Mohr-Coulomb failure criterion friction angle and cohesion

To further understand the shear behavior of the soil, the Mohr-Coulomb criterion is used, and the failure lines of all the soils are shown in Fig. 4.3 in the [*p'*, *q*] plane. The slopes of the failure lines (M) and the friction angles (ϕ) are deduced from the steady state strength. M (ϕ values) are equal to 1.50 (36.9°), 1.47 (36.2°), 1.46 (36°), 1.42 (35°) and 1.40 (34.6°) for MS6.0, MS6.20, MS6.40, MS6.60 and MS6.100, respectively. There is no cohesion in all the untreated soils.

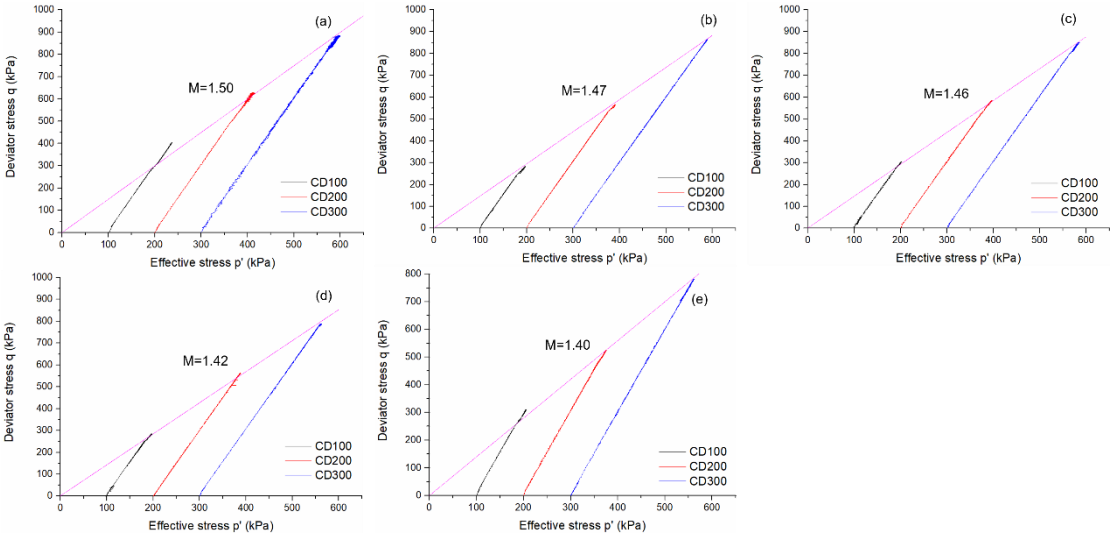

Fig. 4.3 q-p' paths of untreated samples under 100, 200, 300 kPa confining pressures

In Fig 4.3 (a), the residual strength of MS6.0 under 100 kPa confining pressure surpasses a bit the failure envelope. This might be because of the effect of coarse grains particle breakage. Coarse grains have less contact points per unit area. During shearing, the concentration of stress at the contact points may lead to particle breakage, and fine particles are produced. The larger the confining pressure, the more the soil particles break. This leads to a rearrangement of the grains that lowers the possibility of dilatancy and reduces the measured shear strength. This explanation is confirmed by the result of a sieving test on the sand after triaxial tests, shown in Fig. 4.4. After two triaxial tests, around 6% of fines (<1mm) were produced in the sand matrix.

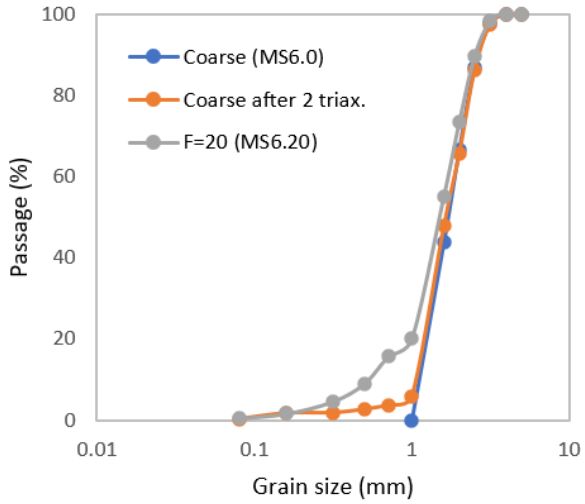

Fig. 4.4 Grain size distribution of MS6.0 after 2 monotonic consolidated drained triaxial tests

4.2.3 Critical state line

The critical state lines (*CSLs*) derived from the triaxial tests are compared with

those of correlations based on the values of e_{max} and e_{min} according to (Biarez & Hicher, 1994) (Fig. 4.5). As shown in Fig.4.5 (a), in general the slopes of the CSL are similar to the slopes of the correlation lines. The larger the C_u value, the lower the critical state line is located. Larger C_u corresponds to a better gradation and a smaller void ratio.

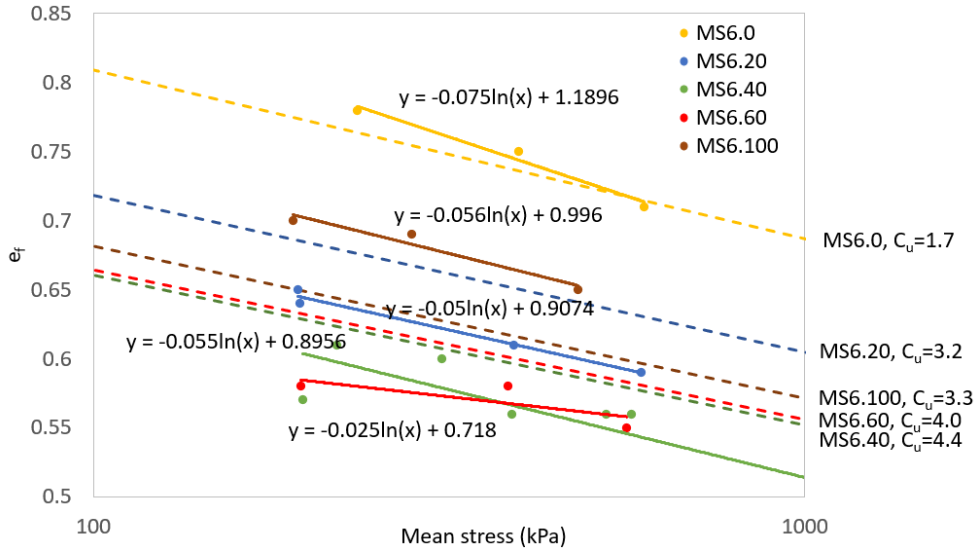

Fig. 4.5 Comparison between the experimental critical state lines (*CSL*) and those derived from e_{max}-e_{min} (Biarez & Hicher, 1994), e_f-p'; (b) Slopes of CSL & e_{max}-e_{min} correlation-*FC*; (c) Slopes of *CSL* & e_{max}-e_{min} correlation-C_u

In Fig. 4.5, it can be noticed that there are large differences between the positions of the measured *CSL*s and those of the e_{max}-e_{min} correlation. For MS6.20, MS6.40 and MS6.60, the *CSL*s are below the corresponding correlations, while the *CSL* of MS6.100 is above the corresponding e_{max}-e_{min} correlation. The reason for this might be the difference between the measured values of e_{max} and e_{min} and the values derived from the correlation with C_u (Biarez & Hicher, 1993) (Fig. 2.4). The measured e_{max} values of MS6.20, MS6.40 and MS6.60 are smaller (around 0.05-0.08) than the corresponding e_{max} values obtained from the correlation, whereas it is the contrary for MS6.100. The measured e_{min} values of MS6.20, MS6.40 and MS6.60 are similar to the values of the correlation, whereas the e_{min} value (0.608) of MS6.100 is much larger than the correlation value (0.494). These differences are reflected in the position of the lines.

4.2.4 Effect of grain size distribution

How the grain size distribution affects the mechanical behavior of soil is still debatable (Tejada & Antolin, 2020). Results obtained in various studies sometimes contradicted to each other based on the literature review.

Figs. 4.6 (a) and (b) show the comparison between the slopes of the *CSL*s and e_{max}-e_{min} correlations for the various fine content (%) and C_u values. We observe that the slope of the *CSL*s decreases when the fine content increases up to *FC* = 40%, then becomes stable at higher fine contents. MS6.0 presents a steeper slope of the *CSL* than the other sands. It may be due to the larger soil grains and the dilative behavior. For

the e_{max}-e_{min} correlation, when the fine content is less than the critical fine content (50%), the slope slightly decreases with increasing fine content. When the fine content is larger than the critical fines content, the slope slightly increases. The slopes of the e_{max}-e_{min} correlation at various fine contents do not change very much compared to the slopes of the measured *CSL*s.

In general, the larger the C_u values, the smaller the slope of the *CSL*s, except for MS6.60. Note that the points are very few and the scatter is high, changes might happen with more plotted points. The slope of the e_{max}-e_{min} correlation follows the same trend as the measured *CSL*s, but the difference between the slopes of the e_{max}-e_{min} correlation at various C_u is less apparent.

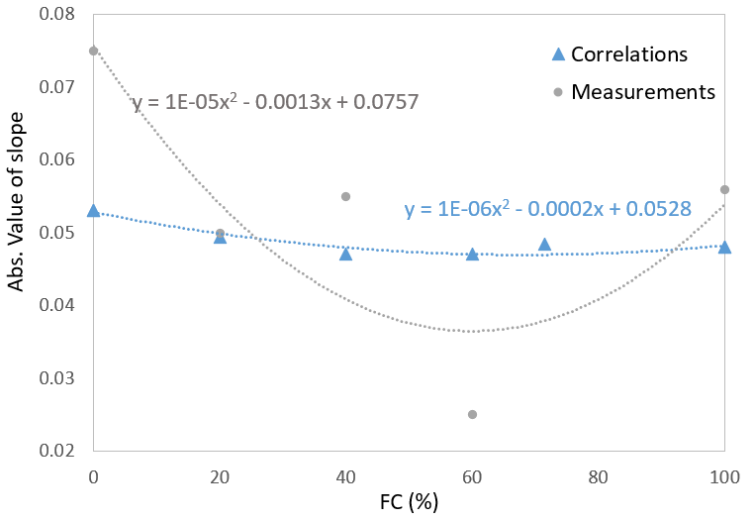

(a) Absolute value of slope vs. *FC*

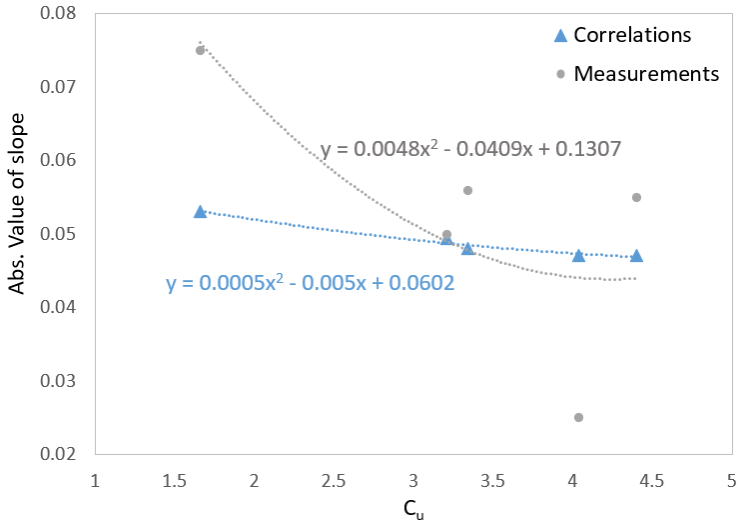

(b) Absolute value of slope vs. C_u

Fig. 4.6 (a) Slopes of the CSL & e_{max}-e_{min} correlation lines versus *FC*; (b) Slopes of the *CSL* & e_{max}-e_{min} correlation lines vs. C_u

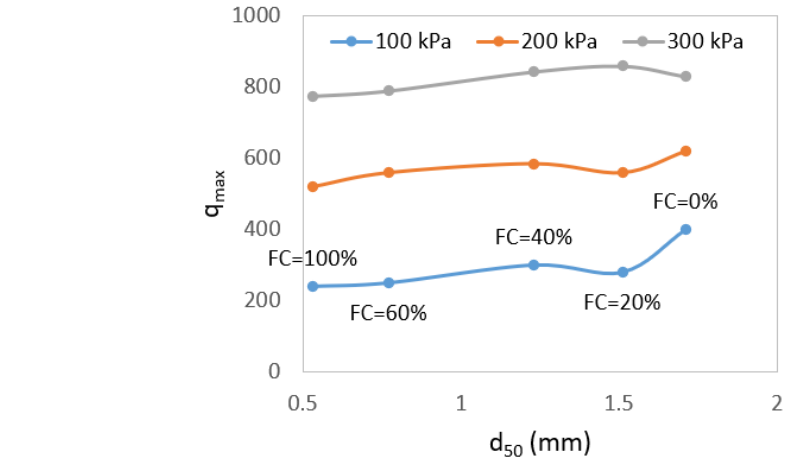

(a) q_{max} (kPa) vs. d_{50} (mm)

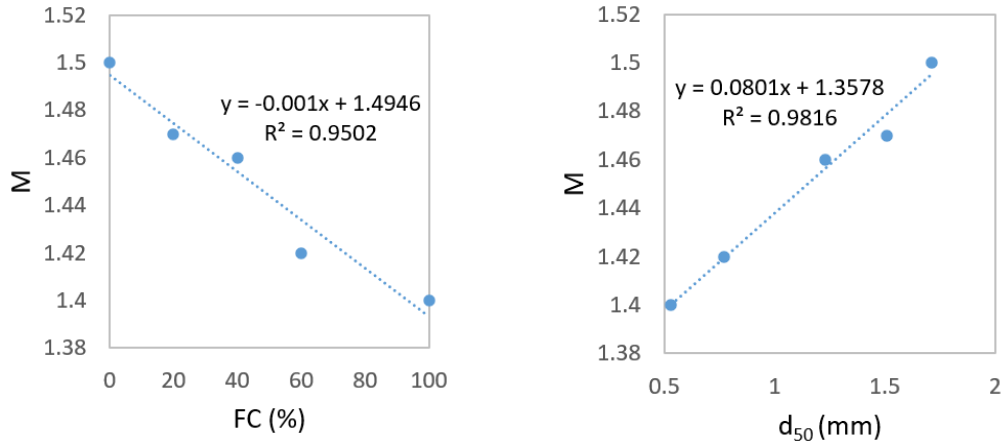

(b) & (c) M vs. FC (%) & d_{50} (mm)

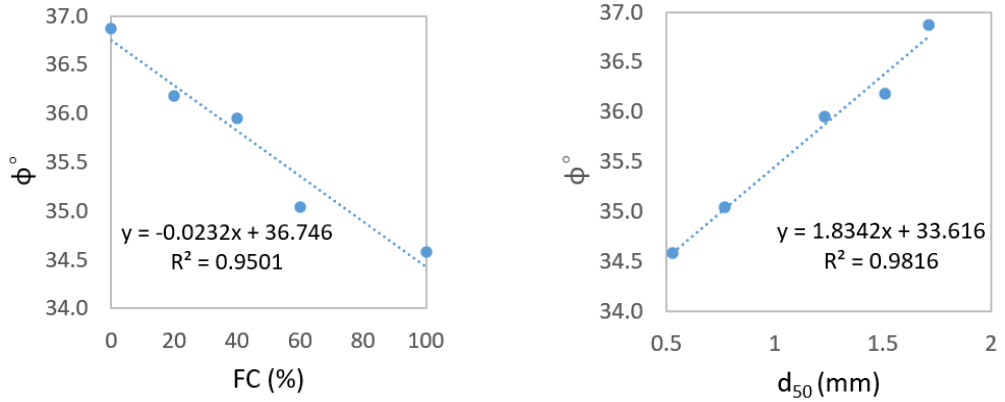

(d) & (e) ϕ° vs. FC (%) & d_{50} (mm)

Fig. 4.7 (a) Effect of mean diameter (d_{50} mm) on the peak deviator stress; (b)&(c) Effect of fine content (FC, %) and mean diameter (d_{50} mm) on the slope M of the CSL; (d)&(e) Effect of fine content (FC, %) and mean diameter ($d_{50,}$ mm) on the friction angle (ϕ, °)

Fig. 4.7 shows the change in the values of maximum strength (q_{max}), the slope of the failure criterion (M) and friction angle (ϕ°) as a function of the fines content (FC, %) and mean grain diameter (d_{50}, mm).

Fig. 4.7 (a) shows the change in the peak deviator stress q_{max} with the mean diameter (d_{50} mm) of the soil. The peak deviator stress generally increases with the mean grain size and decreases when the fine content increases. The difference between the q_{max} of the different sands decreases with increasing confining pressure. The slightly larger strengths of the MS6.40 specimens, compared to the MS6.20 specimens may be due to the higher relative densities after consolidation of the MS6.40 specimens (D_{rc} = 70% for MS6.40 and 50% for MS6.20).

As shown in Figs. 4.7 (b) & (d), the values of M and the friction angles decrease when the fine content increases. Linear relationships are given with a R^2 value equal to 0.95. With 20% more fine content, M approximately decreases of 0.02 and the friction angle decreases of 0.46°. In Figs. 4.7 (c) & (e), the larger the size of the grains, the larger the M value and the friction angle. Linear relationships are given with R^2 = 0.98. With a 0.5 mm increase in mean diameter, M increases of approximately 0.04 and the friction angle increases of approximately 0.9°.

Contractive behavior of the sands seems to be well related to C_u. According to Table 4.1, the contraction of the sands with the largest C_u (MS6.40, MS6.60, C_u around 4) is less obvious than the contraction of the soils with the smallest C_u (MS6.20, MS6.100, C_u around 3) whatever the confining pressure: The contraction is 1-1.75% in MS6.40 and 1.75-2.5% in MS6.60, compared to 0.5-3.5% in MS6.20 and 0-2.5% in MS6.100. This is obviously related to the change in the compressibility of the soil with the uniformity coefficient.

4.3 Monotonic response of MICP-treated soils

4.3.1 Typical curves of MICP-treated samples at various cementation levels

In order to compare the strength of MICP-treated sands with various grain size distributions and calcite percentages, a normalized q_{max} is calculated by the following equation,

$$q_{max,norm} = \frac{q_{max,T}}{q_{max,NT}}$$

where $q_{max,T}$ represents the q_{max} of MICP-treated specimen and $q_{max,NT}$, the corresponding q_{max} of untreated specimen.

According to the literature review (Chapter 1) and the results of our triaxial tests, using only $CaCO_3$ content to quantify the cementation level may be sometimes misleading, even if is indicative. Indeed, there is a large scatter in $CaCO_3$ content (%) for sands with the same strength. The $CaCO_3$ content required to reach a certain strength level depends largely on the precipitation location and the homogeneity of $CaCO_3$ crystals inside the specimen. The scatter becomes even larger when considering various experimental conditions, such as sands with various grain size distributions. Therefore, some researchers (De Jong et al., 2006; Montoya & DeJong, 2015; Gomez et al., 2018; Xiao et al., 2019; Zamani et al., 2021) also used a parameter directly related to the effect of cementation, which is the shear wave velocity measured by

bender elements. In our study, the soils with different grain size distributions need different $CaCO_3$ contents to reach the same $q_{max,norm}$. As a consequence, in order to compare the various sands, we tentatively define the cementation level by the level of achieved $q_{max,\ norm}$ (in Table 4.2). For instance, if $q_{max,\ norm}$ is in the range of 1.05-1.25, the soil will be considered as lightly treated (LT), if it is between 1.25-1.45, it will be moderately treated (MT), and from 1.45-1.65, it will be heavily treated (HT).

Table 4.2 Results of the MICP treatment

Soil	No.	$CaCO_3$%	$q_{max,\ norm}$	cementation level
MS6.0	CD100LT	7.83	1.11	lightly treated
	CD100MT	8.52	1.34	moderately treated
	CD100HT	9.82	1.57	heavily treated
	CD200LT	7.96	1.08	lightly treated
MS6.20	CD100LT	3	1.07	lightly treated
	CD200LT	3	1.1	lightly treated
	CD300LT	4.08	1.14	lightly treated
MS6.40	CD100LT	2.86	1.19	lightly treated
	CD100MT	3.69	1.32	moderately treated
	CD100HT	4.24	1.64	heavily treated
	CD200LT	3.04	1.06	lightly treated
	CD300LT	2.93	1.12	lightly treated
MS6.60	CD100LT	3.74	1.23	lightly treated
	CD100MT	4.28	1.35	moderately treated
	CD100HT	5.11	1.48	heavily treated
	CD200LT	3.88	1.21	lightly treated
	CD300LT	4	1.23	lightly treated
MS6.100	CD100MT	4.18	1.41	moderately treated
	CD100HT	5.24	1.61	heavily treated
	CD200LT	2.61	1.13	lightly treated
	CD300LT	2.61	1.09	lightly treated

Note: Cementation level is defined based on q_{max}/q value: 1.05-1.25, lightly treated soils. 1.25-1.45, moderately treated soils. 1.45-1.65, heavily treated soils.

This part concentrates on the results of multi-level (LT, MT, HT) treated samples under 100 kPa confining pressure. The aim here is to give a general idea of the change in the mechanical behavior of multi-level MICP-treated soils.

The conditions of the tests are indicated in Table 4.3. Stress-strain and volumetric behavior of multi-level treated specimens is shown in Fig. 4.8. The results of MS6.20 are not shown because of lack of data. In the ε_1-q diagrams, remarkable peaks and increases in stiffness are observed in MICP-treated samples. The peak strength of MICP-treated soils increases with the cementation level. The failure mode of the soils changes from a strain hardening behavior in untreated soils to a strain softening behavior in MICP-treated soils. These results are consistent with those of other studies (De Jong et al., 2010; Feng & Montoya, 2016; Cui et al., 2021). It is interesting to note that the maximum deviator stress is obtained for an axial stress in the range from 4-8%, which is larger than the peak axial strain of lime-treated and cement-treated soils, often lower than 5%. This characteristic is especially useful in the framework of hydraulic structures in which brittleness may lead to the formation of cracks.

Table 4.3 Conditions of the consolidated drained monotonic triaxial tests on treated sands

Soil	Name of the test	Fines content (%)	Confining pressure (kPa)	e_c	e_f	$D_{r,c}$ (%)	$D_{r,f}$ (%)	$\rho_{d,c}$ (%)	$\rho_{d,f}$ (%)	$\varepsilon_{v,c}$ (%)	$\varepsilon_{v,f}$ (%)
MS6.0	CD100LT	0	100	0.750	0.783	38	24	1.543	1.514	1.17	-1.89
	CD100MT	0	100	0.662	0.755	77	36	1.625	1.539	1.09	-5.59
	CD100HT	0	100	0.667	0.768	74	30	1.619	1.527	1.33	-8.05
	CD200LT	0	200	0.857	0.888	-	-	1.454	1.430	2.45	-1.69
MS6.20	CD100LT	20	100	0.606	0.654	66	45	1.682	1.633	1.66	-3.00
	CD200LT	20	200	0.593	0.597	72	70	1.695	1.691	2.89	-0.23
	CD300LT	20	300	0.533	0.534	99	98	1.762	1.760	3.09	-0.11
MS6.40	CD100LT	40	100	0.656	0.656	33	33	1.631	1.631	0.53	-0.50
	CD100MT	40	100	0.737	0.773	-	-	1.554	1.523	1.00	-2.05
	CD100HT	40	100	0.580	0.589	70	66	1.708	1.699	0.87	-0.53
	CD200LT	40	200	0.620	0.600	50	61	1.667	1.688	2.69	1.24
	CD300LT	40	300	0.644	0.675	49	35	1.642	1.612	1.99	-1.88
MS6.60	CD100LT	60	100	0.578	0.598	60	51	1.711	1.690	1.05	-1.21
	CD100MT	60	100	0.548	0.563	73	67	1.744	1.728	1.23	-0.92
	CD100HT	60	100	0.588	0.668	56	21	1.700	1.618	1.24	-5.05
	CD200LT	60	200	0.581	0.591	58	54	1.707	1.697	1.87	-0.59
	CD300LT	60	300	0.563	0.563	67	67	1.728	1.728	2.48	0.00
MS6.100	CD100MT	100	100	0.635	0.682	69	52	1.651	1.605	0.77	-2.87
	CD100HT	100	100	0.669	0.669	57	57	1.618	1.618	0.75	0.00
	CD200LT	100	200	0.720	0.720	39	39	1.570	1.570	1.90	-0.02
	CD300LT	100	300	0.652	0.639	63	68	1.634	1.648	1.66	0.80

Note: CD: consolidated drained triaxial test; LT: light treatment, MT: moderate treatment, HT: heavily treatment; e_c: e after consolidation, e_f: e after compression; $D_{r,c}$: D_r, after consolidation, $D_{r,f}$: D_r after compression; $\rho_{d,f}$: ρ_d after consolidation, $\rho_{d,c}$: ρ_d after compression; $\varepsilon_{v,c}$: ε_v during consolidation, $\varepsilon_{v,f}$: ε_v during compression

The analysis of the low residual strength of our specimens, often lower than those of untreated samples, is more complex. In the study of (Feng & Montoya, 2016), residual strength was enhanced in MICP-treated samples except for lightly treated samples that were similar to untreated samples. They attributed the increment to the larger roughness of sand surface due to the treatment and the increase in fines formed by fragmentized $CaCO_3$ due to shearing. (Gowthaman et al., 2020) also recognized the increase in residual strength of treated soil (for 12-23% $CaCO_3$), which they explained by the same reason as (Feng & Montoya, 2016). In our study, the change in the residual strength of all the treated sand specimens is not clear, either due to unreached steady state (even at 25% axial strain) or low final strength (smaller than for untreated samples). For MS6.0 and MS6.60, the strength of treated samples at large strain (> 15%) is even lower than that of untreated samples. For MS6.0, it might be caused by particle breakage. In some cases (e.g., MS6.60), the reason may be the large deformation of the specimen during shearing or the sliding of two blocks, which influences the calculation of the related stress. Indeed, the stress value is derived from the calculation of the area of the sample that is based on the hypothesis of homogenous strains. In the case of two blocks sliding on each other, there is a gross error in the calculation of the area deduced from the measured volumetric strains. For MS6.40 and MS6.100, the strength of all the treated samples decreases continuously with increasing axial strain without reaching a steady state, which is consistent with the findings of (Cui et al.,

2021). The final strength of the lightly treated sample of MS6.40 is almost the same as that of the corresponding untreated sample. Moderately treated and heavily treated samples of MS6.40 and MS6.100 feature a larger final strength than untreated samples. Another reason for explaining the unclear changes in the residual strength of MICP-treated specimens among various sands might be the smaller $CaCO_3$ used in this study, compared to other studies.

Dilative behavior increases as a result of MICP treatment, which is in agreement with other studies (Feng & Montoya, 2016; Gao et al., 2019; Wang et al., 2021; Wu et al., 2021). Dilative amplitude of MS6.0 obviously increases with increasing cementation level: Dilation increases from 2% (for untreated specimen) to 8% (for heavily treated specimen). This might be owing to the effective cohesion of the soil, as explained later (Wu et al., 2021). The increase in density due to MICP-treatment, which results in the formation of calcium carbonate and a net increase in the dry weight of the specimens, can also be a reason. In the case of the other soils (MS6.40, MS6.60 and MS6.100), the untreated specimens contract while the treated samples dilate (except MS6.100_CD100_HT, probably due to a leak during the test). As reported in other studies (Feng & Montoya, 2016; Wu et al., 2021), dilation increases with increasing cementation level. But the result of dilation is not always as regular as reported, especially for MS6.100_CD100_HT and MS6.40_CD100_HT. The reason might be the formation of the shear band when shearing specimens with higher $CaCO_3$ content (Lin et al., 2016).

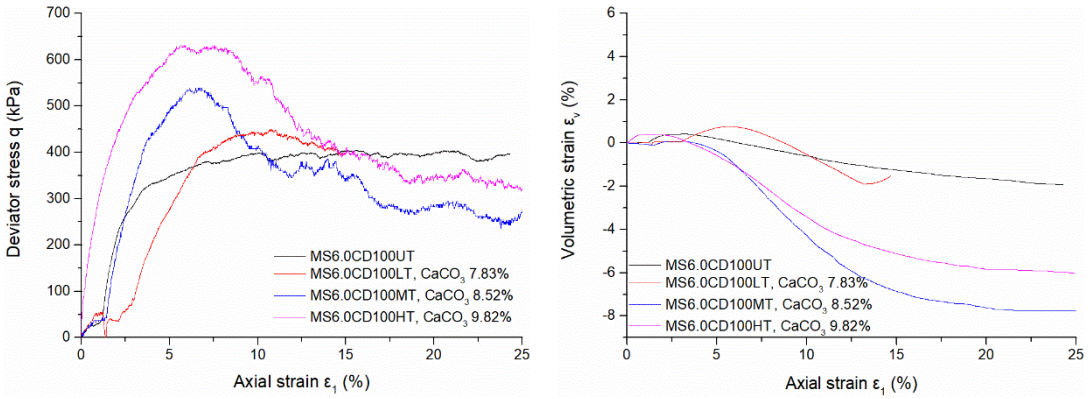

(a) & (b) Stress strain and volumetric behavior of MICP-treated MS6.0

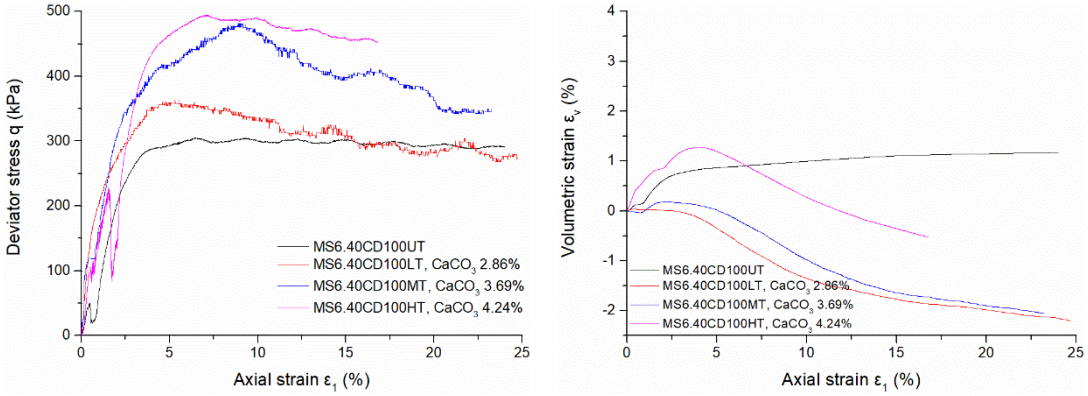

(c) & (d) Stress strain and volumetric behavior of MICP-treated MS6.40

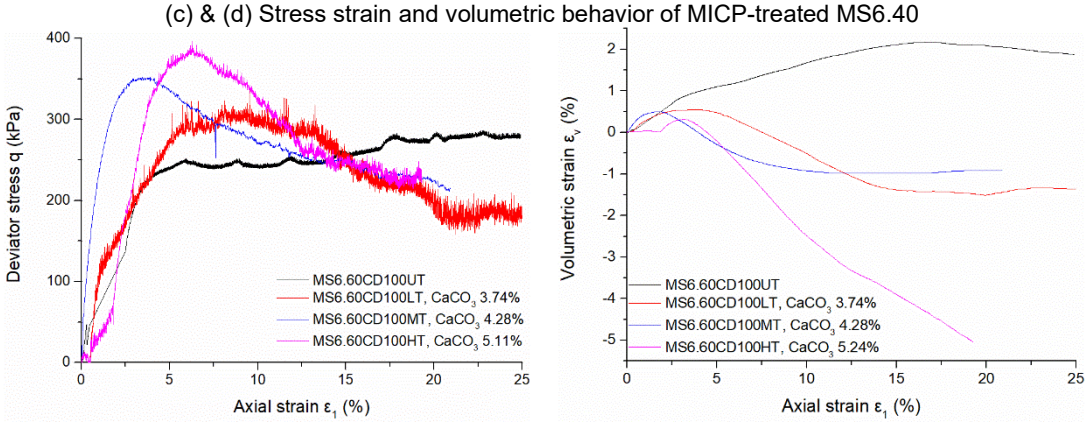

(e) & (f) Stress strain and volumetric behavior of MICP-treated MS6.60

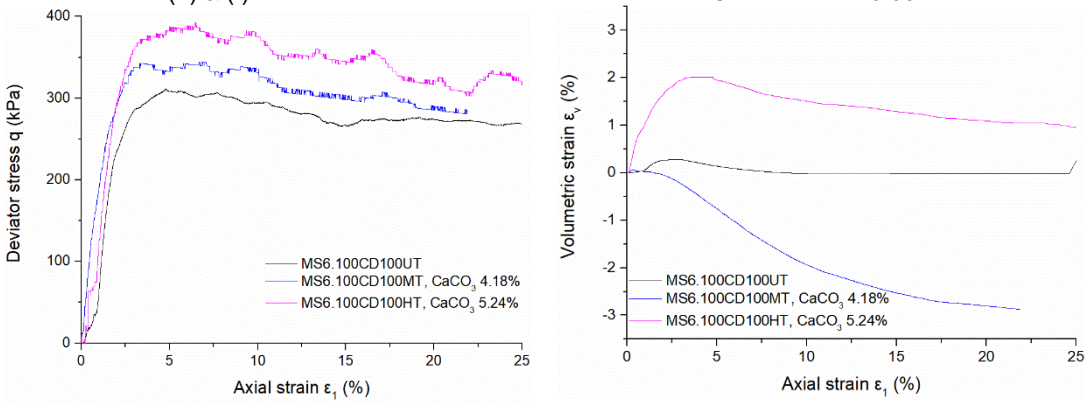

(g) & (h) Stress strain and volumetric behavior of MICP-treated MS6.100

Fig. 4.8 Stress strain and volumetric behavior of untreated and treated samples of different soils at various cementation level: (a), (c), (e), (g) and (i) q-ε_1, (b), (d), (f), (h) and (j) ε_v-ε_1; (a), (b) MS6.0, (c), (d) MS6.40, (e), (f) MS6.60, (g), (h) MS6.100. CD100: CD triaxial test under 100 kPa confining pressure; UT: untreated, LT: light treatment, MT, moderate treatment, HT, heavy treatment

4.3.2 Stress strain behavior of lightly treated soils under various confining pressures

Tables 4.2 and 4.3 show the quantitative results of MICP-treatment and the conditions of monotonic triaxial tests. Fig. 4.9 exhibits the typical stress-strain behavior of lightly treated soils under 100, 200 and 300 kPa confining pressures. Figs. 4.9 (a), (c), (e), (g) and (i) show an increase in strength and a small peak compared to untreated loose samples. As shown in Figs. 4.9 (b), (d), (f), (h) and (j), almost all the treated samples show a more dilative behavior than untreated soils, except MS6.0_CD100, MS6.40_CD200 and MS6.100_CD300. This might be explained by the quite small amount of $CaCO_3$ content that gives a very limited improvement in both strength and dilative behavior. The lightly treated bonds are relatively vulnerable; thus, the effect of treatment is limited.

As shown in Figs. 4.9 (a), (c), (e), (g) and (i), the larger the confining pressure, the larger the strength of the treated soils. With 100 kPa increase in confining pressure, 225-365 kPa more strength is seen. Compared to untreated samples, the increase in strength is small (220-300 kPa). Concerning the volumetric strain behavior, as for untreated samples, the larger the confining pressure, the smaller the dilation of the treated samples.

At the beginning of some of the triaxial tests shown in Fig. 4.9, as observed in some untreated samples, the force increase is very slow, e.g., for MS6.0_CD100_UT&T, MS6.40_CD200T. One reason can be that the sample cap is not centrally placed and not in full contact with the load transducer. Another reason may be that the samples are not homogenously compacted or consolidated, which causes an initial weakness. For treated samples, there are probably small weak zones at the top of the specimen due to unevenly distributed $CaCO_3$ crystals. Another explanation for this might be the partial damage of lightly treated samples during the demolding process.

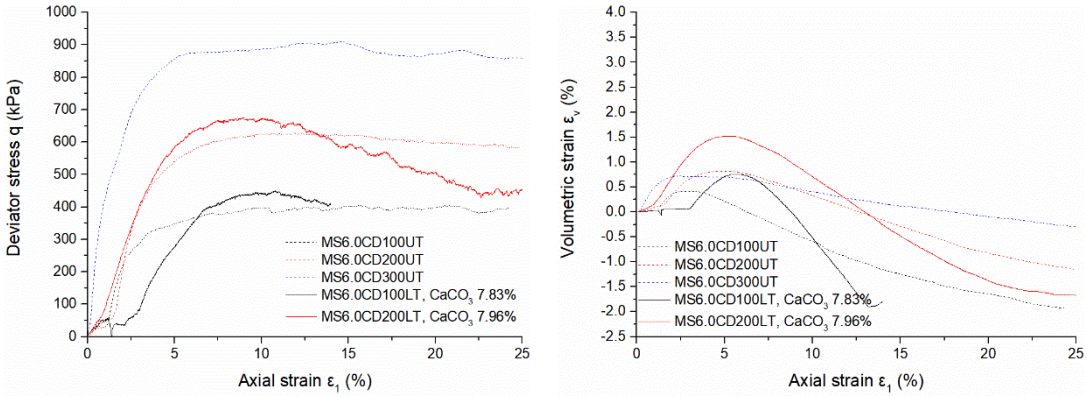

(a) & (b) Stress strain and volumetric behavior of untreated and lightly treated MS6.0

Fig. 4.9 Stress strain and volumetric behavior of untreated and lightly treated samples under 100, 200 and 300 kPa confining pressures

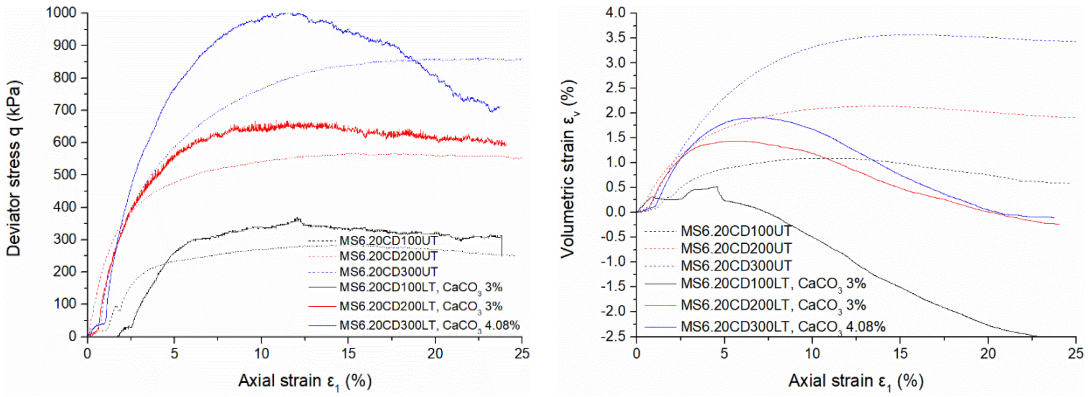

(c) & (d) Stress strain and volumetric behavior of untreated and lightly treated MS6.20

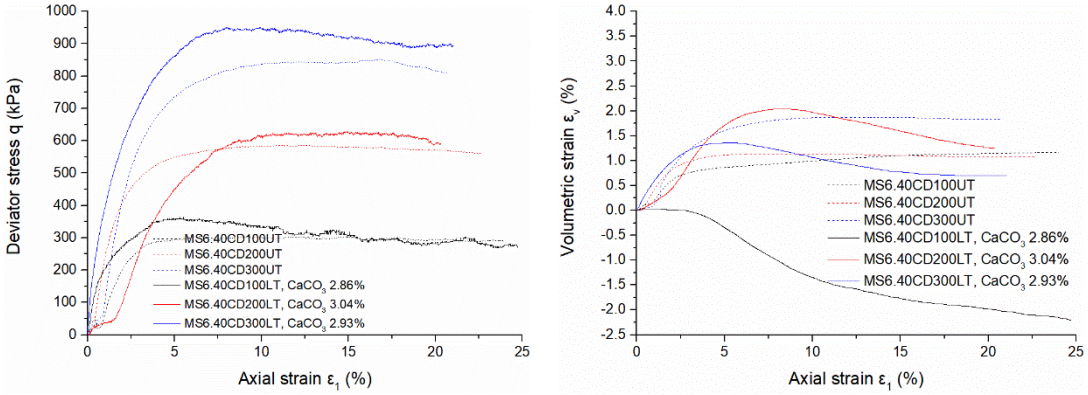

(e) & (f) Stress strain and volumetric behavior of untreated and lightly treated MS6.40

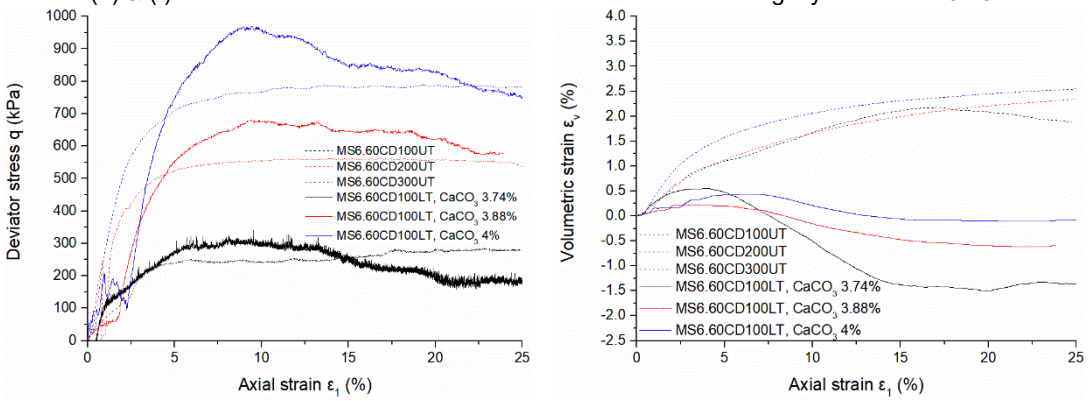

(g) & (h) Stress strain and volumetric behavior of untreated and lightly treated MS6.60

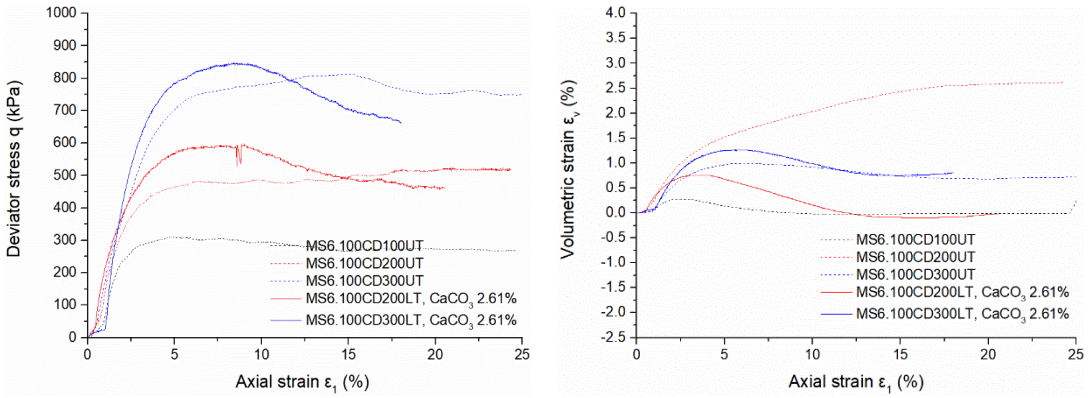

(i) & (j) Stress strain and volumetric behavior of untreated and lightly treated MS6.100

Fig. 4.9 (continued) Stress strain and volumetric behavior of untreated and lightly treated samples under 100, 200 and 300 kPa confining pressures

4.3.3 Effect of $CaCO_3$ content

Fig. 4.10 (a) shows the change in *Normalized* q_{max} with the $CaCO_3$ content. The strength of the treated samples increases with the $CaCO_3$ content. However, this evolution is very different for MS6.0 and the other soils. The curve of MS6.0 is on the far right, while the others are close to each other on the left side. MS6.40 falls in between MS6.100 and MS6.60. To reach the same strength, the $CaCO_3$ content required for MS6.100 is around 0.5% less than for MS6.60, and around 5.2% less than that for MS6.0. For MS6.20, the number of points is not sufficient to conclude.

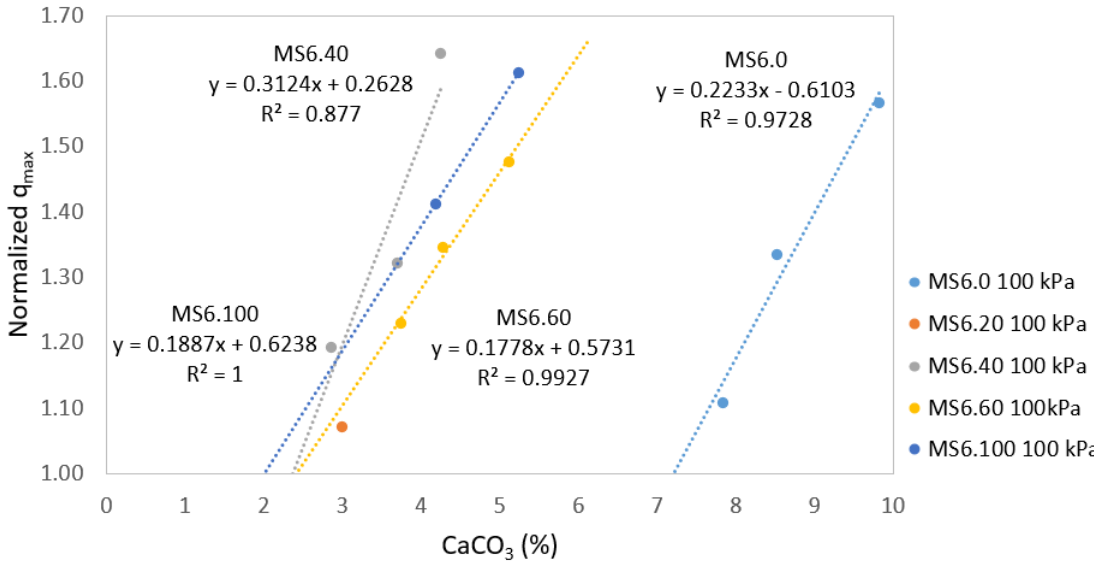

(a) Normalized q_{max} vs. $CaCO_3$% of various sands

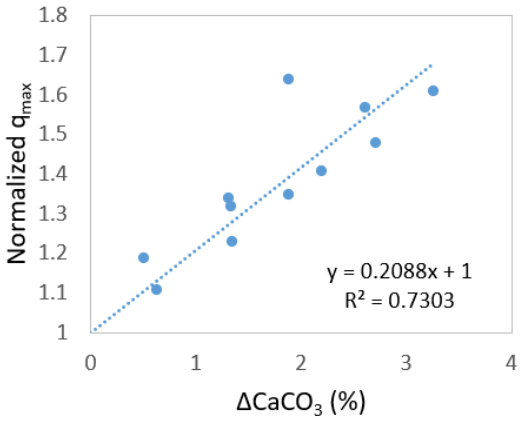

(b) Normalized q_{max} vs. $\Delta CaCO_3$% of various sands

Fig. 4.10 Normalized q_{max} of treated samples under 100 kPa confining pressure versus $CaCO_3$ content (%)

For each soil (MS6.0, MS6.40, MS6.60 and MS6.100) in Fig. 4.10 (a), a linear relationship between the *Normalized* q_{max} and the $CaCO_3$ content (%) is given, with R^2 values larger than 0.9. In these equations, the x-intercept value for each soil represents

the minimum content of $CaCO_3$ necessary to observe an effect of MICP-treatment in increasing the strength of the samples. The minimum contents for MS6.100, MS6.60, and MS6.40 are 1.99, 2.40 and 2.36, which is quite the same. However, for MS6.0, the minimum $CaCO_3$ content is 7.21%. It is quite interesting to note that MS6.0 and MS6.100 have similar void ratio, but a big gap in the minimum $CaCO_3$ content.

When the $CaCO_3$ content exceeds the minimum $CaCO_3$ content, the more $CaCO_3$ precipitated, the larger the strength of the treated samples. The slopes of the lines are more or less the same, i.e., the effect of continuous accumulation of $CaCO_3$ crystals seems similar for the various sands. Thus, we define $\Delta CaCO_3$ as the difference between the real $CaCO_3$ content and the minimum $CaCO_3$ content, to give a general correlation for the different sands. We can see that the strength of the treated samples increases linearly with the same amount $CaCO_3$ crystals precipitated. The equation with R^2=0.73 is as follows (Fig. 4.10 (b),

$$q_{max,norm} = 0.2088 \times \Delta CaCO_3 + 1$$

It indicates that with 1% more $CaCO_3$ precipitates, around 0.21-fold more strength is expected to be seen in the treated sample. It should be noted that these lines are done with a limited number of points. More results might broaden these lines to bands. However, the basic trend will probably remain unchanged.

4.3.4 Failure criterion friction angle and cohesion

The slopes of the failure criteria of the treated samples (M_T) are derived from the peak strength. Fig. 4.11 shows the [q, p'] planes of all the sands. Table 4.4 shows the numerical values of the parameters for untreated and MICP-treated specimens of all the soils.

As shown in Fig. 4.11 and Table 4.4, because of the lack of points (2 points), it is difficult to give a precise value of M. The M values of lightly treated MS6.0 and MS6.100 (M_T) are considered to be the same as those of the untreated specimens (M_{UT}). For the soils with 20, 40 and 60% fines, with 3-4% $CaCO_3$ content, the M_T values of lightly treated samples are slightly higher than those of untreated samples. To compare the various sands, a $\phi°_{norm}$ is calculated by dividing the $\phi_T°$ of treated specimens by those of the corresponding untreated specimens $\phi_{UT}°$. With 3-4% of $CaCO_3$ content, the $\phi°_{norm}$ of MS6.20, MS6.40 and MS6.60 are equal to 1.04, 1.02, and 1.07, respectively. The relative density after consolidation of the untreated samples of MS6.20, MS6.40 and MS6.60 are equal to 50%, 70%, and 50%, respectively. Those of the treated samples of the same soils after consolidation are equal to 70%, 50%, and 60%, respectively. Therefore, the relative densities of the treated samples are not very far from those of the untreated samples, and the increase in friction angle can be partly attributed to the small increase in density (pore-filling $CaCO_3$), but mainly to the increased surface roughness of the sands (images in the following section 4.4.1) (Montoya & DeJong, 2015; Cui et al., 2017).

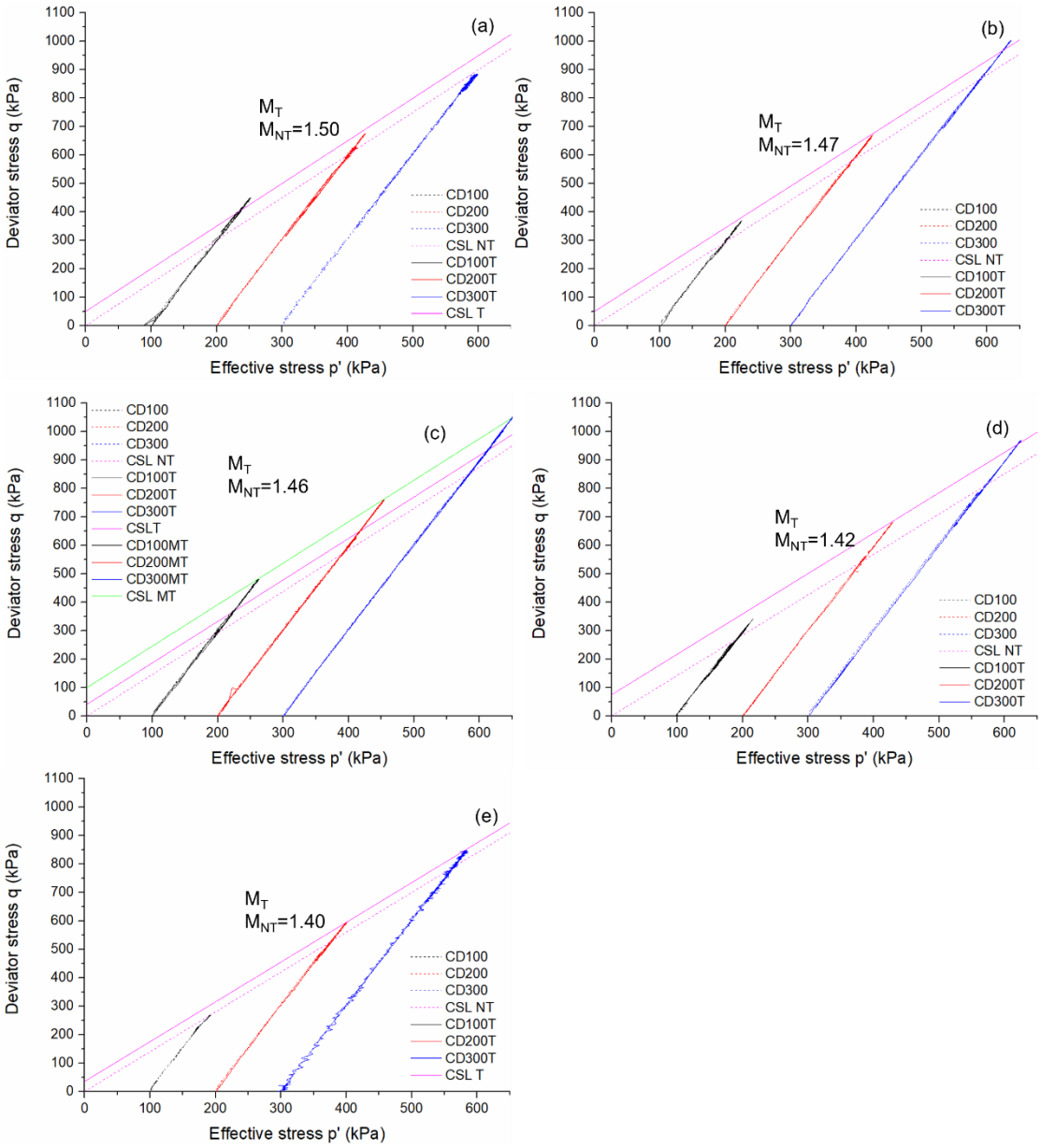

Fig. 4.11 q-p' paths of treated samples under 100, 200, 300 kPa confining pressures: (a) MS6.0, (b) MS6.20, (c) MS6.40, (d) MS6.60 and (e) MS6.100

According to the previous literature review (Chapter 1), various $CaCO_3$ contents (up to 30%) were used for bio-treatment. In the results presented here, the increase in friction angle is small, smaller than those of other studies on silica sand with similar small amounts of $CaCO_3$. This might be due to the larger grain size used in this study. The mean diameter d_{50} of MS6.20, MS6.40 and MS6.60 are equal to 1.51, 1.23 and 0.77 mm, respectively, compared to d_{50} smaller than 0.7 mm in most of the previous studies. If we refer to the previous conclusion on the effect of $CaCO_3$, larger grains might need larger $CaCO_3$ contents to obtain the same treatment effect. The $CaCO_3$ percentage required to reach the same strength is therefore larger in this study than in the other studies using very fine grains. Hence, with a similar $CaCO_3$ content, it is reasonable to see a smaller increment in friction angle.

Table 4.4 *M* values, friction angles and cohesions

Soil	$q_{max,norm}$	$CaCO_3$ (%)	Untreated specimens		MICP-treated specimens				
			M_{UT}	$\phi°_{UT}$	M_T	$\phi°_T$	$\phi°_{norm}$	q_0 (kPa)	c (kPa)
MS6.0_LT	1.10	7.90	1.50	36.9	1.50	36.9	1.00	50	25
MS6.20_LT	1.11	3.36	1.47	36.2	1.53	37.6	1.04	25	13
MS6.40_LT	1.12	2.94	1.46	36.0	1.49	36.6	1.02	25	12
MS6.60_LT	1.23	3.87	1.42	35.0	1.53	37.6	1.07	20	10
MS6.100_LT	1.11	2.61	1.40	34.6	1.40	34.6	1.00	35	17
MS6.40_MT	1.30	3.55	1.46	36.0	1.49	36.6	1.02	85	42

M_{UT}: *M* value of untreated specimen; M_T: *M* value of treated specimen; $\phi°_{UT}$: friction angle of untreated specimens; $\phi°_T$: friction angle of treated specimens; q_0: y-intercept in [*p'*-*q* plane], kPa; *c*: cohesion, kPa

Changes in friction angle after MICP-treatment is also correlated to the mineralogy of the used sands. Some researchers observed the increase in friction angle due to MICP-treatment (Feng & Montoya, 2016; Cui et al., 2017; Gowthaman et al., 2020; Terzis & Laloui, 2019; Wu et al., 2021) in silica sands. (Cui et al., 2021) observed a decrease in friction angle because of particle breakage in calcareous sand. In this study, our sand is non-calcareous sand, and the results are consisted with the results obtained in silica sands.

Cohesion appears in all the treated samples. Cohesion values of lightly treated samples are equal to 25, 13, 12, 10 and 17 kPa for soils with 0, 20, 40, 60 and 100% fines. For the treated MS6.40, there is no change in M values (Table 4.4) between lightly treated and moderately treated specimens, but a large increase in cohesion (42 kPa) in moderately treated samples (1.30 *Normalized q*) due to the presence of a larger number of bonds. This is in line with the result of (Wu et al., 2021). In their study, with 5-13% $CaCO_3$ content, the failure envelopes were parallel. Based on the literature review (Chapter 1), for 3-4% $CaCO_3$ content, between 9 kPa (Feng & Montoya, 2016) and 100 kPa (Terzis & Laloui, 2019) cohesion can be expected. The result in this study (10-42 kPa) is in this (very large) range.

A more quantitative result is shown in Figs. 4.12 and 4.13. The relationship here is based on a limited number of points. The trend can serve as a basis for future studies. Fig. 4.12 shows the normalized friction angle ($\phi°_{norm}$) changes with (a) $CaCO_3$ (%), (b) d_{50} (mm). Fig. 4.13 shows the Cohesion (kPa) changes with (a) C_u; (b) $CaCO_3$ (%) and (c) $\Delta CaCO_3$ (%).

As shown in Fig. 4.12, the normalized friction angle increases with the $CaCO_3$ content. The normalized friction angle decreases when d_{50} increases.

As shown in Fig. 4.13 (a), at the same cementation level (light treatment), the cohesion decreases linearly (R^2 = 0.82) with increasing C_u. Moreover, the cohesion increases with the $CaCO_3$ content and the $\Delta CaCO_3$ content. In Fig. 4.12 (b) & (c), linear relationships are highlighted.

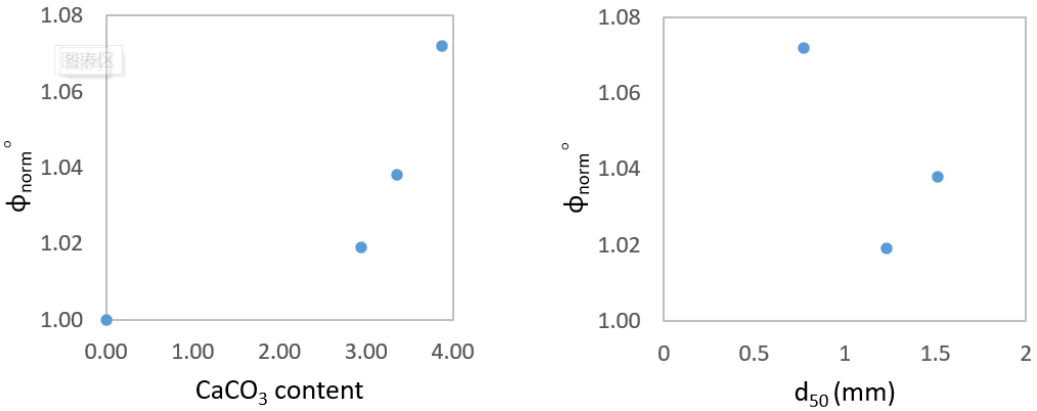

(a) $\phi°_{norm}$ vs. $CaCO_3$ content (b) $\phi°_{norm}$ vs. d_{50} (mm)

Fig. 4.12 Normalized friction angle ($\phi°_{norm}$) changes with (a) $CaCO_3$ (%), (b) d_{50} (mm)

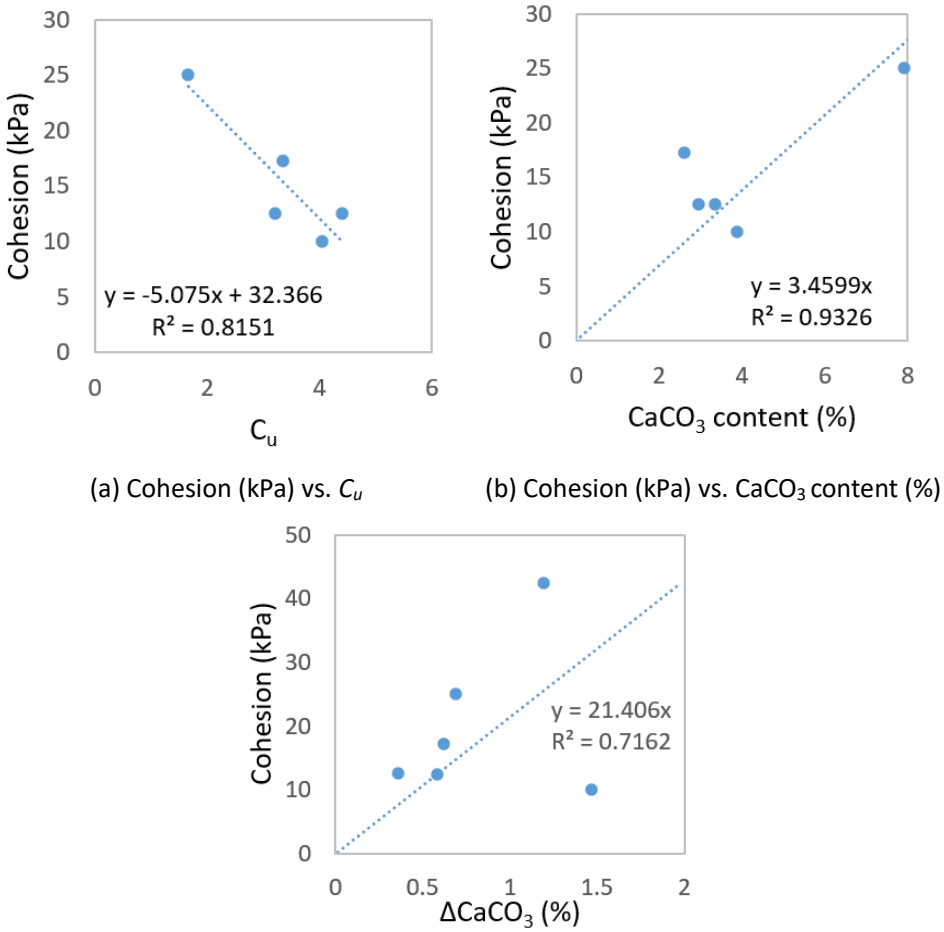

(a) Cohesion (kPa) vs. C_u (b) Cohesion (kPa) vs. $CaCO_3$ content (%)

(c) Cohesion (kPa) vs. $\Delta CaCO_3$ content (%)

Fig. 4.13 Change in cohesion (kPa) with (a) C_u; (b) $CaCO_3$ (%) and (c) $\Delta CaCO_3$ (%)

The main reason for the increase in shear resistance of MICP treated specimen seems to be the increased cohesion, whereas the increased friction angle plays a limited role. As shown in Table 4.4, comparing moderately treated MS6.40 and lightly treated MS6.40, we can see an unchanged friction angle and an increase in cohesion.

Hence the larger strength of MS6.40_MT specimens is mainly caused by the effective cohesion. This result is also confirmed by the study of (Wu et al., 2021).

4.3.5 Void ratios of treated specimens

Fig 4.14 (a) & (b) shows the void ratios after consolidation (e_c) and the final void ratios (e_f) of MICP-treated specimens. If we compare Fig. 4.2 (a) & (b) and Fig. 4.14 (a) & (b), we can conclude that the scatter in e_c and e_f is more important in treated specimens. This scatter is attributed to the difference in cementation levels.

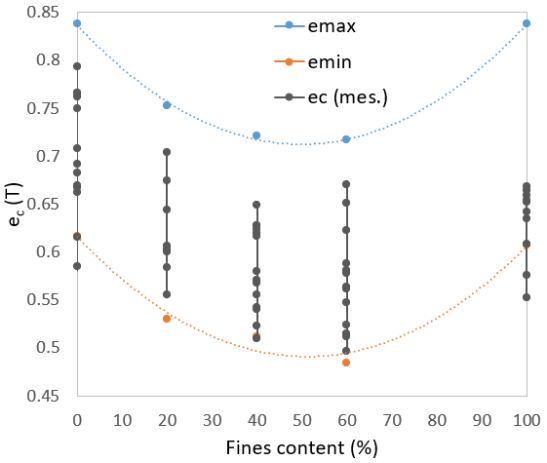

(a) e_c vs. *FC* (%)

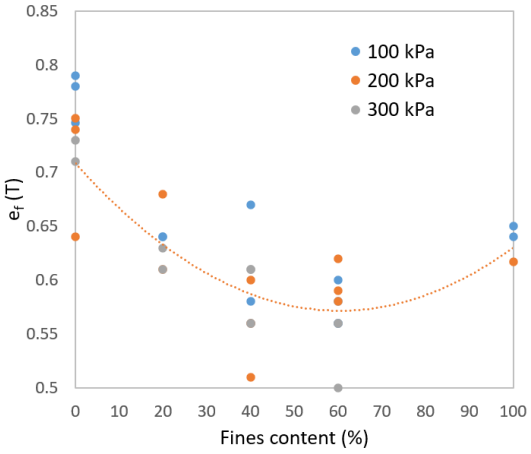

(b) e_f vs. *FC* (%)

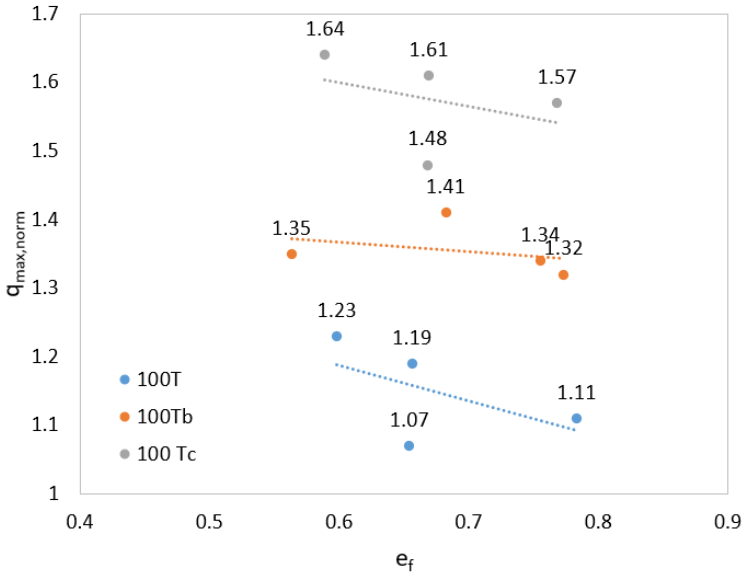

(c) $q_{max,\,norm}$ vs. e_f

Fig.4.14 (a) Void ratios of treated specimens after consolidation (e_c) as a function of fine content (*FC*, %); (b) final void ratios (e_f) of treated specimens as a function of fine content (*FC*, %); (c) normalized maximum strength ($q_{max,norm}$) as a function of final void ratio (e_f)

Except for some extreme points, the final void ratios of treated samples do not seem too different from those of untreated samples. Fig. 4.14 (c) shows the change in

normalized q with the final void ratios. Whatever the value of the *Normalized* q_{max}, little difference in e_f is seen. The interpretation for these results could be the compensation effect of MICP-treatment and dilation. On one hand, the increasing cementation level produces more precipitated crystals, which lowers the void ratio. On the other hand, the higher the cementation level, the larger the dilation when shearing, which increases the void ratio. These two opposite effects cause little change in final void ratios.

4.3.6 Effect of grain size distribution

After treatment, sands are cemented together. Commonly used parameters concerning grain size distribution of untreated sands, such as C_u, d_{50} and fines content, seem not be able to predict the mechanical behavior of treated sands. However, these parameters still have indicative function in determining how much $CaCO_3$ content is required to see the effect of MICP treatment, i.e., minimum $CaCO_3$ content. Fig. 4.14 shows the minimum $CaCO_3$ content (%) changes with (a) C_u, (b) d_{50} and (c) fines content.

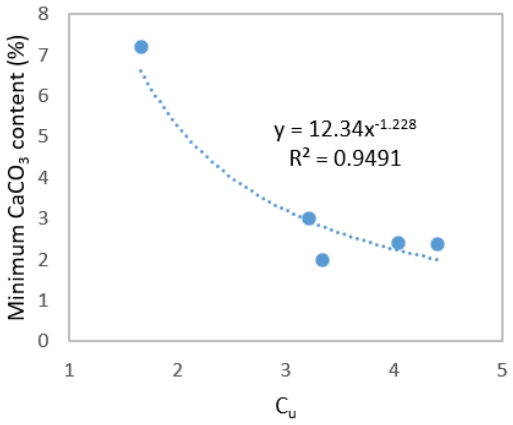

(a) Minimum $CaCO_3$ content (%) vs. C_u

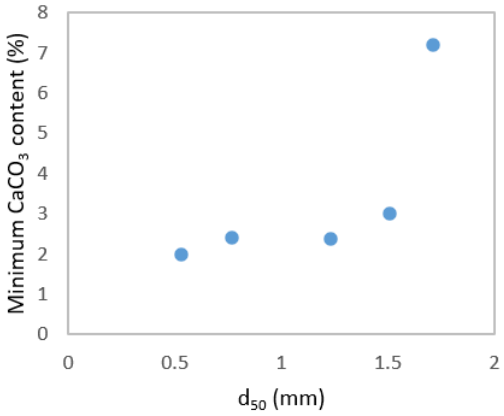

(b) Minimum $CaCO_3$ content (%) vs. d_{50} (mm)

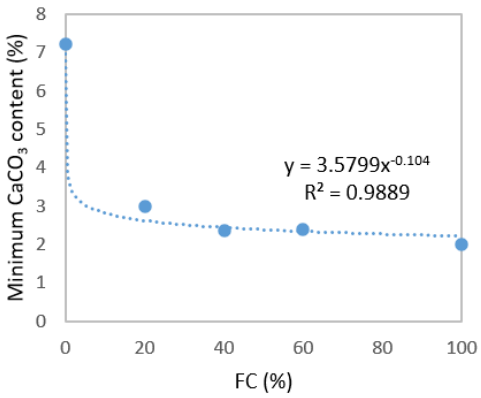

(c) Minimum $CaCO_3$ content (%) vs. *FC* (%)

Fig.4.15 Minimum $CaCO_3$ content (%) vs. (a) C_u; (b) d_{50}; (c) fines content (*FC*, %)

In Fig. 4.15 (a), minimum $CaCO_3$ content decreases with increasing C_u. It seems that relatively well-graded sands are easier to form effective bonds. In Fig. 4.15 (b),

minimum $CaCO_3$ content increases with increasing d_{50}. This might because the smaller the grains, the larger the specific area, the more the contact points in unit volume. Hence, the chances to precipitate at particle contacts are larger. As shown in Fig. 4.15 (c), the larger the fines content, the smaller the quantity of $CaCO_3$ crystals is needed to reach the same improvement in strength. There is a big gap in minimum $CaCO_3$ content between sand without fines (MS6.0) and sands with fines (MS6.20, MS6.40, MS6.60 and MS6.100), especially the minimum $CaCO_3$ content gap between MS6.0 and MS6.20. In addition, the difference between the $CaCO_3$ contents in MS6.60 and MS6.100 is rather small. This illustrates that the presence of fines (such as 20%) helps a lot to increase the efficiency of the MICP treatment process. This enhancement decreases with increasing fines content and becomes quite small after reaching 40% fines content.

4.4 Characterization of the MICP-treated specimens

4.4.1 Optical microscope and SEM observations

Fig. 4.16 shows the images captured by scanning electron microscopy (SEM) (a) & (b) and optical microscopy (c)-(f) of treated coarse sand (MS6.0) and fine sand (MS6.100).

Figs. 4.16 (a) & (b) are SEM images of treated sands. Figs. 4.16 (c), (d), (e) and (f) show images of the treated MS6.0 and MS6.100 samples. Based on the literature review, there are several precipitation modes of $CaCO_3$ crystals: (1) at sand-sand contacts, establishing $CaCO_3$ bridges, (2) on the sand surface, increasing the surface roughness of the sand, and (3) distributed in the pore space, having a pore-filling effect. These three effects can be found in these images, which can explain the increased strength, peak friction angle, cohesion, and dilation. According to the SEM images, the most common morphology of the precipitated $CaCO_3$ crystals is calcite (cubic shape), and also some vaterite crystals are captured. This is maybe because the soil specimens are treated at ambient temperature (20-30°C) and are kept at constant temperature (25°C) in incubator, which is the temperature range that favors the formation of calcite and vaterite crystals (10-35°C) (Trushina et al., 2014). We can also observe that the $CaCO_3$ crystals formed in the treated MS6.0 are larger than the $CaCO_3$ crystals in the treated MS6.100. The difference might be that the volume of single pores in MS6.0 is larger than in MS6.100. Smaller single pore volume can restrict the growth of $CaCO_3$ crystals by confining effect.

In section 4.3.3, we have mentioned that the void ratios of MS6.0 and MS6.100 are similar, however, MS6.0 needs a larger $CaCO_3$ content (6% more) to reach the same improvement in strength than MS6.100. Comparing Fig. 4.15 (c) & (e), we can also observe that more $CaCO_3$ crystals are needed to form valid particle bridges in MS6.0 than in MS6.100. Moreover, in MS6.100, there are more particle contacts in a unit volume, hence the chances to precipitate at the particle contact is bigger. These remarks could partly explain why MS6.0 needs more $CaCO_3$ content than the other sands.

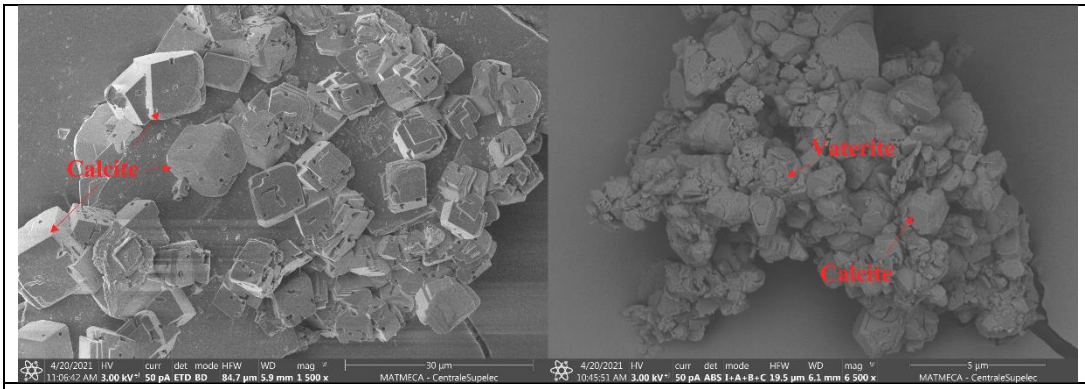

(a) & (b) SEM images of $CaCO_3$ crystals

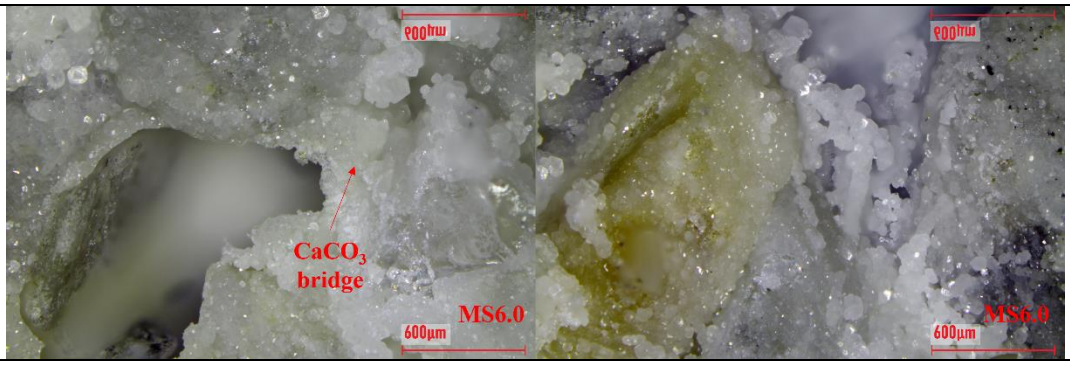

(c) & (d) Images of treated MS6.0

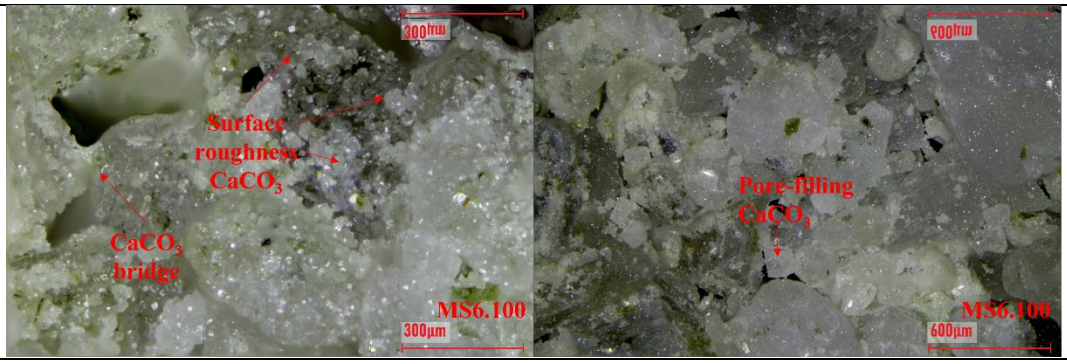

(e) & (f) Images of treated MS6.100

Fig 4.16 SEM images of $CaCO_3$ crystals (a) & (b) at the two magnifications: (a) 1500×, (b) 6500×; and Microscope images (c)-(f) of treated MS6.0 and MS6.100 at two magnifications: (e) 62×, (c), (d), (f) 31×

4.4.2 XRD characterization

The comparison of XRD results on untreated and treated MS6.0 is shown in Fig. 4.17. For untreated specimen, the main peak is quartz. For treated samples, new peaks appear, such as calcite, $CaCl_2$ and vaterite. According to the references (Van Paassen, 2009; Xu et al., 2020), 4 kinds of morphologies of $CaCO_3$ crystals are usually captured in bio-cemented soil, i.e., vaterite, calcite (cubic crystals), aragonite (acicular crystals), amorphous $CaCO_3$. And different morphologies of $CaCO_3$ crystals have various characteristic peaks (Kontoyannis & Vagenas, 2000). In this study, the main crystals

formed seem to be calcite, and vaterite crystals are also seen. These results are consistent with the result of SEM. The presence of $CaCl_2$ is probably due to the blocked bottoms in some treated specimens, which impedes the process of injecting water to flush out the chemicals after MICP treatment. In consequence, these un-reacted and un-flushed salt of the cementation solution remain in the treated specimen.

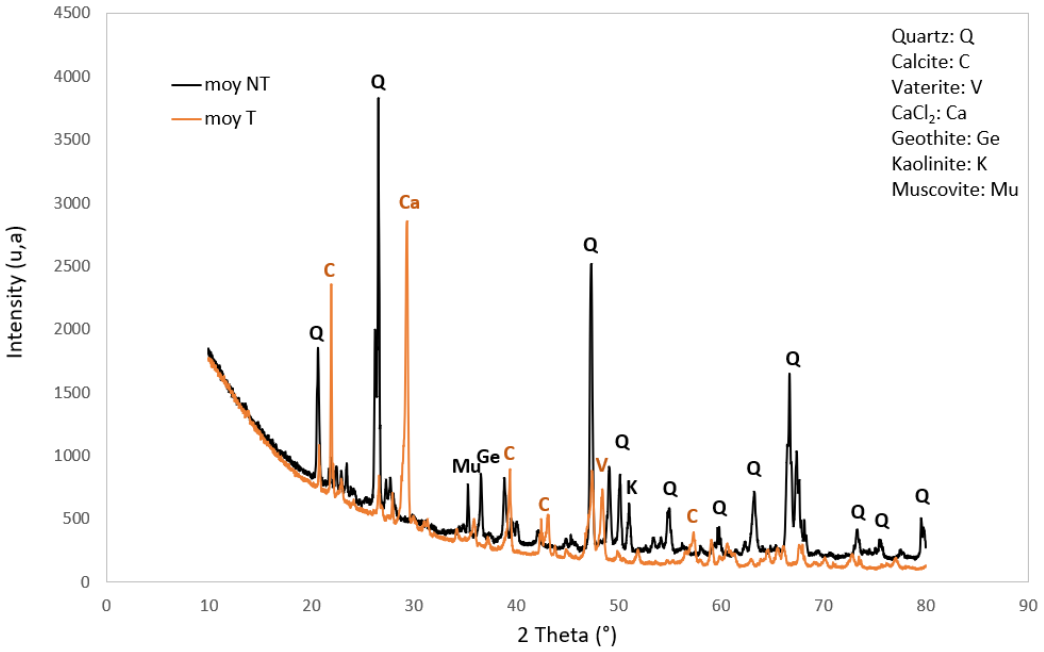

Fig. 4.17 X-Ray diffractograms of untreated and treated MS6.0 specimens

4.5 Conclusions

For untreated sands:

- Untreated loose specimens become medium dense after consolidation.
- Untreated loose samples show stress hardening failure mode, and the strength of the specimens increases with the confining pressure and mean grain size (d_{50}). Specimens of MS6.0 dilate while other specimens contract. The dilation decreases when the confining pressure is increased.
- The maximum strength of the sands decreases with increasing fines content and increases with increasing sand mean diameter. The difference in q_{max} between the sands is attenuated when increasing the confining pressure.
- The slopes M of the failure envelopes, i.e., the friction angles, decrease linearly with increasing fines content and increase with increasing mean grain size (d_{50}). There is no cohesion in untreated samples.
- The larger the uniformity coefficient C_u, the lower the critical state lines (*CSL*s) in the [e vs. p'] diagram are located, the smaller the slope of the *CSL*. The slopes of the *CSL*s decrease with increasing fines content below the Transition Fine Content (TFC = 50%), then become stable at higher fine contents. The change in the slopes of the critical state lines (*CSL*s) with C_u and *FC* are consistent with those derived

from the e_{max}-e_{min} correlations of Biarez & Hicher (1994). The difference between the slopes of the various sands is more obvious in the case of the experimental CSL than in the case of the e_{max}-e_{min} correlations.

For treated sands with small amounts of $CaCO_3$:

- MICP treatment enhances the peak strength and dilation of the soil, and the strength increases with the cementation level. The soil shows a transitional behavior from strain hardening failure mode (for untreated specimens) to strain softening (for treated specimens). The effect of MICP-treatment on residual strength is unclear maybe because that small amount of $CaCO_3$ has little effect in enhancing residual strength.
- The effect of confining pressure on peak strength and dilation is unclear within the range of 100-300 kPa confining pressure and the studied $CaCO_3$ content.
- The concept of minimum $CaCO_3$ content is introduced to quantitatively define the minimum $CaCO_3$ content required to see MICP effect on strength. $CaCO_3$ limit for MS6.0, MS6.40, MS6.60 and MS6.100 are equal to 7.21, 2.36, 2.40 and 1.99%, respectively. Minimum $CaCO_3$ content decreases with increasing C_u and fine content and increases with increasing mean diameter of the sand.
- To give a generalized quantitative relationship between the *Normalized* q_{max} (i.e., the ratio of $q_{max,\ T}$ to $q_{max,\ UT}$) and the minimum $CaCO_3$ content for sands with various grain size distributions, $\triangle CaCO_3$ (which is the difference between the actual $CaCO_3$ content and the minimum $CaCO_3$ content) is introduced. The conclusion that can be drawn is that, after reaching the minimum $CaCO_3$ content, 1% more $CaCO_3$ precipitate can be expected to bring about 0.21-fold more strength.
- For lightly treated MS6.20, MS6.40 and MS6.60 soils, with 3-4% $CaCO_3$ content, there is a small (0.02-0.07) increase in peak friction angle. Friction angle seems to increase with the $CaCO_3$ content and decrease with increasing mean grain size. However, these results must be considered with caution due to the small number of data available.
- For lightly treated MS6.20, MS6.40 and MS6.60, with 3-4% $CaCO_3$ content, a cohesion of about 10-13 kPa appears. The cohesion increases linearly with increasing $CaCO_3$ content, and decreases linearly with increasing C_u.
- The increasing shear resistance of MICP treated specimens is mainly due to the increasing cohesion, while the increasing friction angle (mainly due to the increasing sand grain surface roughness, partially due to increasing density) plays a limited role.
- Almost no change in final void ratio e_f was observed between untreated and treated specimens because of the compensation effect of MICP treatment and dilation.
- Optical microscope images show the pore-filling, surface coating and particle-bridging effect of MICP treatment, which provides evidence of the mechanical behavior enhancement. The result of SEM images and XRD patterns confirm that the main morphology of the $CaCO_3$ crystals formed is calcite, a small amount of vaterite crystals is seen.

Chapter 5 Cyclic behavior of untreated soils

5.1 Introduction

The aim of this chapter is (1) to assess the cyclic behavior of untreated sand in terms of excess pore pressure generation and axial strain accumulation, (2) to analyze how various factors (density, grain size distribution, cyclic stress ratio) affect the cyclic resistance of the soil, and (3) to pave the way for the following chapter to analyze the effect of MICP-treatment on the cyclic behavior of soil.

Sand specimens were prepared with various grain size distributions and densities (i.e., loose D_r=0.3 and dense D_r=0.9). Stress-controlled consolidated undrained (CU+u) cyclic triaxial tests were conducted under 100 kPa confining pressure. Different levels of cyclic loadings, i.e., different cyclic stress ratios (*CSR*) representing the intensity of shaking, are applied. The *CSR* is derived from the following equation: $CSR = \frac{\sigma_d}{2\times\sigma_c'}$, where σ_d represents the applied cyclic deviator stress and σ_c' the effective consolidation stress. Evolution of axial strain and pore-pressure generation is measured during the test.

Section 5.1 gives the objectives and plan of this chapter. The sections 5.2-5.5 show the results of one-stage cyclic triaxial tests. At first, a few examples of the typical cyclic behavior of untreated soils are presented (§ 5.2). Then, the excess pore pressure generation mode is described and fitted with Seed Model (§ 5.3). Next, the effects of various factors, i.e., stress level and grain size distribution, are discussed (§ 5.4-5.5). Paragraphs 5.6-5.8 present the results of both one-stage and multi-stage cyclic triaxial tests. Results consist of (1) discussion on the axial strain development and the effect of soil density in both one-stage and multi-stage tests; and (2) modelling of multi-stage pore water generation mode. Finally, conclusion is summarized in section 5.9.

5.2 Typical cyclic undrained triaxial test result of untreated soil

As indicated in Chapter 2, the grain size distribution of the used sand are within the range of materials susceptible to liquefaction. In this study, liquefaction is considered to occur either (1) when the pore water pressure of the specimen reaches the confining stress (100 kPa), i.e., when the excess pore pressure ratio r_u becomes equal to 1, or (2) when a 5% double amplitude strain (±2.5% axial strain) is reached, whichever happens first. The excess pore pressure ratio r_u is calculated by the following equation,

$$r_u = \frac{\Delta u}{\sigma_c'}$$

where Δu represents the pore pressure increment (kPa), and σ_c' the initial effective confining pressure (100 kPa in this study).

Table 5.1 shows the properties of the untreated samples and the number of cycles necessary to initiate liquefaction (N_L) based on the two above-mentioned criteria. In this study, the r_u = 1 criterion is reached faster than the 5% double amplitude strain criterion in most cases. There seems to be no difference, or little difference, in most cases, between the N_L derived from the two criteria (e.g., Fig. 5.1 (b) & (d), Table 5.1).

Fig. 5.1 shows a typical test result of an untreated specimen of MS6.40 sand (with 40% fine content, $D_{r,c}$=0.6, *CSR*=0.25) as an example. It should be noted that there might be some differences between the tests because of the changing factors, e.g., relative density D_r, grain size distribution of the specimen, applied *CSR,* etc. However, there exists some common typical patterns shown in Fig. 5.1.

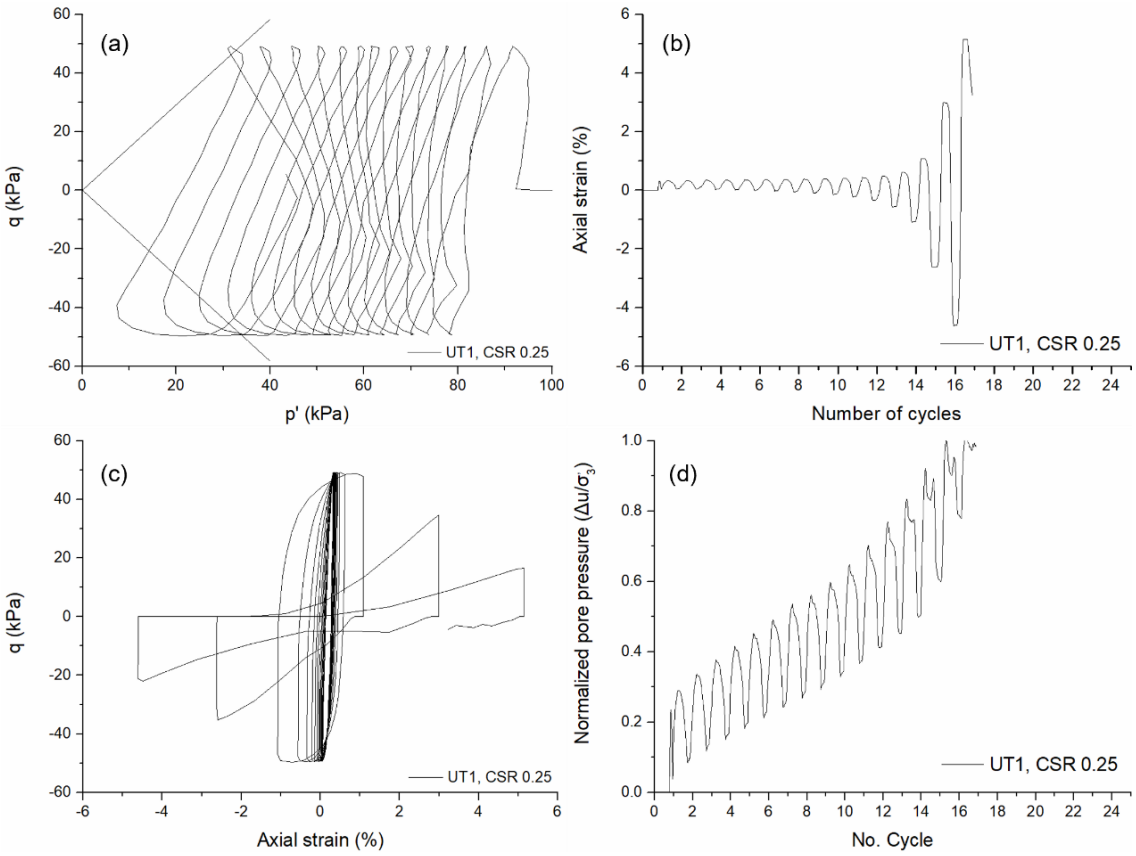

Fig. 5.1 Typical cyclic undrained triaxial test result (MS6.40 UT1)

Table 5.1 Summary of undrained cyclic triaxial tests for the untreated samples

Name of the sample		*B*-value	e_c	$\rho_{d,c}$ (g/cm^3)	$D_{r,c}$ (%)	*CSR*	$^*N_L$ 5% double amplitude strain criterion	$^*N_L$ r_u=1 criterion
MS6.0	UT1	0.99	0.71	1.58	56	0.3	16	18
	UT2	0.98	0.80	1.50	18	0.25	38	39
	UT3	0.96	0.70	1.59	61	0.22	-	320
	UT4 dense	0.94	0.62	1.67	94	0.25→0.5	665	658
	UT5 dense	0.97	0.61	1.67	98	0.5	13	13
	UT6 dense	0.92	0.58	1.71	113	0.4	-	101
MS6.20	UT1	0.9	0.66	1.63	42	0.25	30	30
	UT2	0.94	0.65	1.63	45	0.22	113	106
	UT3	0.98	0.66	1.62	40	0.2	-	593
	UT4 dense	0.97	0.54	1.76	97	0.25→0.4	590	584
	UT5 dense	0.94	0.51	1.79	110	0.4	-	101
MS6.40	UT1	0.9	0.60	1.69	62	0.25	15	15
	UT2	0.9	0.60	1.69	61	0.2	90	89
	UT3	0.9	0.59	1.69	63	0.15	-	217
	UT4 dense	0.93	0.54	1.76	91	0.25	-	120
MS6.60	UT1	0.96	0.63	1.66	37	0.25	13	12
	UT2	0.96	0.61	1.67	44	0.2	118	116
	UT3	0.94	0.63	1.65	36	0.15	654	637
	UT4 dense	0.92	0.53	1.76	79	0.25	-	139
MS6.100	UT1	0.98	0.73	1.56	34	0.25	15	14
	UT2	0.96	0.76	1.54	26	0.2	-	175
	UT3	0.92	0.70	1.59	47	0.17	-	1776
	UT 4dense	0.94	0.59	1.70	87	0.25	-	120

The index c represents the values after consolidation of the specimens

$^*N_L$: number of cycles to liquefaction

-: test stopped without reaching 5% double amplitude strain (±2.5% axial strain)

In Fig. 5.1 (a), when the loading goes on, the effective stress decreases due to pore water pressure build-up. In Fig. 5.1 (b), the axial strain slowly accumulates at the beginning of the test. After reaching around ±0.5%, the axial strain starts to increase rapidly and reaches ±2.5% strain in 2-3 cycles. In Fig. 5.1 (d), the excess pore pressure accumulates steadily with round peaks. After reaching r_u = 0.5, the excess pore pressure grows faster, and the peaks become sharper. When the axial strain exceeds ±0.5%, the increase in excess pore pressure speeds up towards the initiation of liquefaction, and the peaks become irregular. In this study, the applied stresses are constantly controlled with reasonable accuracy. We can observe in Fig. 5.1 (c) that, in the last cycles of the test, the applied cyclic stress decreases. The decrease is caused by the significant softening of the soil under cyclic loading and the difficulty of the loading frame to maintain the same stress associated with large displacements.

5.3 Excess pore pressure generation

Fig. 5.2 shows the *N*-r_u curve of the untreated sand, taking MS6.0 sand as an example. The excess pore pressure generation of the other sands at various *CSR* is similar to that of MS6.0. As shown in Fig. 5.2, when decreasing the *CSR*, the rate of excess pore pressure generation becomes lower. For MS6.0_UT1, the increase in excess pore pressure is rather rapid with a steep slope and liquefaction occurs after 16 cycles due to the large *CSR,* equal to 0.3. For MS6.0_UT2, in accordance with (Georgiannou & Konstadinou, 2014), there seems to be a three-stage development in the *N*-r_u curve. At first, for *CSR* = 0.25 (curve in black), the excess pore pressure increases rapidly with a decreasing slope, to around 0.3 in the first cycles. The decreasing slope is due to the adaption of the soil to the cyclic load. Then, the curve continues to increase in a relatively stable way to a 0.5 excess pore pressure ratio. Finally, the excess pore pressure ratio reaches 1 in the last cycles, with a rapid increase and an increasing slope. The increasing slope is due to the softening of the sand. In the case of MS6.0_UT3 (in blue), the three-stage development is more obvious, and the curve is S-shaped. More cycles are needed for each stage.

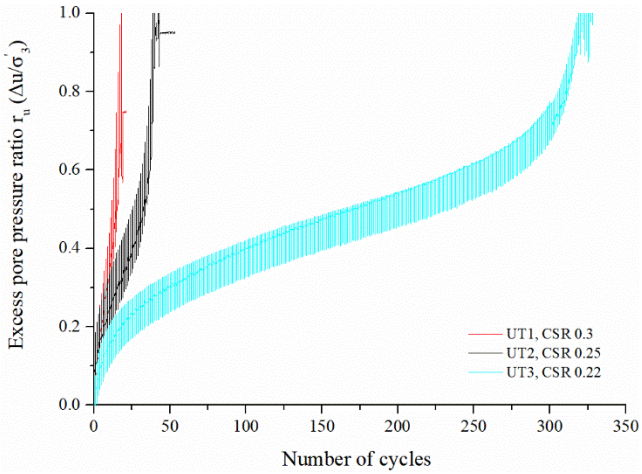

Fig 5.2 Excess pore pressure ratio changes with number of cycles at various *CSR* of loosely prepared specimens of MS6.0

Fig. 5.3 shows the excess pore pressure ratio (r_u) versus the normalized number of cycles (*Normalized N*) for the various sands. The r_u used in all the *Normalized N*-r_u diagrams is the maximum r_u in each cycle. Modeling is based on the upper value of the excess pore pressure. *Normalized N* is calculated by dividing the cycle number (*N*) by the number of cycles required to reach liquefaction (N_L). In Fig.5.3, in accordance with Fig. 5.2, when the CSR decreases, the excess pore pressure ratio of all the sands evolves from an almost linear shape to more and more obvious S-shapes. For instance, under the high *CSR* value of 0.25, the shape of the *Normalized N*-r_u curves of MS6.40_UT1 and MS6.60_UT1 is almost linear. At an intermediate *CSR*, MS6.0UT1, MS6.0_UT2, MS6.20_UT1 and MS6.100_UT2 show a transitional shape. Under a *CSR* lower than

0.22, the samples MS6.0_UT3, MS6.20_UT2, MS6.20_UT3, MS6.40_UT2, MS6.40_UT3, MS6.60_UT2, MS6.60_UT3, MS6.100_UT2 and MS6.100_UT3 feature a clear S-shape.

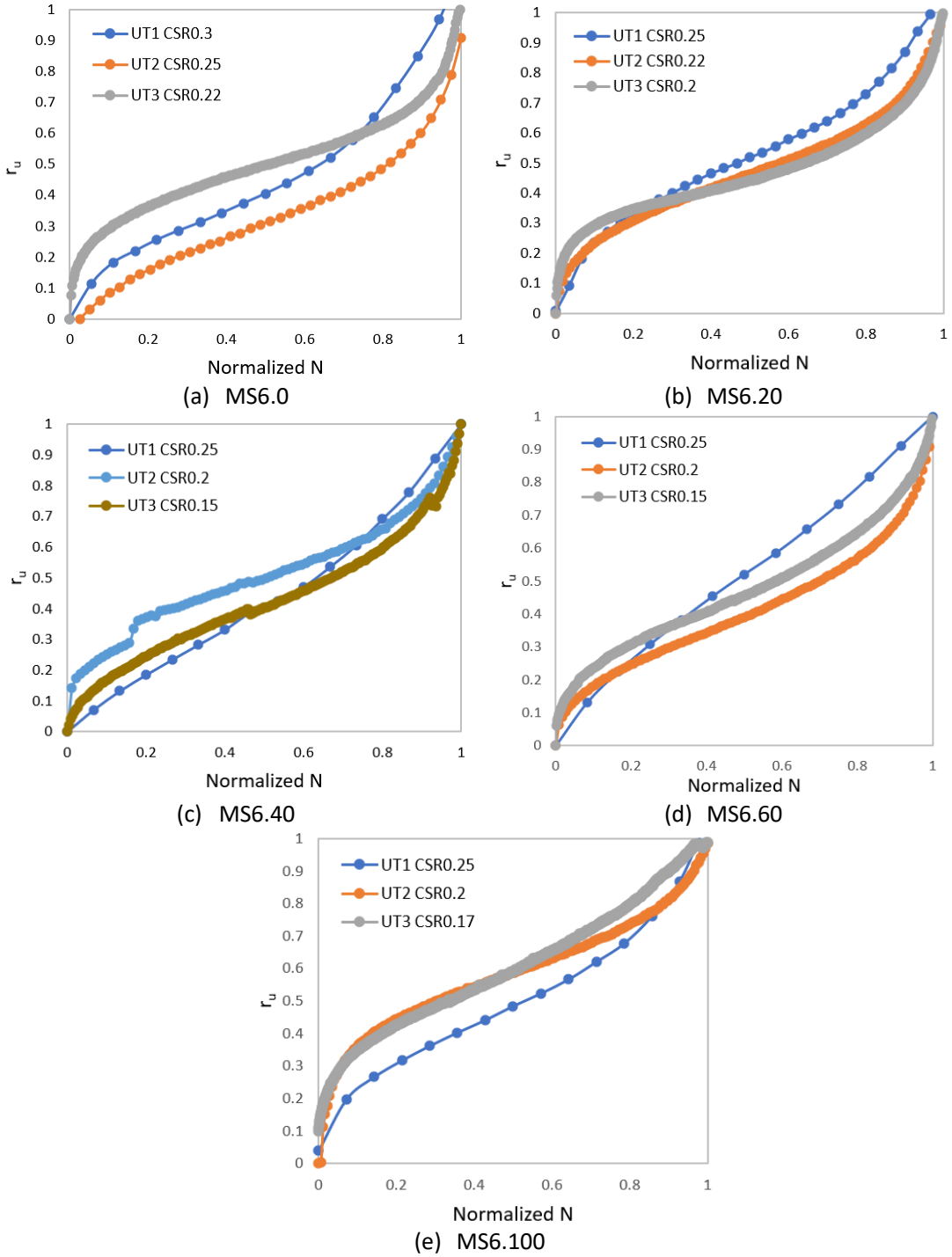

Fig. 5.3 Excess pore pressure ratio (r_u) versus normalized number of cycles (*Normalized N*) for the various loose sands under several *CSR*

To better understand and predict the pore water pressure generation, the results of the triaxial tests were fitted using Seed Model (Seed, Martin, & Lysmer, 1975). The r_u and *Normalized N* data of the untreated specimens at *CSR* = 0.25 are selected for this analysis. The equation is as follows,

$$r_u = \frac{1}{2} + \frac{1}{\pi}\sin^{-1}\left(2 \times \left(\frac{N}{N_L}\right)^{1/\alpha} - 1\right)$$

Curve fitting results are shown in Figs. 5.4 & 5.5. The dots represent the experimental data of the triaxial tests, and the lines represent the results of the simulation. The related parameters and α values are given in Table 5.2. The *SSE* (Sum of squared errors) is equal to the sum of the squares of the differences between the real data and the fitted values. *SSE* values close to 0 mean that the difference between the real data and the fitted value is small, i.e., that the fitting is good. The closer to 1 the R^2 value, the better the equation.

Table 5.2 shows that, according to *SSE* values and R^2 values, the pore pressure generation in the untreated specimens is well simulated by Seed Model. For MS6.0_UT2 and MS6.40_UT4_dense, the result is relatively less good than for the other samples. For all the untreated specimens, the simulated results feature *SSE* values lower than 0.04 and R^2 values larger than 0.97, except for MS6.0_UT2 (0.96) and MS6.40_UT4_dense (0.94). In Figs. 5.4 & 5.5, one can clearly see that the model captures well the shape of the curves, except for MS6.0_UT2 and MS6.40_UT4_dense. The curvature of the fitting curves for these two specimens is relatively far from the real data. For instance, the input data in the early stage of MS6.0_UT2 and MS6.40_UT4_dense show that r_u increases with a decreasing slope, whereas the corresponding simulation result show a stable increasing trend. When $r_u > 0.35$, the curvature of the real data is larger than that of the simulated data. Thus, larger SSE values and R^2 values are seen for these 2 specimens. The difference is caused by the fact that the shape of MS6.0_UT2 and MS6.40_UT4_dense is far from an S-shape, while the Seed Model captures well the S-shapes.

Table 5.2 Results of curve fitting (untreated one-stage tests) using Seed Model (1975)

Name	FC	$D_{r,c}$	α	95% confidence bounds	SSE	R^2
MS6.0_UT2	0	18	0.4739	(0.4412, 0.5065)	0.0735	0.9647
MS6.20_UT1	20	42	0.9413	(0.9047, 0.9779)	0.0135	0.9922
MS6.40_UT1	40	62	0.6895	(0.6294, 0.7496)	0.0160	0.9877
MS6.60_UT1	60	37	1.0390	(0.8753, 1.204)	0.0297	0.9734
MS6.100_UT1	100	34	0.7921	(0.7425, 0.8417)	0.0070	0.9926
MS6.40_UT4	40	91	0.4753	(0.4548, 0.4958)	0.2852	0.9429
MS6.60_UT4	60	79	1.7140	(1.701, 1.727)	0.0097	0.9982
MS6.100_UT4	100	87	0.9483	(0.9336, 0.963)	0.0365	0.9946

**SSE*: Sum of squared errors (*SSE*), is calculated by the sum of squares of differences between the real data and corresponding fitting values

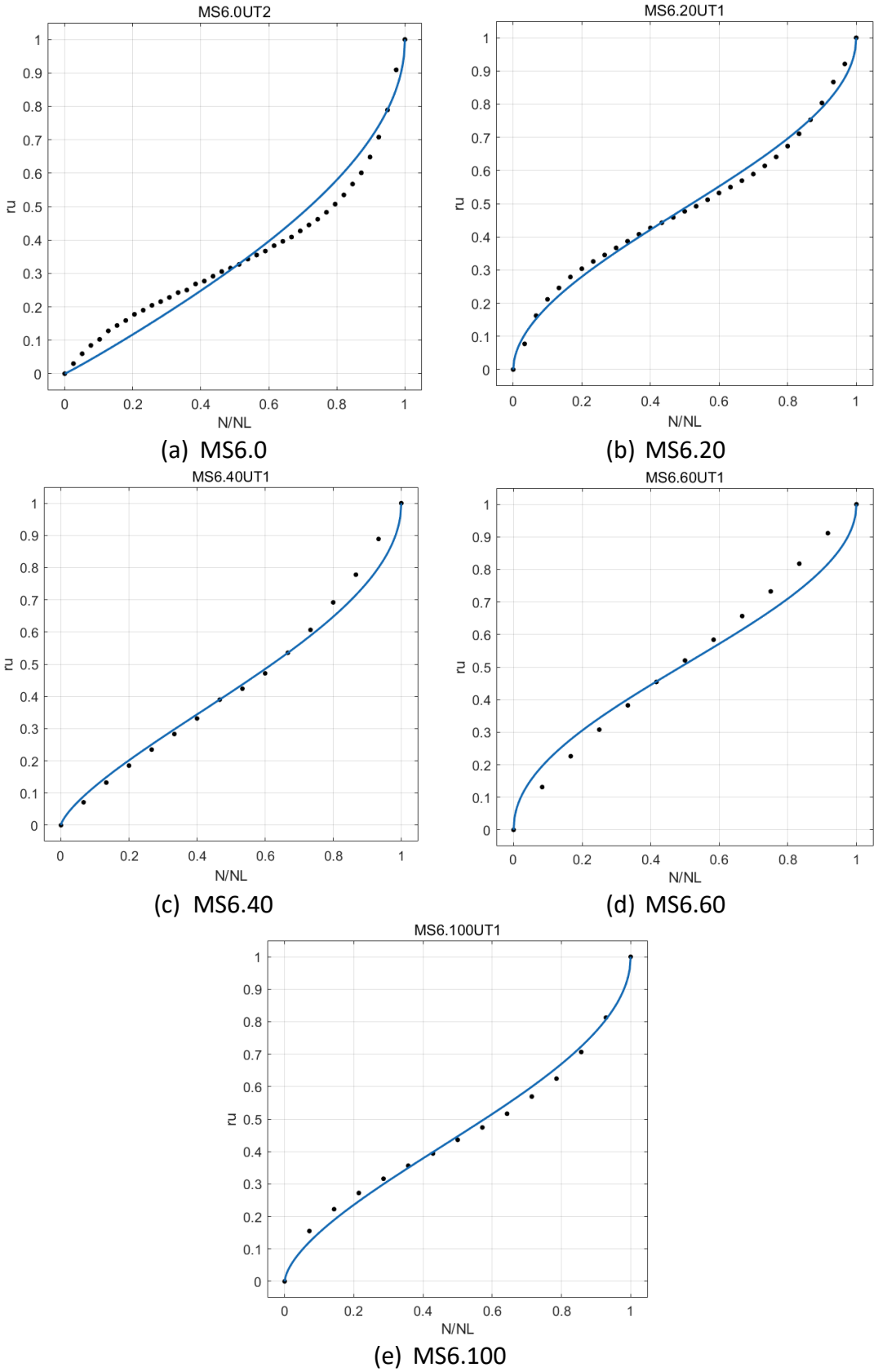

(a) MS6.0 (b) MS6.20

(c) MS6.40 (d) MS6.60

(e) MS6.100

Fig. 5.4 Curve fitting of excess pore pressure (r_u) as a function of normalized number of cycles (normalized N) for the various loose sands at CSR=0.25 (dots: input data, lines: simulated data)

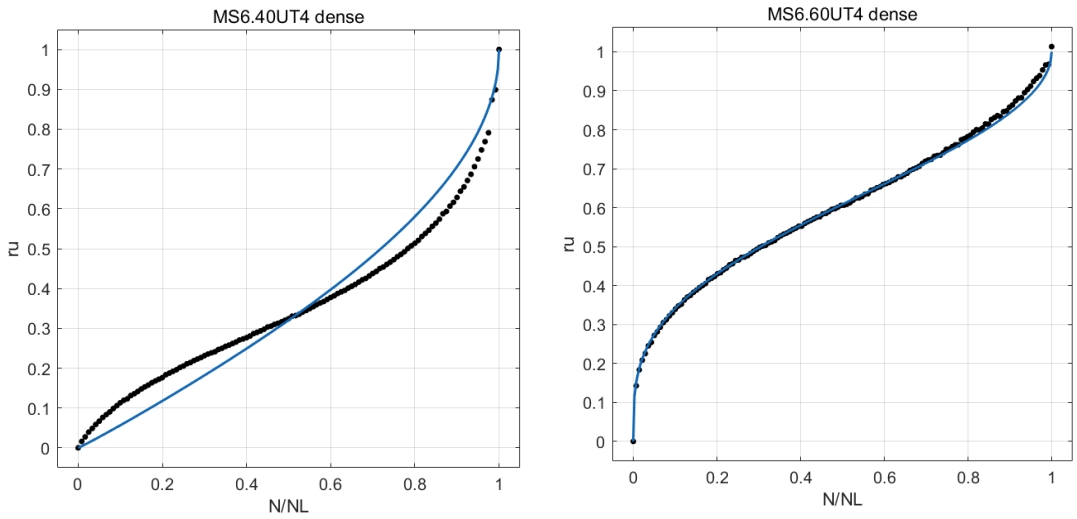

(a) MS6.40 (b) MS6.60

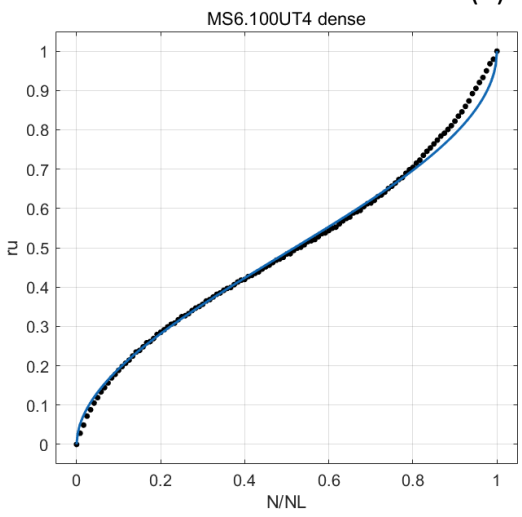

(c) MS6.100

Fig 5.5 Curve fitting of excess pore pressure (r_u) as a function of normalized number of cycles (*Normalized N = N/N$_L$*) for the various dense sands at *CSR*=0.25 (dots: input data, lines: simulated data)

5.4 Liquefaction curves (CSR vs. N$_L$)

Curves of *CSR* as a function of the number of cycles to liquefaction (N_L) are shown in Fig. 5.6. The upper curve corresponds to the sand with the largest cyclic resistance. As shown by many researchers, the number of cycles to the initiation of liquefaction decreases with increasing applied *CSR*. In this study, the largest cyclic resistance is obtained for MS6.0, and it decreases from MS6.0 to MS6.20, MS6.100, MS6.60 and MS6.40, in sequence. To give a quantitative relationship between the applied *CSR* and N_L, exponential functions were derived from (Idriss & Boulanger, 2008) equation for the untreated samples :

$$CSR = a \times N^{-b}$$

where *a* represents the *CSR* required to reach liquefaction in 1 cycle, *b* is a parameter associated with the nature of the soil. Fitting is done for each sand, but a general fitting

is also done for all the sands. It should be noted that extrapolations are made when needed. For example, a final point for $N_L \geqslant 10000$ was added for each sand to obtain a more realistic shape of the curves. Values of *a*, *b* and R^2 are shown in Table 5.3.

For each sand, all the R^2 values of each equation are larger than 0.95, which manifests a well-defined statistical relationship between *CSR* and N_L. The parameters *a* (0.32-0.36) and *b* (0.08-0.14) vary little from one sand to another. For the general fitting of all the sands, the R^2 value is smaller (0.82), due to the differences between the sands.

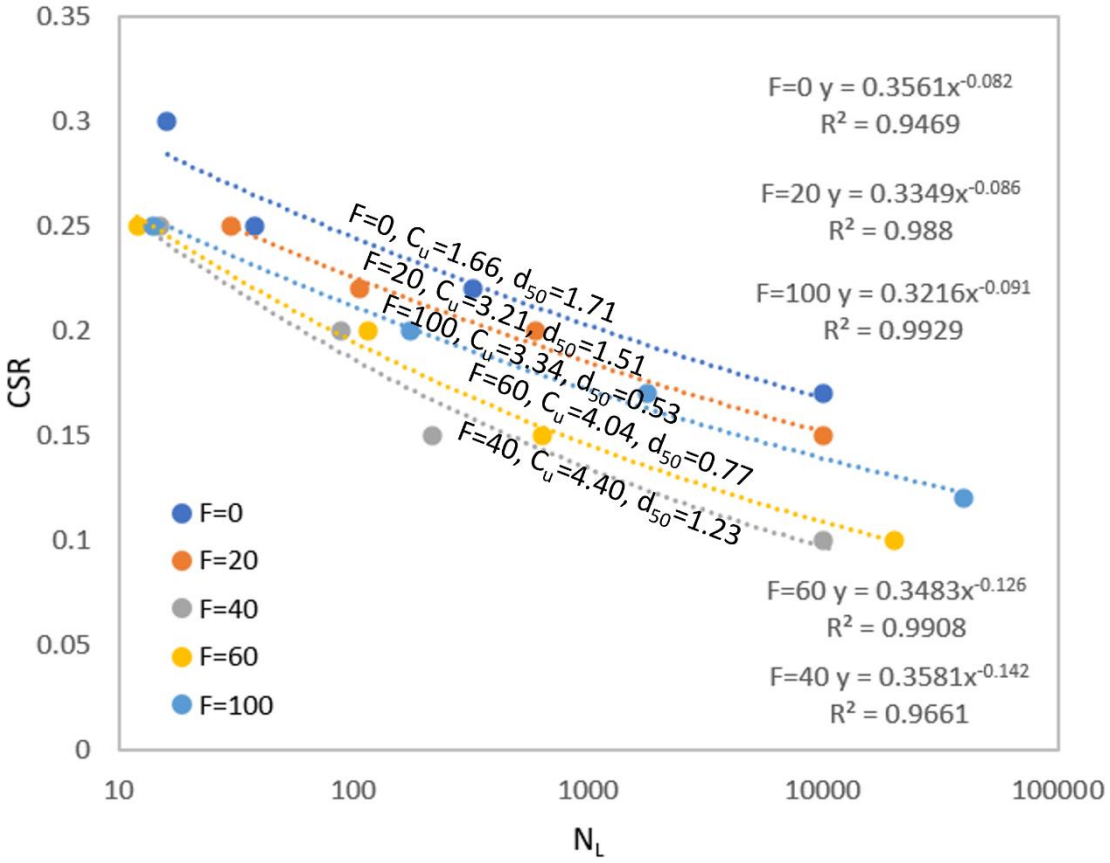

Fig. 5.6 *CSR* versus N_L for the various untreated sands

Table 5.3 Results of the curve fitting (*CSR* vs. N_L) of untreated specimens using (Idriss & Boulanger, 2008) equation

Sand	Fines content (%)	*a*	(-*b*)	R^2	C_u	C_c	d_{50}
MS6.0	0	0.3561	-0.082	0.95	1.66	0.93	1.71
MS6.20	20	0.3349	-0.086	0.99	3.21	1.51	1.51
MS6.40	40	0.3581	-0.142	0.97	4.40	0.98	1.23
MS6.60	60	0.3483	-0.126	0.99	4.04	1.14	0.77
MS6.100	100	0.3216	-0.091	0.99	3.34	1.32	0.53
All sands	-	0.3442	-0.1036	0.82	-	-	-

5.5 Effect of grain size distribution

In spite of the many studies carried out during years, the effect of grain size distribution on cyclic resistance is still controversial. Parameters associated with grain size distribution, i.e., C_u, C_c, d_{50} and the fine content (and also the transitional fines content *TFC*) are chosen for the analysis in this chapter, based on the literature review in Chapter 1. The influence of these parameters on the cyclic resistance, for example, the positions and shapes of the N_L-*CSR* curves (Fig. 5.6) are discussed. The positions and shapes of the N_L-*CSR* curves are reflected by the parameters (later defined $a_{b=0.1036}$ and *b*) in the fitting equation ($CSR = a \times N^{-b}$).

Table 5.3 shows that *a* values are independent of C_u, C_c, d_{50} and the fine content, and *b* values are independent of C_c. To eliminate the effect of curvature of the N_L-*CSR* curves on *a* values, the *b* value was fixed at 0.1036 (i.e., the *b* value of the general fitting line for all the sands), and the corresponding values of *a* ($a_{b=0.1036}$) were calculated. This procedure leads to values of $a_{b=0.1036}$ equal to 0.3928, 0.3664, 0.3045, 0.3144 and 0.3418 for MS6.0, MS6.20, MS6.40, MS6.60 and MS6.100, respectively. The corresponding R^2 values are 0.91, 0.94, 0.89, 0.97 and 0.97, respectively.

CSR_{100} represents the *CSR* required to obtain liquefaction in 100 cycles. CSR_{100} values are extrapolated by using the exponential functions obtained in paragraph 5.4. Similar extrapolations are available in literature (Monkul et al., 2021).

Relationships between *b* or $a_{b=0.1036}$ values and C_u are shown in Figs. 5.7 & 5.8 (a). Cyclic resistance depends on the C_u values of the sands. C_u values affect not only the position of the *CSR*-N_L curve, but also the curvature of the curve. The larger the C_u value, the smaller the cyclic resistance, the more susceptible to liquefaction the sand. This can be seen in Fig. 5.6, where the largest C_u value of the sands corresponds to the lowest and left-handed position of the curve, representing the lowest cyclic resistance. The larger the C_u values, the larger the curvature. This is reflected by the increase in *b* values with increasing C_u values in Fig. 5.6. As shown in Table 5.3, for the studied sands, the *b* values are similar when the C_u values are similar. For example, *b* values are equal to 0.086 and 0.091 for MS6.20 (C_u=3.21) and MS6.100 (C_u=3.34). The *b* values are equal to 0.142 and 0.126 for MS6.40 (C_u=4.40) and MS6.60 (C_u=4.04). The parameter $a_{b=0.1036}$ decreases with increasing C_u. This corresponds to the location of the N_L-*CSR* curves with changing C_u. That is to say, the larger the C_u, the smaller the *CSR* needed to initiate liquefaction. The effect of C_u in this study is contrary to the findings of (Yilmaz et al., 2008) who did not observe a relationship between C_u and the cyclic resistance.

Relationships between *b* or $a_{b=0.1036}$ values and d_{50} are shown in Figs. 5.7 & 5.8 (b). For d_{50} < 1 mm, the cyclic resistance decreases with increasing d_{50}. When d_{50} is comprised between 1-2 mm, the cyclic resistance increases with increasing d_{50}. When d_{50} < 1 mm, the b values increase while $a_{b=0.1036}$ values decrease with increasing d_{50}. When d_{50} is between 1-2 mm, the b values decrease while $a_{b=0.1036}$ values increase with increasing d_{50}.

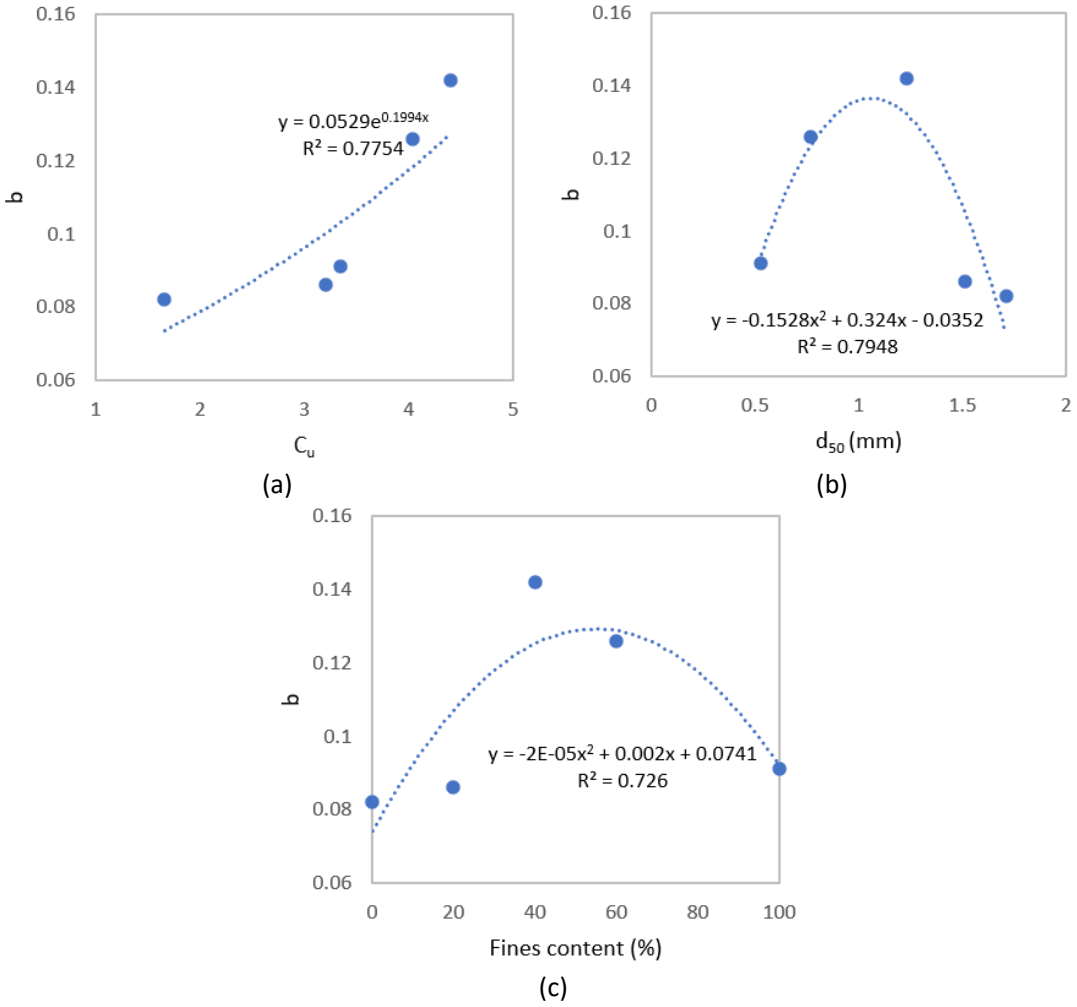

Fig. 5.7 *b* values as a function of (a) C_u, (b) d_{50} and (c) fine content (%)

Figs. 5.7 (c) and 5.8 (c) show how *b* and $a_{b=0.1036}$ values change with the fine content. Fig. 5.9 shows the relationship between the CSR_{100} values and the fine content (%) of the sand. When the fine content is lower than the "transitional fine content" (*TFC* = 50%, refer to Chapter 2), the cyclic resistance decreases when the fine content increases. When the fine content is larger than the *TFC*, the cyclic resistance increases with the fine content. When the fine content is less than the *TFC*, the b values increase with the fine content, whereas the $a_{b=0.1036}$ and CSR_{100} values decrease with an increasing fine content. When the fine content is larger than the *TFC*, the *b* values decrease with an increasing fine content, whereas the $a_{b=0.1036}$ values increase with the fine content. These results are consistent with those of (Xenaki & Athanasopoulos, 2003; Ueng et al., 2004; Papadopoulou & Tika, 2008).

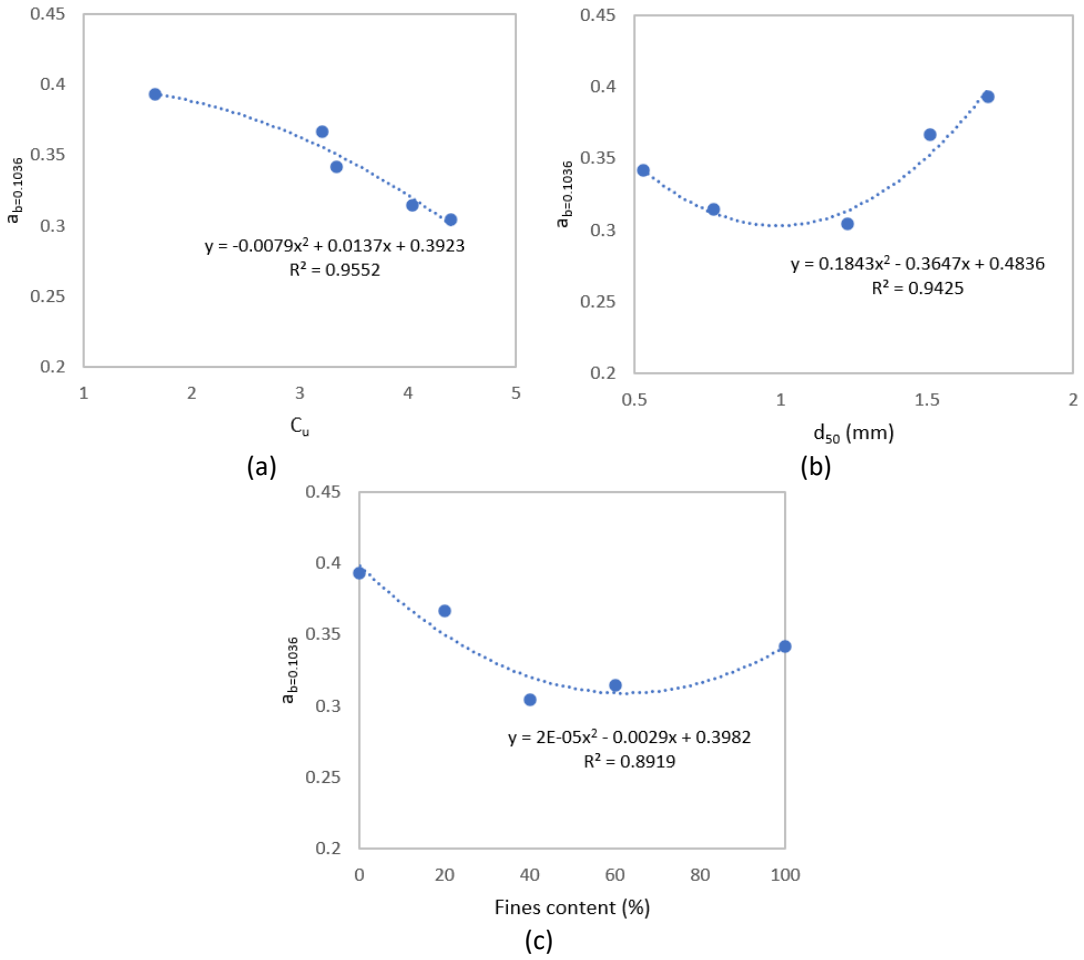

Fig. 5.8 $a_{b=0.1036}$ values as a function of (a) C_u, (b) d_{50} and (c) fine content (%)

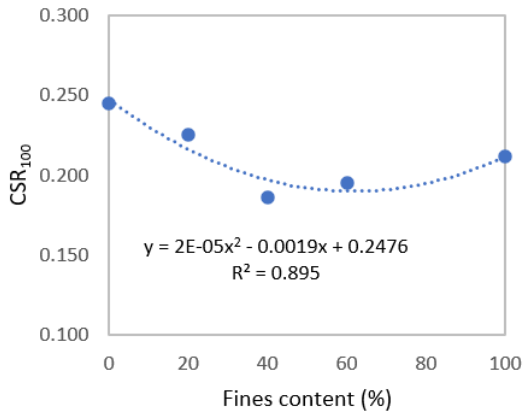

Fig. 5.9 CSR_{100} changes with fine content (%)

5.6 Axial strain accumulation

In the following sections (§ 5.6 to 5.8), we will consider both *mono-stage* cyclic tests (as in the previous paragraphs) and *multi-stage* tests. Indeed, in the case of dense or semi-dense specimens, liquefaction could not always be obtained under the standard initial loading conditions (CSR = 0.25), even after a large number of cycles. To avoid having to carry out a large number of tests, multi-stage tests were performed under the following conditions:

- A first loading stage with CSR = 0.25, up to a maximum of 300 cycles
- Then a loading with CSR = 0.30, up to a maximum of 100 cycles,
- Then a loading with CSR = 0.35, up to a maximum of 100 cycles,
- etc.

Fig. 5.10 shows the axial strain accumulation versus the number of cycles for MS6.0 and MS6.40, chosen as examples. In general, it is accepted that the rate of axial strain accumulation increases with the *CSR*. For example, in Fig. 5.10, the smaller the *CSR*, the greater the number of cycles needed to reach the same amplitude of axial strain.

Untreated loose samples always show a two-side compression and extension strain. After reaching 0.5 % of axial strain, for untreated samples, the amplitude of axial strain in each cycle increases rapidly. 5% axial strain are obtained in the last cycles of loadings.

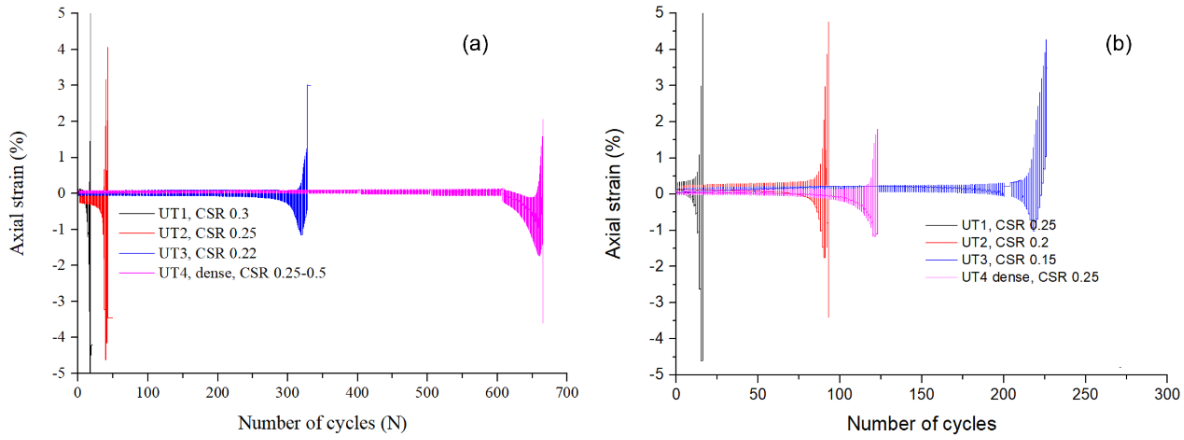

Fig. 5.10 Axial strain versus number of cycles (a) MS6.0 & (b) MS6.40

Let us consider the axial strain amplitude $\delta\varepsilon_1$ of each cycle, which represents the amplitude of the axial strain (contractive and extensive) for each cycle. It is calculated by the following equation,

$$\delta\varepsilon_1 = \varepsilon_{1max,i} - \varepsilon_{1min,i}$$

where $\varepsilon_{1max,i}$ represents the maximum (contractive) axial strain in cycle i, and $\varepsilon_{1min,i}$ represents the absolute value of the minimum axial strain in cycle i.

Fig.5.11 shows the deformation characteristics of MS6.0. The other sands follow

a similar trend. One can see that, when r_u = 1, the larger the *CSR*, the larger the deformation of the specimen. Decreasing *CSR* can decrease the amplitude and rate of deformation. For example, in Fig. 5.11, for the loose specimens MS6.0_UT1, UT2 and UT3, when r_u = 1, for *CSR*=0.3, 0.25 and 0.22, $\delta\varepsilon_1$ are around 9, 8 and 2%, respectively. At the end of the cycles, the slopes of the curves decrease when the *CSR* increases.

Increasing density can decrease the amplitude and rate of deformation. In the same way as for loose samples, decreasing the CSR can decrease the amplitude and rate of deformation of dense samples. For example, in Fig. 5.11, for the dense specimens MS6.0_UT5 and UT6 subjected to one-stage cyclic tests, when r_u = 1, $\delta\varepsilon_1$ is around 3% for *CSR* = 0.5, and 2% for *CSR* = 0.4. For the multi-stage dense specimen MS6.0_UT4, $\delta\varepsilon_1$ (around 2%) is almost same as for the one-stage MS6.0_UT6. The axial strain amplitudes of dense specimens are smaller than those of loose specimens. After reaching a $\delta\varepsilon_1$ around 0.5%, the rate of increase of $\delta\varepsilon_1$ is smaller for the dense samples than for the loose samples. This can be verified in Fig. 5.11 by observing the smaller slopes of dense specimens at the end of the cycles, compared to those of loose specimens. More cycles are needed for dense specimens to liquefy compared to loose specimens.

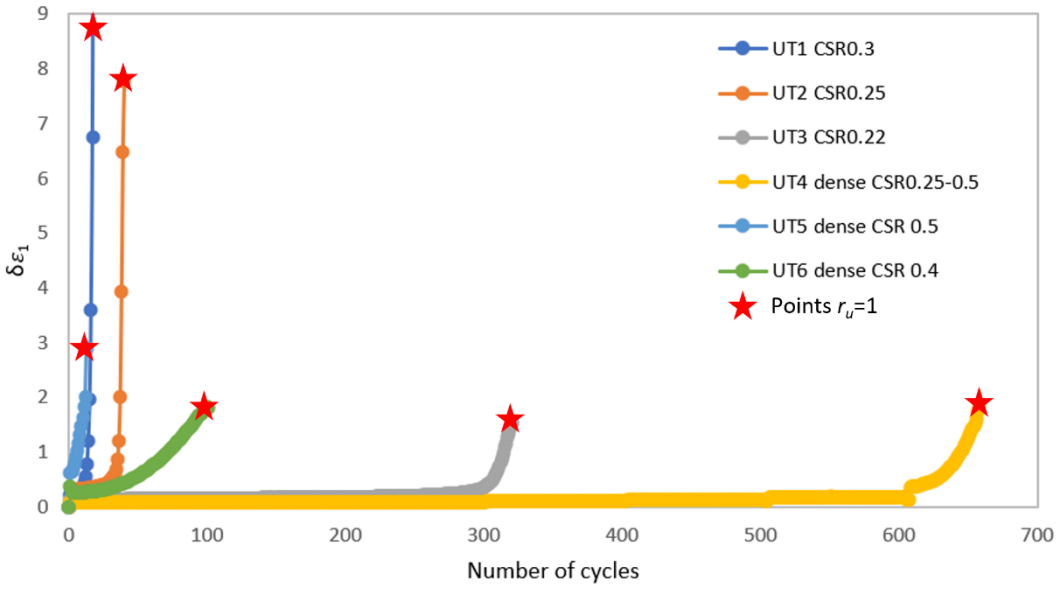

Fig. 5.11 Deformation characteristics of MS6.0: Axial strain amplitude $\delta\varepsilon_1$ vs. Number of cycles

5.7 Effect of soil density

It is generally accepted that cohesionless loose soils are more susceptible to liquefaction than cohesive soils. In addition, densification can enhance the cyclic resistance. Figure 5.12 shows the excess pore pressure ratio (r_u) and axial strain (ε_1) accumulation as a function of the number of loading cycles (*N*) for the various soils prepared in loose and dense states. In general, in line with the expectations, loose specimens are much more susceptible to liquefaction, and the rates of accumulation

of excess pore pressure and axial strain are more rapid than in dense specimens. The result of this increase in cyclic resistance with density is more remarkable in the specimens with the coarsest grains (MS6.0 and MS6.20). For these soils, loose samples liquefy at 30-39 cycles under 0.25 *CSR*. Corresponding dense samples do not liquefy at 0.25 *CSR*, but only when increasing the applied *CSR* to 0.4-0.5. When the fine content is larger than 40 % (i.e., MS6.40, MS6.60, MS6.100), differences in the cyclic resistance between loose and dense specimens among different soils are similar. Under 0.25 *CSR*, the loose specimens liquefy at around 12-15 cycles and the dense specimens liquefy at around 120-135 cycles.

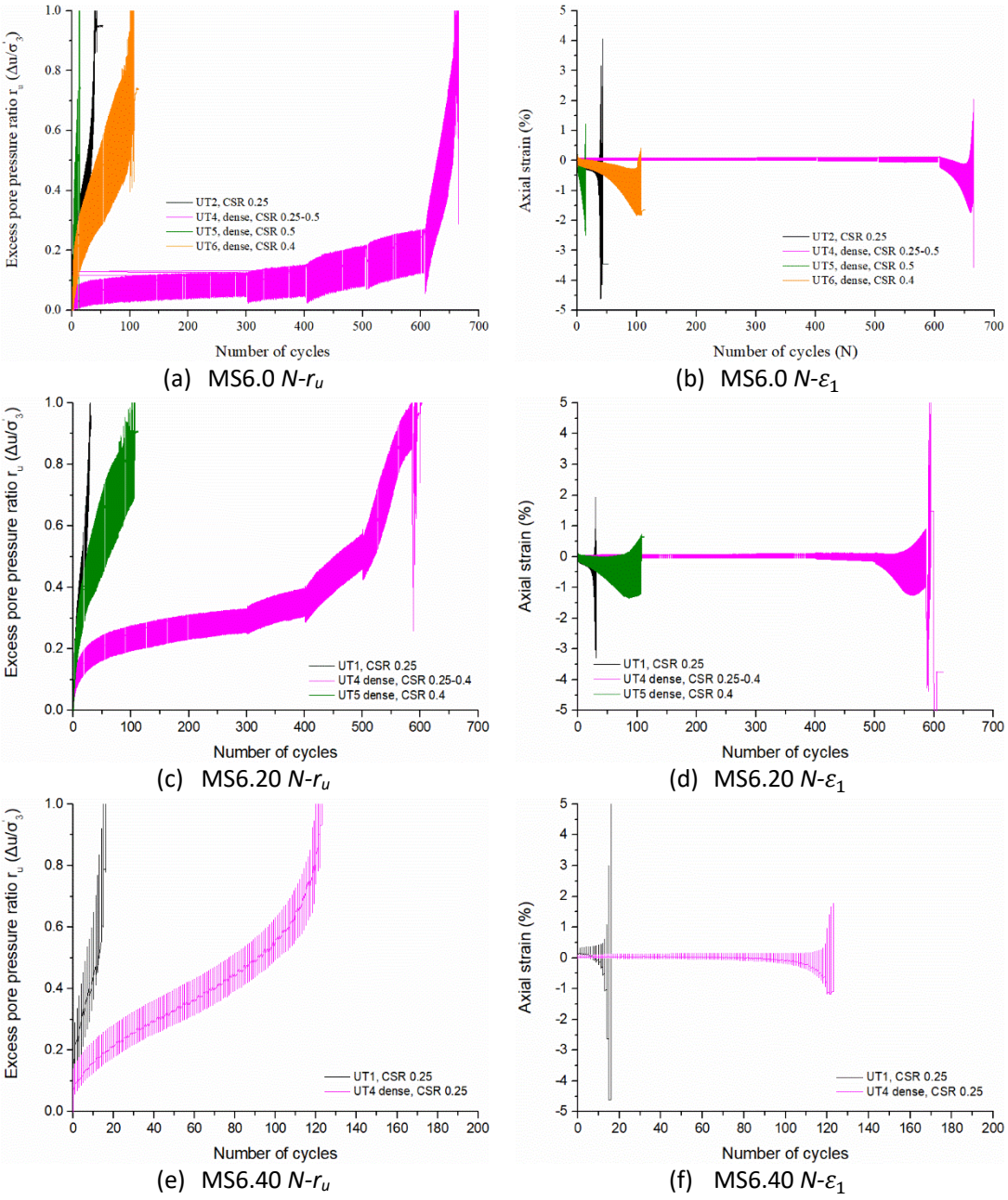

(a) MS6.0 *N*-r_u (b) MS6.0 *N*-ε_1

(c) MS6.20 *N*-r_u (d) MS6.20 *N*-ε_1

(e) MS6.40 *N*-r_u (f) MS6.40 *N*-ε_1

Fig. 5.12 Comparison of the results of cyclic undrained triaxial tests on dense and loose untreated sands

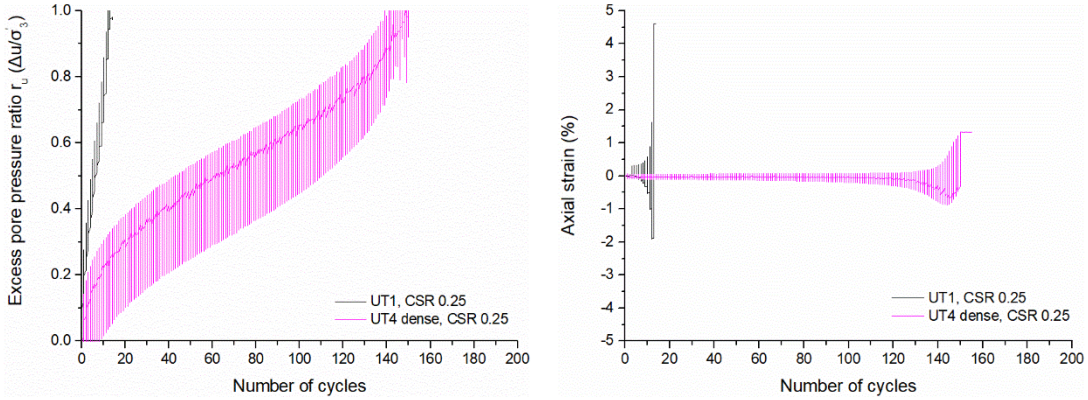

(g) MS6.60 N-r_u

(h) MS6.60 N-ε_1

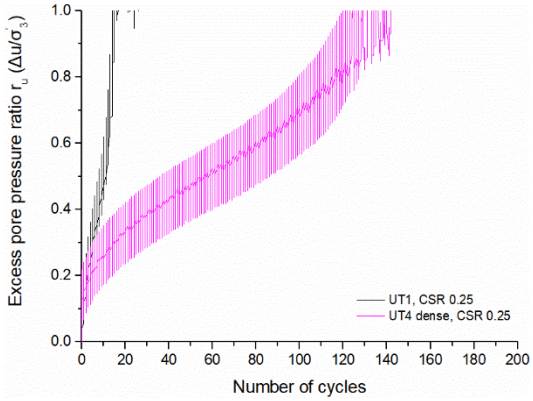

(i) MS6.100 N-r_u

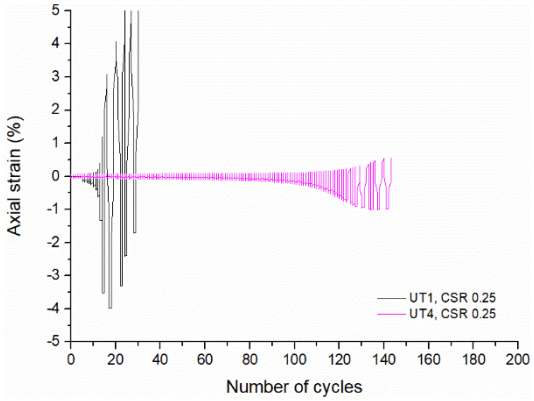

(j) MS6.100 N-ε_1

Fig. 5.12 (continued) Comparison of the results of cyclic undrained triaxial tests on dense and loose untreated sands

5.8 Modelling of multi-stage tests

For the specimens that required multi-stage loadings to initiate liquefaction, e.g., the dense specimens MS6.0_UT4 and MS6.20_UT4, one-stage loading tests were also carried out to see the equivalence between the cyclic resistance obtained in multi-stage and one-stage loadings (Figs. 5.12 (a) & (c)). Seed Model has proved efficient to model pore pressure generation in the untreated specimens in this study. For the multi-stage tests, curve fitting using Seed Model is made to give a likely number of cycles required to initiate liquefaction under the maximum applied *CSR*. The data of excess pore water pressure (r_u) for the last stage (i.e., the stage with the maximum *CSR*) are used. For example, the curve fittings for the 2 multi-stage tests MS6.0_UT4_dense and MS6.20_UT4_dense use the maximum r_u in each cycle from cycle 601 (r_u = 0.27) to cycle 658 (r_u = 1) at *CSR* = 0.5, and the maximum r_u from cycle 502 (r_u = 0.57) to cycle 584 cycles (r_u = 1) at *CSR* = 0.4.

Fig. 5.13 shows the fitting curves. Table 5.4 shows the formula used and the values of the parameters. For MS6.0_UT4_dense, the fit is quite good, reflected by R^2 = 0.99. For MS6.20_UT4_dense, the R^2 is lower (0.81) because the initial value of r_u is very high (0.57). Hence, the corresponding α value (2.92) is much larger than the others (0.47-1.71, Table 5.2). For all the tests, when r_u is between 0.45-0.6, the

Normalized N-r_u relationship is quasi-linear, with $R^2 > 0.99$. Hence, an attempt has been made to extrapolate the data of MS6.20 from $r_u = 0.57$ (Fig. 6.13 (a)) to $r_u = 0.45$ (Fig. 5.13 (b)) based on the slope of $r_u = 0.57$-$r_u = 0.60$. The R^2 value (0.83) is a little bit improved, and the α value (1.85) becomes equivalent to the others.

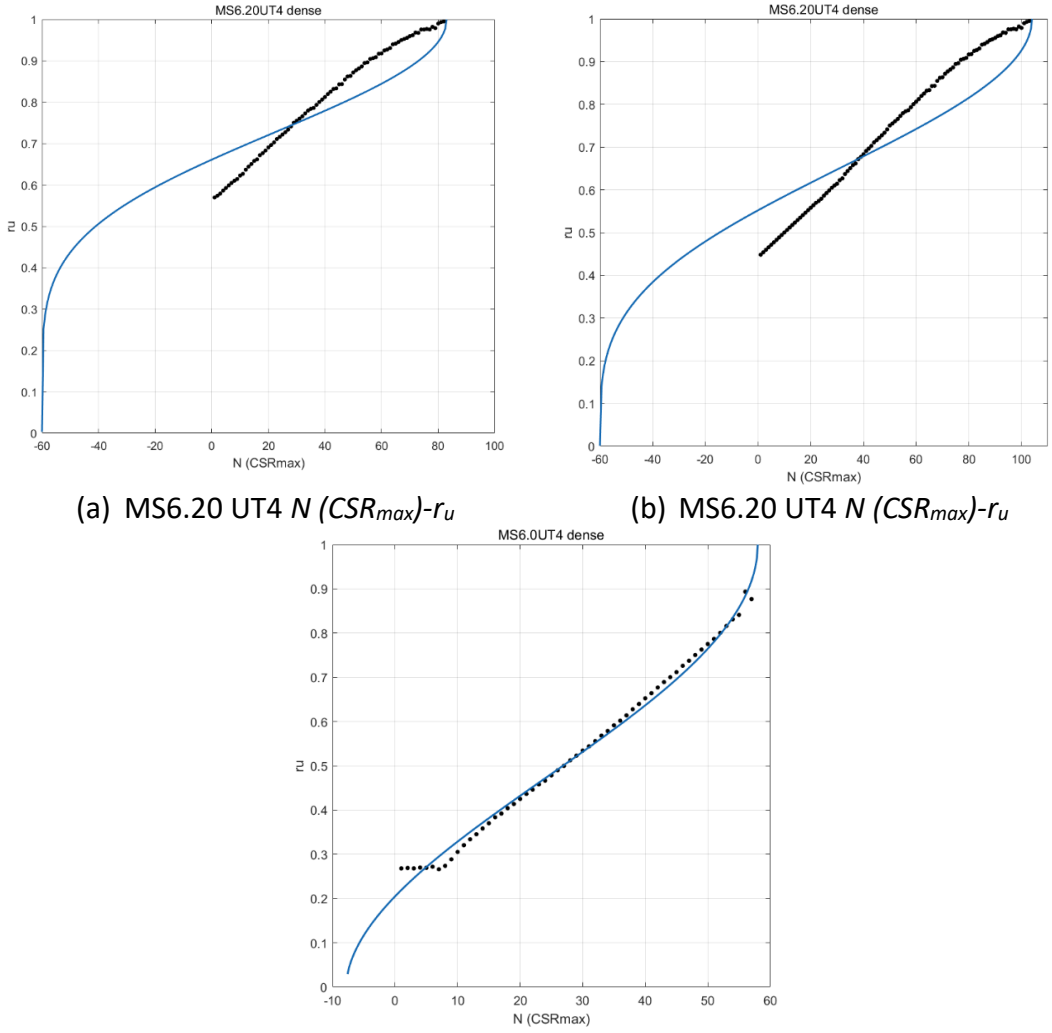

(a) MS6.20 UT4 *N (CSR_{max})-r_u* (b) MS6.20 UT4 *N (CSR_{max})-r_u*

(c) MS6.0_UT4 *N (CSR_{max})-r_u*

Fig. 5. 13 Extrapolation of the pore water pressure generation of multi-stage tests. Black points represent the real data; blue lines represent the simulation results

Table 5.4 Formula and fitting parameters of the multi-stage tests of untreated specimens

Name of the test	Fitting formula	α	β	R^2
MS6.0UT4 dense	$r_u = \frac{1}{2} + \frac{1}{\pi}\sin^{-1}\left(2 \times \left(\frac{\beta + N}{\beta + 58}\right)^{1/\alpha} - 1\right)$	0.925	7.82	0.99
MS6.20UT4 dense	$r_u = \frac{1}{2} + \frac{1}{\pi}\sin^{-1}\left(2 \times \left(\frac{\beta + N}{\beta + 83}\right)^{1/\alpha} - 1\right)$	2.916	60	0.81
MS6.20UT4 dense extension	$r_u = \frac{1}{2} + \frac{1}{\pi}\sin^{-1}\left(2 \times \left(\frac{\beta + N}{\beta + 104}\right)^{1/\alpha} - 1\right)$	1.854	60	0.83

*β: NL=$N_L = \beta + N_{data}, N = [1, 2, 3 \ldots N_{data}]$

For MS6.0 (Table 5.1), in one-stage tests, the dense specimens liquefy at either

13 cycles for *CSR* = 0.5 (MS6.0_UT5 dense) or 101 cycles for *CSR* = 0.4 (MS6.0_UT6_dense). In multi-stage tests, the maximum applied *CSR* is 0.5 (MS6.0_UT4_dense). The number of cycles to liquefaction inferred from this procedure is 66. In the one-stage test, the dense sample MS6.20_UT4_dense liquefies after 101 cycles under 0.4 *CSR*. In the multi-stage test, the maximum applied *CSR* is 0.4. The number of cycles inferred from the procedure are 143 and 164. These results confirm that the cyclic resistance of the specimens in a multi-stage test is more or less equivalent to the cyclic resistance obtained for the same maximum *CSR* - or between the maximum *CSR* and the maximum *CSR* minus 0.1 - applied in a one-stage test.

5.9 Conclusions

For loose specimens,

- When increasing the *CSR*, the rate of excess pore pressure generation becomes lower. With decreasing *CSR*, excess pore pressure generation of all the sands evolves from an almost linear shape to a more and more obvious S-shape.
- The number of cycles to the initiation of liquefaction decreases with increasing applied *CSR*. Exponential functions ($CSR = a \times N^{-b}$) are given with $R^2 > 0.95$ to model *CSR* vs. N_L curves. The effect of grain size distribution on the values of the parameters is discussed. The a values are independent of C_u, C_c, d_{50} and the fine content. The *b* values and $a_{b=0.1036}$ are independent of C_c., but are correlated with C_u, d_{50} and *FC* (*TFC*).
- The effect of the grain size distribution on the cyclic resistance is discussed. Cyclic resistance depends on C_u values. When the C_u value increases, the curvature of the *CSR vs.* N_L curve increases, the cyclic resistance of the sand decreases, the sand is more susceptible to liquefaction. C_c seems to have no influence on cyclic resistance. When d_{50} < 1 mm, the cyclic resistance decreases with increasing d_{50}. When d_{50} is between 1-2 mm, the cyclic resistance increases with d_{50}. When the fine content is lower than the TFC (50%), the cyclic resistance decreases with increasing fine content. When the fine content is larger than the TFC (50%), the cyclic resistance increases with the fine content.
- Increasing *CSR* can increase the amplitude and the rate of deformation. The larger the *CSR*, the larger the axial deformation of the specimen when liquefaction happens. Untreated loose samples always feature a two-side compressive and extensive axial strain. After reaching 0.5% of axial strain, the amplitude of the axial strain in each cycle increases rapidly. 5% axial strain is obtained in the last loading cycles.
- Concerning the effect of density, dense specimens are less susceptible to liquefaction than loose specimens. One can see slower pore pressure generation and decrease in the amplitude and rate of deformation in dense specimens. The effect of increasing density on cyclic resistance increase is remarkable in the specimens of sands with higher fine content (MS6.40, MS6.60 and MS6.100). The cyclic resistance enhancement in specimens with the coarsest grains (MS6.0 and MS6.20) is even much more remarkable.

- To better understand and predict the pore water pressure generation mode, curve fitting using Seed Model was carried out for one-stage test (*CSR*=0.25) and multi-stage tests (MS6.0 & MS6.20 dense). Seed Model simulates well the pore pressure generation of all the one-stage tests on the untreated specimens. In most cases, for loose samples, R^2 values > 0.96, α is in the range of 0.5-1. For dense samples, R^2 values > 0.94, α is in the range of 0.9-1.9.
- Based on the cases analyzed in this work, it seems that the *CSR* that leads to liquefaction in less than 100 cycles in multi-stage tests (CSR_{multi}) can be used to approach the *CSR* leading to liquefaction in less than 300 cycles in mono-stage tests (CSR_{mono}). In our results, the CSR_{mono} is comprised between the CSR_{multi} and the (CSR_{multi}–0.1) for the same number of cycles to liquefaction. This equivalence is all the more valid as the pore pressure increase is small at the end of the penultimate stage of the multi-stage test.

Chapter 6 Cyclic behavior of bio-cemented soils

6.1 Introduction

The data concerning the resistance of bio-cemented soils to cyclic loadings are still not sufficient in the literature. The procedure of the cyclic triaxial tests is the same as that for the untreated specimens. At first, a one-stage test at *CSR* = 0.25 with 300 cycles of loading is carried out. In the case of the untreated specimens, all the loose specimens and some of the dense specimens could liquefy under this loading condition. Hence, we used this procedure for treated specimens. If the specimen did not liquefy, to avoid having to carry out a large number of tests, multi-stage tests were performed by increasing the CSR by steps of 0.05, each time for another 100 loading cycles. The multi-stage tests procedure is therefore the following one:

- A first loading stage with CSR = 0.25, up to a maximum of 300 cycles
- Then a loading with CSR = 0.30, up to a maximum of 100 cycles,
- Then a loading with CSR = 0.35, up to a maximum of 100 cycles,
- etc.

The evolution of strains and pore-pressure is measured during the tests. The parameters are mainly:

1. For the solicitation: cyclic stress ratio;
2. For the soil samples: the grain size distribution and density;
3. For the MICP treatment: the cementation level ($CaCO_3$ content)

The objective is to determine the relationship between the pore-pressure or axial strain increase (and, notably, the conditions of liquefaction) and the parameters cited above. Cyclic test results on MICP-treated soils are compared with those on untreated loose and dense soils. Seed model is also used to model the pore pressure generation of both one-stage and multi-stage tests.

6.2 Typical cyclic behavior of treated specimens

The criterion used to determine liquefaction is almost the same as for untreated specimens (§ 6.2). Except in some cases, liquefaction is considered to happen when 5% single amplitude strain is reached. Typical cyclic behavior of treated specimens is shown in Figs. 6.1-6.3. The following paragraphs show the typical cyclic behavior of treated specimens compared to that of loosely prepared untreated specimens. Differences in pore pressure generation and strain development of treated specimens due to various grain size distributions are also mentioned and will be discussed in detail in the following sections.

Table 6.1 shows the properties of the treated specimens. The notations T1, T2 and T3 represent *lightly treated, moderately treated* and *heavily treated* specimens,

respectively. Fig. 6.1 shows typical pore pressure generation and axial strain development of untreated and lightly treated samples of MS6.100 and MS6.0 at the same *CSR* (0.25). The pore pressure generation of the treated samples (Figs. 6.1 (a) & (c)) is slower than that of the untreated samples. In the case of the finest material MS6.100, lightly treated sample T1 liquefies at N_L = 322 cycles, compared to N_L = 14 for the corresponding untreated specimen. In the case of the coarsest sand MS6.0, lightly treated sample T1 liquefies at N_L = 66 and moderately treated sample T2 liquefies at N_L = 300, compared to N_L = 38 for the corresponding untreated specimen. For lightly treated samples, the pore pressure generation either features a similar S-shape as that of untreated sand under a lower *CSR*, e.g., MS6.100_T1 shown in Fig 6.1 (a), or takes a polynomial shape, e.g., MS6.0_T1, as shown in Fig 6.1 (c).

The treated specimens exhibit vastly different deformation characteristics from those of untreated samples (see details in § 6.4). The strain development of the treated samples is slower than that of the untreated ones. When the excess pore pressure ratio r_u reaches 1, the axial strain of the treated samples is smaller than that of the untreated samples. For instance, in Figs. 6.1 (b) & (d), when r_u reaches 1, the axial strain of the treated sample is less than 2%, whereas the axial strain of the untreated samples is around 5%. In the last cycles of loading, the lightly treated sample sometimes shows both contractive and dilative behavior like untreated samples, e.g., MS6.100_T1 shown in Fig.6.1 (b). In other tests, unlike untreated specimens, lightly treated samples show a single-amplitude dilative strain accumulation, e.g., MS6.0_T1 shown in Fig.6.1 (d).

Table 6.1 Properties of MICP-treated specimens

Name of the sample		$CaCO_3$ content (%)	e_c	$\rho_{d,c}$ (g/cm^3)	$D_{r,c}$ (%)	*CSR*	$^*N_L$ (5% double amplitude strain criterion)	$^*N_L$ (r_u=1 criterion)
MS6.0	T1	8.62	0.77	1.53	31	0.25	-	66
	T2	10.06	0.62	1.67	97	0.25	417	300
	T3	11.53	0.58	1.70	110	0.25→0.5	-	700
MS6.20	T2	6.15	0.58	1.70	76	0.25→0.3	411	380
	T3	8.27	0.56	1.74	88	0.25→0.4	-	557
MS6.40	T1	4.5	0.56	1.74	83	0.25	-	134
	T2	5.4	0.57	1.72	77	0.25→0.3	-	355
	T3	7.5	0.54	1.75	90	0.25→0.35	-	494
	T4	8.4	0.51	1.79	105	0.25→0.5	697	677
MS6.60	T1	2.07	0.56	1.73	66	0.25	-	182
	T2	4.17	0.56	1.73	67	0.25→0.35	527	529
	T3	7.24	0.50	1.80	95	0.25→0.5	723	733
MS6.100	T1	1.37	0.67	1.62	57	0.25	-	322
	T2	2.59	0.66	1.62	59	0.25→0.3	-	431
	T3	5.99	0.66	1.63	61	0.25→0.5	678	676

-: test stops when r_u=1, without reaching 5% strain

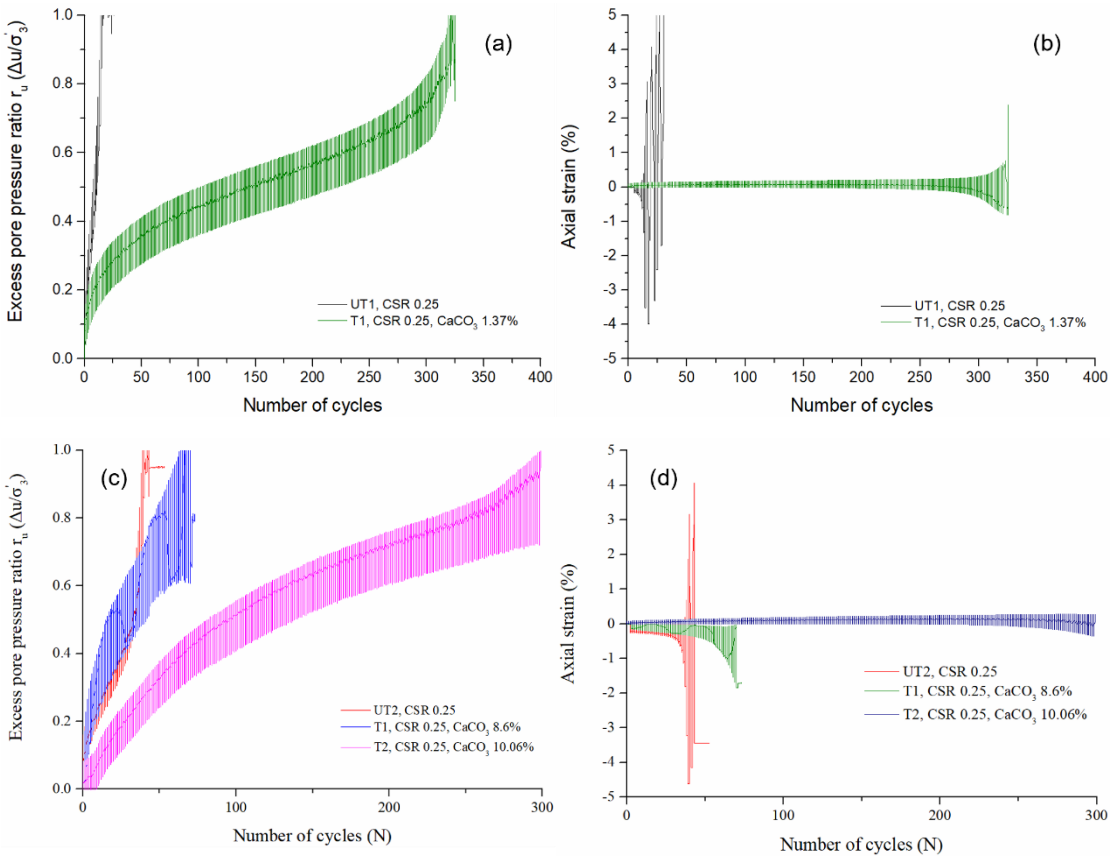

Fig. 6.1 Typical pore pressure generation (a) & (c) and axial strain development (b) & (d), (a) & (b) untreated and lightly treated MS6.100 at *CSR*=0.25; (c) & (d) untreated, lightly treated and moderately treated MS6.0 at *CSR*=0.25

Fig. 6.2 shows typical stress-strain curves and cyclic effective stress paths for untreated and lightly treated specimens of MS6.100. Fig. 6.3 shows the typical stress-strain curves of untreated and lightly treated specimens of MS6.0. In general, compared to untreated samples, the decrease in effective stress and the development of axial strain are slower in the case of treated samples. If we compare Figs. 6.2 (a) & (c) and Figs. 6.3 (a) & (b), we observe that the untreated sand shows obvious softening and is unable to maintain the stress in the last cycles. The treated specimens resist much better and the stress is more or less maintained to the end. Comparing Figs. 6.2 (b) & (d), when loading goes on, the effective stress of the untreated specimen decreases continuously due to pore pressure accumulation, and the decrease in effective stress speeds up in the last cycles. For the treated specimens, the decrease in effective stress in the last cycles remains stable.

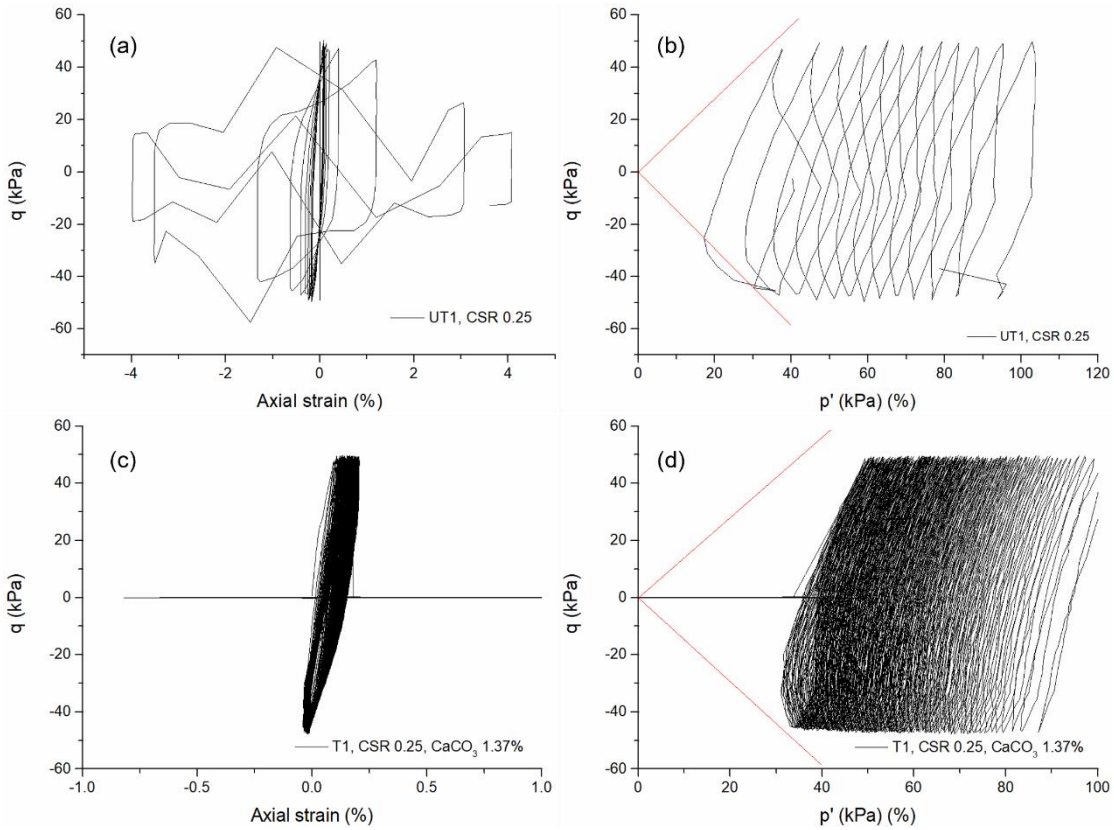

Fig. 6.2 Stress strain behavior and stress path of samples of MS6.100 at *CSR*=0.25
(a) & (b) untreated, and (c) & (d) lightly treated

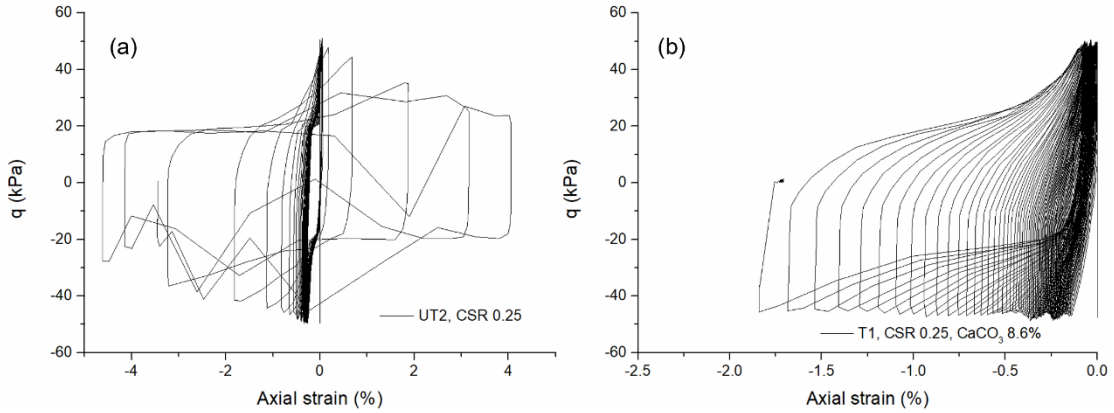

Fig. 6.3 Stress-strain behavior of samples of MS6.0 at *CSR*=0.25
(a) untreated, and (b) lightly treated

Fig. 6.4 shows the typical *CSR* vs. N_L diagram of untreated and treated specimens of MS6.0 and MS6.100. For the treated samples of MS6.0 shown in Fig. 6.4 (a), the points are all located above the *CSR vs.* N_L curve of the untreated soil, which highlights the improvement in cyclic resistance. When the cementation level increases, i.e., with more $CaCO_3$ content, the points are located further and further from the *CSR* vs. N_L curve of the untreated samples, which means that a larger increase in cyclic resistance is seen. The effect of the cementation level will be discussed in detail in § 6.7. For MS6.100 shown in Fig. 6.4 (b). Similar conclusions can be drawn for MS6.0, except the

difference between dense and treated specimens. The effect of the density will be discussed in detail in § 6.5.

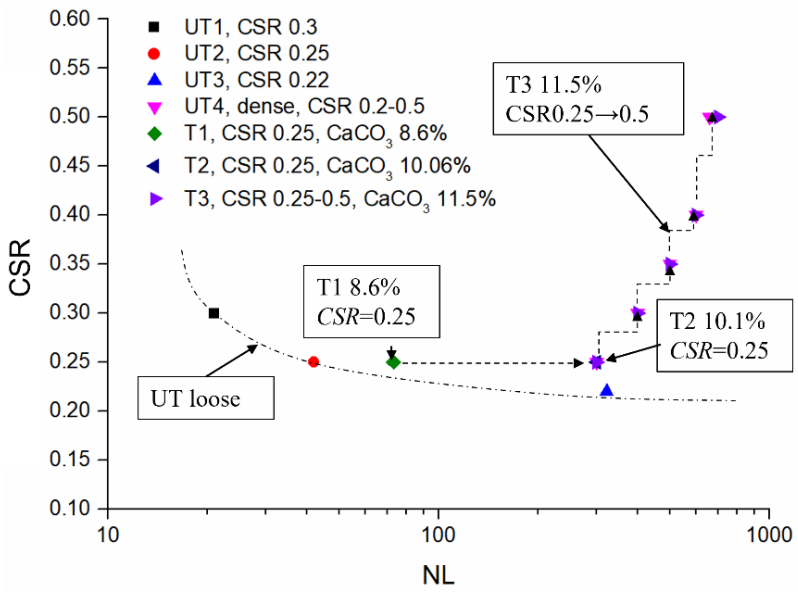

(a) MS6.0

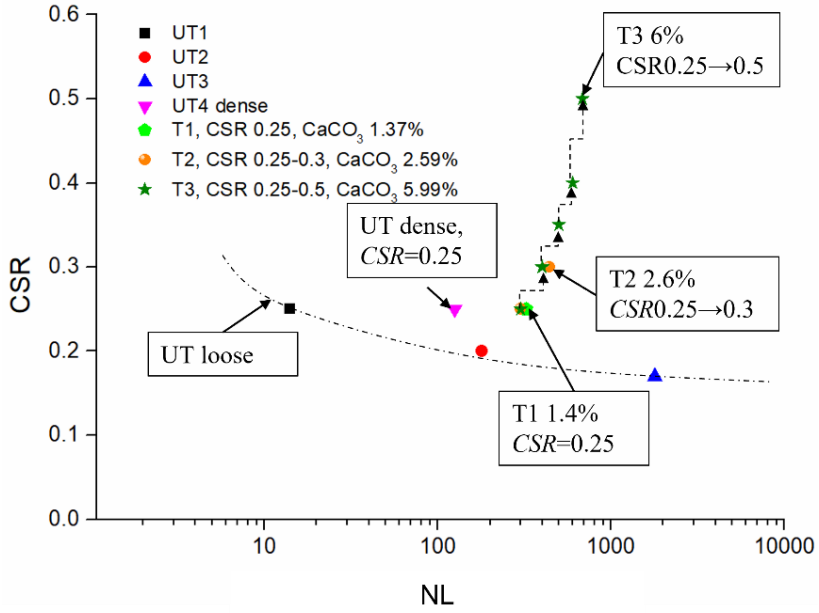

(b) MS6.100

Fig.6.4 Typical diagram of *CSR* vs. N_L of untreated and treated (a) MS6.0 and (b) MS6.100

Based on the literature, there are three cyclic failure mechanism based on the deformation characteristics (Pan et al., 2022): flow failure, cyclic mobility and residual deformation accumulation. Cyclic mobility failure mechanism has been seen in the case of the untreated and treated fine sands of MS6.60_UT & T1 and MS6.100_UT, T1 & T2. All the other treated specimens show a residual deformation accumulation failure.

6.3 Excess pore pressure generation

Fig. 6.5 shows the excess pore pressure generation as a function of the number of cycles. Results for untreated and treated samples of MS6.0 and MS6.40 are shown as examples. In agreement with the results of the other studies, the excess pore pressure generation is slower in bio-treated samples than in untreated samples. (Xiao et al., 2018) considered that this phenomenon was due to the increase in strength and decrease in void ratio in MICP-treated specimens. In some cases, especially in heavily treated specimens, such as MS6.0_T3 and MS6.40_T3, r_u never reaches 1.

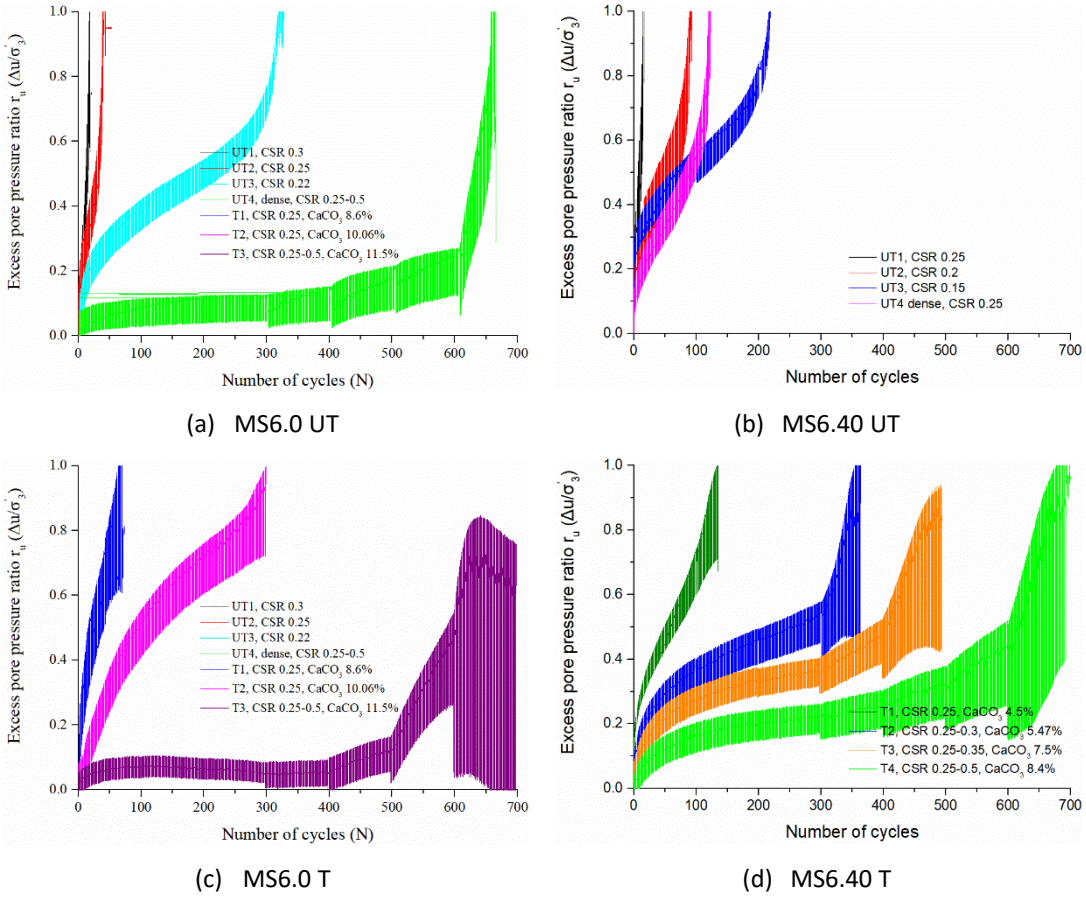

(a) MS6.0 UT (b) MS6.40 UT

(c) MS6.0 T (d) MS6.40 T

Fig. 6.5 Excess pore pressure ratio versus number of cycles for untreated and treated samples of MS6.0 & MS6.40

The shape of the excess pore pressure generation curves for one-stage tests is shown in Fig. 6.6. As in the case of untreated soils, analysis of excess pore pressure generation is based on the upper pore pressure values in each cycle. Results of one-stage cyclic tests (*CSR* = 0.25) on untreated and treated sand specimens are selected for better comparison. Usually, samples with light treatment liquefy in one-stage cyclic tests. In the case of moderately and heavily treated samples, a *CSR* value of 0.25 is not sufficient to cause liquefaction after a few hundreds of cycles. Hence, moderately and heavily treated samples are often associated with multi-stage tests. There is no one-stage cyclic test on treated MS6.20, so that MS6.20 is not shown in Fig. 6.6. However

according to the untreated and treated sand behavior of MS6.20, the pore pressure generation mode of MS6.20 might be similar to that of MS6.0.

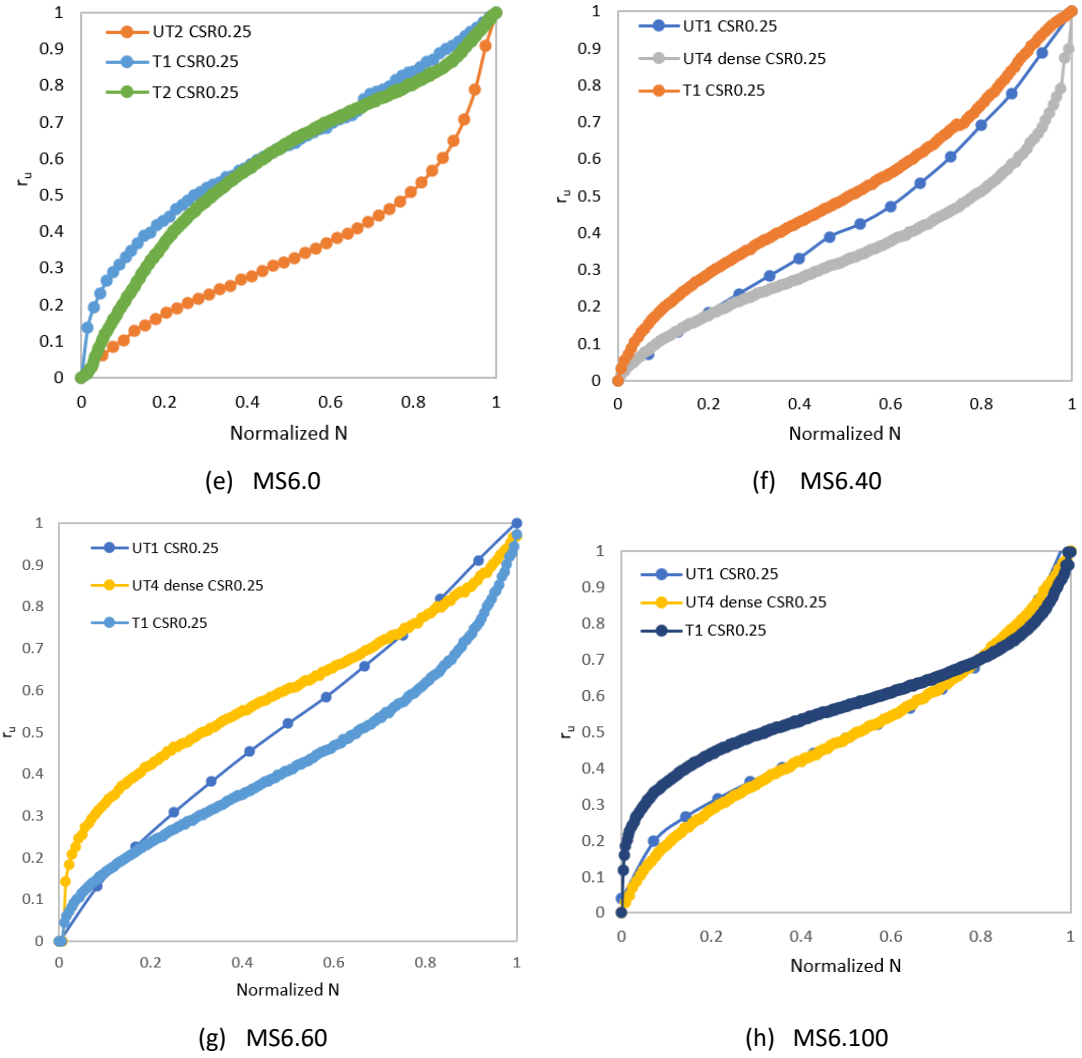

Fig. 6.6 Pore pressure generation of treated and untreated sand during one-stage loading tests (at *CSR* = 0.25)

The shapes of the curves of treated and untreated specimens shown in Fig. 6.6 are sometimes different. For the lightly treated specimens with the highest fine content (MS6.60 & MS6.100), the development of pore pressure follows a nice S-shape (a three-stage development) as for the untreated specimens, i.e., a rapid increasing stage with a decreasing slope, a trend toward stabilization followed by a rapid increasing stage with increasing slope. For treated soil samples with a smaller fine content (MS6.0 & MS6.40), the difference is mainly in the last stage of the curve. For instance, when the normalized number of cycles *N* is in the range from 0.8-1, for untreated samples, the slopes of the curves increase with the *Normalized N*. The slope of the curves of the treated specimens becomes more stable or the slope decreases with increasing *Normalized N*. This is in agreement with Liu et al. (2020) and Xiao et al. (2019). These researchers claimed that, with increasing cementation level, the shape

of the curves evolved from an S-shape to a hyperbolic shape. In comparison, untreated samples evolved from an almost linear shape to an S-shape when the *CSR* decreased.

In the literature, modelling of excess pore pressure generation in MICP-treated sands is quite rare. To compare the untreated and treated pore water pressure generation modes, curve fitting using Seed Model (Seed et al., 1975) is also used for treated samples. Fig. 6.7 shows the r_u vs. *Normalized N* curves of one-stage loading tests (*CSR* = 0.25) where the real data are represented by black dots and the corresponding fitting curves by blue lines. Table 6.2 shows the corresponding parameters and results of the fitting curves using Seed Model.

Often, modelling of lightly treated sand by Seed Model is a bit less good than for untreated sand but still acceptable. Relatively better results are seen in lightly treated specimens containing more fines (> 40%). The α values of treated samples are larger than those of untreated samples. Usually, the α values of treated samples are in the range of 1-2, compared to 0.4-1 for untreated loose samples. In most cases (except MS6.0_T2), the R^2 values of treated samples remain larger than 0.93, while the R^2 values of untreated samples are larger than 0.96. However, the SSE values are much larger. The larger SSE values reflect the effect of the shape of the curves shown in Fig. 6.7, through the large difference between the real data and the fitting curves. Seed Model is based on modelling clean sand curves, which is why it is reasonable to see more deviations in the fitting curves. Modelling of a hyperbolic-shaped curve is not very good, especially when cementation level is high. For example, modelling of MS6.0_T2 is less good than that of MS6.0_T1.

Table 6.2 Fitting parameters and results for one-stage cyclic triaxial tests using Seed Model

Name	FC	D_r	α	95% confidence bounds	SSE	R^2
MS6.0T1	0	31	1.8860	(1.785, 1.988)	0.101	0.97
MS6.0T2	0	97	1.5170	(1.458, 1.575)	1.239	0.93
MS6.40T1	40	83	1.0230	(0.9901, 1.055)	0.191	0.98
MS6.60T1	60	66	0.7191	(0.7061, 0.7321)	0.119	0.99
MS6.100T1	100	57	1.1270	(1.103, 1.151)	0.481	0.96

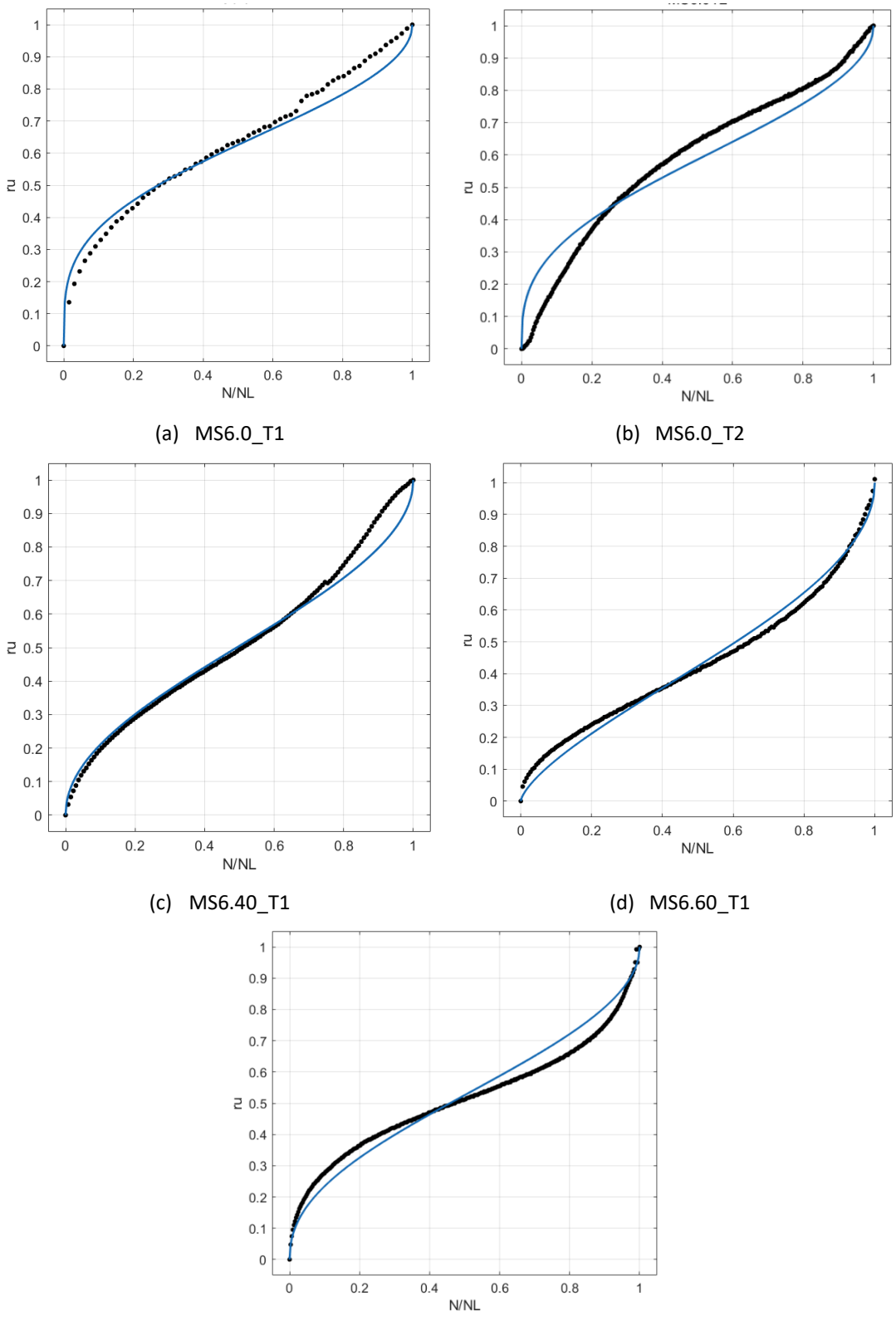

(a) MS6.0_T1 (b) MS6.0_T2

(c) MS6.40_T1 (d) MS6.60_T1

(e) MS6.100_T1

Fig. 6.7 Curve fitting of excess pore pressure ratio (r_u) versus normalized number of cycles (*Normalized N*) for various treated sands subjected to one-stage cyclic loading at CSR=0.25 (dots: input data, lines: simulated data)

Figs. 6.8-6.10 show the fitting curves of treated specimens of the various sand fractions. Table 6.3 shows the corresponding formulas and parameters. Attempts to extend the data (as in Chapter 6) were made when the initial value of r_u was in the linear range (i.e., r_u between 0.4 and 0.6), and when the fitting result with the original data was not good. In the case of MS6.20_T3, the initial value of r_u is too high (> 0.8), and data extension was not carried out.

The fitting results for the finest sands (MS6.60 & MS6.100) during multi-stage cyclic tests are good. The fitting results of the sands with larger d_{50} (MS6.0, MS6.20 & MS6.40) are not very good. For these sands, extension of data improved the fitting. The R^2 values for T2 & T3 of MS6.60 & MS6.100 are larger than 0.92, which is acceptable. The fitting results of MS6.40 with extension of data are also good, better than using the original results. The R^2 values for MS6.40_T2, T3 & T4 are larger than 0.85, and the α values range from 2.8-5. The R^2 values of these soils with extension of data are larger than 0.9, and the α values are comprised between 1.6 and 2.7, which is similar to the values for the untreated dense samples (1-3). The fitting results of MS6.20_T2 & T3 with the original data are not very good (R^2 = 0.74 and 0.82 for T2 & T3), the α values are quite large (5 for T2 and 10 for T3). The result of MS6.20_T2 with extended data is good (R^2=0.94), and the α value decreases to 2, within the range of 1-3 like the α value of fine sand. The result of MS6.0_T3 after data extension is acceptable, with R^2 value equal to 0.85.

Considering all the tests, the fitting results of one-stage tests are better than those of multi-stage tests. For lower cementation levels, the fitting results are better.

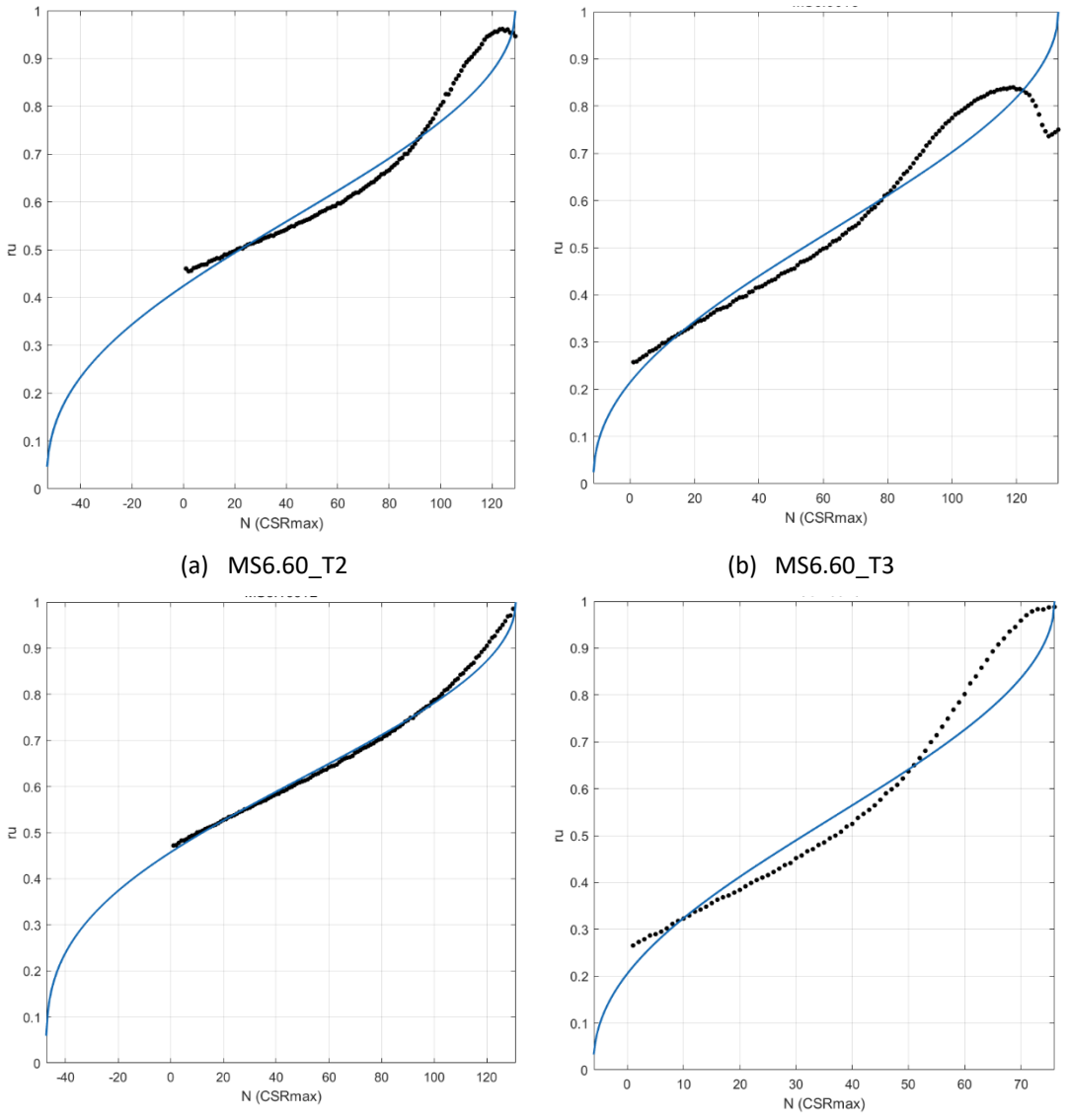

(a) MS6.60_T2 (b) MS6.60_T3

(c) MS6.100_T2 (d) MS6.100_T3

Fig. 6.8 Curve fitting of excess pore pressure ratio (r_u) versus normalized number of cycles (*Normalized N*) for treated MS6.60 & MS6.100 subjected to multi-stage cyclic loadings (dots: input data, lines: simulated data)

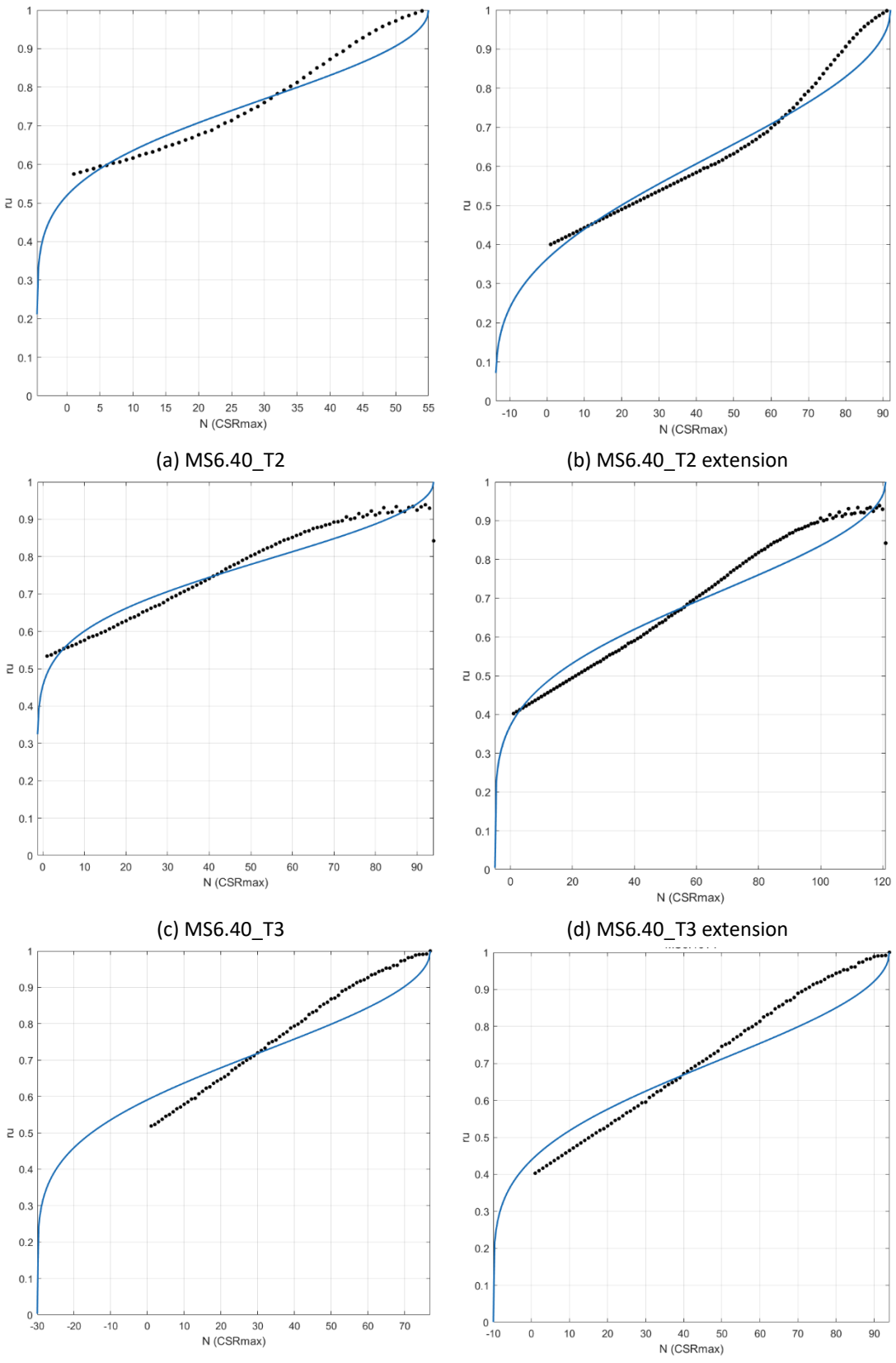

(a) MS6.40_T2

(b) MS6.40_T2 extension

(c) MS6.40_T3

(d) MS6.40_T3 extension

(e) MS6.40_T4

(f) MS6.40_T4 extension

Fig. 6.9 Curve fitting of excess pore pressure ratio (r_u) versus normalized number of cycles (*Normalized N*) for treated MS6.40 subjected to multi-stage cyclic loadings (dots: input data, lines: simulated data)

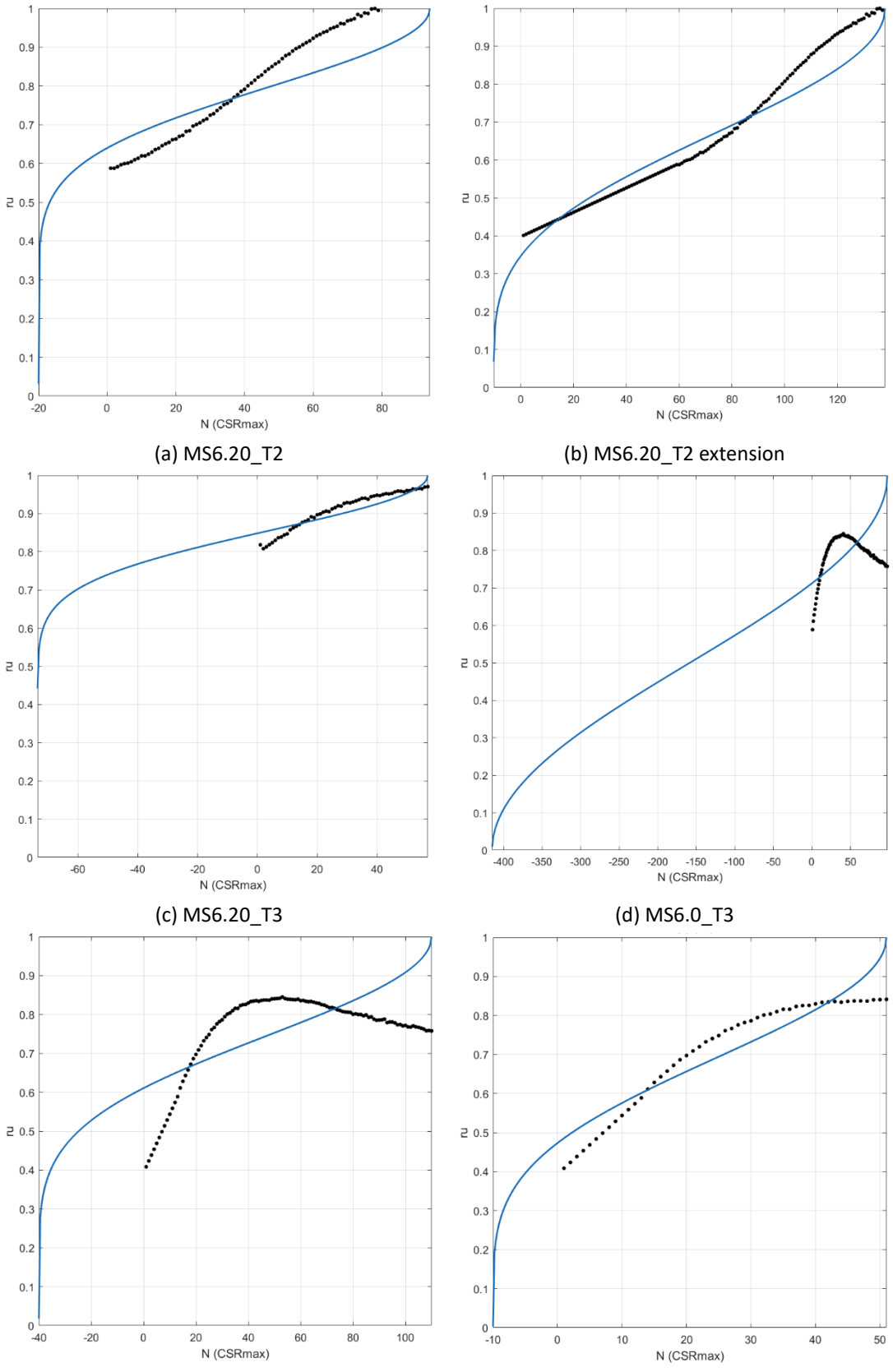

(a) MS6.20_T2

(b) MS6.20_T2 extension

(c) MS6.20_T3

(d) MS6.0_T3

(e) MS6.0_T3 extension 1

(f) MS6.0_T3 extension 2

Fig. 6.10 Curve fitting of excess pore pressure ratio (r_u) versus normalized number of cycles (*Normalized N*) for treated MS6.0 & MS6.20 subjected to multi-stage cyclic loadings (dots: input data, lines: simulated data)

Table 6.3 Fitting parameters and result for multi-stage cyclic triaxial tests using Seed Model

Name of the test	Fitting formulas	α	β	R^2	CSR_{max}	N (CSR_{max})	$N_{L,\,eq}$
MS6.0T3	$r_u = \frac{1}{2} + \frac{1}{\pi}\sin^{-1}\left(2 \times \left(\frac{\beta + N}{\beta + 98}\right)^{1/\alpha} - 1\right)$	1	415.1	-1.54	0.5	98	513
MS6.0T3 extension 1	$r_u = \frac{1}{2} + \frac{1}{\pi}\sin^{-1}\left(2 \times \left(\frac{\beta + N}{\beta + 110}\right)^{1/\alpha} - 1\right)$	3.303	40	0.15	0.5	110	150
MS6.0T3 extension 2	$r_u = \frac{1}{2} + \frac{1}{\pi}\sin^{-1}\left(2 \times \left(\frac{\beta + N}{\beta + 51}\right)^{1/\alpha} - 1\right)$	2.314	10	0.85	0.5	51	61
MS6.20T2	$r_u = \frac{1}{2} + \frac{1}{\pi}\sin^{-1}\left(2 \times \left(\frac{\beta + N}{\beta + 94}\right)^{1/\alpha} - 1\right)$	5.142	20	0.74	0.3	94	114
MS6.20T2 extension	$r_u = \frac{1}{2} + \frac{1}{\pi}\sin^{-1}\left(2 \times \left(\frac{\beta + N}{\beta + 138}\right)^{1/\alpha} - 1\right)$	2.031	10.32	0.94	0.3	138	148
MS6.20T3	$r_u = \frac{1}{2} + \frac{1}{\pi}\sin^{-1}\left(2 \times \left(\frac{\beta + N}{\beta + 57}\right)^{1/\alpha} - 1\right)$	10	73.52	0.82	0.4	57	131
MS6.40T2	$r_u = \frac{1}{2} + \frac{1}{\pi}\sin^{-1}\left(2 \times \left(\frac{\beta + N}{\beta + 55}\right)^{1/\alpha} - 1\right)$	4.055	4.607	0.93	0.3	55	60
MS6.40T2 extension	$r_u = \frac{1}{2} + \frac{1}{\pi}\sin^{-1}\left(2 \times \left(\frac{\beta + N}{\beta + 92}\right)^{1/\alpha} - 1\right)$	1.654	13.78	0.96	0.3	92	106
MS6.40T3	$r_u = \frac{1}{2} + \frac{1}{\pi}\sin^{-1}\left(2 \times \left(\frac{\beta + N}{\beta + 94}\right)^{1/\alpha} - 1\right)$	5.037	1.37	0.94	0.35	94	95
MS6.40T3 extension	$r_u = \frac{1}{2} + \frac{1}{\pi}\sin^{-1}\left(2 \times \left(\frac{\beta + N}{\beta + 121}\right)^{1/\alpha} - 1\right)$	2.708	5	0.94	0.35	121	126
MS6.40T4	$r_u = \frac{1}{2} + \frac{1}{\pi}\sin^{-1}\left(2 \times \left(\frac{\beta + N}{\beta + 77}\right)^{1/\alpha} - 1\right)$	2.86	30	0.85	0.5	77	107
MS6.40T4 extension	$r_u = \frac{1}{2} + \frac{1}{\pi}\sin^{-1}\left(2 \times \left(\frac{\beta + N}{\beta + 94}\right)^{1/\alpha} - 1\right)$	2.583	10	0.90	0.5	94	104
MS6.60T2	$r_u = \frac{1}{2} + \frac{1}{\pi}\sin^{-1}\left(2 \times \left(\frac{\beta + N}{\beta + 129}\right)^{1/\alpha} - 1\right)$	1.278	53.22	0.95	0.35	129	182
MS6.60T3	$r_u = \frac{1}{2} + \frac{1}{\pi}\sin^{-1}\left(2 \times \left(\frac{\beta + N}{\beta + 133}\right)^{1/\alpha} - 1\right)$	1.145	11.48	0.92	0.5	133	144
MS6.100T2	$r_u = \frac{1}{2} + \frac{1}{\pi}\sin^{-1}\left(2 \times \left(\frac{\beta + N}{\beta + 131}\right)^{1/\alpha} - 1\right)$	1.586	47.39	0.99	0.3	131	178
MS6.100T3	$r_u = \frac{1}{2} + \frac{1}{\pi}\sin^{-1}\left(2 \times \left(\frac{\beta + N}{\beta + 76}\right)^{1/\alpha} - 1\right)$	1.133	6.099	0.94	0.5	76	82

- $N_{L,\,eq}$ represent the estimated equivalent cycles at the maximum *CSR* stage

6.4 Deformation characteristics

Fig. 6.11 shows the axial strain accumulation as a function of the number of cycles for both untreated and treated sand specimens. Results of MS6.0 (similar to MS6.20), MS6.40 and MS6.100 (similar to MS6.60) are presented. In general, the results are consistent with the findings of the monotonic triaxial tests in chapter 5 and those of other studies (Montoya & DeJong, 2015; Lin et al., 2016; Xiao et al., 2018; Wu et al., 2021). MICP treatment significantly decreases the contractive tendency and enhances the dilative behavior compared to untreated sand specimens. The number of cycles and *CSR* required to reach liquefaction increases with the cementation level.

In the finest sands (with more than 60% fines), lightly treated and moderately treated samples show both compressive and extensive axial strain behavior like untreated samples. It is the case, for example, of the lightly treated (MS6.100_T1) and moderately treated (MS6.100_T2) samples of the finest sand MS6.100, as shown in Fig. 6.11 (f). This can also be seen in specimen MS6.60_T1. These results are in agreement with those of Lee et al. (2022), who showed that a small amount of cementation resulted in a noteworthy enhancement in the pre-trigger stage of liquefaction but made hardly any difference in post-triggering strain accumulation. With an increase in the cementation level, the axial strain development of bio-cemented fine soils evolves from two-side (compressive and extensive) strain (e.g., for MS6.100_T1 & T2 and MS6.60_T1) to one-side extension (e.g., for MS6.100_T3 and MS6.60_T2 & T3).

For treated samples with larger grains (with 40% fines or less), unlike the compressive and extensive axial strains of untreated specimens, only extensive strains are seen at all cementation levels (Figs. 6.11 (b) & (d)). MICP treatment changes the strain behavior of treated specimen permanently. This aspect are also mentioned in the study of Montoya et al. (Montoya et al., 2013). For soils with a large d_{50}, the cyclic resistance of lightly treated specimens is slightly enhanced, but the axial strain evolves from compression to extension. For instance, at *CSR* = 0.25, MS6.0_T1 liquefies at N_L = 66, which is a bit higher than for untreated MS6.0_UT2 that liquefies at N_L = 38. MS6.0_T1 shows extensive axial strain behavior whereas MS6.0_UT2 shows compressive and extensive axial strain behavior. This is in accordance with (Feng & Montoya, 2016).

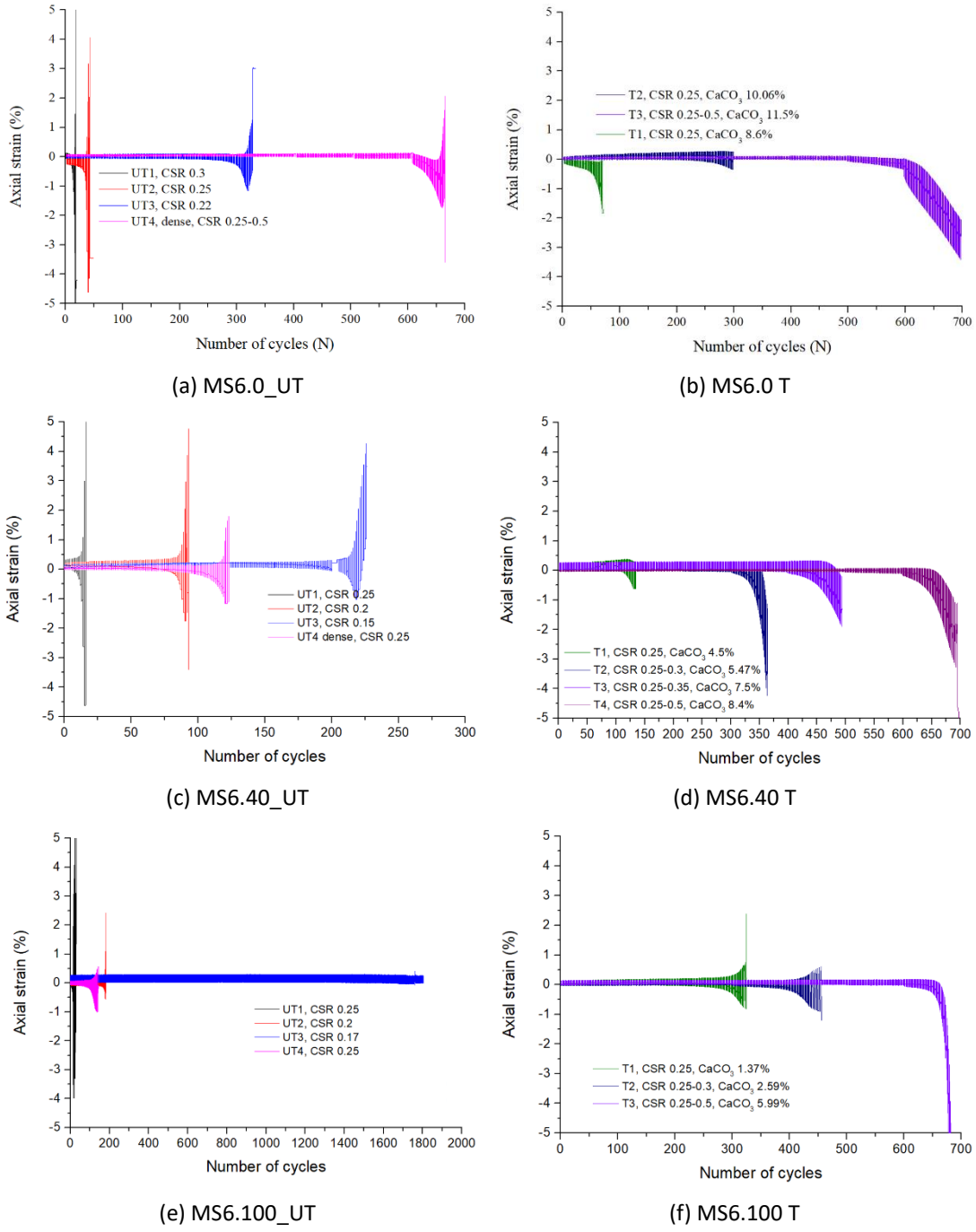

Fig. 6.11 Typical axial strain response of MS6.0, MS6.40 and MS6.100 versus number of loading cycles (UT: untreated samples, T: treated samples)

Fig. 6.12 shows the photos of oven-dried treated specimens after mechanical tests. When the cementation level increases, the oven-dried specimens of cemented soil evolve from pure powder to powder with small blocks, then to big cylindrical blocks with a small amount of powder. As shown in the photos of Fig. 6.12, lightly treated (MS6.100_T1 & MS6.60_T1) and moderately treated (MS6.100_T2) soil samples are made of powder with very few small blocks, which indicates that the bonds formed by cementation are almost all destroyed in these samples. For moderately treated sand, the powder is still present, but we also see blocks with

undestroyed bonds after mechanical tests. These blocks might result from the heterogeneity of the treatment, because the $CaCO_3$ content is often larger in the lower part of the specimens (near the inlet of the injected solutions), as also observed by Feng & Montoya (2016) and Martinez et al. (2013). For heavily-treated specimens of all the sands, intact big blocks are seen after mechanical tests, which is also mentioned in the study of (Xiao et al., 2018). All the heavily treated samples (T3) appear as the superposition of cylindrical blocks separated by quasi-horizontal sections. The extensive axial strain and asymmetrical behavior of heavily treated samples may be due to the oriented micro-cracks created by the loading in a direction parallel to the loading (Cerfontaine & Collin, 2018). The photos point out the interesting fact that a significant enhancement of the soil properties does not require the calcification of the whole specimen. The formation of cemented nodules (with diameters of 1-3 cm) in various parts of the sample is enough to improve its properties, as clearly evidenced for instance by the sample MS6.0_T3 who failed to reach liquefaction after 700 cycles under a *CSR* of 0.5, compared to the untreated sample who liquefied after 38 cycles under the *CSR* of 0.25.

Fig. 6.12 Treated specimens of various sands with various cementation levels after cyclic triaxial tests

Fig. 6.13 shows the evolution of the axial strain amplitude ($\delta\varepsilon_1 = \varepsilon_{1max,i} - \varepsilon_{1min,i}$) of untreated and treated samples as a function of the number of cycles. MS6.0 & MS6.100 are selected as examples, considering that the axial strain behavior of MS6.20 is similar to that of MS6.0, while the strain behavior of MS6.40 & MS6.60 is similar to that of MS6.100. In addition to the dilative character, the axial strain amplitude of treated specimens increases more slowly than that of untreated sand. For MS6.0, during a one-stage cyclic test at *CSR* = 0.25, when r_u = 1, the axial strain amplitude of untreated MS6.0_UT2 is larger than 5% while that of lightly treated MS6.0_T1 is only 1.1%. Even for the dense untreated specimen MS6.0_UT4, the

$\delta\varepsilon_1$ reaches 1.88% during a multi-stage cyclic test at *CSR* ranging from 0.25 to 0.5. For heavily treated MS6.0_T3, r_u never reaches 1: at the maximum r_u value, $\delta\varepsilon_1$ is 1.87%, similar to MS6.0_UT4. For MS6.100, during a one-stage cyclic test at *CSR*=0.25, when r_u = 1, the $\delta\varepsilon_1$ of untreated loose MS6.100_UT1 is 4.7% while the $\delta\varepsilon_1$ of dense untreated MS6.100_UT4 is 0.9%, similar to that of the lightly treated MS6.100_T1 (1%).

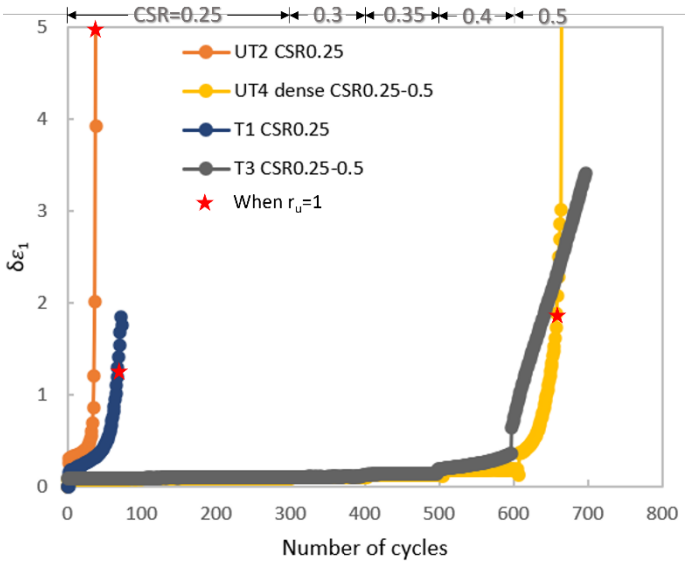

(a) MS6.0

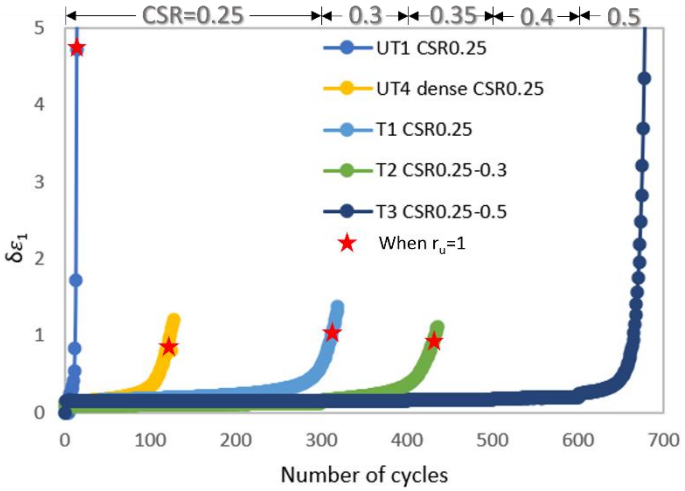

(b) MS6.100

Fig. 6.13 Evolution of axial strain amplitude $\delta\varepsilon_1$ as a function of the number of cycles for untreated and treated samples of (a) MS6.0, (b) MS6.100

The lower rate of increase of the axial strain amplitude in the treated specimens, compared to the untreated ones, can be seen in Fig. 6.13. For example, to reach an amplitude of 0.5% under the same loading conditions, treated samples require more cycles compared to untreated loose specimens. The rate of increase of the axial strain amplitude in treated samples is comparable (in the case of MS6.0 & MS6.20) or smaller than that in dense untreated specimens (e.g., MS6.40, MS6.60 & MS6.100). While

untreated specimens feature a rapid increase of $\delta\varepsilon_1$ between 0.5% and 5%, especially in the last cycles, treated sand specimens show a relatively gentler slope, i.e., a relatively slower and more stable increase in axial strain amplitude. Treated specimens need several tens to one hundred or more cycles to reach 5% of axial strain amplitude. This is consistent with the findings of (Xiao et al., 2019) who concluded that MICP-treated sand exhibited gradual loss of stiffness and needed more cycles for the same magnitude of deformation, compared to untreated samples.

6.5 Effect of soil density

Figs. 6.14, 6.15 and 6.16 show the pore pressure generation and axial strain accumulation as a function of the number of cycles for loose and dense untreated and treated specimens of MS6.0 (similar to MS6.20), MS6.40 and MS6.100 (similar to MS6.60), respectively. In general, the cyclic resistance of bio-cemented sand is improved compared to that of untreated loose samples. Xiao et al. (2018) claimed that the increased extensive behavior and the bonds formed by MICP treatment could explain the significantly enhanced cyclic resistance, similar to what is observed in dense sand.

For the coarsest sands (MS6.0 & MS6.20), the enhanced cyclic resistance of heavily treated specimens is comparable to that of dense untreated specimens. As shown in Figs. 6.14 (a) & (b), MS6.0_UT4 and MS6.0_T3 liquefy under *CSR* = 0.25 after a similar number of cycles. Our results agree with (Xiao et al., 2019), who concluded that, during the bio-cementation process, $CaCO_3$ precipitates gradually occupy the voids, and soil behavior changes from loose to dense type. They concluded that bio-cementation plays a similar role to an increase in relative density and results in improved cyclic resistance. However, the mechanical behavior of heavily treated and dense samples is not the same, especially as regards the pore pressure generation and axial strain accumulation, as shown in Figs. 6.14 (a) & (b),

- the excess pore pressure of MS6.0_UT4 begins to increase significantly under the maximum *CSR* = 0.5 at around $r_{u,max}$ = 0.25 and the sample liquefies within 60 cycles.
- on the other hand, for MS6.0_T3, the excess pore pressure begins to increase at approximately the same value of $r_{u,max}$ under the CSR of 0.4, but with a decreasing slope, then increases again under the maximum CSR of 0.5 at around $r_{u,max}$ = 0.6, also with a decreasing slope, to a maximum value close to 0.9, and does not increase anymore.

As shown in Figs. 6.14 (c) & (d), MS6.0_T3 shows a steadily increasing extensive axial strain, while MS6.0_UT4 first features an extensive axial strain, followed by both compressive and extensive axial strain in the last cycles.

On the contrary, for soils with a fine content equal to, or larger than, 40 % (MS6.40, MS6.60, MS6.100), a more remarkable enhancement of cyclic resistance is seen, due to bio-cementation, compared to sands with a larger d_{50}. Even the lightly treated loose samples resist better to liquefaction than the dense samples. For example, in Figs. 6.15 and 6.16, at the same CSR = 0.25, lightly treated samples of MS6.40 and MS6.100

require a larger number of cycles than dense samples of MS6.40 and MS6.100: 134 and 322 cycles for MS6.40_T1 and MS6.100_T1, versus 120 cycles for MS6.40_UT4 and MS6.100_UT4, respectively. The cohesion brought by the MICP-treatment in fine sands plays a more important part in increasing the cyclic resistance than the increase in density due to the formation of $CaCO_3$ crystals. These results are consistent with the findings of Porcino et al., (2011), Gao et al. (2019), and Xiao et al. (2019) who stated that a slight bio-cementation could be similar to, or surpass, densification in improving strength and controlling deformation.

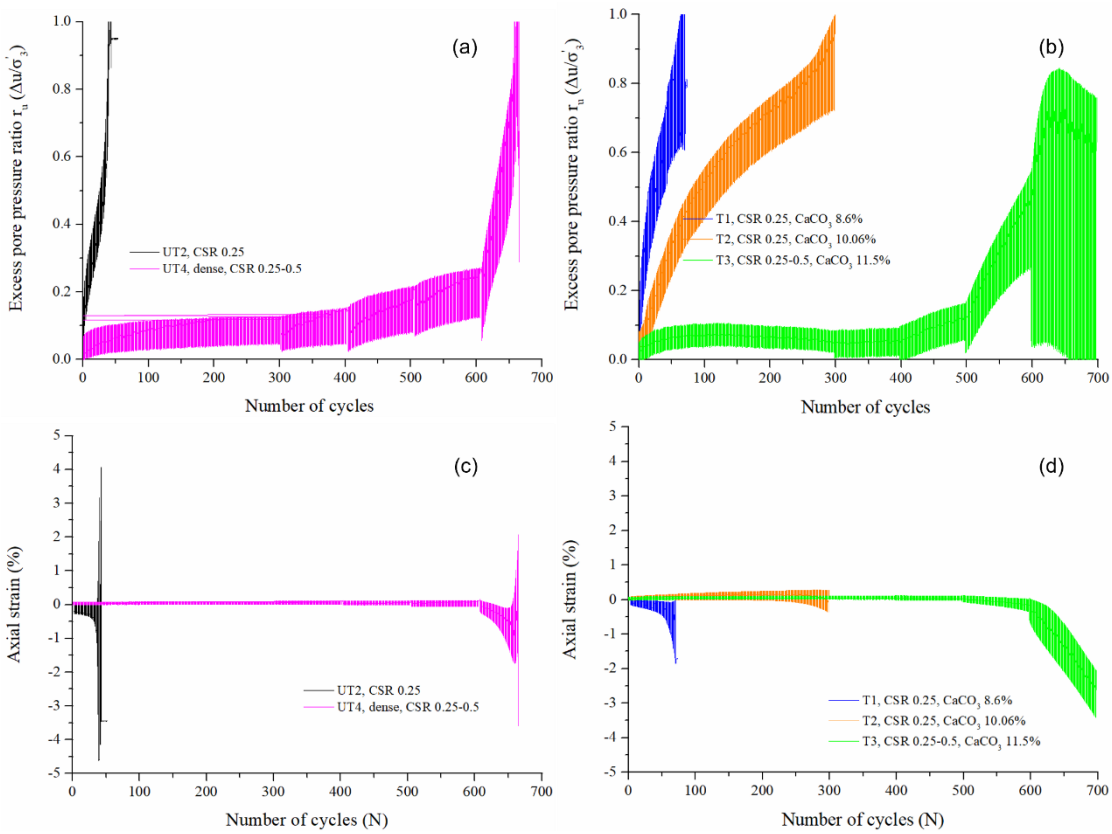

Fig. 6.14 Effect of soil density for MS6.0 (a)&(c) untreated, and (b) & (d) treated

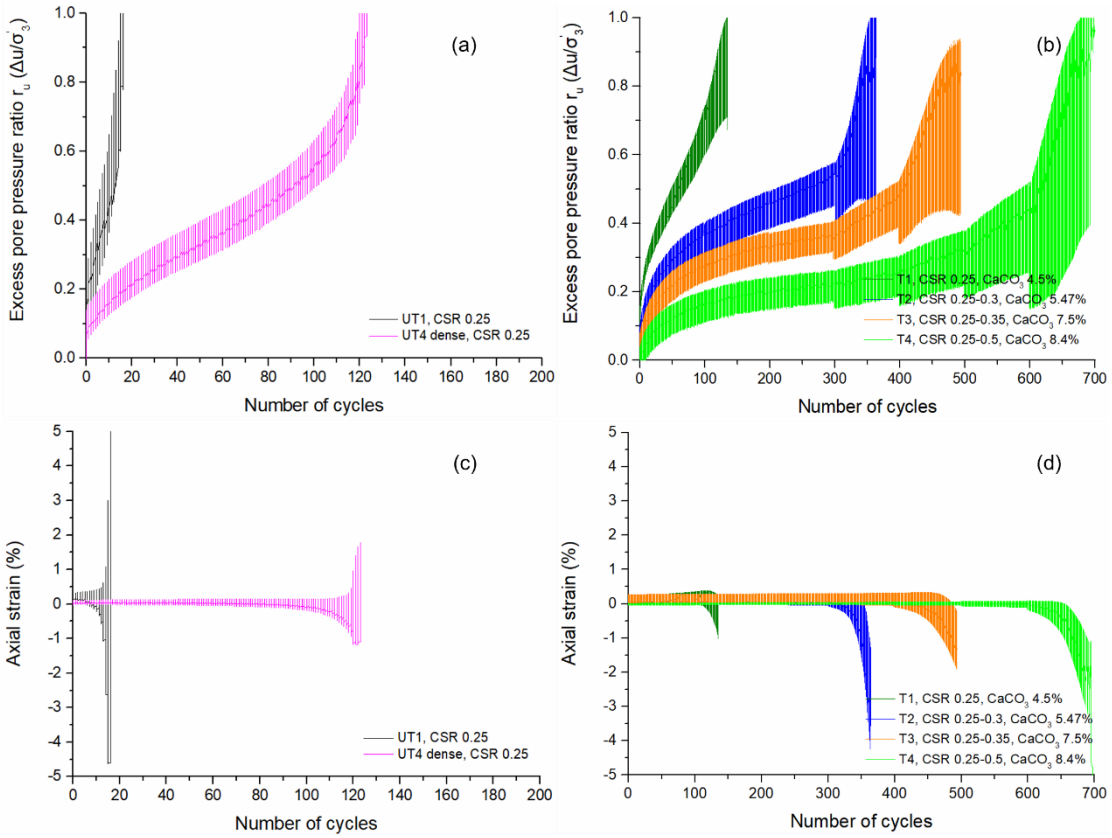

Fig. 6.15 Effect of soil density for MS6.40 (a)&(c) untreated, and (b) & (d) treated

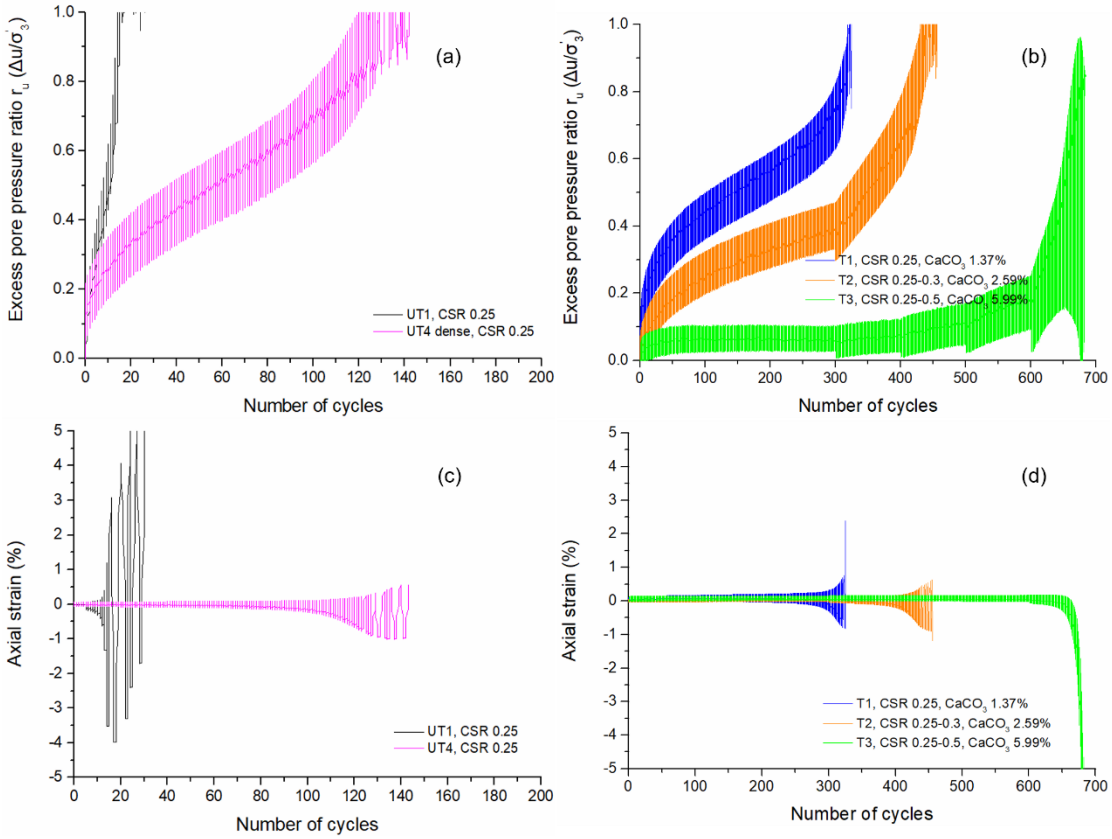

Fig. 6.16 Effect of soil density for MS6.100 (a)&(c) untreated, and (b) & (d) treated

6.6 Effect of cementation level

To compare the effect of MICP for the different used soils, we calculated the magnitude of *CSR* required to initiate liquefaction in 100 cycles of uniform cyclic loading, called CSR_{100}. This parameter has already been introduced in § 5.5. Fig. 6.17 shows the CSR_{100} versus the $CaCO_3$ content for the various sand fractions with various cementation levels.

As shown in Fig. 6.17 (a), the larger the $CaCO_3$ content, the larger the CSR_{100}, and the larger the resistance to liquefaction. This result is consistent with those of other studies (Montoya et al., 2013; Xiao et al., 2018).

It has been reported in various studies (Simatupang & Okamura, 2017; Almajed et al., 2019; Gao et al., 2019; Lee et al., 2022) that notable improvements of mechanical behavior could be seen in lightly treated samples with the presence of a small amount of $CaCO_3$ precipitation (around or less than 1%). In our study, small amounts of $CaCO_3$ manifested their effectiveness in enhancing cyclic resistance and changing stress-strain behavior in soils with a large percentage of small grains (small d_{50}). For instance, lightly treated MS6.60_T1, with 2.1% of $CaCO_3$ content showed a more than 15-fold increase in N_L (182) compared to an untreated loose sample (12). As shown in Table 6.2, for MS6.100_T1, even less $CaCO_3$ content (1.4%) is needed to achieve a more than 20-fold improvement in resistance to liquefaction. This might be due to the fact that, when there are more small grains, the number of contacts between the particles is higher, and the chance of precipitation of $CaCO_3$ crystals at the particle contacts is higher. Smaller grains might need less $CaCO_3$ crystals to create bridges between particles. But a small amount of $CaCO_3$ is still not sufficient in the treatment of soils with a smaller content of fine grains (i.e., MS6.0, MS6.20 and MS6.40).

The results obtained for the different fine fractions of the sand were plotted in Fig. 6.17 (a) in terms of CSR_{100} value as a function of the precipitated carbonate content. This figure illustrates the fact that there is a minimum $CaCO_3$ content below which the effect of MICP treatment is very small, and that this minimum value depends on the soil. For example, when CSR_{100} equals 0.25, the minimum $CaCO_3$ contents to see the effect of MICP treatment is around 9% for MS6.0, 5.3% for MS6.20, 4.4% for MS6.40, 1.8% for MS6.60 and 1% for MS6.100. After reaching these minimum values of $CaCO_3$ content, the increase in CSR_{100} with the $CaCO_3$ percentage is approximately linear, and the lines are more or less parallel. Thus, we can define $\Delta CaCO_3\%$ as the percentage of $CaCO_3$ minus the $CaCO_3$ percentage corresponding to the limit (CSR_{100} = 0.25). Therefore, in Fig.6.17 (b), a unified linear relationship of CSR_{100} change with $\Delta CaCO_3\%$ for all the treated specimens of various gradings is given with a R^2 value of 0.85. We can deduct from the equation that, after reaching the minimum content of $CaCO_3$ (CSR_{100} = 0.25), an extra 1% of $CaCO_3$ precipitation can contribute to an additional CSR_{100} of about 0.056.

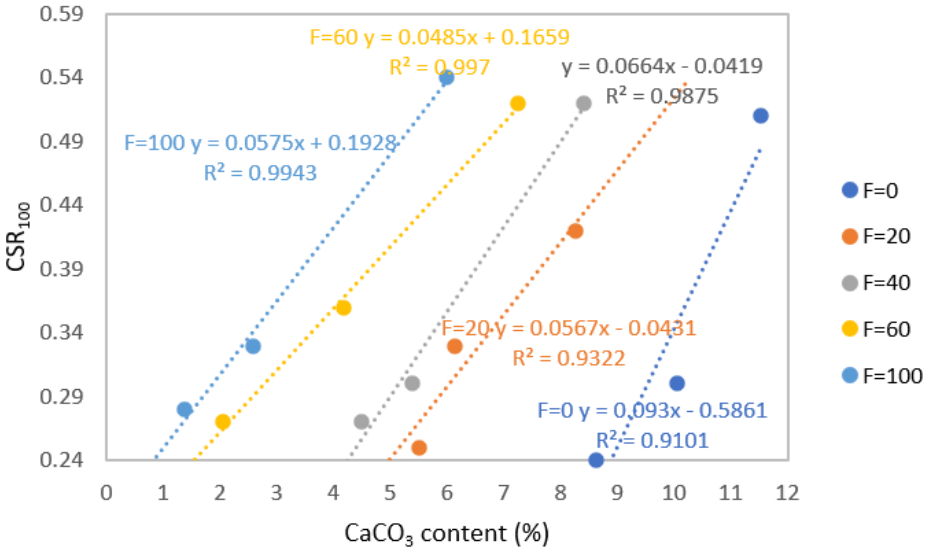

(a) *CSR100* vs. $CaCO_3$ content

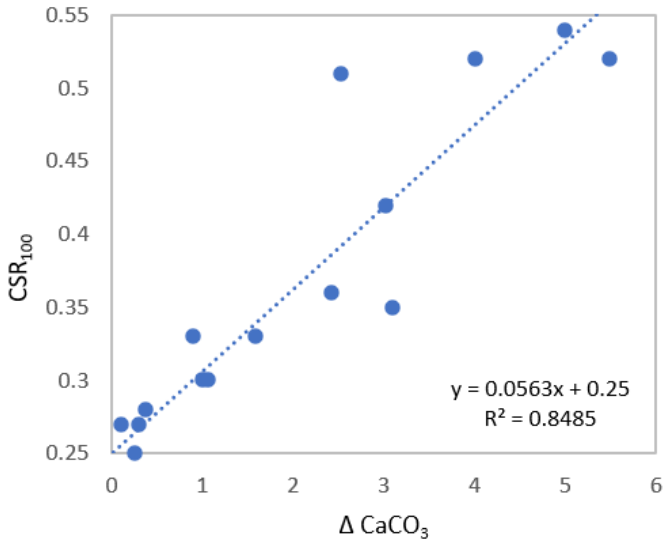

(b) *CSR100* vs. $\Delta CaCO_3$ content

Fig. 6.17 CSR_{100} versus (a) $CaCO_3$ and (b) $\Delta CaCO_3$ content for the soils with different fine contents at various cementation levels

The results of Fig. 6.17 (a) are similar to, but slightly different from, those shown in Fig. 5.10 (a). In chapter 5, the minimum carbonate contents were very close to each other for all the soils containing fines (< 1 mm), and significantly different for the only soil that did not contain fines (i.e. MS6.0). In Fig. 6.17 (a), we see that there is a progressive increase in the minimum carbonate content when the fine content decreases (i.e., from MS6.100 to MS6.0). The reason is that the two main mechanisms influencing the effect of carbonate content on the mechanical properties of the soil – the formation of "bonds" between the particles and the density – play a slightly

different part in monotonic and cyclic tests. Though the initial densities after consolidation at 100 kPa are the same in both tests, the density at the maximum stress is lower in monotonic CD tests than in cyclic CU tests because dilation has already begun at that time. Thus, the main effect of the MICP-treatment in monotonic tests is probably the cementation of particles and, in a minor way, the increased roughness of the particles, and we saw that the influence of fines is very important in that case. In cyclic tests, density is an important parameter of resistance to liquefaction as shown by many authors in the past. This is also what appears in the similarities between treated and dense specimens. As a conclusion, there is an interplay between the effects of these two mechanisms, which is different in monotonic and cyclic tests and might explain the observed differences in minimum carbonate contents.

6.7 Effect of grain size distribution

Fig. 6.18 shows the relationship between the minimum $CaCO_3$ content (%), the mean diameter d_{50} and the fine content (%).

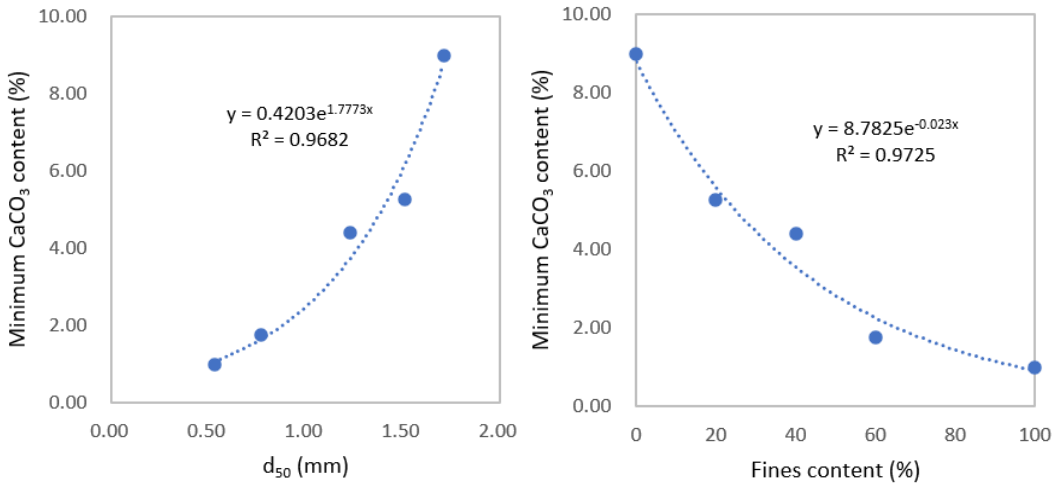

Fig. 6.18 Minimum $CaCO_3$ content (%) versus (a) d_{50}, (b) fine content (%)

The influence of C_u on the mechanical behavior of the treated sand specimens is not as important as the influence of C_u in untreated sands. The conclusion is that the larger the d_{50} of the grains, the larger the percentage of $CaCO_3$ % required to observe the effect of bio-cementation. An exponential relationship has been given in Fig.6.18 (a) with R^2 = 0.97. When the fine content increases, the percentage of $CaCO_3$ needed to obtain the same CSR_{100} value decreases. The presence of fines in the soil matrix can significantly lower the required $CaCO_3$ content. An exponential relationship is given in Fig. 6.18 (b) with R^2 = 0.97. Fig. 6.17 (a) shows that, between the soil without fines (MS6.0) and the soil containing only 20% of fines (< 1 mm) in the soil matrix (MS6.20), the minimum $CaCO_3$ content falls from 9% to nearly half (5.3%). Fine particles help a lot in increasing the efficiency of the MICP process. This is consistent with the results

of (Mahawish et al., 2018). This is probably due to (i) the enhancement of the adsorption of bacteria in the presence of fines, (ii) the fact that the fines partly fill the pore space, which lowers the amount of $CaCO_3$ needed to create bonds between soil grains, (iii) the fact that the presence of fines greatly contributes to the multiplication of contact points.

6.8 Mercury intrusion porosimetry (MIP)

Results of mercury intrusion porosimetry (MIP), i.e., the change in cumulative volume of pores (mL/g) and incremental volume of pores (mL/g) vs. diameter of the pores (µm) in some treated specimens, are shown in Fig. 6.19.

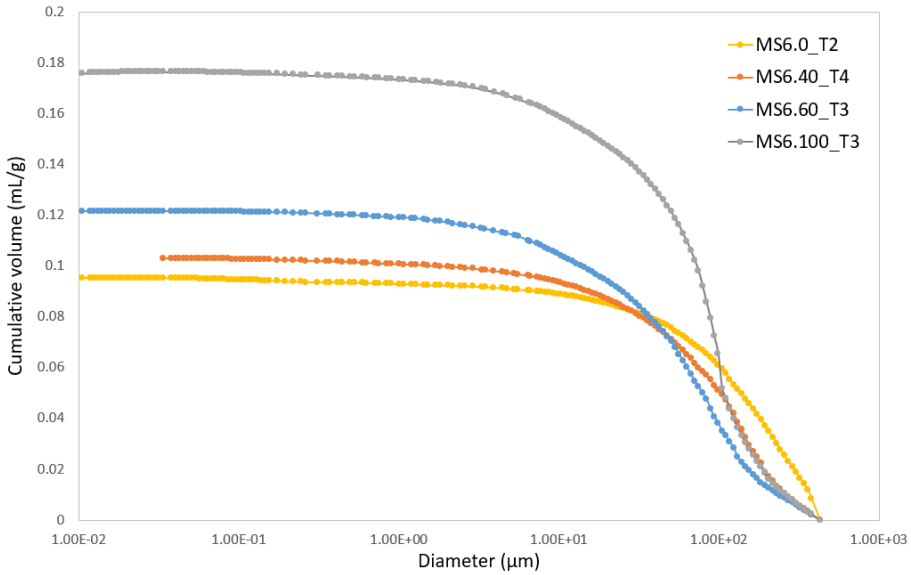

(a) Cumulative volume of pores (mL/g) vs. diameter of the pores (µm)

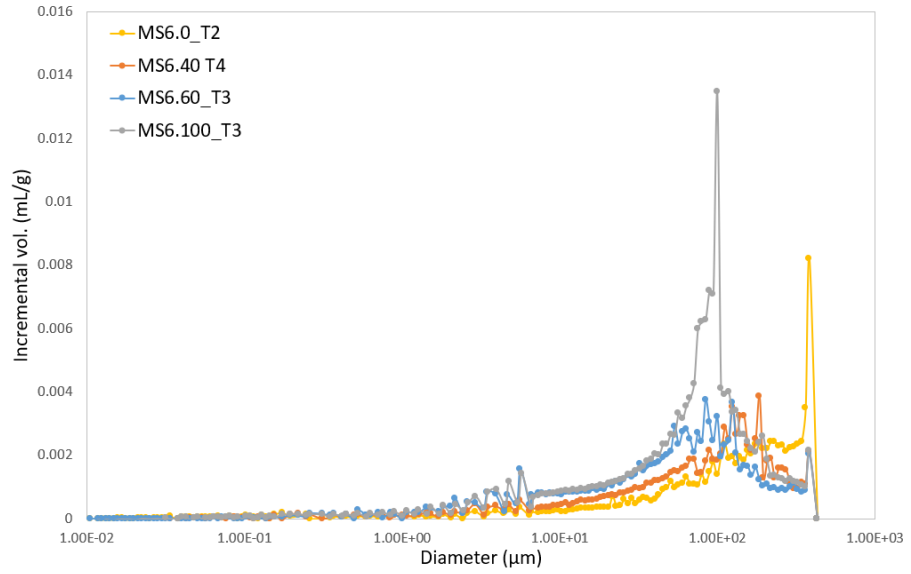

(b) Incremental volume of pores (mL/g) vs. diameter of the pores (µm)

Fig. 6.19 (a) Cumulative volume of pores (mL/g) and (b) Incremental volume of pores (mL/g) vs. diameter of the pores (µm) in treated specimens

The results concern moderately treated MS6.0 (10 $CaCO_3$%) and heavily treated MS6.40 (8.4 $CaCO_3$%), MS6.60 (7.2 $CaCO_3$%) and MS6.100 (6 $CaCO_3$%). For the untreated specimens, with a target D_r = 30%, the porosity is in the following order: MS6.60 < MS6.40 < MS6.100 < MS6.0. For the treated samples, the diameter of the pores is in the same order: MS6.100 = MS6.60 < MS6.40 < MS6.0. However, the total volume of the pores accessible to mercury in the treated specimens is in the order: MS6.0 < MS6.40 < MS6.60 < MS6.100, which is in the opposite order from the $CaCO_3$ content. It is reasonable that a larger $CaCO_3$ content occupies more space in the pores or makes more pores inaccessible.

6.9 Conclusions

The effect of MICP treatment depends on the percentage of fine grains in the soil. In this study, the "fines" or "fine grains" are the grains whose diameter is smaller than 1 mm. The following conclusions can be drawn from this chapter as follows,

- In general, the cyclic resistance of treated specimens is improved compared with untreated samples and the improvement increases with the cementation level. During cyclic loading, the pore pressure generation, the decrease in effective stress and the development of axial strain are slower in treated samples.
- For lightly treated specimens with the largest fine grains contents (MS6.60 & MS6.100), the development of pore pressure features a nice S-shape as for untreated specimens. For the soils with lower fine grains contents (MS6.0 & MS6.40), the difference between untreated and treated samples mainly appears in the last part of the curve.
- In general, the Seed Model can efficiently model the excess pore pressure generation curves of lightly treated sand in one-stage cyclic triaxial tests. Good results are generally seen in specimens with fine contents larger than 40% (MS6.60 & MS6.100). For these samples, the α values are larger for the lightly treated samples (1-2) than for the untreated loose samples (around 0.4-1). R^2 values of lightly treated samples remain larger than 0.93, a bit smaller than those of untreated loose samples (0.96).
- In general, the Seed Model is satisfactory ($R^2 > 0.92$) in modelling the moderately- and heavily treated finest sands (MS6.60 & MS6.100) in multi-stage cyclic tests, but less good in modelling coarser sands. In this case, a procedure of data extension is used to improve the fitting. The fitting results for coarse sands (MS6.0, MS6.20 & MS6.40) are better ($R^2 > 0.9$) with extension of data.
- The number of cycles and the *CSR* required to reach liquefaction increase with the cementation level.
- Regarding the axial strain behavior, MICP treatment significantly decreases the contractive tendency of loosely prepared specimens. In addition to the more extensive behavior, the amplitude of the axial strains increases more slowly in treated specimens than in untreated ones. In the finest sands (MS6.60 & MS6.100), lightly treated and moderately treated samples show both contractive and

extensive axial strain behavior like untreated samples. With an increase in cementation level, the axial strain development of bio-cemented fine soils evolves from two-side (compressive and extensive) axial strain to one-side extension. For treated samples with larger grains (MS6.0, MS6.20 & MS6.40), on the other hand, only extensive axial strain is seen at all cementation levels. For larger grains, the cyclic resistance of lightly treated specimens is slightly enhanced, but the axial strain behavior evolves from compressive (for untreated samples) to extensive (for treated samples).

- For the coarsest sands (MS6.0 & MS6.20), the enhancement of the cyclic resistance of heavily treated specimens is comparable to that of untreated dense specimens. However, the mechanical behavior of the heavily treated samples, e.g., pore pressure generation mode and axial strain behavior, is different from that of the untreated dense specimens. The enhancement in cyclic resistance due to bio-cementation is more remarkable in soils with 40% fines and more (MS6.40, MS6.60, MS6.100) than in coarse sands. Even the lightly treated samples resist better than the dense samples though their density is smaller.
- A small amount of $CaCO_3$ (1-2%) can efficiently enhance the cyclic resistance and stress-strain behavior of the finest soils (MS6.60 & MS6.100), but a small amount of $CaCO_3$ is not sufficient to improve the behavior of soils with larger grains (MS6.0, MS6.20 and MS6.40)
- When the CSR_{100} is equal to 0.25, the minimum $CaCO_3$ content to see the effect of MICP treatment varies from 9.0 to 5.3, 4.4, 1.8 and 1.0% when the fine content increases from 0 to 20, 40, 60 and 100%, respectively. After reaching these minimum values of $CaCO_3$ content in each sand, a unified linear relationship between CSR_{100} and $\Delta CaCO_3$% for all the treated specimens of the various sands was established ($y = 0.0563x + 0.25$) with a R^2 value of 0.85.
- The results shown in chapters 5 and 7 concerning the effect of carbonate content are similar but with slightly differences concerning the values of minimum carbonate content. This is probably due to the interplay of the different effects of MICP in increasing cohesion (bridging), surface roughness (coating) and density (pore-filling) on the mechanical properties of the soil
- Concerning the effect of the grain size distribution, C_u is an important parameter of the mechanical behavior of untreated sand specimens, but it does not seem to be as important for the cyclic behavior of treated specimens. The larger the grains (increasing d_{50}), the larger the percentage of $CaCO_3$ required to observe the effect of bio-cementation. With increasing fine contents, less $CaCO_3$ is needed to obtain the same CSR_{100} value: Fines in soil matrix can significantly lower the required $CaCO_3$ content.
- According to the results of mercury intrusion porosimetry (MIP), the coarser the sand grains, the larger the pores, the smaller the total pore volume in treated specimens due to the larger calcium carbonate content.

Chapter 7 Conclusion and future perspectives

7.1 Conclusions

This thesis studies the effect of the low-carbon microbial induced calcium carbonate precipitation (MICP) method in enhancing the monotonic and cyclic behavior of treated sands (up to 5 mm in diameter) with different grain size distributions (i.e., various fines contents *FC* and uniformity coefficients C_u). In this study, the "fines" or "fine grains" are the grains whose diameter is smaller than 1 mm. The mean diameter (d_{50}) of the fines used in this study is comparable to, or even a bit larger than, the d_{50} of the sands used in most previous studies. Many biological, chemical, and physical experiments were carried out to analyze qualitatively and quantitatively the influence of the used soils (five grain size distributions) and bacteria (DSM33 from Leibniz Institute and SB from Solétanche Bachy), the MICP processes and protocols, and the monotonic (through consolidated drained triaxial tests) and cyclic (through consolidated undrained triaxial tests) mechanical behavior of MICP-treated sands, always with reference to the behavior of the untreated sands. The difference between the effect of MICP-treatment on monotonic and cyclic behavior is analyzed as well. Additional optical & electronic microscopy observations, X-ray diffraction and mercury intrusion porosimetry tests help in interpreting the results.

The following conclusions can be drawn:

(1) Concerning the bacteria and related MICP process and protocol,

- For DSM 33, oxygen availability is important. Insufficient oxygen quantity prevents bacterial growth. Oxygen transfer rate increases with the bacterial activity (biomass) and decreases rapidly with oxygen depletion. The advantages of DSM33 includes longer preservation time after the preparation of the bacterial solution and relatively stable rate of MICP reactions for longer treatments. DSM33 bacterial solution is appropriate and sustainable to be used in-situ trials with longer treatment period.
- At ambient temperature (around 20°C), a dramatic decrease in the viability and urease activity of the cells can be seen. Significant advantages of using SB bacteria include a much simpler preparation and a faster rate of MICP treatment, which are essential for right-away treatment in real sites.
- However, for SB, tests in solution show a rapid MICP reaction rate and 100% of MICP efficiency can be achieved up to 3.5 hours after mixing.
- Urease activity of the two bacteria increases with increasing biomass. The two kinds of bacteria feature similar specific urease activity (around 5 mM/min/OD), comparable to, or stronger than, what is found in the literature.

- SB bacteria were chosen to be used for the preparation of treated soil column specimens because of the above-mentioned advantages. For establishing MICP protocol, the effects of injection mode, injection speed of cementation solution, soil used and some other considerations on the efficiency of MICP were discussed. The injection mode consisting of 1 bacterial solution followed by 1 cementation solution, and an injection rate of 25 mL/min for the cementation solution, were chosen for the final MICP protocol.

(2) Concerning the monotonic and cyclic behavior of untreated sands

For the monotonic behavior of untreated loose sands:

- A noticeable increase in density occurs during saturation and consolidation of untreated loose specimens, which become medium dense after consolidation. However, during shearing, the specimens keep their "loose" behavior, and feature a stress-hardening failure mode, with an increase in strength with increasing confining pressure, mean grain size (d_{50}) and decreasing fines content. All the specimens contract, except MS6.0 that dilates. The dilation decreases when the confining pressure is increased.
- The slope M of the failure envelopes, i.e., the friction angle, decreases linearly with increasing fines content and increase with increasing mean grain size (d_{50}). There is no cohesion in untreated samples.
- The larger the uniformity coefficient C_u, the lower the critical state lines (*CSL*s) in the [e vs. p'] diagram, the smaller the slope of the *CSL*. The slope of the *CSL*s decreases with increasing fines content below the Transitional Fine Content (*TFC* $\cong$ 50%), then become stable at higher fine contents.

For the cyclic behavior of untreated specimens,

- The rate of excess pore pressure generation, the amplitude and rate of deformation, and the final axial strain at liquefaction, increase with increasing CSR. The excess pore pressure generation curve of all the sands, in the [δu vs. N] plane, evolves from an almost linear shape to a more and more obvious S-shape with decreasing CSR.
- Untreated loose samples always feature a two-side compressive and extensive axial strain. After reaching 0.5% of axial strain, the amplitude of the axial strain in each cycle increases rapidly. 5% axial strain is often obtained in the last loading cycles, even if the effective pore pressure criterion is first reached.
- The number of cycles to the initiation of liquefaction decreases with increasing applied *CSR*. Exponential functions ($CSR = a \times N^{-b}$) are given with $R^2 > 0.95$ to model *CSR* vs. N_L curves. The effect of the grain size distribution on the values of the fitting parameters a and b is discussed. The a values are independent of C_u, C_c, d_{50} and the fine content *FC*. The b values and $a_{b=0.1036}$ are independent of C_c.,

but are correlated with C_u, d_{50} and *FC* (*TFC*).

- The effect of the grain size distribution on the cyclic resistance is discussed. The cyclic resistance depends on C_u values. When C_u increases, the curvature of the [*CSR vs.* N_L] curve increases, the cyclic resistance of the sand decreases, and the sand is more susceptible to liquefaction. C_c seems to have no influence on cyclic resistance. When d_{50} is lower than 1 mm, the cyclic resistance decreases with increasing d_{50}. When d_{50} is between 1-2 mm, the cyclic resistance increases with d_{50}. When the fine content is lower than the *TFC* (50%), the cyclic resistance decreases with increasing fine content. When the fine content is larger than the *TFC*, the cyclic resistance increases with the fine content.
- Concerning the effect of density, as it is well known, dense specimens are less susceptible to liquefaction than loose specimens. One can see slower pore pressure generation and decrease in the amplitude and rate of deformation in dense specimens. The effect of density on cyclic resistance is remarkable in the specimens of sands with the highest fine contents (MS6.40, MS6.60 and MS6.100). The cyclic resistance enhancement in the specimens with the lowest fine contents (MS6.0 and MS6.20) is even much more remarkable.
- To better understand and predict the pore water pressure generation mode, curve fitting using Seed Model was carried out for both one-stage tests (*CSR* = 0.25) and multi-stage tests (MS6.0 & MS6.20 dense). The Seed Model simulates well the pore pressure generation of all the one-stage tests on the untreated specimens. In most cases, for the loose samples, the R^2 values are larger than 0.96, α is in the range of 0.5-1. For the dense samples, the R^2 values are larger than 0.94, α is in the range of 0.9-1.9.
- Based on the cases analyzed in this work, it seems that the *CSR* that leads to liquefaction in less than 100 cycles in multi-stage tests (CSR_{multi}) can be used to approach the *CSR* leading to liquefaction in less than 300 cycles in mono-stage tests (CSR_{mono}). Based on our test results, the CSR_{mono} is comprised between the CSR_{multi} and the (CSR_{multi}–0.1) for a similar number of cycles to liquefaction. This equivalence is all the more valid as the pore pressure increase is small at the end of the penultimate stage of the multi-stage test.

(3) Monotonic and cyclic behavior of treated sands

Regarding the monotonic behavior of treated sands with small amounts of $CaCO_3$,

- MICP treatment enhances the peak strength and dilation of the soil, and the strength increases with the cementation level. The soil shows a transitional behavior from strain hardening failure mode (for untreated specimens) to strain softening (for treated specimens). It is important to note for practical applications that the peaks are generally observed for axial strains larger than 4%, which shows that cemented specimens keep some ductility. The effect of MICP-treatment on residual strength is unclear maybe because that small amount of $CaCO_3$ has little effect in enhancing residual strength.

- The concept of minimum $CaCO_3$ content is introduced to quantitatively define the minimum $CaCO_3$ content required to see MICP effect on strength. Minimum $CaCO_3$ contents for MS6.0, MS6.40, MS6.60 and MS6.100 are equal to 7.21, 2.36, 2.40 and 1.99%, respectively. The minimum $CaCO_3$ content decreases with increasing C_u and fine content and increases with increasing mean diameter of the sand.
- To give a generalized quantitative relationship between the *Normalized* q_{max} (i.e., the ratio of the $q_{max\,T}$ of treated specimens to the $q_{max\,UT}$ of untreated specimens) and the $CaCO_3$ content for our sands with various grain size distributions, the $\Delta CaCO_3$ (which is the difference between the actual $CaCO_3$ content and the minimum $CaCO_3$ content) is introduced. The conclusion that can be drawn is that, after reaching the minimum $CaCO_3$ content, 1% more $CaCO_3$ precipitate can be expected to bring about a 0.21-fold increase in strength.
- For lightly treated MS6.20, MS6.40 and MS6.60 soils, with 3-4% $CaCO_3$ content, there seems to be a small (1-3°) increase in peak friction angle, and there is a definite increase in cohesion of about 10-13 kPa. The friction angle seems to increase with the $CaCO_3$ content and decrease with increasing mean grain size. However, these results must be considered with caution due to the small number of available data. The cohesion increases linearly with increasing $CaCO_3$ content, and decreases linearly with increasing C_u.
- The increasing shear resistance of MICP-treated specimens is mainly due to the increase in cohesion, the increasing friction angle (that is probably mainly the result of the increasing sand grain surface roughness, and maybe partially due to increasing density) plays a limited role.
- Almost no change in final void ratio e_f was observed between untreated and treated specimens because of the compensation effect of MICP treatment and dilation on density.
- Optical microscope images show the pore-filling, surface coating and particle-bridging effect of MICP-treatment, which provides evidence of the mechanical behavior enhancement. The result of SEM images and XRD patterns confirm that the main morphology of the formed $CaCO_3$ crystals is calcite, but a small amount of vaterite crystals is also seen. According to the result of mercury intrusion porosimetry (MIP), the coarser the sand grains, the larger the pores, the smaller the total pore volume in treated specimens.

Concerning the cyclic behavior of treated sands with multi-level cementations:

- In general, the cyclic resistance of treated specimens is improved compared with untreated samples and the improvement increases with the cementation level. During cyclic loading, the pore pressure generation, the decrease in effective stress and the development of axial strain in treated samples are slower than in untreated ones.
- It is important to note that it is not necessary to have cementation of the whole soil specimen but that the presence of cemented lumps of one or two centimeters inside the specimen may be sufficient to observe the effect of MICP-treatment.

- In the lightly treated specimens with the largest fine grains contents (MS6.60 & MS6.100), the development of pore pressure features a nice S-shape as in the untreated specimens. For the soils with lower fine grains contents (MS6.0 & MS6.40), the difference between untreated and treated samples mainly appears in the last part of the curve.
- The modified Seed model shows good results in modelling the excess pore pressure generation, using data extension when needed. For treated specimens, R^2 values are larger than 0.9, α is in the range of 1-3. In general, the Seed Model is less efficient in the case of specimens with less fines and higher $CaCO_3$ contents.
- Regarding the axial strain behavior, MICP treatment significantly decreases the axial strain contractive tendency of loosely prepared specimens. In addition to the more extensive behavior, the amplitude of the axial strains increases more slowly in treated specimens than in untreated ones. In the finest sands (MS6.60 & MS6.100), lightly treated and moderately treated samples show both contractive and extensive axial strain behavior like untreated samples. With an increase in cementation level, the axial strain development of bio-cemented fine soils evolves from two-side (compressive and extensive) axial strain to one-side extension. For treated samples with the largest mean grain diameter (MS6.0, MS6.20 & MS6.40), on the other hand, only extensive axial strain is seen at all cementation levels. For larger grains, the cyclic resistance of lightly treated specimens is slightly enhanced, but the axial strain behavior evolves from compressive (for untreated samples) to extensive (for treated samples).
- For the coarsest sands (MS6.0 & MS6.20), the enhancement of the cyclic resistance of heavily treated specimens is comparable to that of untreated dense specimens. However, the mechanical behavior of the heavily treated samples, e.g., the pore pressure generation mode and axial strain behavior, is different from that of the untreated dense specimens. The enhancement in cyclic resistance due to bio-cementation is more remarkable in soils with 40% fines and more (i.e., MS6.40, MS6.60, MS6.100) than in coarse sands. Even the lightly treated samples resist better than the dense samples though their density is smaller.
- A small amount of $CaCO_3$ (1-2%) can efficiently enhance the cyclic resistance and stress-strain behavior of the finest soils (MS6.60 & MS6.100), but a small amount of $CaCO_3$ is not sufficient to improve the behavior of soils with larger grains (MS6.0, MS6.20 and MS6.40)
- When the CSR_{100} is equal to 0.25, the minimum $CaCO_3$ content to see the effect of MICP treatment varies from 9.0 to 5.3, 4.4, 1.8 and 1.0% when the fine content increases from 0 to 20, 40, 60 and 100%, respectively. After reaching these minimum values of $CaCO_3$ content in each sand, a unified linear relationship between CSR_{100} and $\Delta CaCO_3$% for all the treated specimens of the various sands is established ($y = 0.0563x + 0.25$) with a R^2 value of 0.85.
- Concerning the effect of the grain size distribution, the larger the grains (increasing d_{50}), the larger the percentage of $CaCO_3$ required to observe the effect of bio-cementation. With increasing fine contents, less $CaCO_3$ is needed to obtain the same CSR_{100} value: Fines in soil matrix can significantly lower the required

$CaCO_3$ content.

For all the treated specimens

- In spite of the similar results concerning the minimum calcium carbonate contents, the slight observed differences between monotonic tests and cyclic tests probably result from the different significance and interplay of the different mechanisms involved in MICP-treatment: increase in cohesion (bridging), increase in surface roughness (coating) and increase in density (pore-filling). All these mechanisms influence the mechanical properties of the soil, but in different ways.
- Small amounts of $CaCO_3$ result in more significant improvement in cyclic behavior than in monotonic behavior. For the finest sands (≥ 40% fines), a small amount of $CaCO_3$ (3-4 %) can significantly increase the peak strength (20-40%), the dilative behavior, the cohesion (10-15kPa), but with only a small increase in friction angle (1-3◦) and hardly any change in residual strength. Similar or even smaller amounts of $CaCO_3$ (1-4%) can improve a lot the cyclic resistance, i.e., increase N_L from 10-30 folds.
- Though there are sometimes uncertainties in using the $CaCO_3$ content to characterize and quantify the results concerning MICP-treated sands, because of the uneven distribution and precipitation location, this parameter is still indicative and easy to obtain.
- The mechanical behavior of MS6.0 is always different from that of the others, probably because this material is the only one without fines. Though specimens of MS6.0 and MS6.100 have similar void ratios, for a similar improvement in mechanical behavior, the required $CaCO_3$ content is much larger for MS6.0 than for MS6.100. This is certainly due to the larger specific surface area of MS6.100.
- C_u is an important parameter to analyze the cyclic behavior of untreated soils; it does not seem as important in the case of the cyclic behavior of MICP-treated specimens.

7.2 Future perspectives

Recommendations regarding future experimental work include,

- More kinds of soils should be tested to see the efficiency of MICP treatment. For example, soils with a much larger range of maximum diameters, soils with larger C_u, soils with various fine contents, different mineralogy and morphology, etc.
- To optimize the industrial bacteria, several aspects from a microbial perspective can be strengthened. For example, try to find the maximum growth rate and biomass (urease) through balancing culture time, culture medium (adding additives, using economic materials or wastes) and environment (pH, oxygen, temperature…). Strain improvement through genetic engineering and

mutagenesis is optional. The hunting for new bacteria with high activity and environmental tolerance (pH, temperature, and oxygen requirement), environmental-friendly by-products is always desirable.

- The location of $CaCO_3$ crystals is important to improve the mechanical behavior of treated specimens. Oriented precipitation $CaCO_3$ is quite interesting.
- With the development of new sensors, e.g., optical fibers, research for new parameters with less uncertainties should be carried out to characterize the properties of treated specimens.

Recommendations concerning future modelling work include,

- Create a database, with different scenarios of effective MICP protocols that include soil characteristics (grain size distribution, mineralogy, and morphology), environmental parameters (temperature, oxygen availability, etc.), injection strategy (injection mode, injection rate, etc.), concentration of the materials (bacterial and cementation solutions, etc.), etc.
- Relate the monotonic and cyclic behavior of the sands to the resulting $CaCO_3$ content is important.
- Modelling pore pressure generation axial strain accumulation using constitutive models taking into account all the aspects of the soil behavior.

References

A

Abu-Ashour, J., Joy, D. M., Lee, H., Whiteley, H. R., and Zelin, S. (1994). Transport of microorganisms through soil. Water, Air and Soil Pollution, 75(519), 141–158.

Achal, V., and Mukherjee, A. (2015). A review of microbial precipitation for sustainable construction. Construction and Building Materials, 93, 1224–1235. https://doi.org/10.1016/j.conbuildmat.2015.04.051

Adalier, K., et al. (2003) Stone columns as liquefaction countermeasure in non-plastic silty soils. Soil Dynamics and Earthquake Engineering 23.7 (2003): 571-584. https://doi.org/10.1016/S0267-7261(03)00070-8

Adamczyk, Z., and Weroński, P. (1999). Application of the DLVO theory for particle deposition problems. Advances in Colloid and Interface Science, 83(1), 137–226. https://doi.org/10.1016/S0001-8686(99)00009-3

Ahmadi, M.M. and Akbari Paydar, N. (2014). Requirements for soil-specific correlation between shear wave velocity and liquefaction resistance of sands, Soil Dyn. Earthq. Eng., 57, 152–163. https://doi.org/10.1016/j.soildyn.2013.11.001.

Almajed, A., Tirkolaei, H. K., Kavazanjian, E., and Hamdan, N. (2019). Enzyme Induced Biocemented Sand with High Strength at Low Carbonate Content. Nature, 9(1135), 1–7. https://doi.org/10.1038/s41598-018-38361-1

Al Qabany, A., Mortensen, B., Martinez, B., Soga, K. and Dejong, J. (2011), “Microbial carbonate precipitation: correlation of S-wave velocity with calcite precipitation”, Geo-Frontiers 2011, pp 3993–4001, Dallas, Texas, USA, March.

Al Qabany, A., Soga, K., and Santamarina, C. (2012). Factors Affecting Efficiency of Microbially Induced Calcite Precipitation. Journal of Geotechnical and Geoenvironmental Engineering, 138(8), 992–1001. https://doi.org/10.1061/(ASCE)GT.1943-5606.0000666

Al Qabany, A. and Soga, K. (2013), “Effect of chemical treatment used in MICP on engineering properties of cemented soils”, Géotechnique, 63, 331–339. https://doi.org/10.1680/geot.SIP13.P.022.

Al-Salloum, Y., Hadi, S., Abbas, H., Almusallam, T., and Moslem, M. A. (2017). Bio-induction and bioremediation of cementitious composites using microbial mineral precipitation – A review. Construction and Building Materials, 154, 857–876. https://doi.org/10.1016/j.conbuildmat.2017.07.203

Ashraf, M. S., Azahar, S. B., and Yusof, N. Z. (2017). Soil Improvement Using MICP and Biopolymers: A Review. IOP Conference Series: Materials Science and Engineering, 226(1).

https://doi.org/10.1088/1757-899X/226/1/012058

B

Bahmani, M., Noorzad A., Hamedi J. and Sali F. (2017). The role of Bacillus pasteurii on the change of parameters of sands according to temperature compresion and wind erosion resistance, J. CleanWAS, 1, 1–5. https://doi.org/10.26480/jcleanwas.02.2017.01.05.

Barkouki, T. H., Martinez, B. C., Mortensen, B. M., Weathers, T. S., de Jong, J. D., Ginn, T. R., … Fujita, Y. (2011). Forward and Inverse Bio-Geochemical Modelling of Microbially Induced Calcite Precipitation in Half-Meter Column Experiments. Transport in Porous Media, 90(1), 23–39. https://doi.org/10.1007/s11242-011-9804-z

Bernardi, D. J. (2012). Biologically Cemented Sandstone Bricks. University of California, Davis, 2012.

Biarez, J. and Hicher, P.Y. (1994), Elementary Mechanics of Soil Behavior: Saturated Remoulded Soils, A.A. Balkema, Lisse, The Netherlands.

Burenkova, V. V. (1993). Assessment of suffusion in non-cohesive and graded soils. Filters in Geotechnical and Hydraulic Engineering. Balkema, Rotterdam, 357–360.

C

Cardoso, R., Pedreira, R., Duarte, S., Monteiro, G., Borges, H. and Flores-Colen, I. (2016). Biocementation as rehabilitation technique of porous materials, New Approaches to Building Pathology and Durability, Springer, pp. 99–120. https://doi.org/10.1007/978-981-10-0648-7_5.

Cardoso, R., Pires, I., Duarte, S.O.D and Monteiro, G.A. (2018). Effects of clay's chemical interactions on biocementation, Appl. Clay Sci, 156, 96–103. https://doi.org/10.1016/j.clay.2018.01.035.

Cerfontaine, B., and Collin, F. (2018). Cyclic and Fatigue Behaviour of Rock Materials: Review, Interpretation and Research Perspectives. Rock Mechanics and Rock Engineering, 51(2), 391–414. https://doi.org/10.1007/s00603-017-1337-5

Chang, I., Im, J., and Cho, G. C. (2016). Introduction of microbial biopolymers in soil treatment for future environmentally-friendly and sustainable geotechnical engineering. Sustainability (Switzerland), 8(3). https://doi.org/10.3390/su8030251

Cheng, L. (2012). Innovative ground enhancement by improved microbially induced $CaCO_3$ precipitation technology, Ph.D. Dissertation, Murdoch University, Perth, Western Australia.

Cheng, L., and Cord-Ruwisch, R. (2012). In situ soil cementation with ureolytic bacteria by surface percolation. Ecological Engineering, 42, 64–72. https://doi.org/10.1016/j.ecoleng.2012.01.013

Cheng, L., Cord-Ruwisch, R., and Shahin, M. A. (2013). Cementation of sand soil by microbially induced calcite precipitation at various degrees of saturation. Canadian Geotechnical Journal, 50(1), 81–90. https://doi.org/10.1139/cgj-2012-0023

Cheng, L., Shahin, M. A., and Cord-Ruwisch, R. (2014). Bio-cementation of sandy soil using microbially induced carbonate precipitation for marine environments. Géotechnique, 64(12), 1010–1013. https://doi.org/10.1680/geot.14.T.025

Cheng, L., Shahin, M. A., Cord-Ruwisch, R., Addis, M., Hartanto, T., and Elms, C. (2014). Soil Stabilisation by Microbial-Induced Calcite Precipitation (MICP): Investigation into Some Physical and Environmental Aspects. In 7th International Congress on Environment Geotechnics, 10 - 14 November, Melbourne, Australia (pp. 1105–1112). Retrieved from https://search.informit.com.au/documentSummary;dn=000879880064866;res=IELENG

Cheng, L., Shahin, M.A. and Mujah, D. (2017). Influence of key environmental conditions on microbially induced cementation for soil stabilization, J. Geotech. Geoenvironmental Eng. https://doi.org/10.1061/(ASCE) GT.1943-5606.0001586.

Cheng, L., Shahin, M. A., and Chu, J. (2019). Soil bio-cementation using a new one-phase low-pH injection method. Acta Geotechnica, 14(3), 615–626. https://doi.org/10.1007/s11440-018-0738-2

Chiaro, G., Koseki, J., and Sato, T. (2012). Effects of initial static shear on liquefaction and large deformation properties of loose saturated Toyoura sand in undrained cyclic torsional shear tests. Soils and Foundations, 52(3), 498–510. https://doi.org/10.1016/j.sandf.2012.05.008

Choi, S. G., Wang, K., and Chu, J. (2016). Properties of biocemented, fiber reinforced sand. Construction and Building Materials, 120, 623–629. https://doi.org/10.1016/j.conbuildmat.2016.05.124

Choi, S.G., Wang, K., Wen, Z. and Chu, J. (2017). Mortar crack repair using microbial induced calcite precipitation method, Cem. Concr. Compos., 83, 209–221. https://doi.org/10.1016/j.cemconcomp.2017.07.013.

Choi, S. G., Wang, K., Wen, Z., and Chu, J. (2017). Mortar crack repair using microbial induced calcite precipitation method. Cement and Concrete Composites, 83, 209–221. https://doi.org/10.1016/j.cemconcomp.2017.07.013

Choi, S.G., Chu, J. and Kwon, T.H. (2019). Effect of chemical concentrations on strength and crystal size of biocemented sand, Geomechanics and Engineering, 17(5), 465–473. https://doi.org/10.12989/GAE.2019.17.5.465.

Choi, S. G., Chang, I., Lee, M., Lee, J. H., Han, J. T. and Kwon, T. H. (2020). Review on geotechnical engineering properties of sands treated by microbially induced calcium

carbonate precipitation (MICP) and biopolymers, Construction and Building Materials, 246, 118415. https://doi.org/10.1016/j.conbuildmat.2020.118415.

Chou, C.-W., Seagren, E. A., Aydilek, A. H., and Lai, M. (2011). Biocalcification of Sand through Ureolysis. Journal of Geotechnical and Geoenvironmental Engineering, 137(12), 1179–1189. https://doi.org/10.1061/(asce)gt.1943-5606.0000532

Chu, J., Ivanov, V., Naeimi, M., Stabnikov, V., and Liu, H. L. (2014). Optimization of calcium-based bioclogging and biocementation of sand. Acta Geotechnica, 9(2), 277–285. https://doi.org/10.1007/s11440-013-0278-8

Connolly, J., Kaufman, M., Rothman, A., Gupta, R., Redden, G., Schuster, M., Colwell, F., and Gerlach, R. (2013). Construction of two ureolytic model organisms for the study of microbially induced calcium carbonate precipitation, J Microbiol Methods, 94, 290–299. https://doi.org/10.1016/j.mimet.2013.06.028.

Cui, M. J., Zheng, J. J., and Lai, H. J. (2017). Effect of method of biological injection on dynamic behavior for bio-cemented sand. Yantu Lixue/Rock and Soil Mechanics, 38(11), 3173–3178. https://doi.org/10.16285/j.rsm.2017.11.012

Cui, M.J., Zheng, J.J., Zhang, R.J., Lai, H.J. and Zhang, J. (2017). Influence of cementation level on the strength behavior of bio-cemented sand, Acta Geotech., 12, 971–986. https://doi.org/10.1007/s11440-017-0574-9.

Cui, M.J., Zheng, Chu, J., Wu, C.C., and Lai, H.J. (2021), Bio-mediated calcium carbonate precipitation and its effect on the shear behaviour of calcareous sand, Acta Geotech.. https://doi.org/10.1007/s11440-020-01099-0.

D

Dadda, A., Geindreau, C., Emeriault, F., Rolland du Roscoat, S., Garandet, A., Sapin, L. and Esnaut Filet, A. (2017), Characterization of microstructural and physical properties changes in biocemented sand using 3D X-ray microtomography, Acta Geotech., 12, 955–970. https://doi.org/10.1007/s11440-017-0578-5.

Danjo, T., and Kawasaki, S. (2016). Microbially induced sand cementation method using pararhodobacter sp. strain SO1, inspired by beachrock formation mechanism. Materials Transactions, 57(3), 428–437. https://doi.org/10.2320/matertrans.M-M2015842

Darby, K.M., Hernandez, G.L., Dejong, J.T., Boulanger, R.W., Gomez, M.G. and Wilson, D.W. (2019), Centrifuge Model testing of liquefaction mitigation via microbially induced calcite precipitation, J. Geotech. Geoenvironmental Eng., 145, 1–13. https://doi.org/10.1061/(ASCE)GT.1943-5606.0002122.

Decho, A.W. (2010), Overview of biopolymer-induced mineralization: What goes on in biofilms?, Ecol. Eng., 36, 137–144. https://doi.org/10.1016/j.ecoleng.2009.01.003.

Dejong, J.T., Fritzges, M.B. and Nüsslein, K. (2006), Microbially induced cementation to control sand response to undrained shear, J. Geotech. Geoenvironmental Eng., 132, 1381–1392. https://doi.org/10.1061/(ASCE)1090-0241(2006)132:11(1381).

Dejong, J.T., Mortensen, B.M., Martinez, B.C. and Nelson, D.C. (2010), Bio-mediated soil improvement, Ecol. Eng., 36, 197–210. https://doi.org/10.1016/j.ecoleng.2008.12.029.

Dejong, J. T., Soga, K., E., K., Burns, S., van Paassen, L. A., Qabany, A. Al, … T., W. (2013). Biogeochemical processes and geotechnical applications: progress, opportunities and challenges. Géotechnique, 63(4), 287–301. https://doi.org/10.1680/geot.SIP13.P.017

Dejong, J.T., Soga, K., Kavazanjian, E., Burns, S., Van Paassen, L.A., Al Qabany, A., Aydilek, A., Bang, S.S., Burbank, M., Caslake, L.F., Chen, C.Y., Cheng, X., Chu, J., Ciurli, S., Esnault-Filet, A., Fauriel, S., Hamdan, N., Hata, T., Inagaki, Y., Jefferis, S., Kuo, M., Laloui, L., Larrahondo, J., Manning, D.A.C., Martinez, B., Montoya, B.M., Nelson, D.C., Palomino, A., Renforth, P., Santamarina, J.C., Seagren, E.A., Tanyu, B., Tsesarsky, M. and Weaver, T. (2013), Biogeochemical processes and geotechnical applications: progress, opportunities and challenges, Géotechnique, 63, 287–301. https://doi.org/10.1680/geot.SIP13.P.017.

Dejong, J.T., Martinez, B.C., Ginn, T.R., Hunt, C., Major, D. and Tanyu, B. (2014), Development of a scaled repeated five-spot treatment model for examining microbial induced calcite precipitation feasibility in field applications, Geotech. Test J., 37, 424–435. https://doi.org/10.1520/GTJ20130089.

De Muynck, W., Verbeken, K., De Belie, N., and Verstraete, W. (2010). Influence of urea and calcium dosage on the effectiveness of bacterially induced carbonate precipitation on limestone. Ecological Engineering, 36(2), 99–111. https://doi.org/10.1016/j.ecoleng.2009.03.025

Dhami, N.K., Reddy, M.S. and Mukherjee, A. (2013), Biomineralization of calcium carbonate polymorphs by the bacterial strains isolated from calcareous sites, J. Microbiol. Biotechnol., 23, 707–714. https://doi.org/10.4014/jmb.1212.11087.

De, J., Montoya, B.M. and Gabr, M.A. (2019), Debonding of microbially induced carbonate precipitation-stabilized sand by shearing and erosion, Geomechanics and Engineering, 17(5), 429–438. https://doi.org/10.12989/GAE.2019.17.5.429.

E

El-Latief, M.A.A., Ashour, M.B. and El-Tahrany, A.C. (2015). Strengthening of the permeability of sandy soil by different grouting materials for seepage reduction, Glob. J. Res. Eng. Civ. Struct. Eng., 15(3), 39–48.

Ercole, C., Bozzelli, P., Altieri, F., Cacchio, P. and Del Gallo, M. (2012), Calcium carbonate mineralization: involvement of extracellular polymeric materials isolated from calcifying bacteria, Microsc. Microanal., 18(4), 829–839. https://doi.org/10.1017/S1431927612000426.

Eryürük K., Yang S., Suzuki D., Sakaguchi, I. and Katayama, A. (2015), Effects of bentonite and yeast extract as nutrient on decrease in hydraulic conductivity of porous media due to $CaCO_3$ precipitation induced by Sporosarcina pasteurii, J. Biosci Bioeng., 120, 411–418. https://doi.org/10.1016/j.jbiosc.2015.01.020.

Esnault Filet, A., Gutjahr, I., Garandet, A., Viglino, A., Beguin, R., Sibourg, O., Monnier, J.M., Martins, J., Oxarango, L., Spadini, L., Geindreau, C., Emeriault, F., Castanier Perthuisot, S. (2019), BOREAL, Bio-reinforcement of embankments by biocalcification, Digues Maritimes et Fluviales de Protection Contre les Inondations, Aix-en-Provence, France. (In French) https://doi.org/10.5281/zenodo.2532995.

F

Farah, T., Souli, H., Fleureau, J.M., Kermouche, G., Fry, J.J., Girard, B., Aelbrecht, D., Lambert, J. and Harkes, M. (2016), “Durability of bioclogging treatment of soils”, J. Geotech. Geoenvironmental Engineering. https://doi.org/10.1061/(ASCE)GT.1943-5606.0001503.

Fauriel, S., and Laloui, L. (2012). A bio-chemo-hydro-mechanical model for microbially induced calcite precipitation in soils. Computers and Geotechnics, 46, 104–120. https://doi.org/10.1016/j.compgeo.2012.05.017

Feng, K. and Montoya, B.M. (2016). Influence of confinement and cementation level on the behavior of microbial-induced calcite precipitated Sands under monotonic drained loading, J. Geotech. Geoenvironmental Engineering. https://doi.org/10.1061/(ASCE)GT.1943-5606.0001379.

Feng, K. and Montoya, B.M. (2017), Quantifying level of microbial-induced cementation for cyclically loaded Sand, J. Geotech. Geoenvironmental Eng., https://doi.org/10.1061/(ASCE)GT.1943-5606.0001682.

G

Gai, X., and Sánchez, M. (2019). An elastoplastic mechanical constitutive model for microbially mediated cemented soils. Acta Geotechnica, 0123456789, 709–726. https://doi.org/10.1007/s11440-018-0721-y

Gao, Y., Hang, L., He, J. and Chu, J. (2019). Mechanical behaviour of biocemented sands at various treatment levels and relative densities, Acta Geotech., 14, 697–707. https://doi.org/10.1007/s11440-018-0729-3.

Gat, D., Tsesarsky, M., Shamir, D. and Ronen, Z. (2014). Accelerated microbial-induced $CaCO_3$ precipitation in a defined coculture of ureolytic and non-ureolytic bacteria, Biogeosciences, 11, 2561–2569. https://doi.org/10.5194/bg-11-2561-2014.

Gat, D., Ronen, Z., and Tsesarsky, M. (2017). Long-term sustainability of microbial-induced CaCO3precipitation in aqueous media. Chemosphere, 184, 524–531. https://doi.org/10.1016/j.chemosphere.2017.06.015

Ghosh, T., Bhaduri, S., Montemagno, C. and Kumar, A. (2019). Sporosarcina pasteurii can form nanoscale calcium carbonate crystals on cell surface, PLoS One, 14, 1–15. https://doi.org/10.1371/journal.pone.0210339.

Georgiannou, V. N., and Konstadinou, M. (2014). Effects of density on cyclic behaviour of anisotropically consolidated Ottawa sand under undrained torsional loading. Geotechnique, 64(4), 287–302. https://doi.org/10.1680/geot.13.P.090

Gobbi, S., Reiffsteck, P., Lenti, L., d'Avila, M. P. S., and Semblat, J. F. (2021). Liquefaction triggering in silty sands: effects of non-plastic fines and mixture-packing conditions. Acta Geotechnica, 1. https://doi.org/10.1007/s11440-021-01262-1

Gomez, M. G., Martinez, B. C., de Jong, J. T., Hunt, C. E., DeVlaming, L. A., Major, D. W., and Dworatzek, S. M. (2015). Field-scale bio-cementation tests to improve sands. Proceedings of the Institution of Civil Engineers - Ground Improvement, 168(3), 206–216. https://doi.org/10.1680/grim.13.00052

Gomez, M.G. and Dejong, J.T. (2017). Engineering Properties of Bio-Cementation Improved Sandy Soils, Grouting 2017 GSP 288, pp 23–33, Honolulu, Hawaii, July.

Gomez, M. G., Anderson, C. M., Graddy, C. M. R., de Jong, J. T., Nelson, D. C., and Ginn, T. R. (2017). Large-Scale Comparison of Bioaugmentation and Biostimulation Approaches for Biocementation of Sands. Journal of Geotechnical and Geoenvironmental Engineering, 143(5), 04016124. https://doi.org/10.1061/(ASCE)GT.1943-5606.0001640

Gomez, M.G., Dejong, J.T. and Anderson, C.M. (2018). Effect of bio-cementation on geophysical and cone penetration measurements in sands, Can. Geotech. J. https://doi.org/10.1139/cgj-2017-0253.

Gomez, M. G., Graddy, C. M. R., de Jong, J. T., Nelson, D. C., and Tsesarsky, M. (2018). Stimulation of native microorganisms for biocementation in samples recovered from field scale treatment depths. Journal of Geotechnical and Geoenvironmental Engineering, 144(1), 1–13. https://doi.org/10.1061/(ASCE)GT.1943-5606.0001804.

Gowthaman, S., Nakashima, K., and Kawasaki S. (2020). Freeze-thaw durability and shear responses of cemented slope soil treated by microbial induced carbonate precipitation, Soils and Foundations, https://doi.org/10.1016/j.sandf.2020.05.012.

H

Hamdan, N., Kavazanjian, J. E., and S., O. (2013). Carbonate cementation via plant derived urease. Proceedings of the 18th International Conference on Soil Mechanics and Geotechnical Engineering, Paris 2013, (480), 2489–2492.

Hammes, F., Boon, N., De Villiers, J., Verstraete, W., and Siciliano, S. D. (2003). Strain-specific ureolytic microbial calcium carbonate precipitation. Applied and Environmental Microbiology, 69(8), 4901–4909. https://doi.org/10.1128/AEM.69.8.4901-4909.2003

Haouzi, F., Esnault Filet, A. and Courcelles, B. (2019). Performance studies of microbial induced calcite precipitation to prevent the erosion of internally unstable granular soils, Advancements on Sustainable Civil Infrastructures, GeoChina 2018, Sustainable Civil Infrastructures, Hangzhou, China, July. https://doi.org/10.1007/978-3-319-96241-2_4.

Harkes, M. P., van Paassen, L. A., Booster, J. L., Whiffin, V. S., and van Loosdrecht, M. C. M. (2010). Fixation and distribution of bacterial activity in sand to induce carbonate precipitation for ground reinforcement. Ecological Engineering, 36(2), 112–117. https://doi.org/10.1016/j.ecoleng.2009.01.004

Hataf, N. and Jamali, R. (2018). Effect of fine-grain percent on soil strength properties improved by biological method, Geomicrobiol. J., 35, 695–703. https://doi.org/10.1080/01490451.2018.1454554.

He, J., Chu, J., and Liu, H. (2014). Undrained shear strength of desaturated loose sand under monotonic shearing. Soils and Foundations. https://doi.org/10.1016/j.sandf.2014.06.020

Hussien, M.N. and Karray, M. (2016). Shear wave velocity as a geotechnical parameter: An overview, Can. Geotech. J., 53, 252–272. https://doi.org/10.1139/cgj-2014-0524.

I

Idriss, I. M., and Boulanger, R. W. (2008). Soil liquefaction during earthquakes. Earthquake Engineering Research Institute.

Imran, M.A., Nakashima, K., Evelpidou, N. and Kawasaki, S. (2019). Factors affecting the urease activity of native ureolytic bacteria isolated from coastal areas, Geomechanics and Engineering, 17(5), 421–427. https://doi.org/10.12989/GAE.2019.17.5.421.

Ishihara, K. (1993). Liquefaction and flow failure during earthquakes. Géotechnique, 43(3), 351–451. https://doi.org/10.1680/geot.1993.43.3.351

Ivanov, V. and Chu, J. (2008). Applications of microorganisms to geotechnical engineering for bioclogging and biocementation of soil in situ, Rev. Environ. Sci Biotechnol., 7, 139–153. https://doi.org/10.1007/s11157-007-9126-3.

Ivanov, V. (2010). Environmental microbiology for engineers, CRC Press, Taylor and Francis Group, Boca Raton, USA

J

Jiang, N.J. and Soga, K. (2017). The applicability of microbially induced calcite precipitation (MICP) for internal erosion control in gravel–sand mixtures, Géotechnique, 67, 42–55. https://doi.org/10.1680/jgeot.15.p.182.

Jiang, N.J., Soga, K. and Kuo, M. (2017). Microbially induced carbonate precipitation for seepage-induced internal erosion control in sand–clay mixtures, J. Geotech. Geoenvironmental Eng. https://doi.org/10.1061/(asce)gt.1943-5606.0001559.

K

Kafarski, P., and Talma, M. (2018). Recent advances in design of new urease inhibitors: A review. Journal of Advanced Research, 13, 101–112. https://doi.org/10.1016/j.jare.2018.01.007

Kawaguchi, T. and Decho, A.W. (2002). A laboratory investigation of cyanobacterial extracellular polymeric secretions (EPS) in influencing $CaCO_3$ polymorphism, J. Cryst. Growth, 240, 230–235. https://doi.org/10.1016/S0022-0248(02)00918-1.

Kenney, T. C., and Lau, D. (1985). Internal stability of granular filters. Canadian Geotechnical Journal, 22, 215–225. https://doi.org/10.1139/t86-068

Kenney, T.C., and Lau, D. (1986). Internal stability of granular filters: reply, Can. Geotech. J. 23: 420-423.

Kim, G., Kim, J., and Youn, H. (2018). Effect of Temperature, pH, and Reaction Duration on Microbially Induced Calcite Precipitation. Applied Sciences, 8(8), 1277. https://doi.org/10.3390/app8081277

Kontoyannis, C. G., and Vagenas, N. V. (2000). Calcium carbonate phase analysis using XRD and FT-Raman spectroscopy. Analyst, 125(2), 251–255. https://doi.org/10.1039/a908609i

L

Ladd, Richard S. (1974). Specimen preparation and liquefaction of sands. Journal of the Geotechnical Engineering Division 100.10: 1180-1184. https://doi.org/10.1061/AJGEB6.0000117

Lade, P. V., and Yamamuro, J. A. (1997). Effects of nonplastic fines on static liquefaction of sands. Canadian Geotechnical Journal, 34(6), 918–928. https://doi.org/10.1139/t97-052

Lapierre, F. M., Schmid, J., Ederer, B., Ihling, N., Büchs, J., and Huber, R. (2020). Revealing nutritional requirements of MICP-relevant Sporosarcina pasteurii DSM33 for growth

improvement in chemically defined and complex media. Scientific Reports, 10(1), 1–14. https://doi.org/10.1038/s41598-020-79904-9

Lauchnor, E. G., Topp, D. M., Parker, A. E., and Gerlach, R. (2015). Whole cell kinetics of ureolysis by Sporosarcina pasteurii. Journal of Applied Microbiology, 118(6), 1321–1332. https://doi.org/10.1111/jam.12804

Lee, L. M., Ng, W. S., Tan, C. K., and Hii, S. L. (2012). Bio-Mediated Soil Improvement under Various Concentrations of Cementation Reagent. Applied Mechanics and Materials, 204–208(September), 326–329. https://doi.org/10.4028/www.scientific.net/AMM.204-208.326

Lee, M., Gomez, M.G., El Kortbawi, M., and Ziotopoulou, K. (2020). Examining the Liquefaction Resistance of Lightly Cemented Sands Using Microbially Induced Calcite Precipitation (MICP), GeoCongress 2020, ASCE, Minneapolis, Minnesota, Feb. 25-28, GSP 320, 53-64. https://doi.org/10.1061/9780784482841.

Lee, M., Gomez, M. G., El Kortbawi, M., and Ziotopoulou, K. (2022). Effect of Light Biocementation on the Liquefaction Triggering and Post-Triggering Behavior of Loose Sands. Journal of Geotechnical and Geoenvironmental Engineering, 148(1). https://doi.org/10.1061/(asce)gt.1943-5606.0002707

Li, B. (2015). Geotechnical properties of biocement treated sand and clay, Ph.D. Dissertation; Nanyang Technological University, Singapore.

Li, C., Yao, D., Liu, S., Zhou, T., Bai, S., Gao, Y. and Li, L. (2018). Improvement of geomechanical properties of bio-remediated aeolian sand, Geomicrobiol. J., 35,132–140. https://doi.org/10.1080/01490451.2017.1338798.

Li, L., Wen, K., Li, C. and Amini, F. (2017). FIB/SEM imaging of microbial induced calcite precipitation in sandy soil, Microsc. Microanal., 23, 310–311. https://doi.org/10.1017/S1431927617002239.

Liang, S., Chen, J., Niu, J., Gong, X. and Feng, D. (2019). Using recycled calcium sources to solidify sandy soil through microbial induced carbonate precipitation, Mar. Georesources Geotechnol.. https://doi.org/10.1080/1064119X.2019.1575939.

Lin, H. (2016). Microbial modification of soil for ground improvement, Ph.D. Dissertation; Lehigh University, USA.

Lin, H., Suleiman, M.T., Brown, D.G. and Kavazanjian, E. (2016). Mechanical behavior of sands treated by microbially induced carbonate precipitation, J. Geotech. Geoenvironmental Eng., 142, 1–13. https://doi.org/10.1061/(ASCE)GT.1943-5606.0001383.

Lin, H., Suleiman, M. T., Jabbour, H. M., Brown, D. G., and Kavazanjian, E. (2016). Enhancing the axial compression response of pervious concrete ground improvement piles using biogrouting. Journal of Geotechnical and Geoenvironmental Engineering, 142(10), 1–12. https://doi.org/10.1061/(ASCE)GT.1943-5606.0001515

Lin, H., Suleiman, M.T., and Brown, D.G. (2021). Investigation of pore-scale $CaCO_3$ distributions and their effects on stiffness and permeability of sands treated by microbially induced carbonate precipitation (MICP), Soils and Foundations. https://doi.org/10.1016/j.sandf.2020.07.003.

Liu, D., Shao, A., Li, H., Jin, C., and Li, Y. (2020). A study on the enhancement of the mechanical properties of weak structural planes based on microbiologically induced calcium carbonate precipitation. Bulletin of Engineering Geology and the Environment, 79(8), 4349–4362. https://doi.org/10.1007/s10064-020-01818-7

Liu, H., Zhang, X., Xiao, P., and Chu, J. (2020). Predictions of dynamic pore water pressure for MICP-treated calcareous sand, (October) (in chinese)

M

Mahanty, B., Kim, S., and Kim, C. G. (2014). Biokinetic modeling of ureolysis in Sporosarcina pasteurii and its integration into a numerical chemodynamic biocalcification model. Chemical Geology, 383, 13–25. https://doi.org/10.1016/j.chemgeo.2014.05.034

Mahawish, A., Bouazza, A. and Gates, W.P. (2018). Effect of particle size distribution on the bio-cementation of coarse aggregates, Acta Geotech., 13, 1019–1025. https://doi.org/10.1007/s11440-017-0604-7.

Martinez, B.C. and Dejong, J.T. (2009). Bio-Mediated Soil Improvement: Load Transfer Mechanisms at the Micro- and Macro- Scales Brian, Advances in Ground Improvement. 2009 US-China. Workshop on ground improvement technologies pp 242–251. https://doi.org/10.1061/41025(338)26.

Martinez, B.C., Dejong, J.T., Ginn, T.R., Montoya, B.M., Barkouki, T.H., Hunt, C., Tanyu, B. and Major, D. (2013). Experimental optimization of microbial-induced carbonate precipitation for soil improvement, J. Geotech. Geoenvironmental Eng., 139, 587–598. https://doi.org/10.1061/(ASCE)GT.1943-5606.0000787.

Marzin, T., Desvages, B., Creppy, A., Lépine, L., Esnault-Filet, A. and Auradou, H. (2020). Using Microfluidic set-up to determine the adsorption rate of Sporosarcina pasteurii bacteria on sandstone, Transp. Porous Media. https://doi.org/10.1007/s11242-020-01391-3.

Mirmohammad Sadeghi, M., Modarresnia, A. R., and Shafiei, F. (2015). Parameters Effects Evaluation of Microbial Strengthening of Sandy Soils in Mixing Experiments Using Taguchi Methodology. Geomicrobiology Journal, 32(5), 453–465. https://doi.org/10.1080/01490451.2014.958206

Mobley, H. L., Island, M. D., and Hausinger, R. P. (1995). Molecular biology of microbial ureases. Microbiological Reviews.

Monkul, M. M., Kendir, S. B., and Tütüncü, Y. E. (2021). Combined effect of fines content and

uniformity coefficient on cyclic liquefaction resistance of silty sands. Soil Dynamics and Earthquake Engineering, 151(September), 106999. https://doi.org/10.1016/j.soildyn.2021.106999

Montoya, B.M., Dejong, J.T., Boulanger, R.W., Wilson, D.W., Gerhard, R., Ganchenko, A. and Chou, J.C. (2012), Liquefaction mitigation using microbial induced calcite precipitation, GeoCongress 2012, Oakland, California, USA, pp 1918–1927. https://doi.org/10.1016/j.soildyn.2016.08.014.

Montoya, B.M., Dejong, J.T. and Boulanger, R.W. (2013), Dynamic response of liquefiable sand improved by microbial-induced calcite precipitation, Géotechnique, 63:302–312. https://doi.org/10.1680/geot.SIP13.P.019.

Montoya, B.M. and Dejong, J.T. (2015). Stress-strain behavior of sands cemented by microbially induced calcite precipitation, J. Geotech. Geoenvironmental Eng. https://doi.org/10.1061/(ASCE)GT.1943-5606.0001302.

Mortensen, B. M., Haber, M. J., Dejong, J. T., Caslake, L. F., and Nelson, D. C. (2011). Effects of environmental factors on microbial induced calcium carbonate precipitation. Journal of Applied Microbiology, 111(2), 338–349. https://doi.org/10.1111/j.1365-672.2011.05065.x

Mujah, D., Cheng, L., Shahin, M.A. (2019). Microstructural and geomechanical study on biocemented sand for optimization of MICP process, J. Mater. Civ. Eng., 31, 1–10. https://doi.org/10.1061/(ASCE)MT.1943-5533.0002660.

N

Nehrke, G. and Nouet, J. (2011). Confocal Raman microscope mapping as a tool to describe different mineral and organic phases at high spatial resolution within marine biogenic carbonates: Case study on Nerita undata (Gastropoda, Neritopsina), Biogeosciences. https://doi.org/10.5194/bg-8-3761-2011.

O

O'Donnell, S.T., and Kavazanjian, E. (2015). Stiffness and Dilatancy Improvements in Uncemented Sands Treated through MICP. Journal of Geotechnical and Geoenvironmental Engineering, 141(11), 02815004. https://doi.org/10.1061/(ASCE)GT.1943-5606.0001407

O'Donnell, S.T., Rittmann, B.E. and Kavazanjian, E. (2017). MIDP: Liquefaction mitigation via microbial denitrification as a two-stage process. II: MICP, J. Geotech. Geoenvironmental Eng. https://doi.org/10.1061/(ASCE)GT.1943-5606.0001806.

Okwadha, G. D. O., and Li, J. (2010). Optimum conditions for microbial carbonate precipitation. Chemosphere, 81(9), 1143–1148. https://doi.org/10.1016/j.chemosphere.2010.09.066

Omoregie, A. I., Khoshdelnezamiha, Ghazaleh Senian, N., Ong, D. E. L., and Nissom, P. M. (2017). Experimental optimisation of various cultural conditions on urease activity for isolated Sporosarcina pasteurii strains and evaluation of their biocement potentials. Ecological Engineering, 65–75. https://doi.org/10.1016/j.ecoleng.2017.09.012

Omoregie, A.I., Ngu, L.H., Ong, D.E.L. and Nissom, P.M. (2019). Low-cost cultivation of Sporosarcina pasteurii strain in food-grade yeast extract medium for microbially induced carbonate precipitation (MICP) application, Biocatal. Agric. Biotechnol., 17, 247–255. https://doi.org/10.1016/j.bcab.2018.11.030.

P

Pan, K., Xu, T. T., Liao, D., and Yang, Z. X. (2022). Failure mechanisms of sand under asymmetrical cyclic loading conditions: experimental observation and constitutive modelling. Geotechnique, 72(2), 162–175. https://doi.org/10.1680/jgeot.20.P.004

Papadopoulou, A., and Tika, T. (2008). The Effect of Fines on Critical State and Liquefaction Resistance Characteristics of Non-Plastic Silty Sands. Soils and Foundations, 48(5), 713–725. https://doi.org/https://doi.org/10.3208/sandf.48.713

Polito, Carmine P., and James R. Martin II. (2001). Effects of nonplastic fines on the liquefaction resistance of sands." Journal of geotechnical and geoenvironmental engineering 127.5: 408-415. https://doi.org/10.1061/(ASCE)1090-0241(2001)127:5(408)

Porcino, D., Marcianò, V. and Granata, R. (2011). Undrained cyclic response of a silicate-grouted sand for liquefaction mitigation purposes, Geomech. Geoengin., 6:155–170. https://doi.org/10.1080/17486025.2011.560287.

Poulos, H.G. (1988) The mechanics of calcareous sediments. Jaeger Memorial Lecture, 5th Australia-New Zealand Geomechanics Conference, 8–41.

R

Riveros, G.A., and Sadrekarimi, A. (2020). Liquefaction resistance of Fraser river sand improved by a microbially-induced cementation, Soil Dyn. Earthq. Eng., 131, 106034, 1-14, https://doi.org/10.1016/j.soildyn.2020.106034.

Rowshanbakht, K., Khamehchiyan, M., Sajedi, R. H., and Nikudel, M. R. (2016). Effect of injected bacterial suspension volume and relative density on carbonate precipitation resulting from microbial treatment. Ecological Engineering, 89, 49–55. https://doi.org/10.1016/j.ecoleng.2016.01.010

Røyne, A., Phua, Y.J., Le, S.B., Eikjeland, I.G., Josefsen, K.D., Markussen, S., Myhr, A., Throne-Holst, H., Sikorski, P. and Wentzel, A. (2019). Towards a low CO_2 emission building material

employing bacterial metabolism (1/2): The bacterial system and prototype production, PLoS One, 14(4). https://doi.org/10.1371/journal.pone.0212990.

S

Salifu, E., MacLachlan, E., Iyer, K. R., Knapp, C. W., and Tarantino, A. (2016). Application of microbially induced calcite precipitation in erosion mitigation and stabilisation of sandy soil foreshore slopes: A preliminary investigation. Engineering Geology, 201, 96–105. https://doi.org/10.1016/j.enggeo.2015.12.027

Sarda, D., Choonia, H.S., Sarode, D.D. and Lele, S.S. (2009). Biocalcification by Bacillus pasteurii urease: A novel application, J. Ind. Microbiol. Biotechnol., 36, 1111–1115. https://doi.org/10.1007/s10295-009-0581-4.

Schultze-Lam, S., Harauz, G. and Beveridge, T.J. (1992), Participation of a cyanobacterial S layer in fine-grain mineral formation, J. Bacteriol., 174, 7971–7981. https://doi.org/10.1128/jb.174.24.7971-7981.1992.

Seed, H.B., and Lee, K.L. (1966). Liquefaction of saturated sands during cyclic loading. Journal of the Soil Mechanics and Foundations Division, 92(6), 105–134.

Seed, H.B., and Idriss, I.M. (1970). National Technical Information Service A Simplified Procedure for Evaluating Soil Liquefaction Potential.

Seed, H. B., and Idriss, I.M. (1971). Simplified procedure for evaluating soil liquefaction potential. Journal of the Soil Mechanics and Foundations division 97.9: 1249-1273. https://doi.org/10.1061/JSFEAQ.0001662

Seed, H. Bolton, Idriss, I. M. and Arango, I. (1983) Evaluation of liquefaction potential using field performance data. Journal of geotechnical engineering 109.3 (1983): 458-482. https://doi.org/10.1061/(ASCE)0733-9410(1983)109:3(458)

Seed, H. B., Martin, P. P., and Lysmer, J. (1975). The generation and dissipation of pore water pressures during soil liquefaction. College of Engineering, University of California.

Shahin, S., Montoya, B.M. and Gabr M.A. (2017), Effect of microbial induced calcium carbonate precipitation on the performance of ponded coal ash, Association of State Dam Safety Officials, Inc., USA.

Sibille, L., Marot, D., and Sail, Y. (2015). A description of internal erosion by suffusion and induced settlements on cohesionless granular matter. Acta Geotechnica, 10(6), 735–748. https://doi.org/10.1007/s11440-015-0388-6

Simatupang, M. and Okamura, M. (2017). Liquefaction resistance of sand remediated with carbonate precipitation at different degrees of saturation during curing, Soils Found., 57, 619–631. https://doi.org/10.1016/j.sandf.2017.04.003.

Son, H.M., Kim, H.Y., Park, S.M. and Lee, H.K. (2018). Ureolytic/Non-ureolytic bacteria co-cultured self-healing agent for cementitious materials crack repair, Materials (Basel). https://doi.org/10.3390/ma11050782.

Song, C., Elsworth, D., Zhi, S. and Wang, C. (2019). The influence of particle morphology on microbially induced $CaCO_3$ clogging in granular media, Mar. Georesources Geotechnol.. https://doi.org/10.1080/1064119X.2019.1677828.

Soon, N.W., Lee, L.M., Khun, T.C. and Ling, H.S. (2013). Improvements in engineering properties of soils through microbial-induced calcite precipitation, KSCE J. Civ. Eng., 17, 718–728. https://doi.org/10.1007/s12205-013-0149-8.

Soon, N.W., Lee, L.M., Khun, T.C. and Ling, H.S. (2014). Factors Affecting improvement in engineering properties of residual soil through microbial-induced calcite precipitation, J. Geotech. Geoenvironmental Eng. https://doi.org/10.1061/(ASCE)GT.1943-5606.0001089.

Skorupa, D. J., Akyel, A., Fields, M. W., and Gerlach, R. (2019). Facultative and anaerobic consortia of haloalkaliphilic ureolytic micro-organisms capable of precipitating calcium carbonate. Journal of Applied Microbiology, 127(5), 1479–1489. https://doi.org/10.1111/jam.14384

Stabnikov, V., Chu, J., Ivanov, V. and Li, Y. (2013). Halotolerant, alkaliphilic urease-producing bacteria from different climate zones and their application for biocementation of sand, World Journal of Microbiology and Biotechnol., 29, 1453–1460. http://dx.doi.org/10.1007/s11274-013-1309-1.

Stocks-Fischer, S., Galinat, J.K. and Bang, S.S. (1999). Microbiological precipitation of $CaCO_3$, Soil Biol. Biochem., 31, 1563–1571. https://doi.org/10.1016/S0038-0717(99)00082-6.

Sun, X., Miao, L., Tong, T., and Wang, C. (2019). Study of the effect of temperature on microbially induced carbonate precipitation. Acta Geotechnica, 14(3), 627–638. https://doi.org/10.1007/s11440-018-0758-y

T

Taïbi, S., Fleureau, J.-M., Hadiwardoyo, S. and Kheirbek-Saoud, S. (2008). Small and large strain behaviour of an unsaturated compacted silt, Eur. J. Environmental Civil Eng., 12, 3, 203-228.

Tejada, I. G., and Antolin, P. (2020). Use of Machine Learning for unraveling hidden correlations between Particle Size Distributions and the Mechanical Behavior of Granular Materials, 5. https://doi.org/10.1007/s11440-021-01420-5

Terzis, D., and Laloui, L. (2019a). A decade of progress and turning points in the understanding of bio-improved soils: A review. Geomechanics for Energy and the Environment, 19. https://doi.org/10.1016/j.gete.2019.03.001

Terzis, D., and Laloui, L. (2019b). Cell-free soil bio-cementation with strength, dilatancy and fabric characterization. Acta Geotechnica, 14(3), 639–656. https://doi.org/10.1007/s11440-019-00764-3

Thevanayagam, S. (1998). Effect of fines and confining stress on undrained shear strength of silty sands. Journal of Geotechnical and Geoenvironmental Engineering, 124(6), 479–491.

Tsuchida, H., and Hayashi, S. (1972). Estimation of liquefaction potential of sandy soils. Publication of: McGraw Hill Book Company, 14.

U

Ueng, T. S., Sun, C. W., and Chen, C. W. (2004). Definition of fines and liquefaction resistance of Maoluo River soil. Soil Dynamics and Earthquake Engineering, 24(9–10), 745–750. https://doi.org/10.1016/j.soildyn.2004.06.011

V

Van Paassen L. (2009). Biogrout: ground improvement by microbially induced carbonate precipitation, Ph.D. Dissertation, Delft University of Technology, The Netherland.

Van Paassen, L. A., Ghose, R., van der Linden, T. J. M., van der Star, W. R. L., and van Loosdrecht, M. C. M. (2010). Quantifying Biomediated Ground Improvement by Ureolysis: Large-Scale Biogrout Experiment. Journal of Geotechnical and Geoenvironmental Engineering, 136(12), 1721–1728. https://doi.org/10.1061/(ASCE)GT.1943-5606.0000382

Venda Oliveira, P. J., da Costa, M. S., Costa, J. N. P., and Fernanda Nobre, M. (2015). Comparison of the Ability of Two Bacteria to Improve the Behavior of Sandy Soil. Journal of Materials In Civil Engineering, 27(1), 6014025. https://doi.org/10.1061/(ASCE)MT.1943-5533.0001138

W

Waller, J.T. (2011). Influence of bio-cementation on shearing behavior in sand using X-ray computed tomography, Ph.D. Dissertation, University of California, Davis, USA.

Wang, Y., Soga, K. and Jiang, N. (2017). Microbial induced carbonate precipitation (MICP): the case for microscale perspective, 19th Int. Conf. on Soil Mechanics and Geotechnical Eng., Seoul, December.

Wang, Y., Soga, K., Dejong, J.T. and Kabla, A.J. (2019). A microfluidic chip and its use in characterising the particle-scale behaviour of Microbial-Induced Carbonate Precipitation

(MICP), Géotechnique, 69, 1086–1094. https://doi.org/10.1680/jgeot.18.p.031.

Wang, Z., Zhang, N., Cai, G., Jin, Y., Ding, N. and Shen, D. (2017). Review of ground improvement using microbial induced carbonate precipitation (MICP), Marine Georesources and Geotechnology, 35(8), 1135-1146. https://doi.org/10.1080/1064119X.2017.1297877.

Wang, L., Chu, J., Wu, S., and Wang, H. (2021). Stress–dilatancy behavior of cemented sand: comparison between bonding provided by cement and biocement. Acta Geotechnica, 16(5), 1441–1456. https://doi.org/10.1007/s11440-021-01146-4

Wei, S., Cui, H., Jiang, Z., Liu, H., He, H., and Fang, N. (2015). Biomineralization processes of calcite induced by bacteria isolated from marine sediments. Brazilian Journal of Microbiology. https://doi.org/10.1590/S1517-838246220140533

Weil, M.H., Dejong, J.T., Martinez, B.C. and Mortensen, B.M. (2012). Seismic and resistivity measurements for real-time monitoring of microbially induced calcite precipitation in sand, Geotech. Test J.. https://doi.org/10.1520/GTJ103365.

Wen, K., Li, Y., Liu, S. et al. (2019). Development of an improved immersing method to enhance microbial induced calcite precipitation treated sandy soil through multiple treatments in low cementation media concentration, Geotech. Geol. Eng., 37, 1015–1027. https://doi.org/10.1007/s10706-018-0669-6.

Whiffin, V.S. (2004). Microbial $CaCO_3$ precipitation for the production of biocement, Ph.D. Dissertation, Murdoch University, Western Australia.

Whiffin, V.S., van Paassen, L. and Harkes, M. (2007). Microbial carbonate precipitation as a soil improvement technique, Geomicrobiology Journal, 24, 417–423.
https://doi.org/10.1080/ 01490450701436505.

Wu, S. (2015). Mitigation of liquefaction hazards using the combined biodesaturation and bioclogging method, Ph.D. Dissertation, Iowa State University, USA.

Wu, S., Li, B., and Chu, J. (2021). Stress-Dilatancy Behavior of MICP-Treated Sand, Int. J. Geomech., 21(3): 04020264-1-12. https://doi.org/ 10.1061/(ASCE)GM.1943-5622.0001923.

X

Xenaki, V. C., and Athanasopoulos, G. A. (2003). Liquefaction resistance of sand-silt mixtures: An experimental investigation of the effect of fines. Soil Dynamics and Earthquake Engineering, 23(3), 1–12. https://doi.org/10.1016/S0267-7261(02)00210-5

Xenaki, V. C., and Athanasopoulos, G. A. (2008). Dynamic properties and liquefaction resistance of two soil materials in an earthfill dam—Laboratory test results, Soil Dynamics and Earthquake Engineering 28.8: 605-620.

https://doi.org/10.1016/j.soildyn.2007.10.001

Xiao, P., Liu, H., Xiao, Y., Stuedlein, A.W. and Evans, T.M. (2018). Liquefaction resistance of bio-cemented calcareous sand, Soil Dyn. Earthq. Eng., 107, 9–19. https://doi.org/10.1016/j.soildyn.2018.01.008.

Xiao, P., Liu, H., Stuedlein, A. W., Evans, T. M., and Xiao, Y. (2019). Effect of Relative Density and Bio-cementation on the Cyclic Response of Calcareous Sand. Canadian Geotechnical Journal, (January). https://doi.org/10.1139/cgj-2018-0573

Xiao, Y., He, X., Evans, T. M., Stuedlein, A. W., and Liu, H. (2019). Unconfined Compressive and Splitting Tensile Strength of Basalt Fiber–Reinforced Biocemented Sand. Journal of Geotechnical and Geoenvironmental Engineering, 145(9), 04019048. https://doi.org/10.1061/(asce)gt.1943-5606.0002108

Xiao, Y., Zhao, C., Sun Y., Wang, S., Wu, H., Chen, H., and Liu, H. (2020). Compression behavior of MICP-treated sand with various gradations, Acta Geotech., https://doi.org/10.1007/s11440-020-01116-2.

Xu, X., Guo, H., Cheng, X., and Li, M. (2020). The promotion of magnesium ions on aragonite precipitation in MICP process. Construction and Building Materials, 263, 120057. https://doi.org/10.1016/j.conbuildmat.2020.120057

Y

Yamamuro, Jerry A., and Poul V. Lade (1998). Steady-state concepts and static liquefaction of silty sands." Journal of geotechnical and geoenvironmental engineering 124.9: 868-877. https://doi.org/10.1061/(ASCE)1090-0241(1998)124:9(868)

Yasuhara, H., Neupane, D., Hayashi, K. and Okamura, M. (2012). Experiments and predictions of physical properties of sand cemented by enzymatically-induced carbonate precipitation, Soils Found., 52, 539–549. https://doi.org/10.1016/j.sandf.2012.05.011.

Yilmaz, Y., Mollamahmutoglu, M., Ozaydin, V., and Kayabali, K. (2008). Experimental investigation of the effect of grading characteristics on the liquefaction resistance of various graded sands. Engineering Geology, 100(3–4), 91–100. https://doi.org/10.1016/j.enggeo.2007.12.002

Yu, T., Souli, H., Péchaud, Y. and Fleureau, J.M. (2020). Optimizing protocols for microbial induced calcite precipitation (MICP) for soil improvement–a review, Eur. J. Environ. Civ. Eng. https://doi.org/10.1080/19648189.2020.1755370.

Z

Zamani, A., Xiao, P., Baumer, T., Carey, T. J., Sawyer, B., DeJong, J. T., and Boulanger, R. W. (2021). Mitigation of Liquefaction Triggering and Foundation Settlement by MICP Treatment. Journal of Geotechnical and Geoenvironmental Engineering, 147(10), 04021099. https://doi.org/10.1061/(asce)gt.1943-5606.0002596

Zhang, X., Chen, Y., Liu, H., Zhang, Z. and Ding, X. (2020). Performance evaluation of a MICP-treated calcareous sandy foundation using shake table tests, Soil Dyn. Earthq. Eng. https://doi.org/10.1016/

Zhao, Q., Li, L., Li, C., Li, M., Amini, F., and Zhang, H. (2014). Factors affecting improvement of engineering properties of MICP-treated soil catalyzed by bacteria and urease. J. Mater. Civ. Eng, 40(6), 1056–1058. https://doi.org/10.1061/(ASCE)MT.1943-5533

Annex 1 Equations

$$B = \frac{\Delta u}{\Delta \sigma_3}$$

$$C_c = \frac{d_{30}^2}{d_{60} \times d_{10}}$$

$$C_u = \frac{d_{60}}{d_{10}}$$

$$e_{if} = \frac{e}{FC}$$

$$e_s = \frac{e + FC}{1 - FC}$$

$$e_{max} = \frac{2.7}{D_{min}} - 1$$

$$e_{min} = \frac{2.7}{D_{max}} - 1$$

$$e = \frac{2.7}{D} - 1$$

$$n = \frac{e}{1 + e}$$

$$\phi = \sin^{-1}\left(\frac{3M}{6 + M}\right)$$

$$c = \frac{(3 - \sin\phi)q_0}{6\cos\phi}$$

$$q_{max,norm} = \frac{q_{max,T}}{q_{max,NT}}$$

$$CSR = \frac{\sigma_d}{2 \times \sigma_c'},$$

$$Specific\ urease\ activity\ (mM/min/OD) = \frac{Urease\ activity\ (mM/min)}{Biomass\ (OD_{600})}$$

$$CaCO_3\ (\%) = \frac{120 \times V_{CO_2}}{m \times (\theta_b + 273)}$$

$$r_u = \frac{\Delta u}{\sigma_c'}$$

$$CSR = a \times N^{-b}$$

$$\delta\varepsilon_1 = \varepsilon_{1max,i} - \varepsilon_{1min,i}$$

Annex 2

Cyclic tests on untreated loose & dense samples

and on treated initially loose samples

MS6.0 (Coarse soil)

No. of samples		CaCO3 content (%)	e after consolid.	dry density after consolid. (g/cm^3)	Dr after consolid. (%)	CSR	NL	Original No. Test
MS6.0	UT1	0	0,710	1,58	56	0,3	18	liq38
	UT2	0	0,796	1,50	18	0,25	39	liq18
	UT3	0	0,698	1,59	61	0,22	320	liq74
	UT4 dense	0	0,621	1,67	94	0.25->0.5	658	liq70
	T1	8,62	0,766	1,53	31	0,25	66	liq20T
	T2	10,06	0,616	1,67	97	0,25	300	liq55T
	T3	11,53	0,585	1,70	110	0,25->0,5	700	liq36T

MS6.0_UT1 (untreated loose specimen), CSR=0.3, 0.1Hz

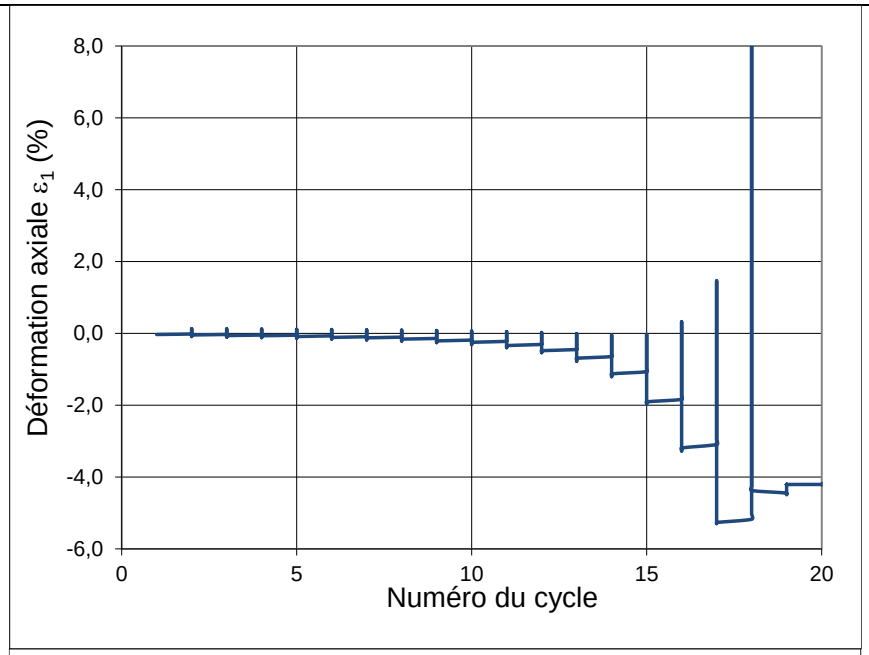

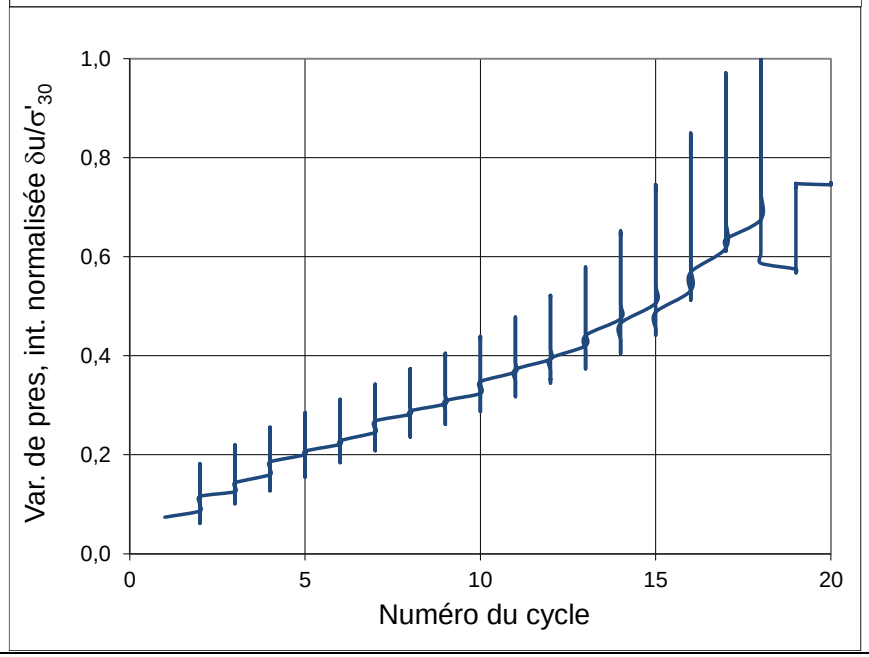

MS6.0_UT2 (untreated loose specimen), CSR=0.25, 0.1Hz

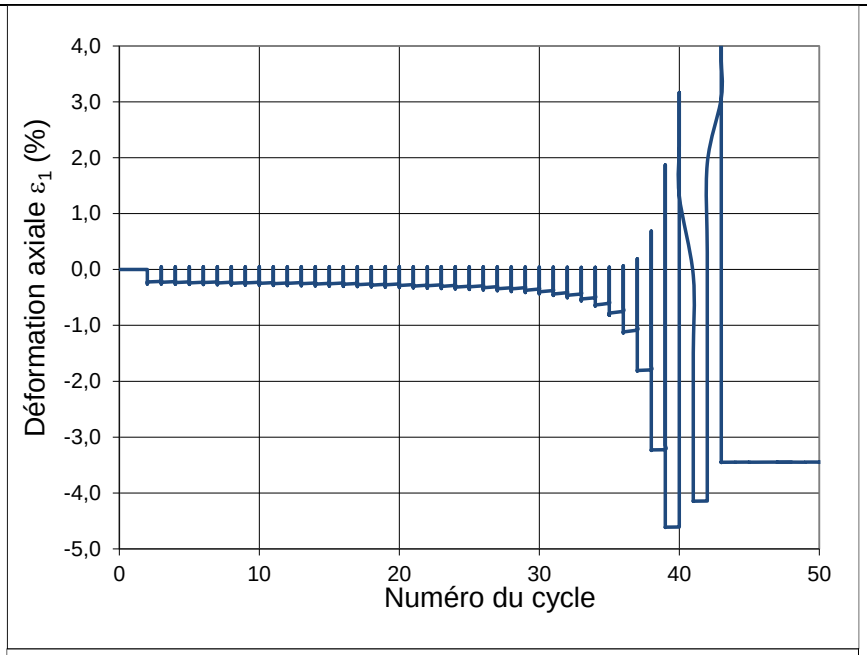

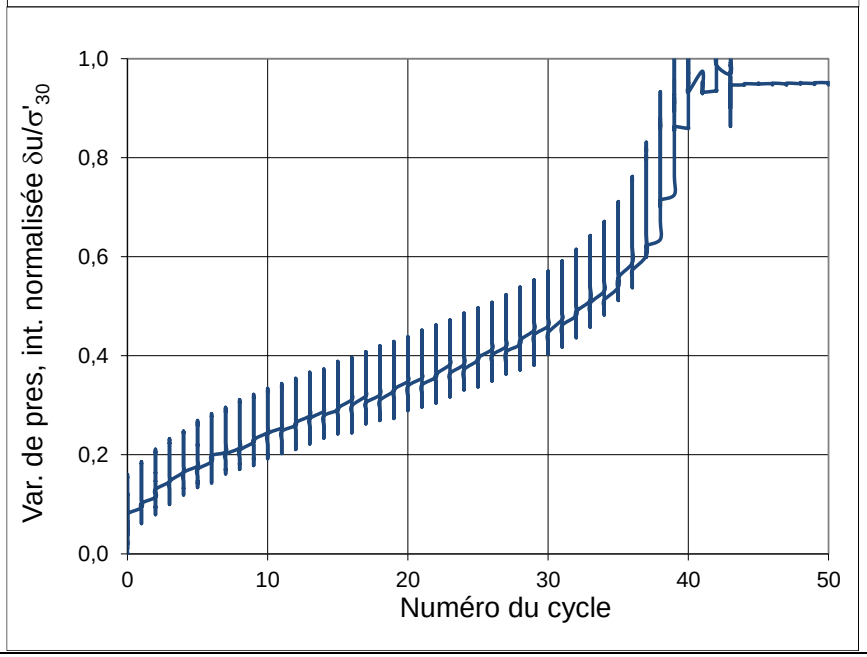

MS6.0_UT3 (untreated loose specimen), CSR=0.22, 0.5Hz

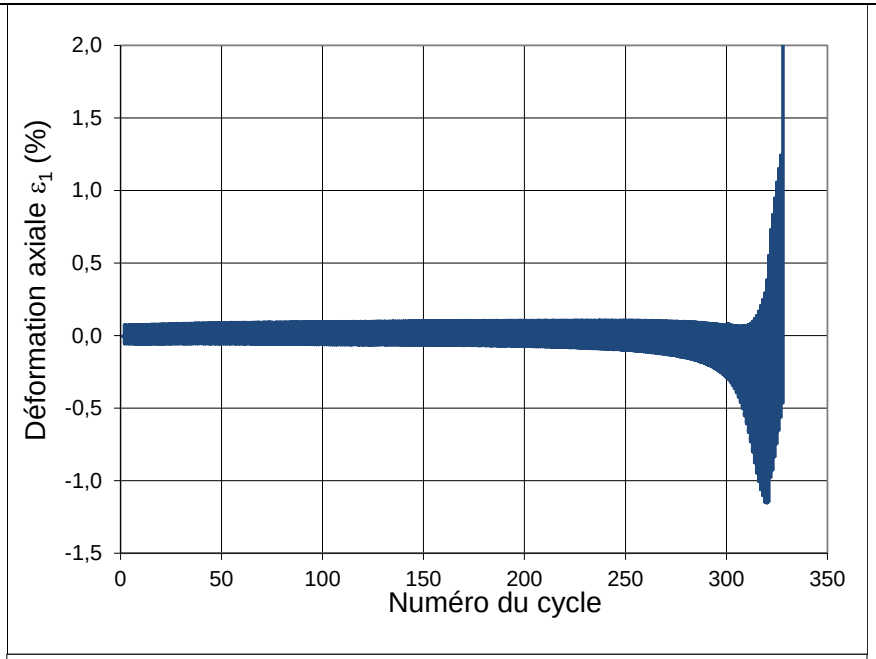

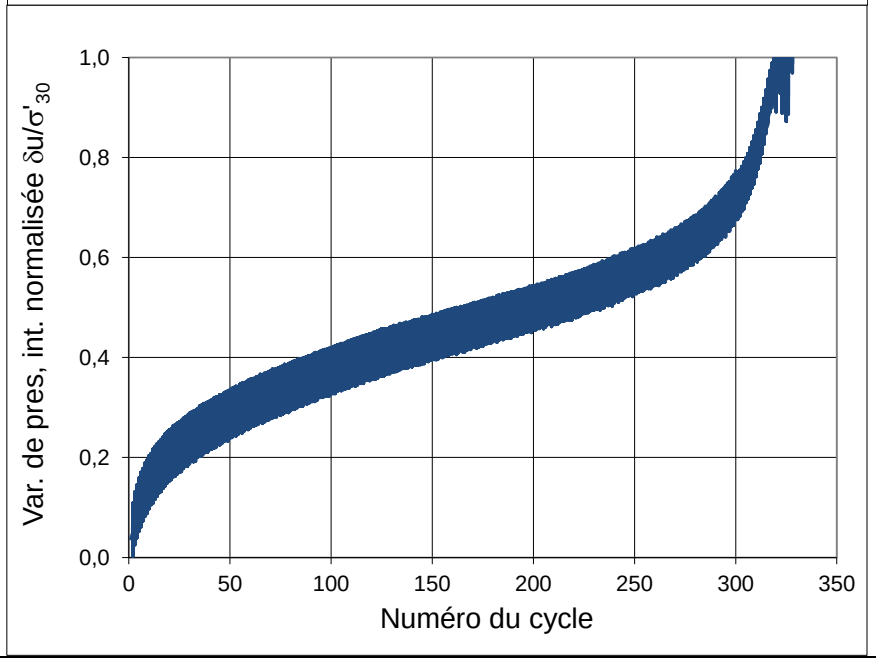

MS6.0_UT4 (untreated dense specimen), CSR=0.25-0.50, 0.5Hz

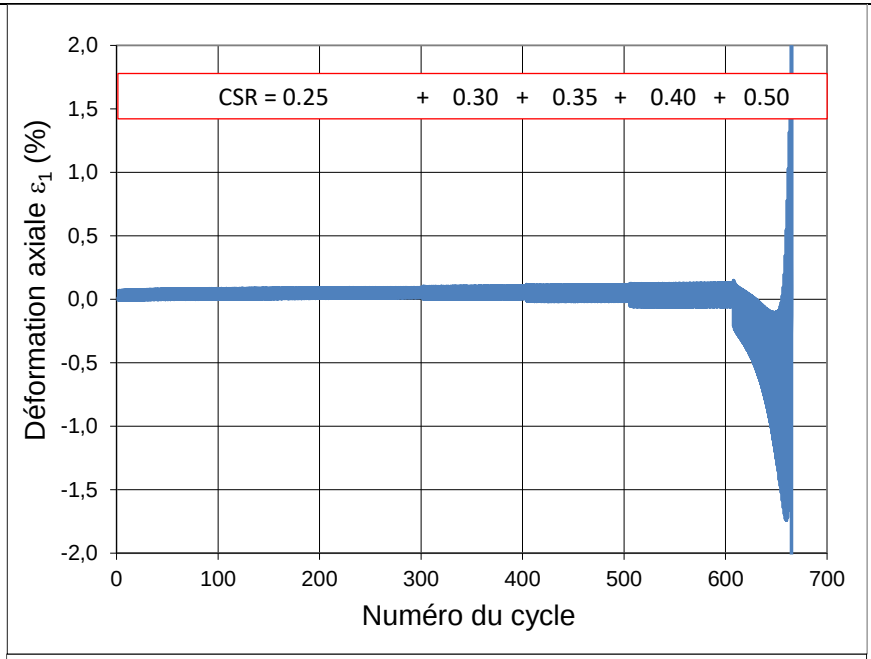

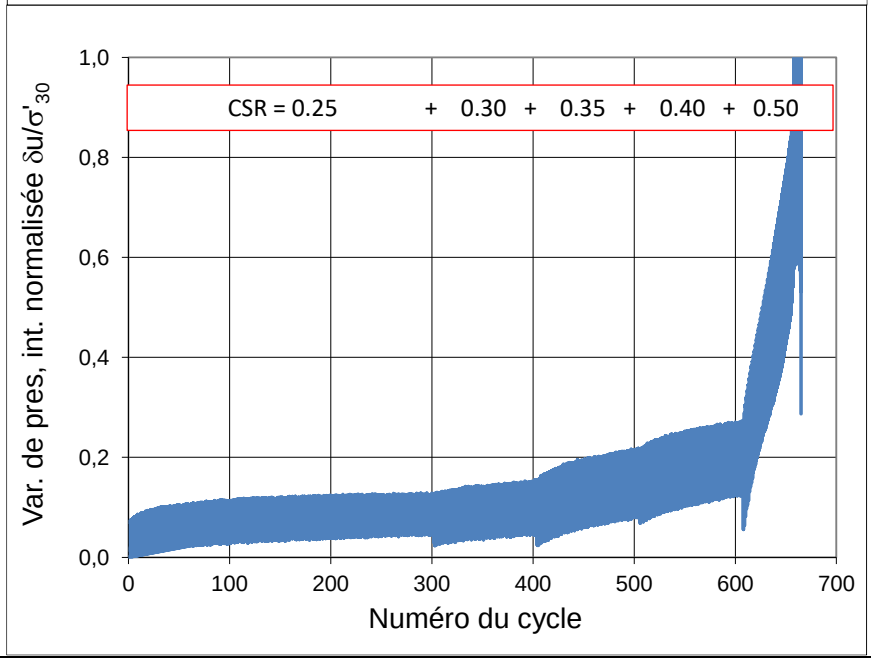

MS6.0_T1 (treated specimen), CSR=0.25, 0.1Hz, C=8.6%

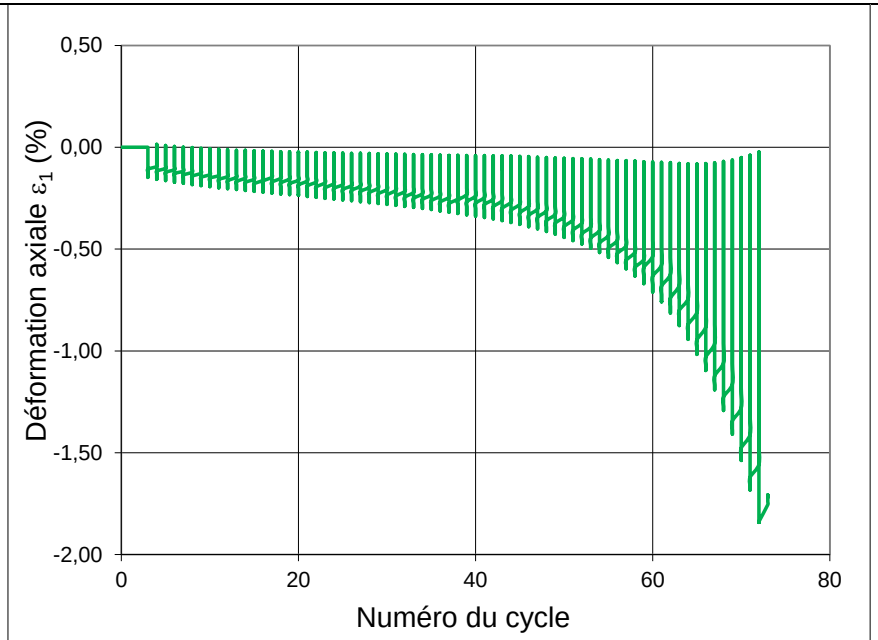

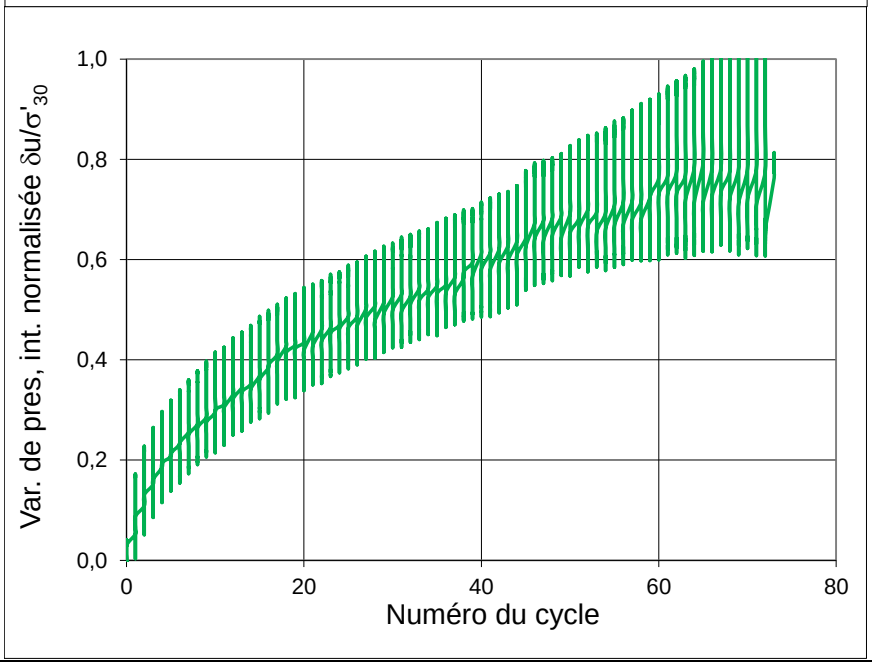

MS6.0_T2 (treated specimen), CSR=0.25, 0.5Hz, C=10.1%

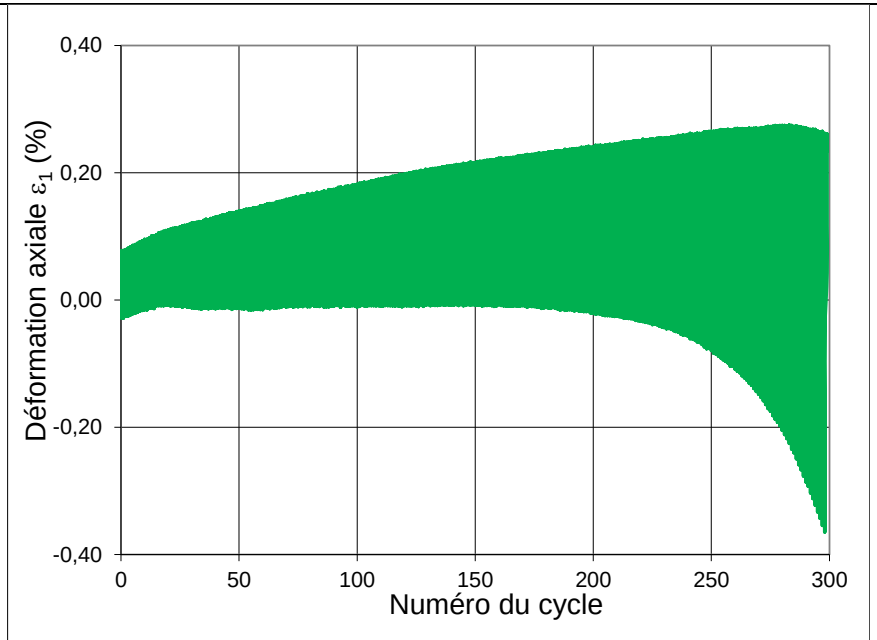

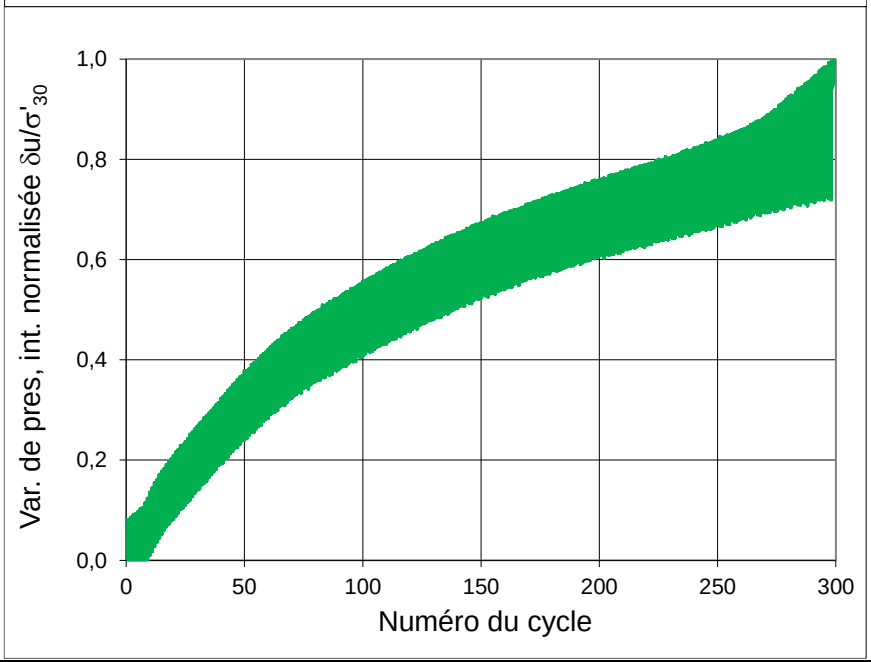

MS6.0_T3 (treated specimen), CSR=0.25-0.5, 0.5Hz, C=11.5%

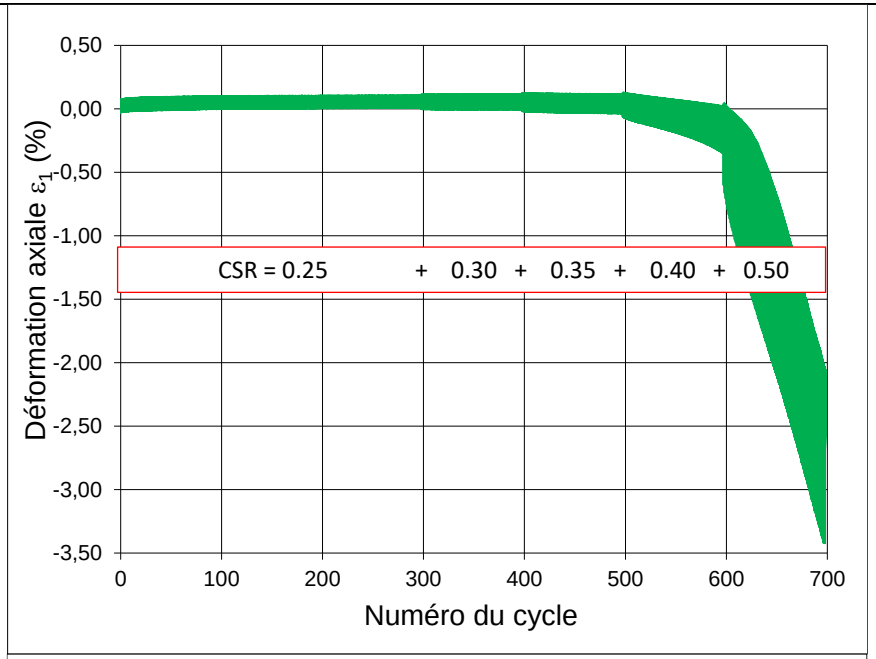

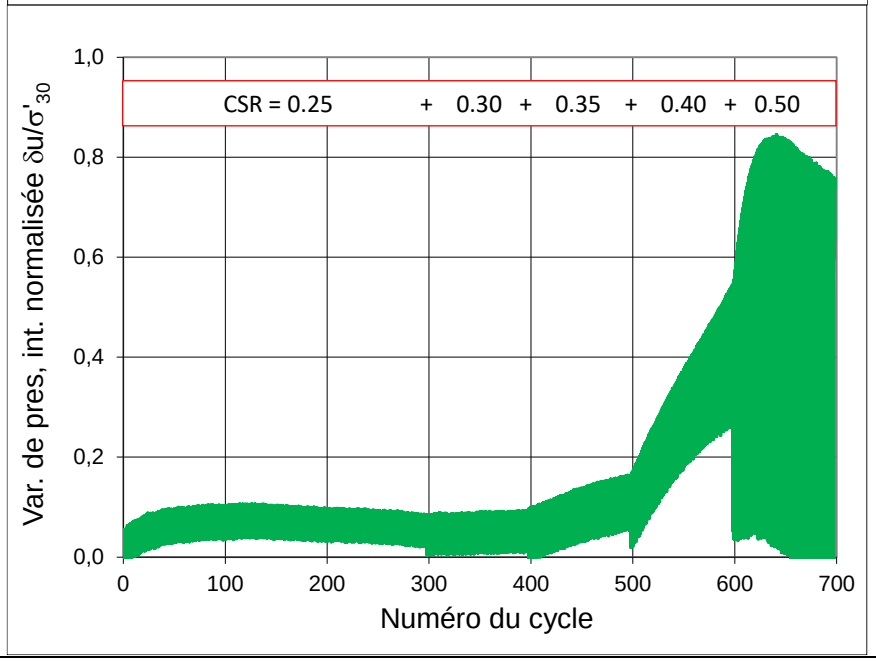

MS6.20 (20% fines < 1 mm)

No. of samples		CaCO3 content (%)	e after consolid.	dry density after consolid. (g/cm^3)	Dr after consolid. (%)	CSR	NL	Original No. Test
MS6.20	UT1	0	0,660	1,63	42	0,25	30	liq10
	UT2	0	0,652	1,63	45	0,22	106	liq93
	UT3	0	0,664	1,62	40	0,2	593	liq88
	UT4	0	0,537	1,76	97	0.25->0.4	584	liq90 dense
	UT5	0	0,508	1,79	110	0,4	101	liq100 dense
	T2	6,15	0,584	1,70	76	0,25-0,3	380	liq91T
	T3	8,27	0,556	1,74	88	0,25-0,4	557	liq85T

MS6.20_UT1 (untreated loose specimen), CSR=0.25, 0.1Hz

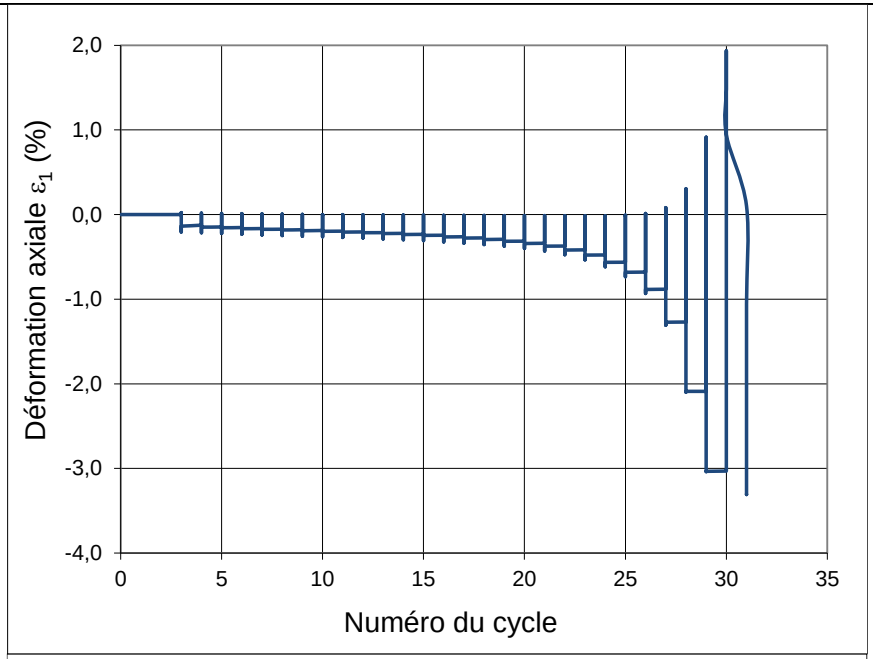

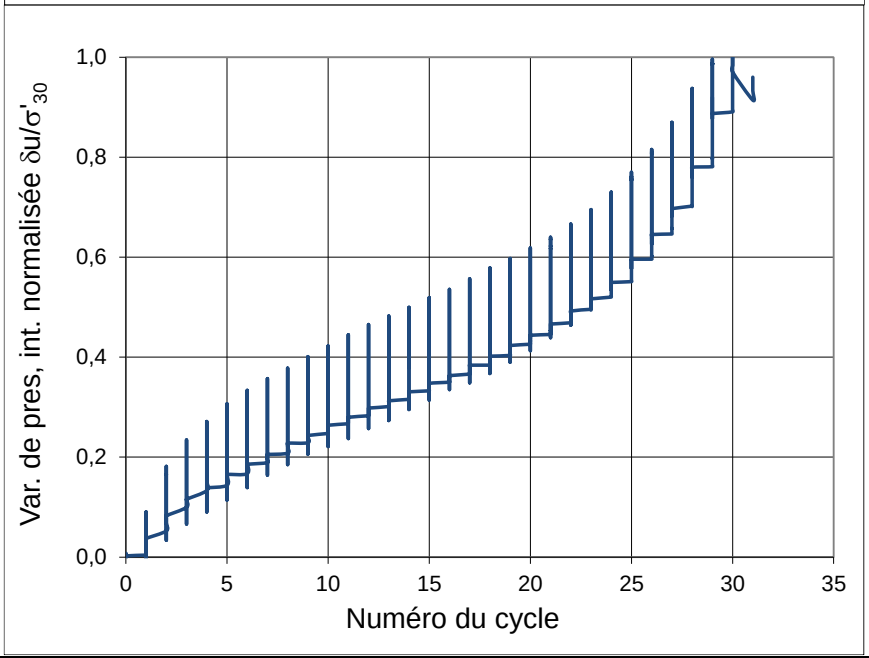

MS6.20_UT2 (untreated loose specimen), CSR=0.22, 0.5Hz

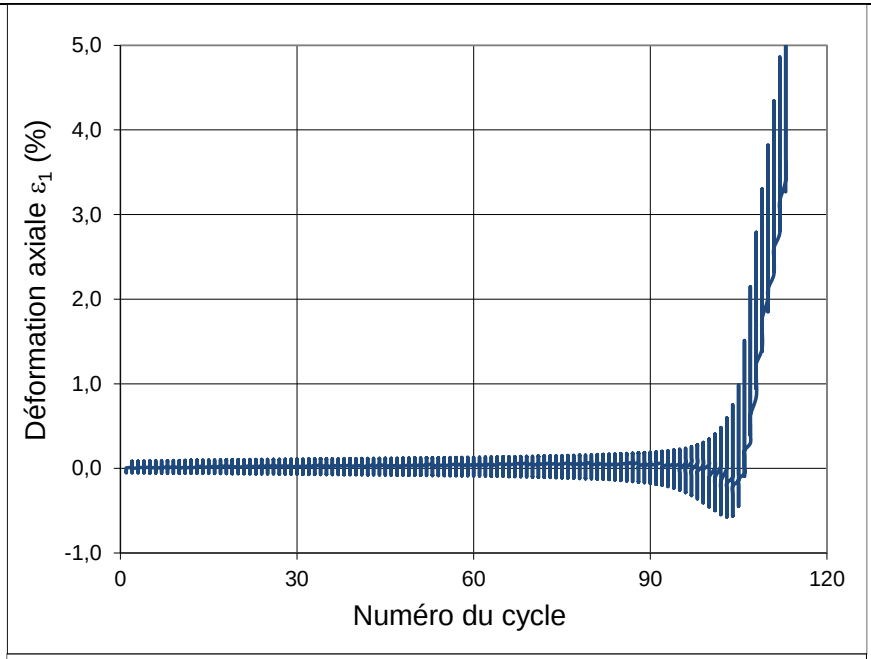

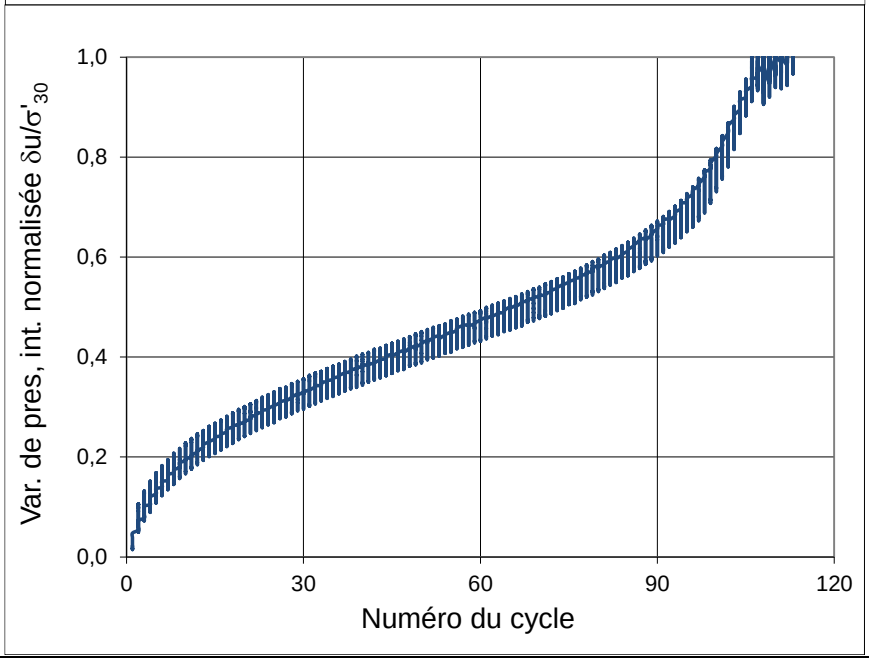

MS6.20_UT3 (untreated loose specimen), CSR=0.2, 0.5Hz

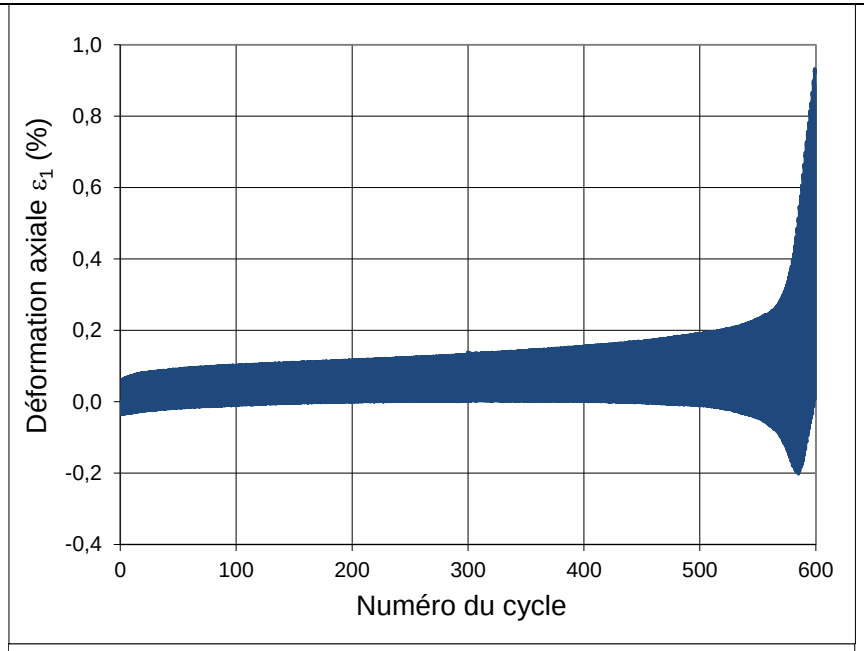

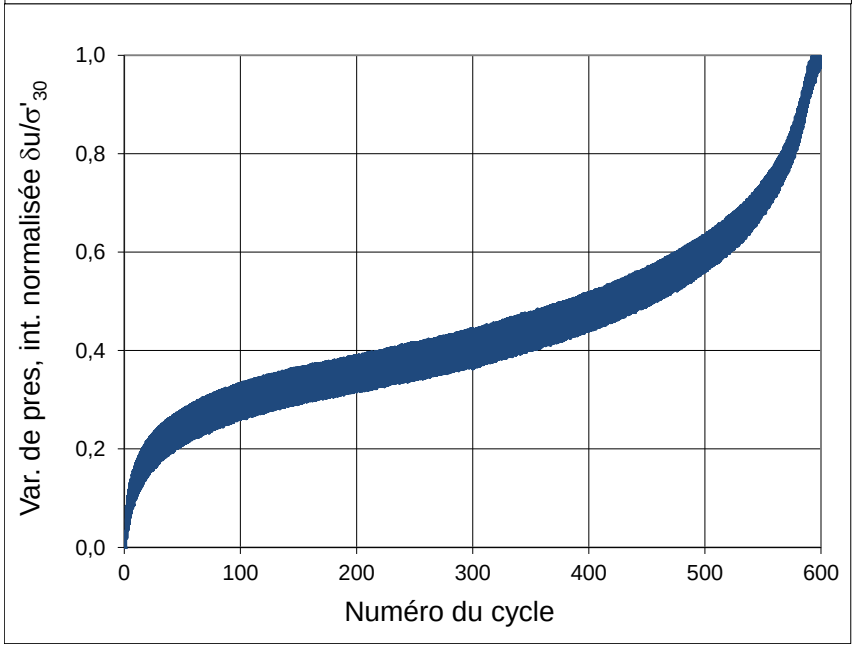

MS6.20_UT4 (untreated dense specimen), CSR=0.25-0.4, 0.5Hz

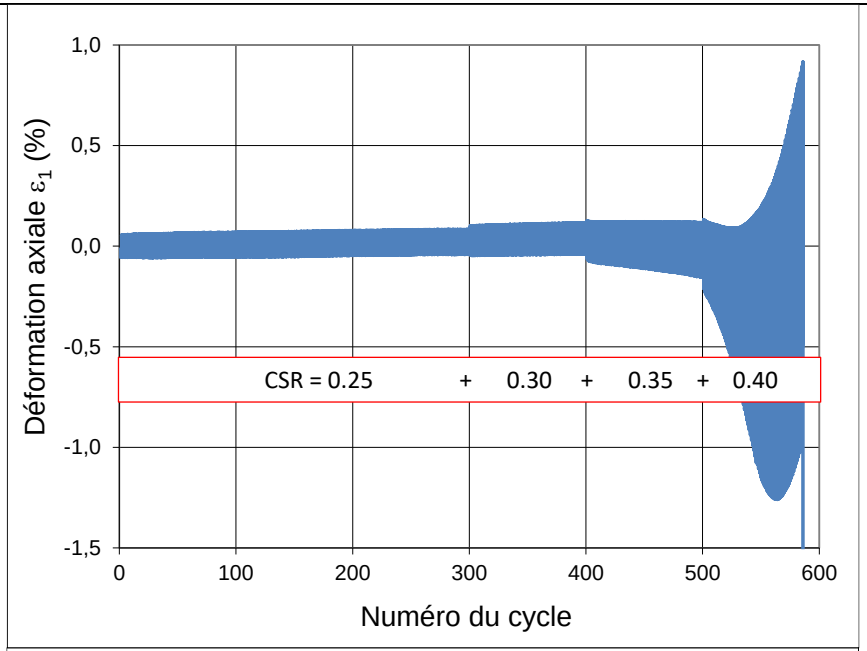

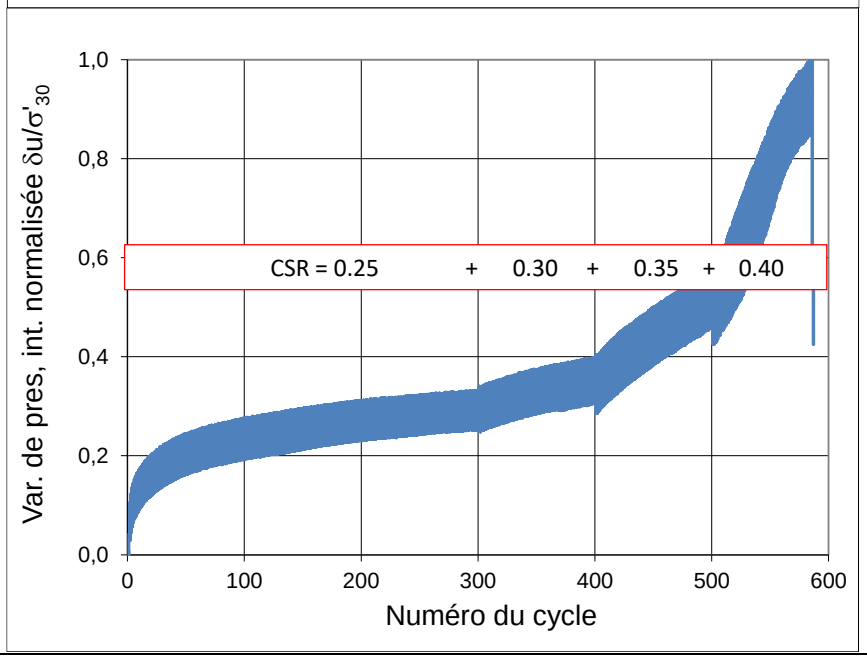

MS6.20_UT5 (untreated dense specimen), CSR=0.4, 0.5Hz

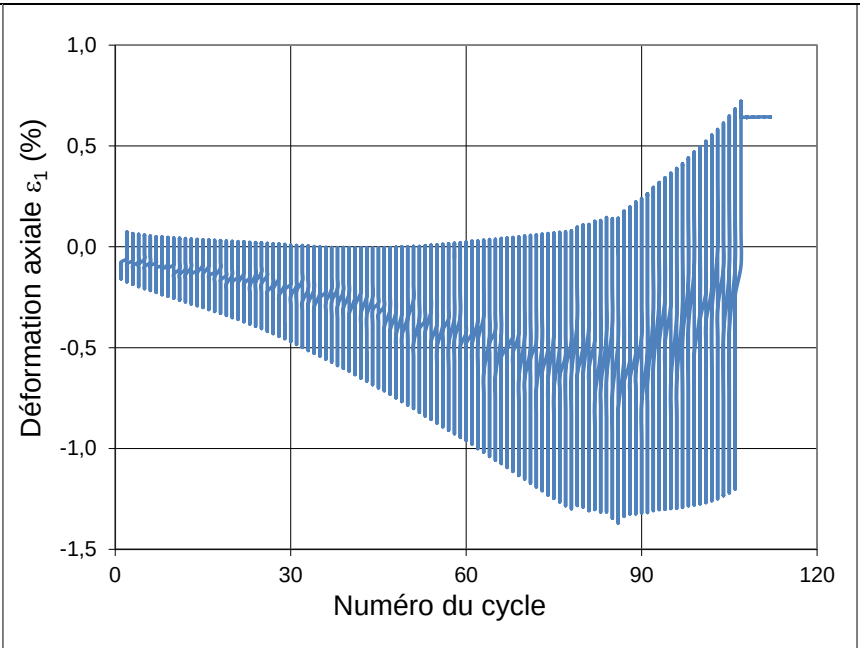

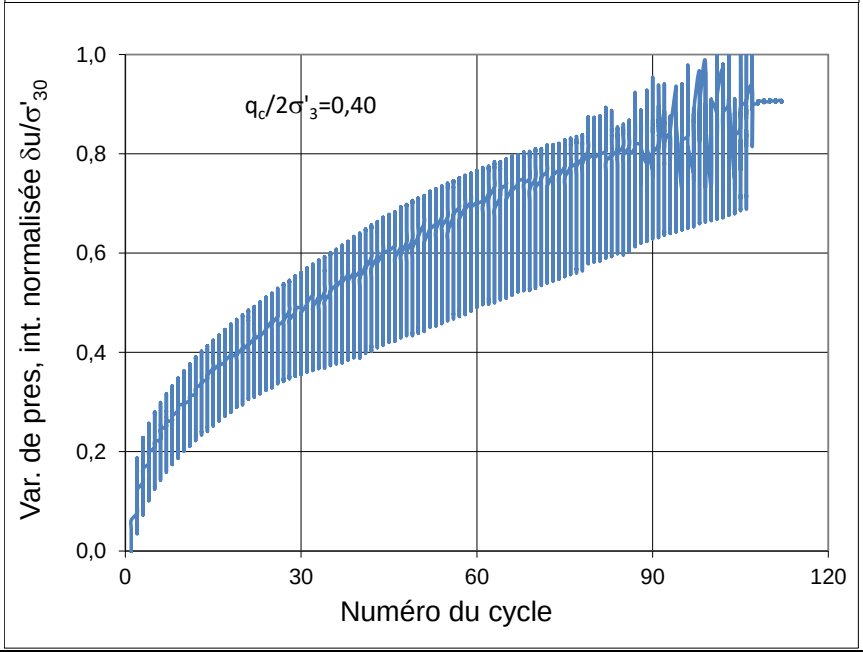

MS6.20_T2 (treated specimen), CSR=0.25-0.3, 0.5Hz, C=6.2%

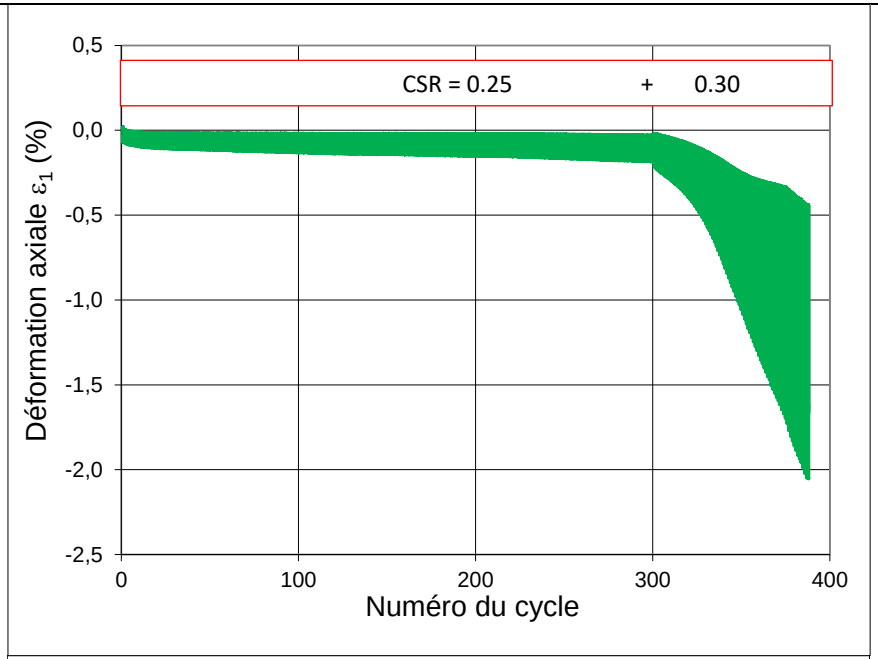

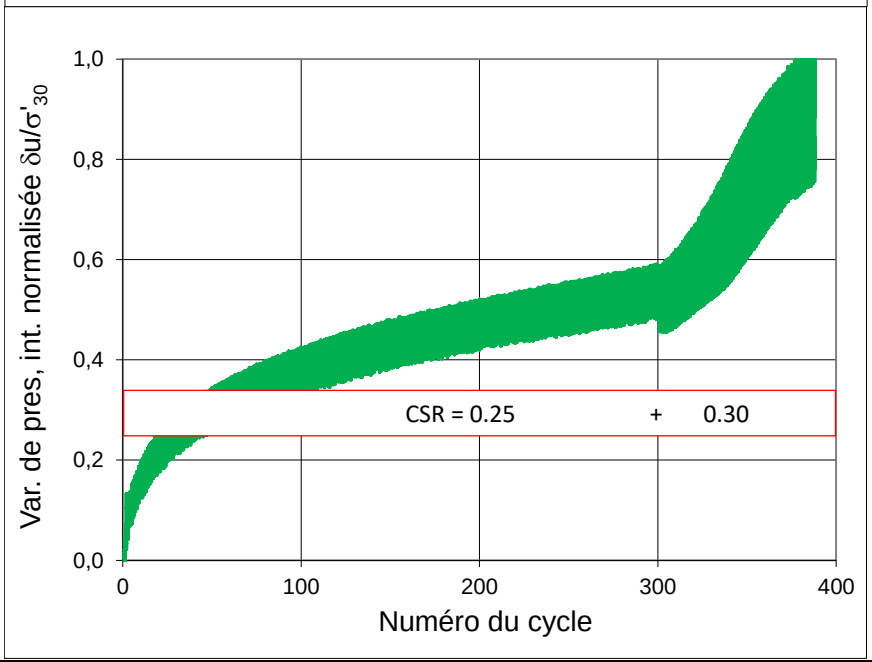

MS6.20_T3 (treated specimen), CSR=0.25-0.4, 0.5Hz, C=8.3%

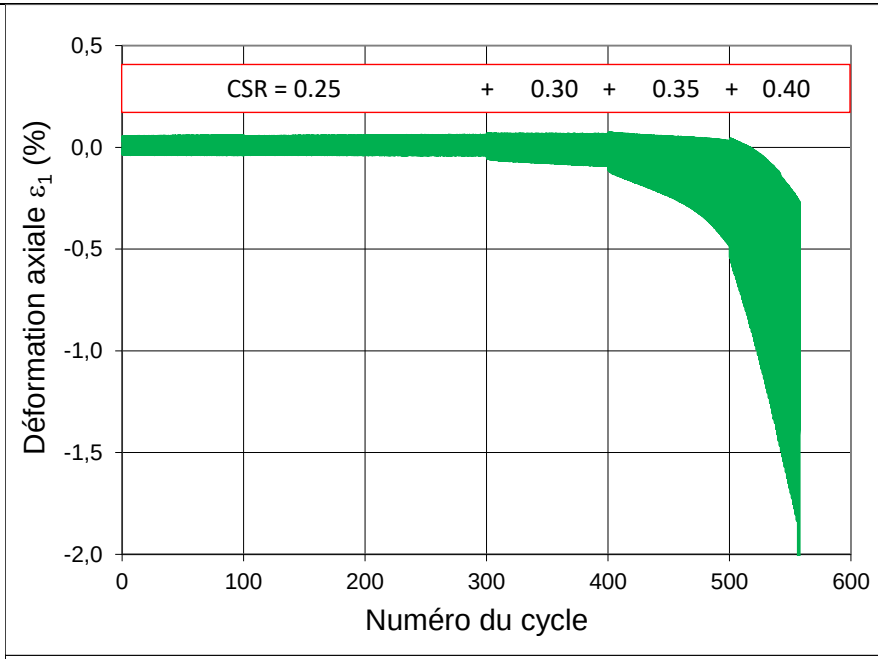

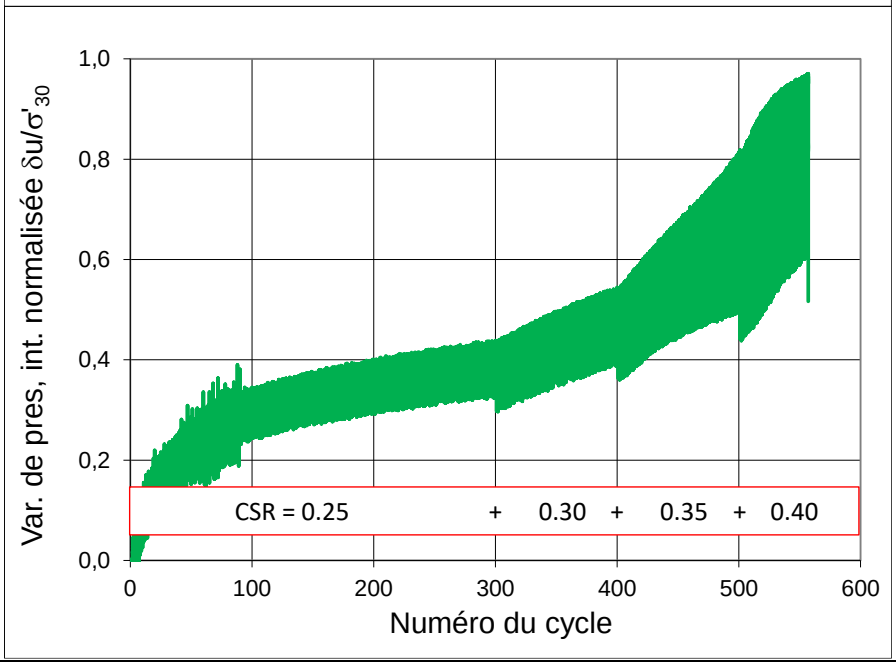

MS6.40 (40% fines < 1 mm)

No. of samples		CaCO3 content (%)	e after consolid.	dry density after consolid. (g/cm^3)	Dr after consolid. (%)	CSR	NL	Original No. Test
MS6.40	UT1	0	0,598	1,69	62	0,25	15	liq3
	UT2	0	0,598	1,69	61	0,2	89	liq5
	UT3	0	0,595	1,69	63	0,15	217	liq4
	UT4 dense	0	0,538	1,76	91	0,25	120	liq71
	T1	4,5	0,556	1,74	83	0,25	134	liq7T
	T2	5,4	0,568	1,72	77	0,25->0,3	355	liq46T
	T3	7,5	0,542	1,75	90	0,25->0,35	494	liq34T
	T4	8,4	0,510	1,79	105	0,25->0,5	677	liq86T

MS6.40_UT1 (untreated loose specimen), CSR=0.25, 0.1Hz

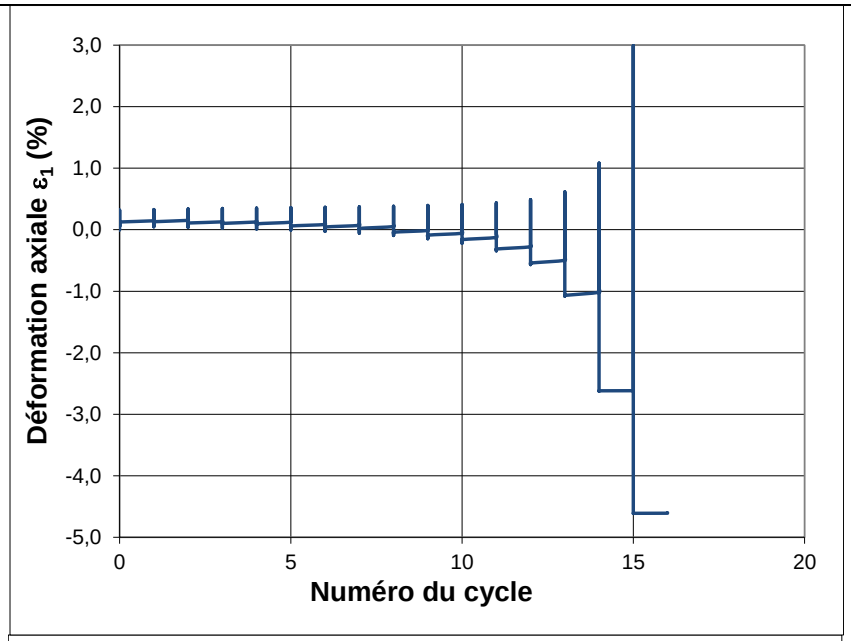

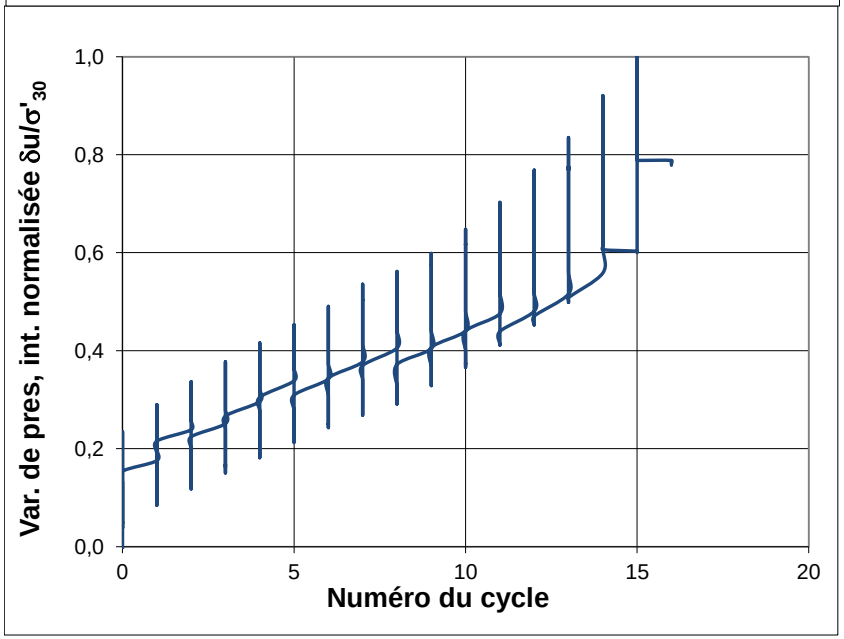

MS6.40_UT2 (untreated loose specimen), CSR=0.2, 0.1Hz

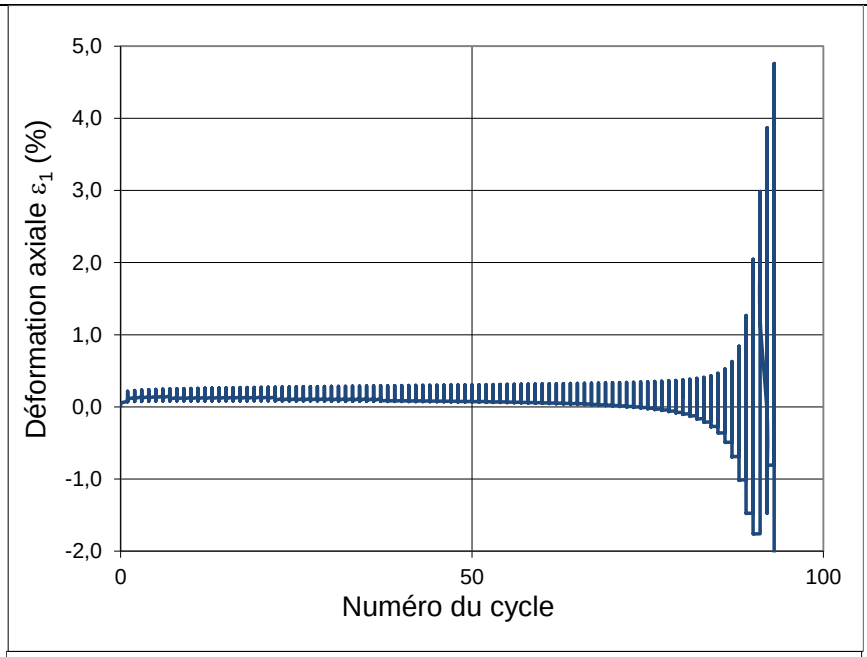

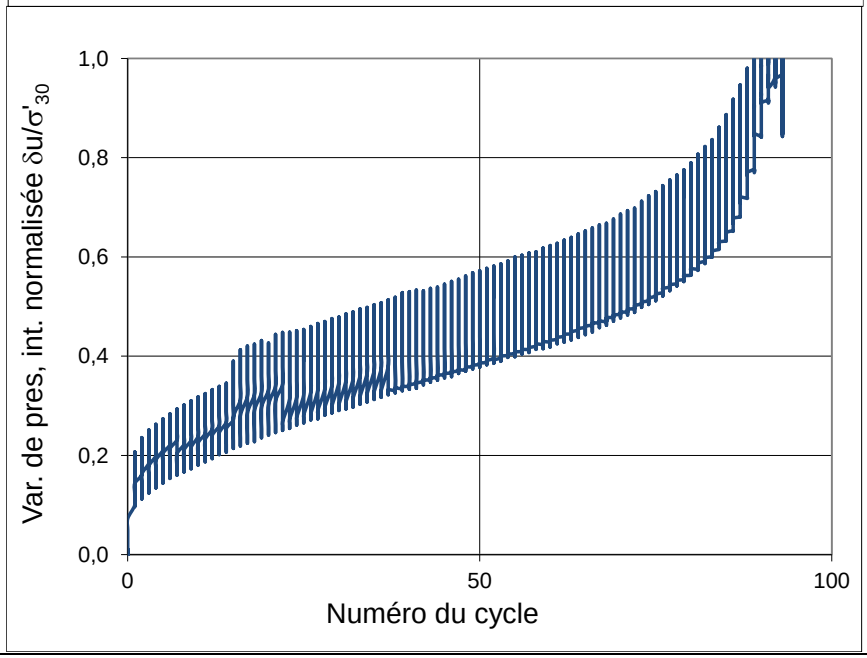

MS6.40_UT3 (untreated loose specimen), CSR=0.15, 0.1Hz

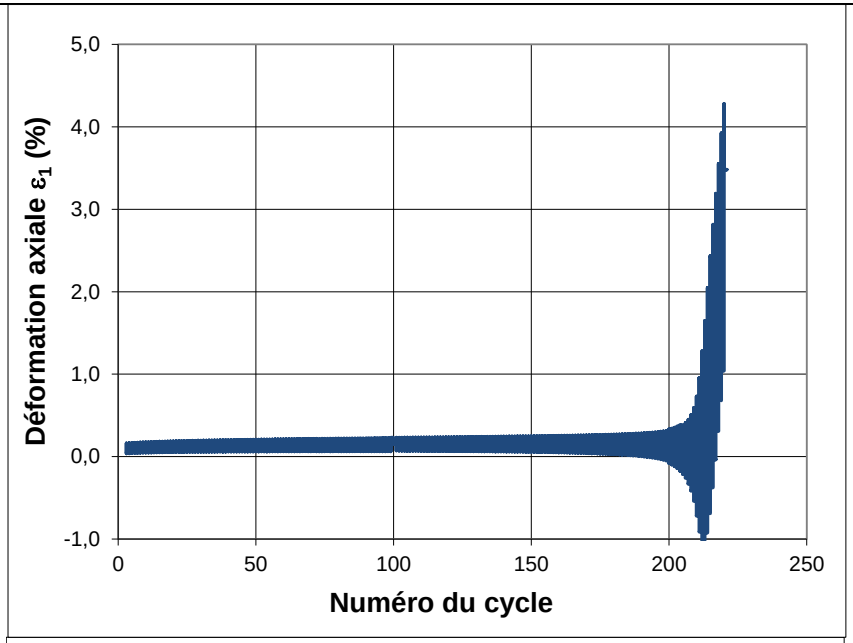

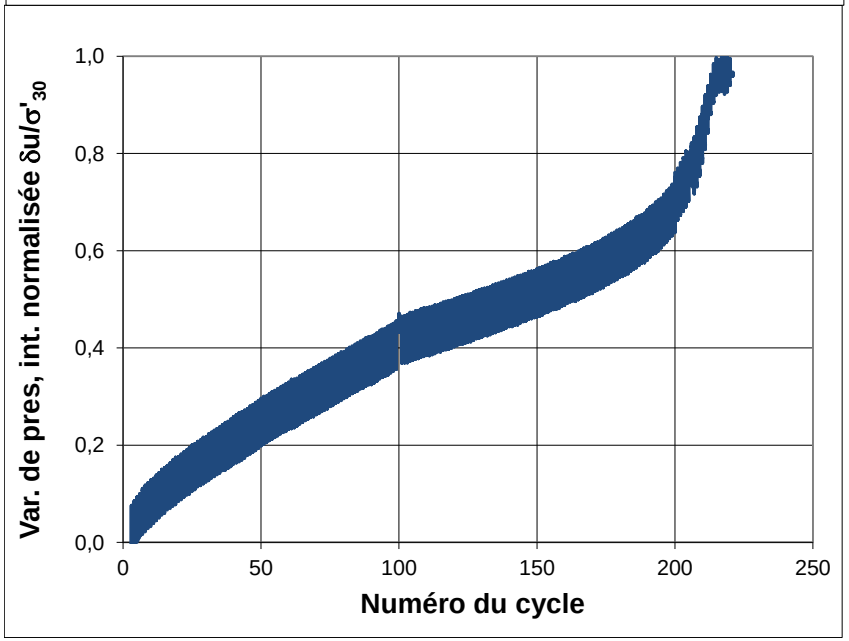

MS6.40_UT4 (untreated dense specimen), CSR=0.25, 0.5Hz

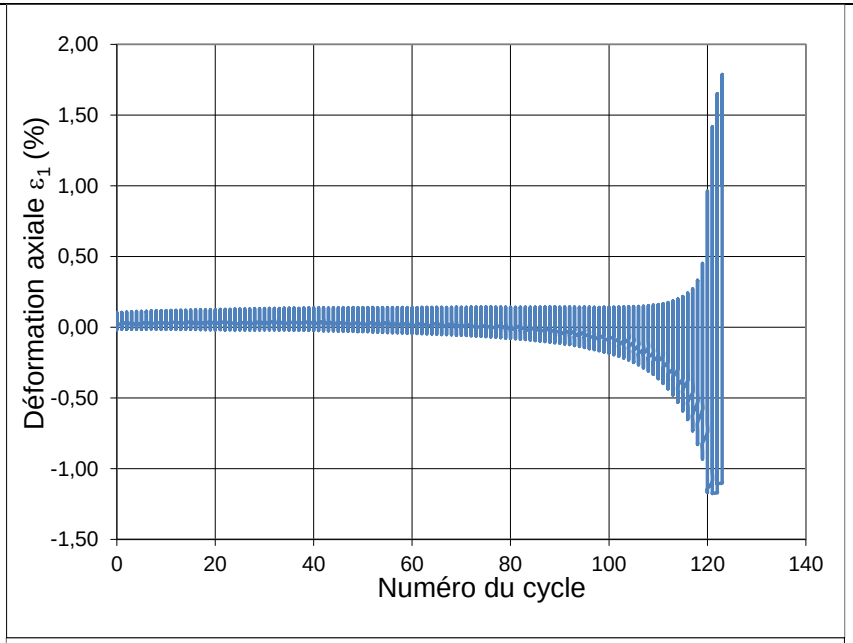

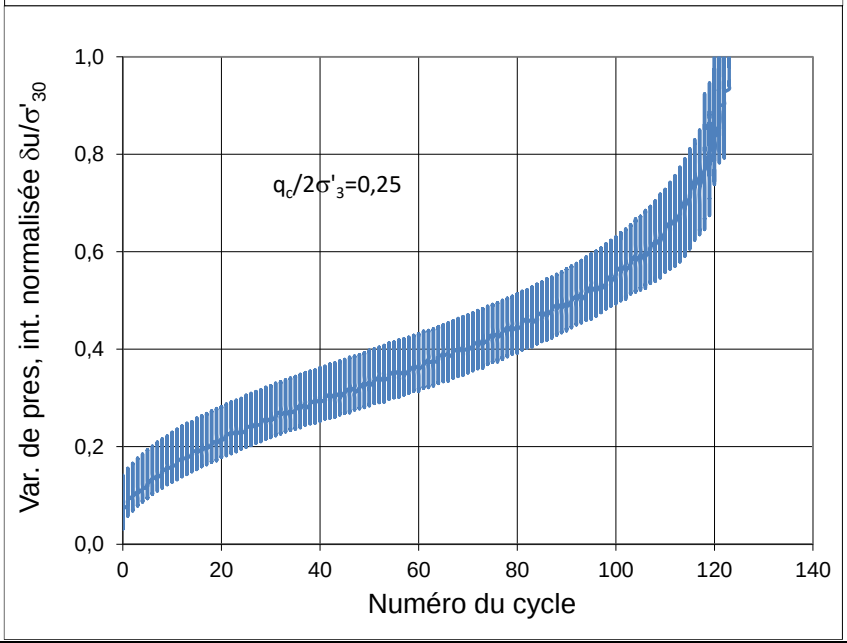

MS6.40_T1 (treated specimen), CSR=0.25, 0.1Hz, C=4.5%

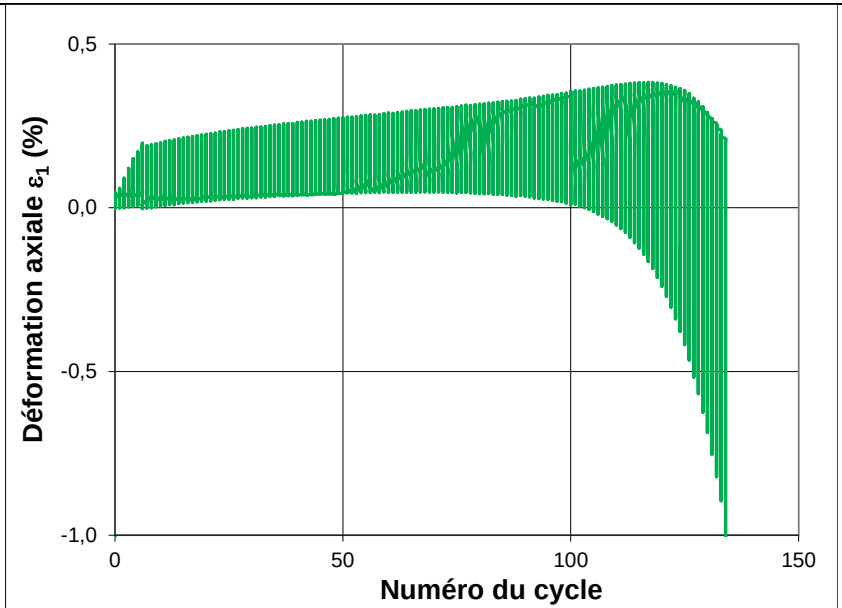

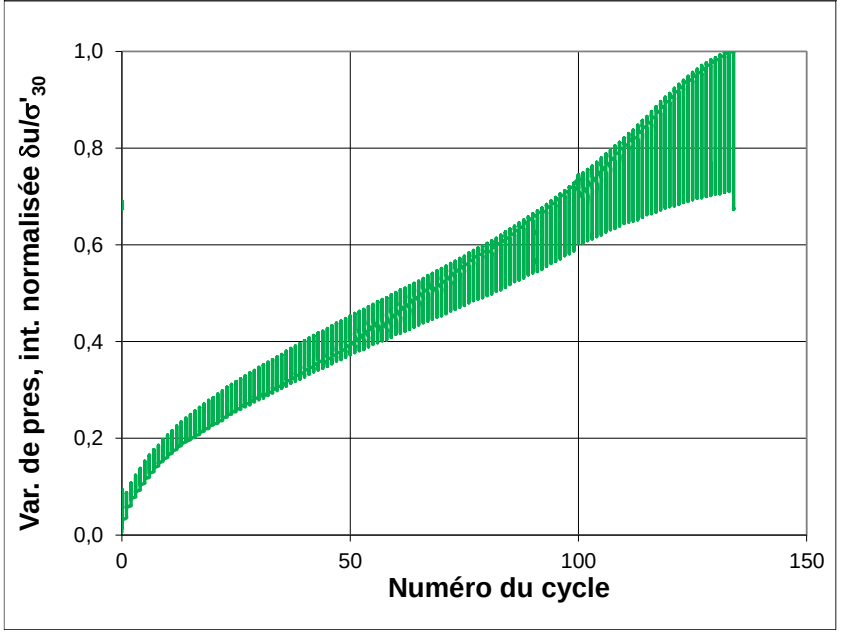

MS6.40_T2 (treated specimen), CSR=0.25-0.3, 0.5Hz, C=5.4%

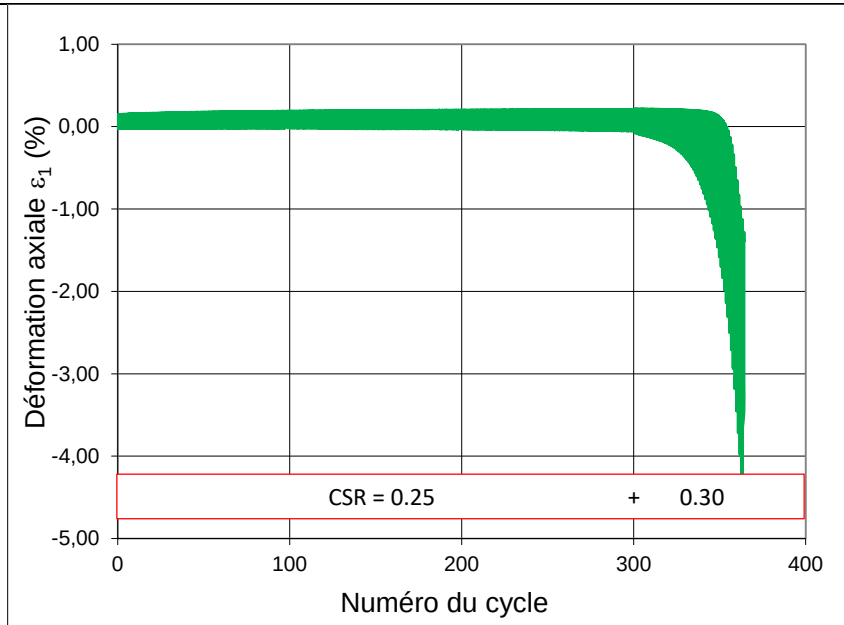

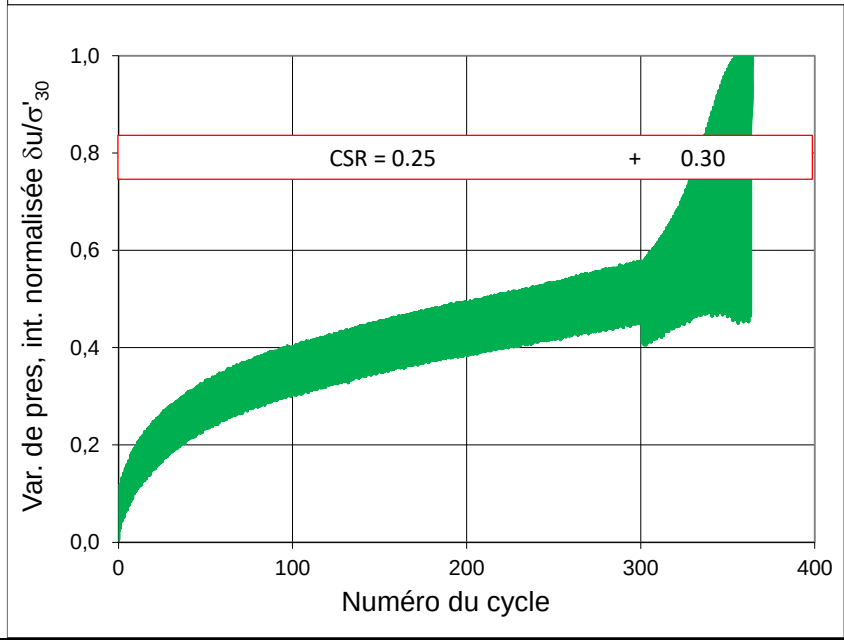

MS6.40_T3 (treated specimen), CSR=0.25-0.35, 0.1Hz, C=7.5%

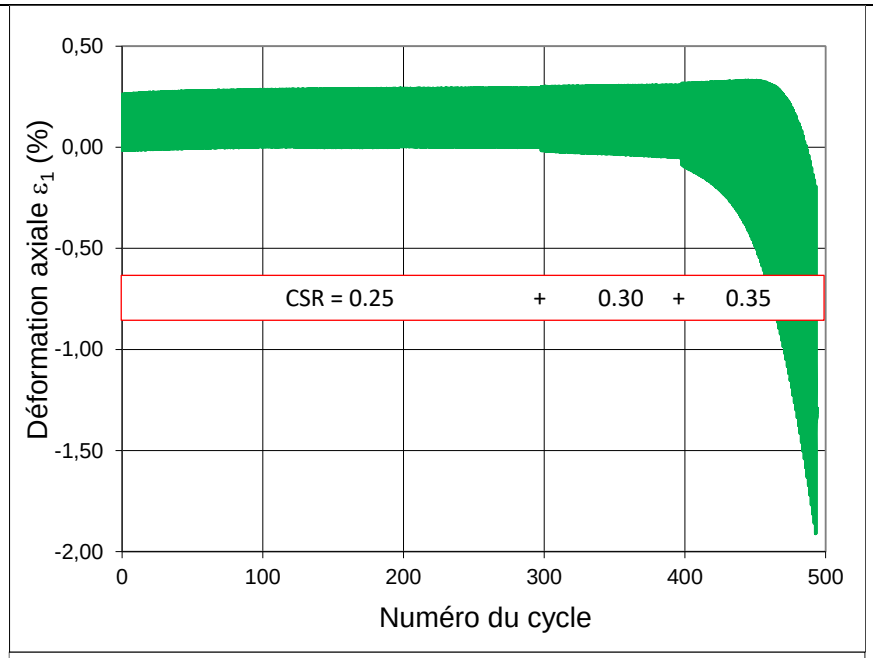

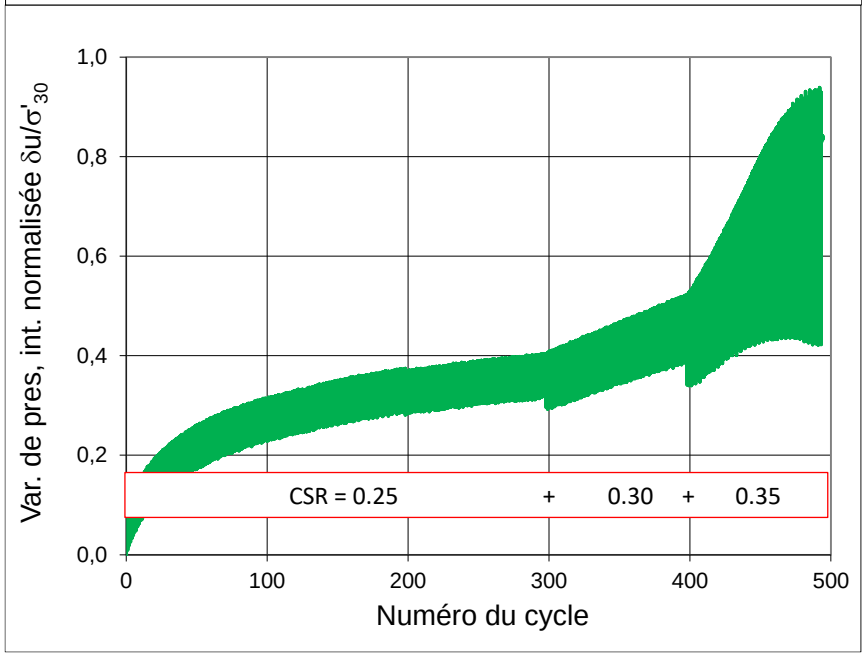

MS6.40_T4 (treated specimen), CSR=0.25-0.5, 0.5Hz, C=8.4%

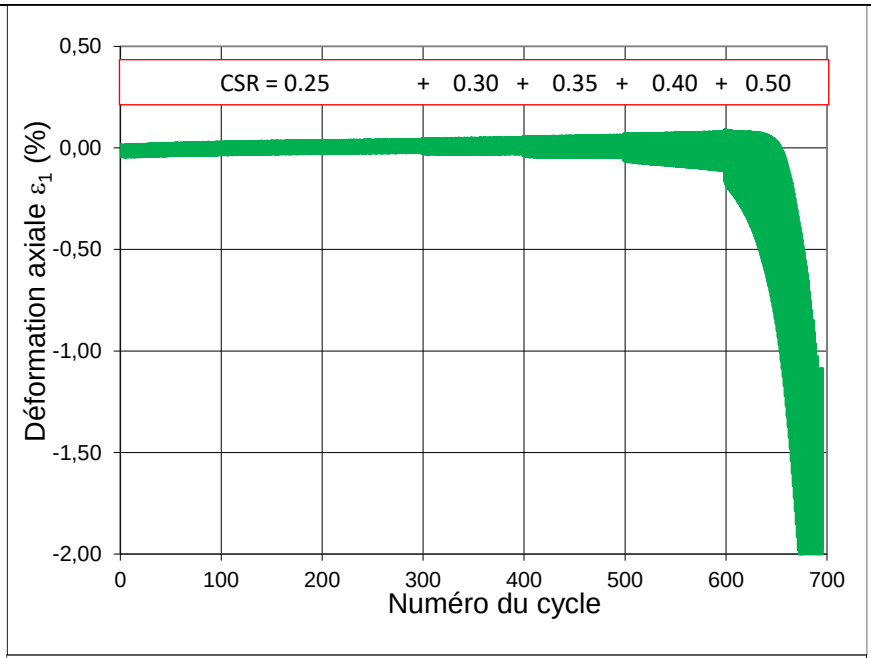

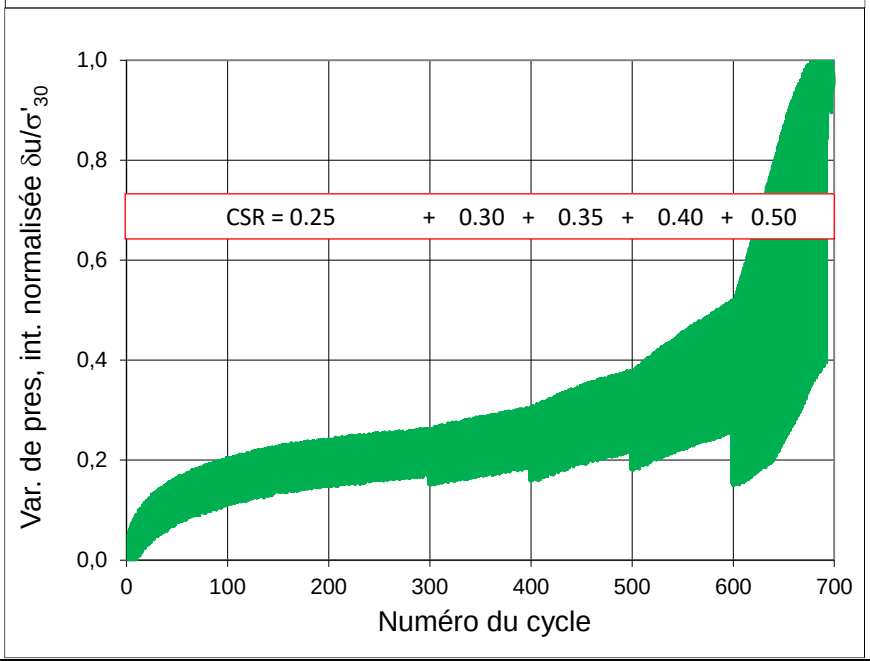

MS6.60 (60% fines < 1 mm)

No. of samples		CaCO3 content (%)	e after consolid.	dry density after consolid. (g/cm^3)	Dr after consolid. (%)	CSR	NL	Original No. Test
MS6.60	UT1	0	0,631	1,66	37	0,25	12	liq15
	UT2	0	0,615	1,67	44	0,2	116	liq83
	UT3	0	0,633	1,65	36	0,15	637	liq79
	UT4 dense	0	0,533	1,76	79	0,25	139	liq82
	T1	2,07	0,564	1,73	66	0,25	182	liq78T
	T2	4,17	0,562	1,73	67	0,25->0,35	529	liq56T
	T3	7,24	0,497	1,80	95	0,25->0,5	733	liq49T

MS6.60_UT1 (untreated loose specimen), CSR=0.25, 0.1Hz

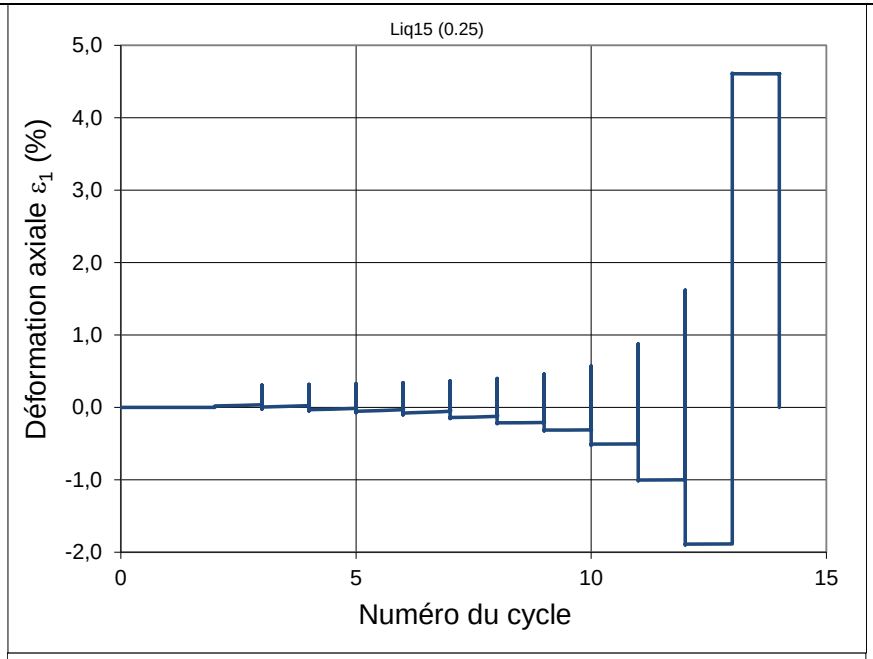

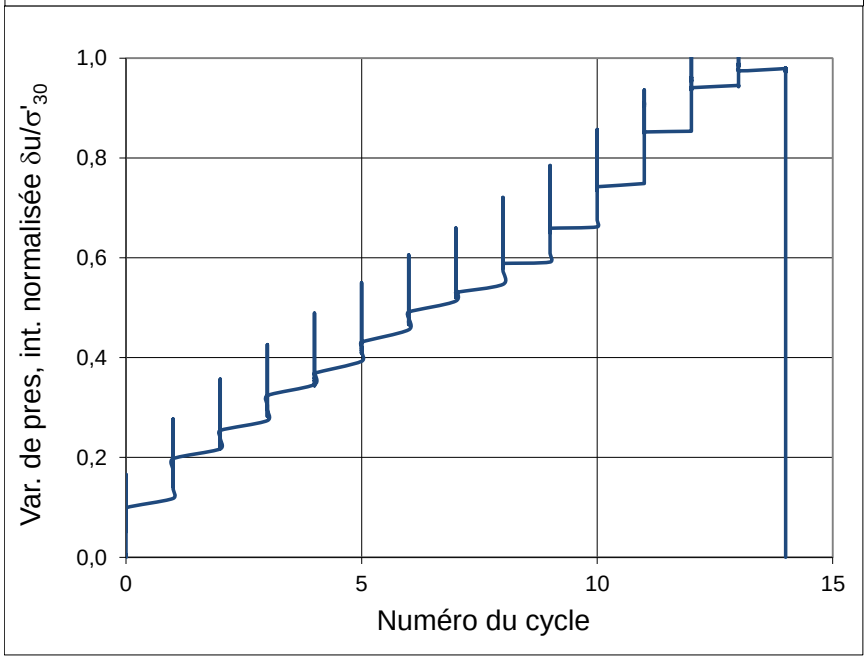

MS6.60_UT2 (untreated loose specimen), CSR=0.2, 0.5Hz

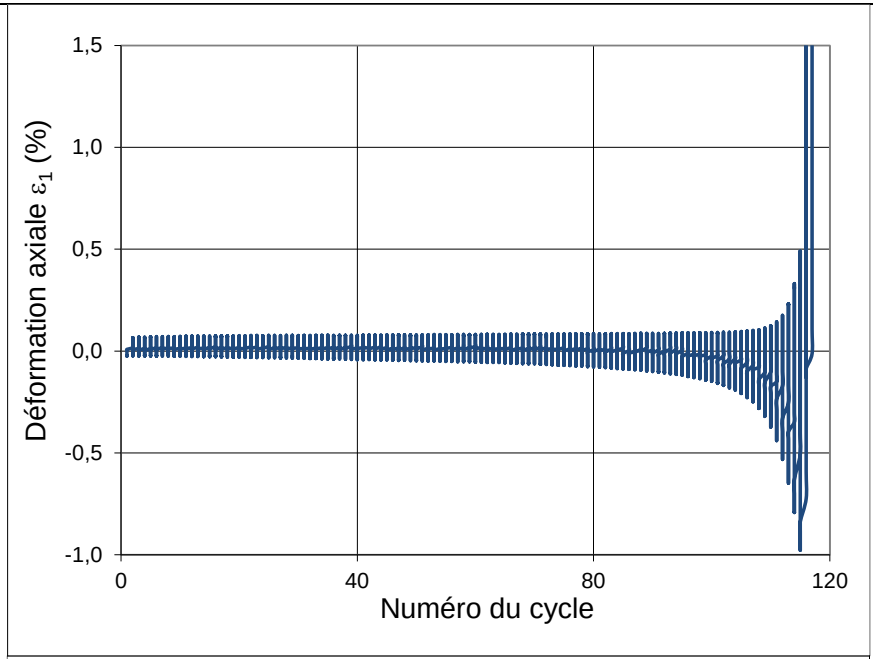

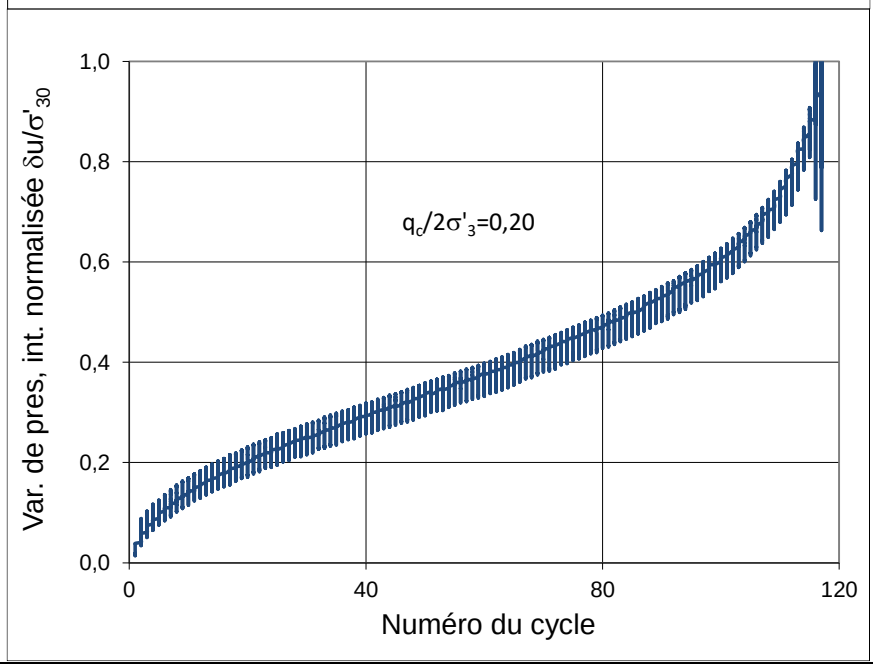

MS6.60_UT3 (untreated loose specimen), CSR=0.15, 0.5Hz

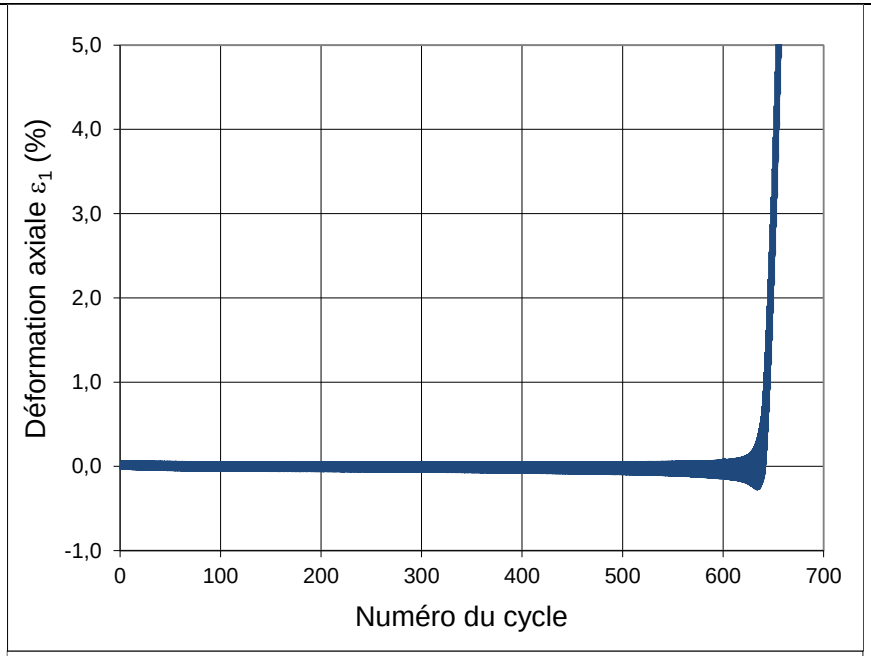

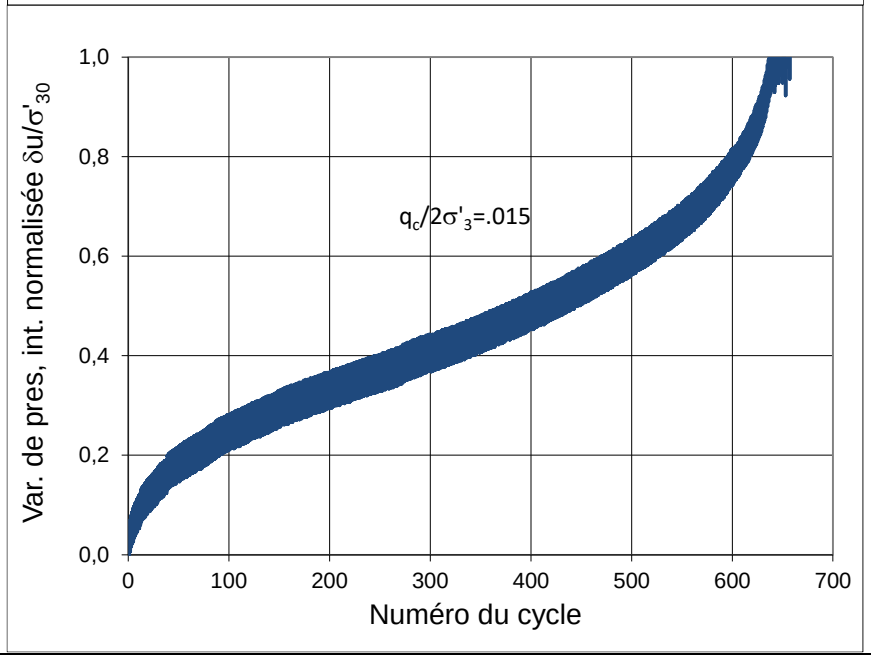

MS6.60_UT4 (untreated dense specimen), CSR=0.25, 0.5Hz

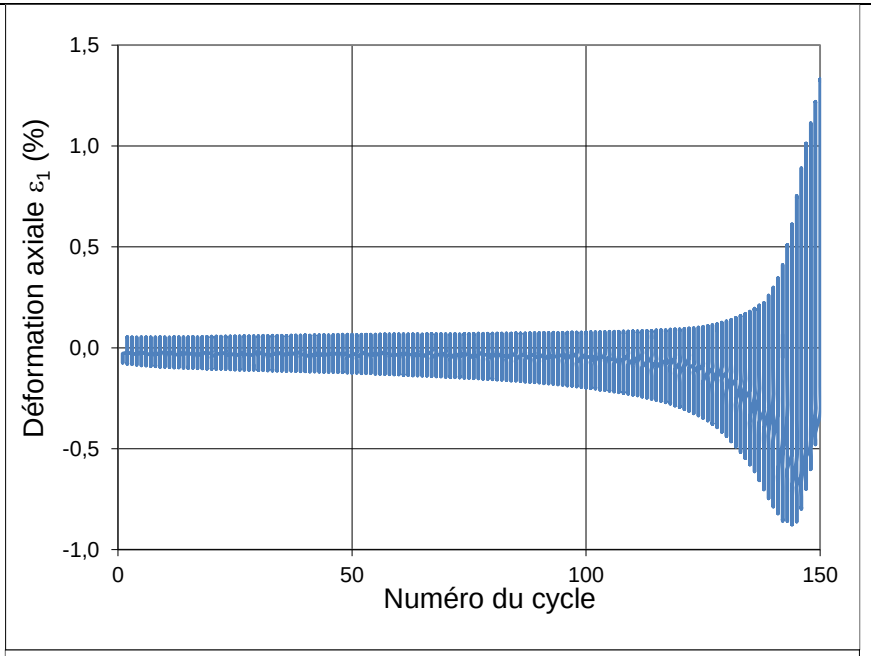

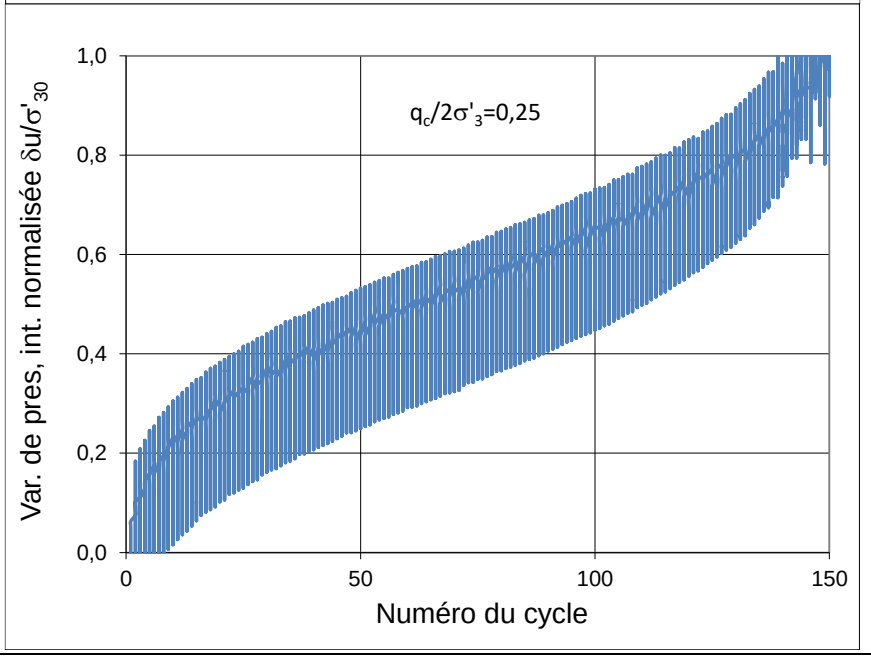

MS6.60_T1 (treated specimen), CSR=0.25, 0.5Hz, C=2.1%

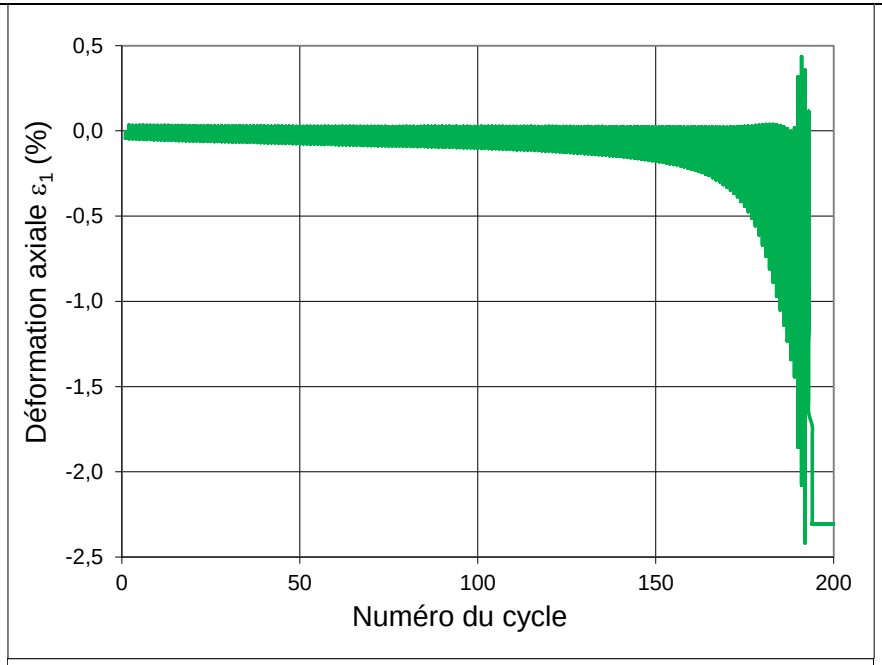

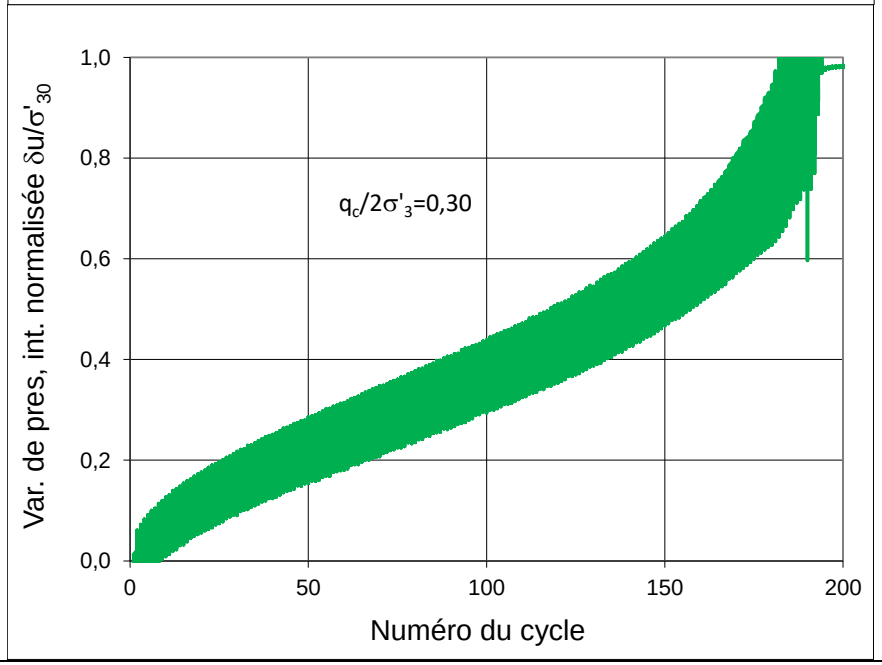

MS6.60_T2 (treated specimen), CSR=0.25-0.35, 0.5Hz, C=4.2%

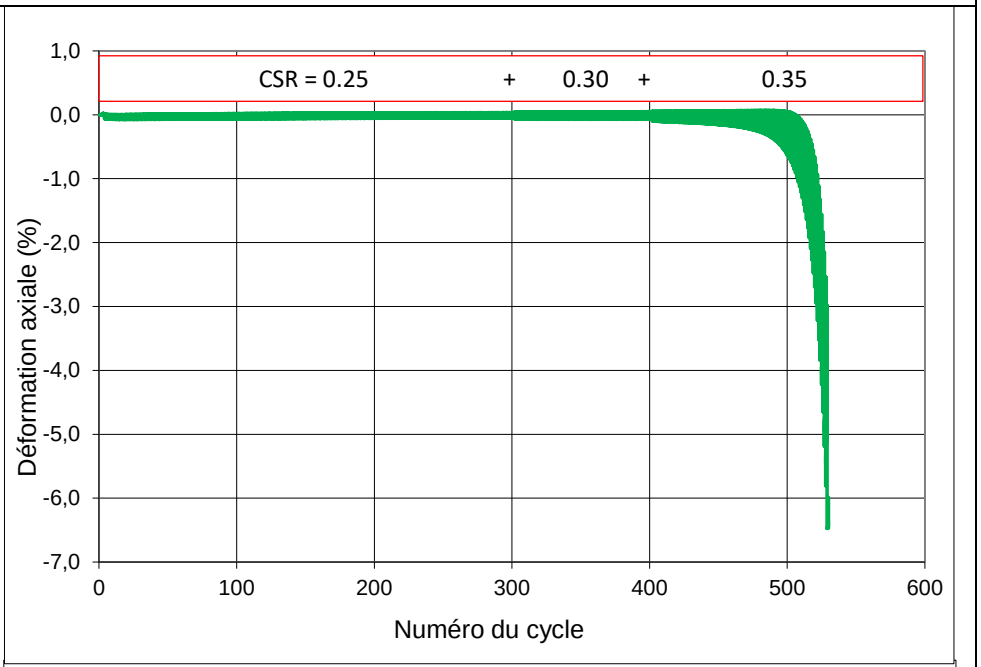

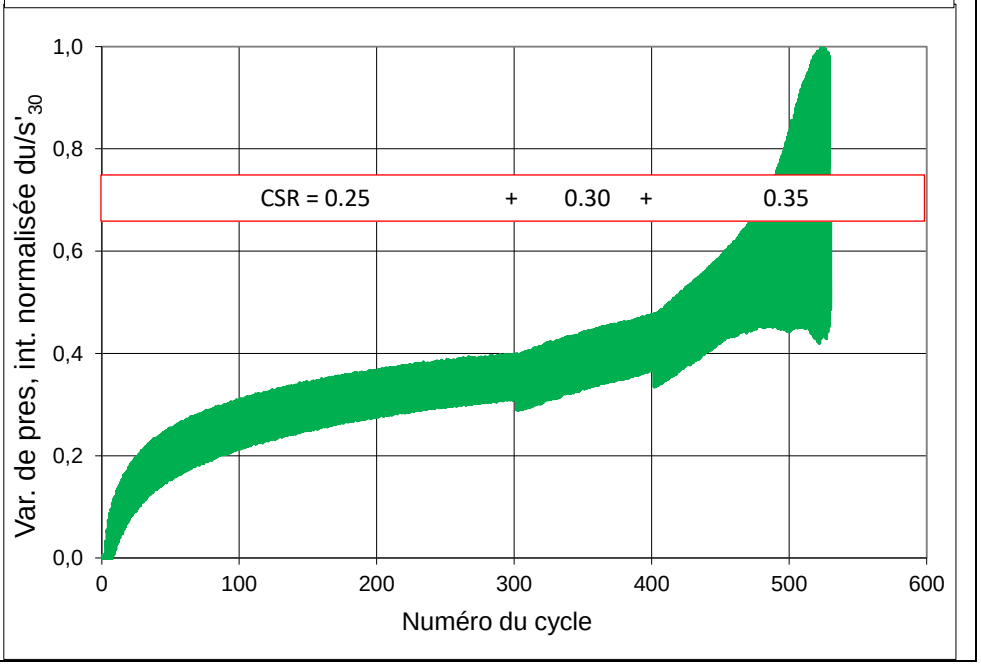

MS6.60_T3 (treated specimen), CSR=0.25-0.5, 0.1Hz, C=7.2%

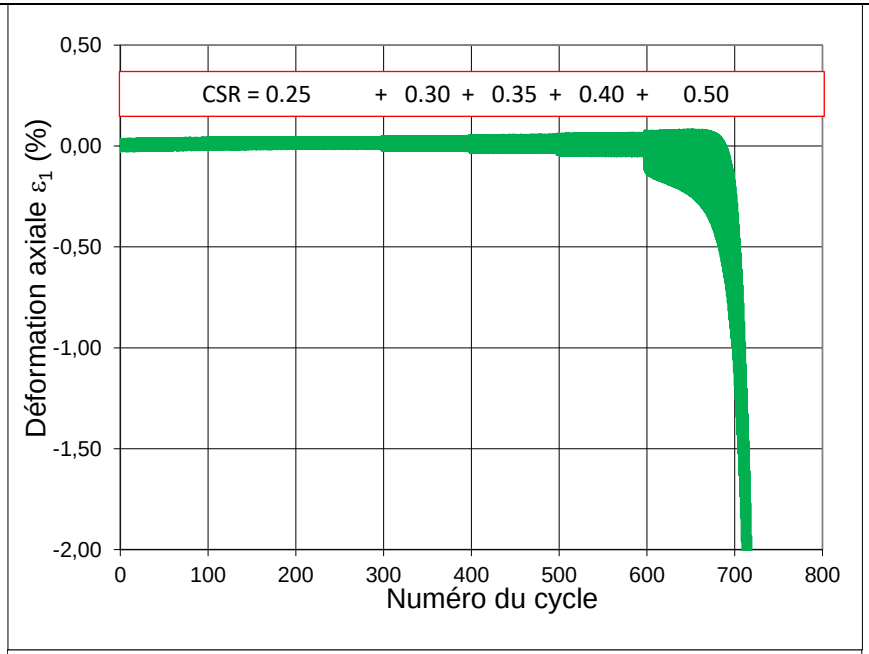

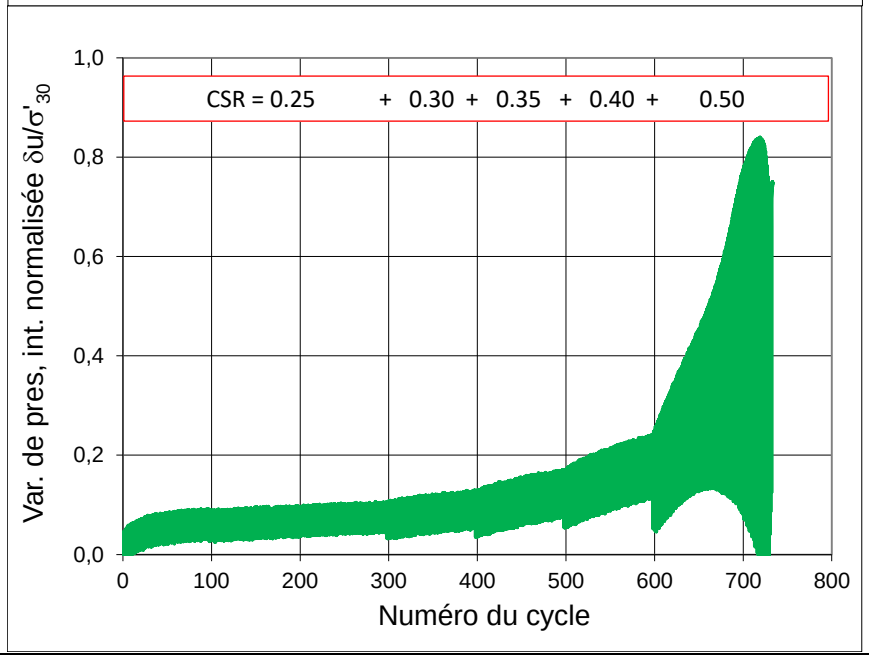

MS6.100 (Fine soil)

No. of samples		CaCO3 content (%)	e after consolid.	dry density after consolid. (g/cm^3)	Dr after consolid. (%)	CSR	NL	Original No. Test
MS6.100	UT1	0	0,735	1,56	34	0,25	14	liq13
	UT2	0	0,757	1,54	26	0,2	175	liq14
	UT3	0	0,696	1,59	47	0,17	1776	liq81
	UT4 dense	0	0,586	1,70	87	0,25	120	liq73 dense
	T1	1,37	0,668	1,62	57	0,25	322	liq92T
	T2	2,59	0,664	1,62	59	0,25->0,3	431	liq80T
	T3	5,99	0,659	1,63	61	0,25->0,5	676	liq52T

MS6.100_UT1 (untreated loose specimen), CSR=0.25, 0.1Hz

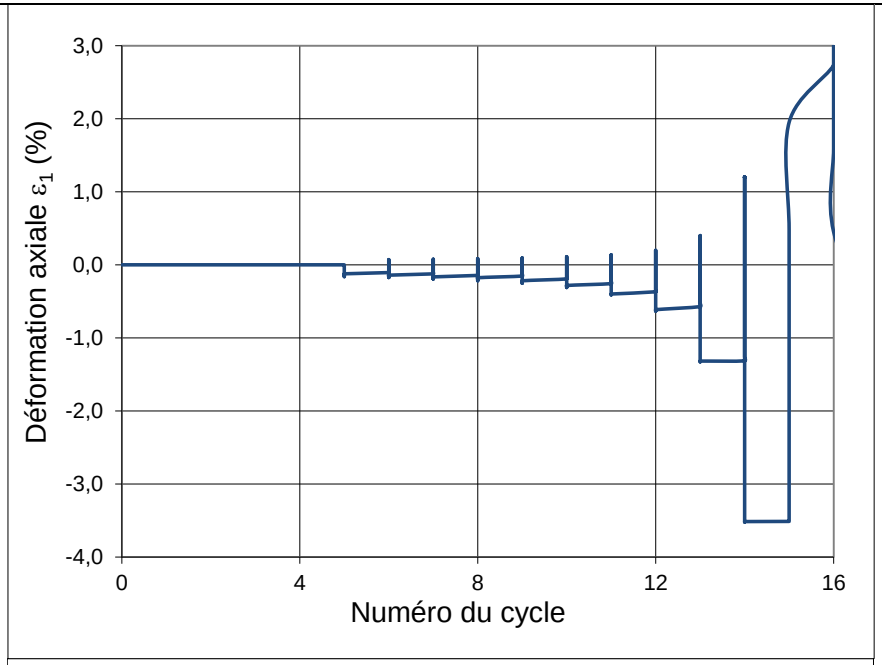

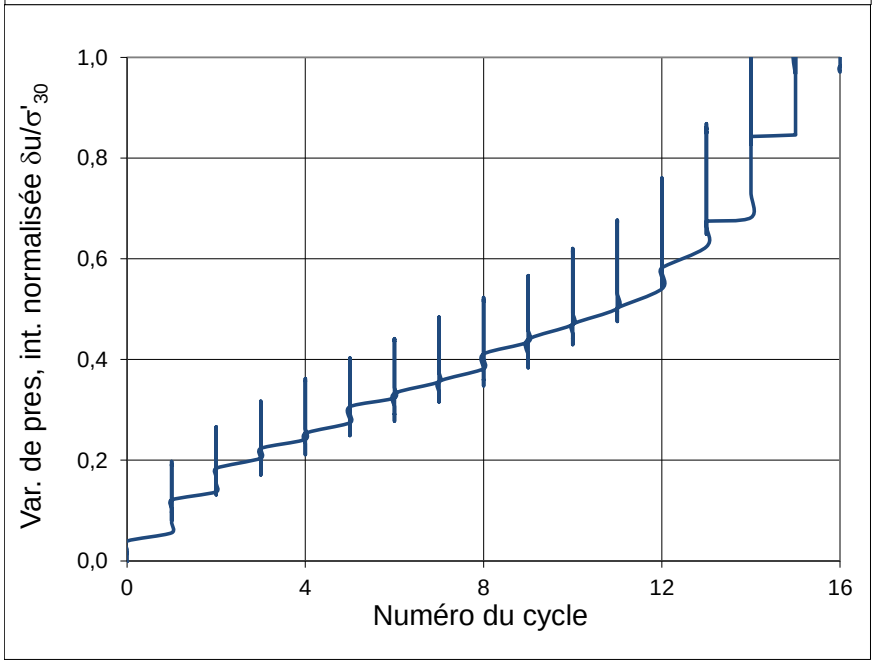

MS6.100_UT2 (untreated loose specimen), CSR=0.2, 0.1Hz

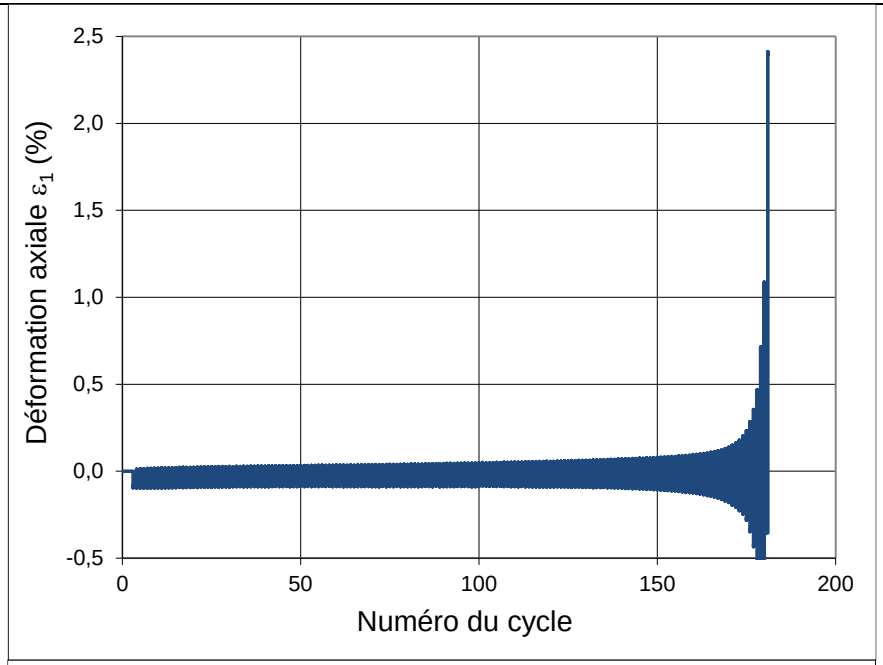

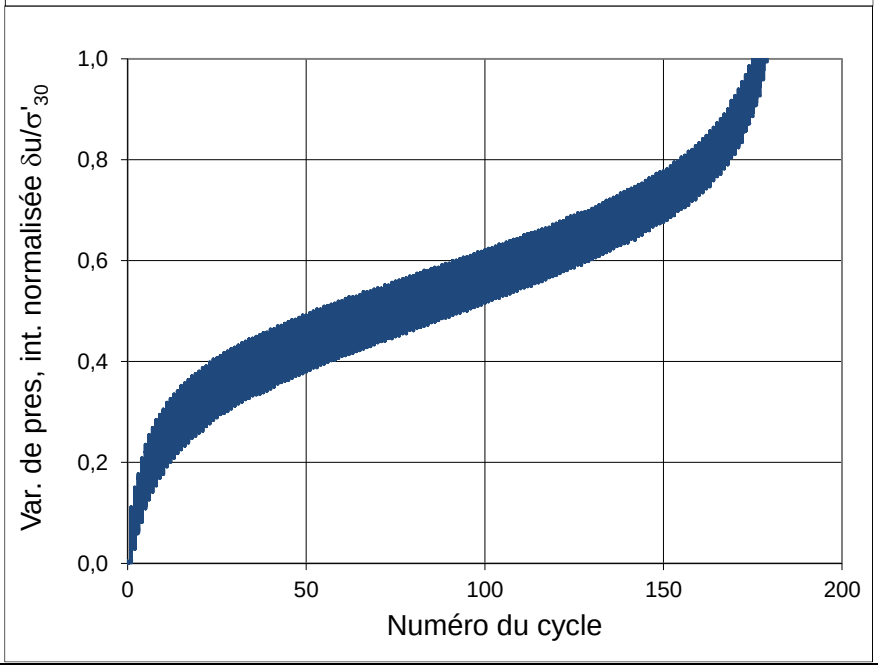

MS6.100_UT3 (untreated loose specimen), CSR=0.17, 0.5Hz

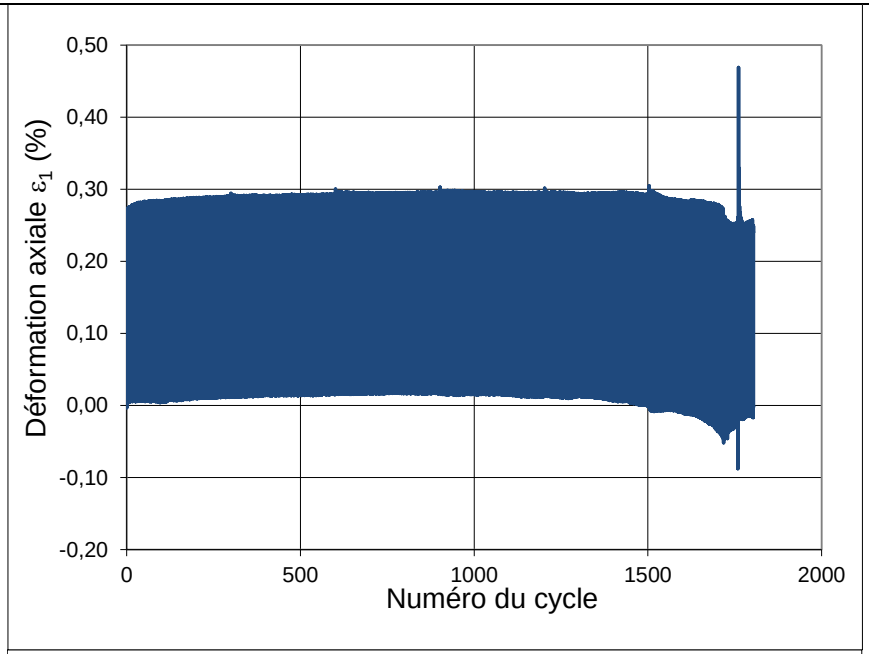

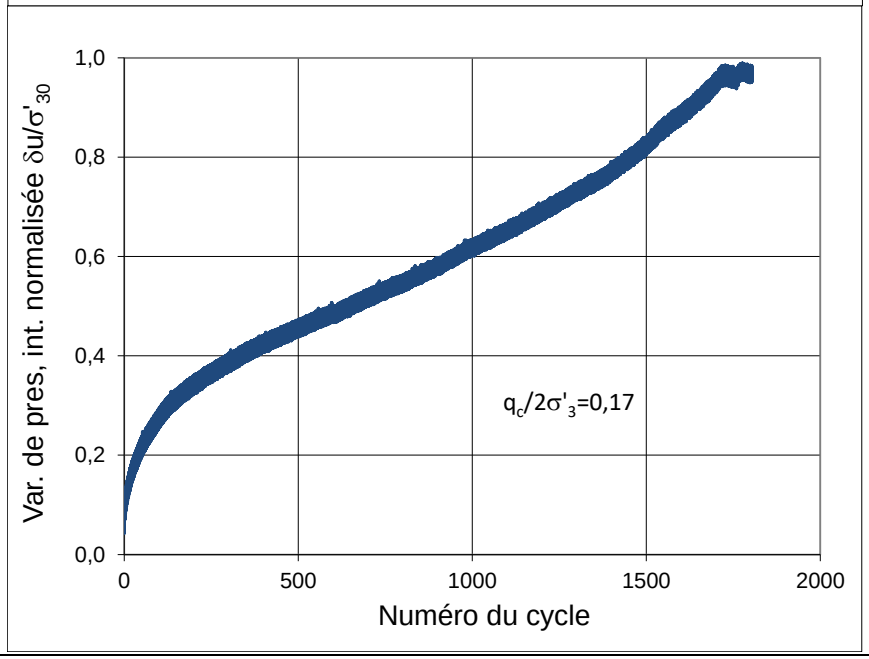

MS6.100_UT4 (untreated dense specimen), CSR=0.25, 0.5Hz

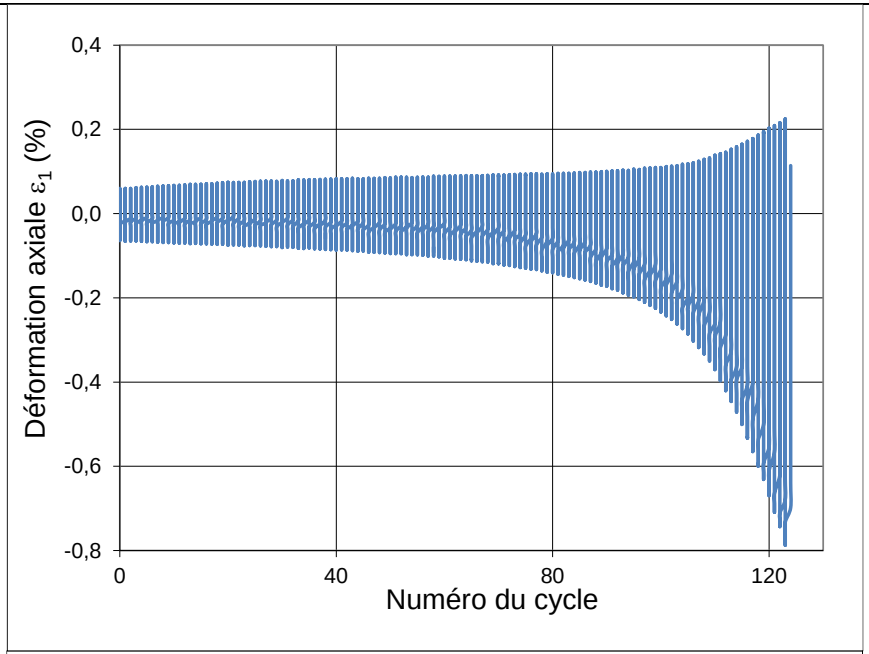

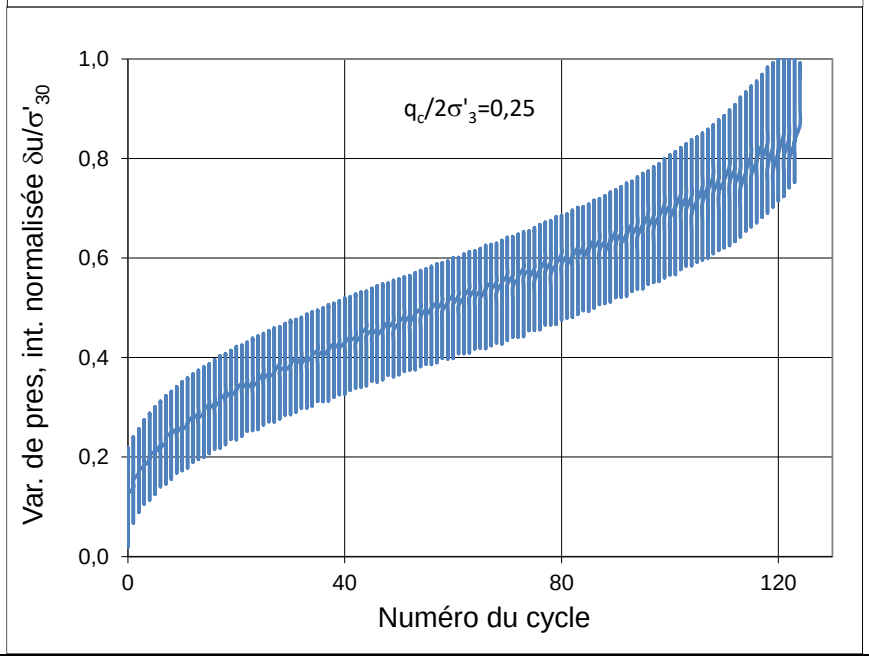

MS6.100_T1 (treated specimen), CSR=0.25, 0.5Hz, C=1.4%

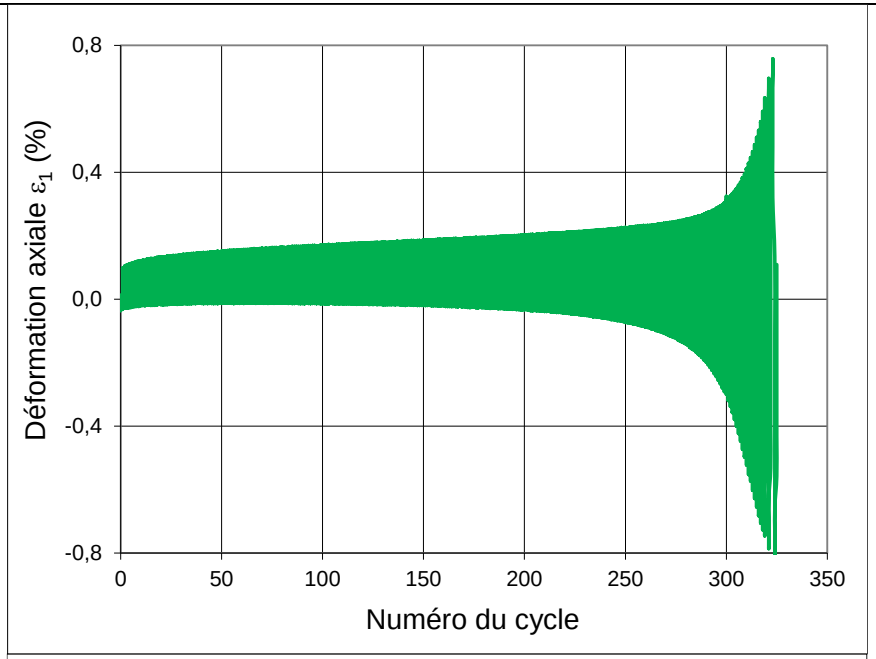

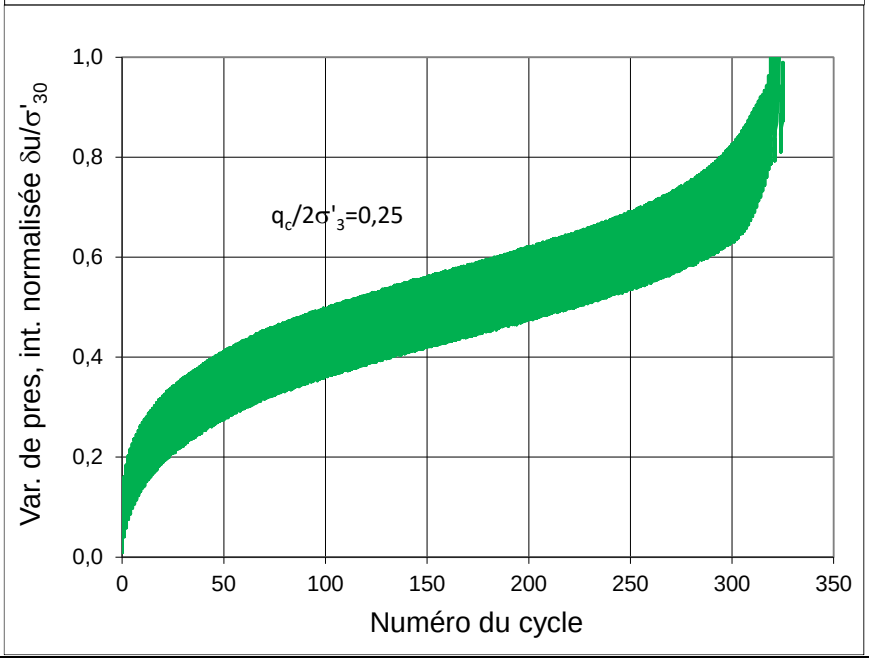

MS6.100_T2 (treated specimen), CSR=0.25-0.3, 0.5Hz, C=2.6%

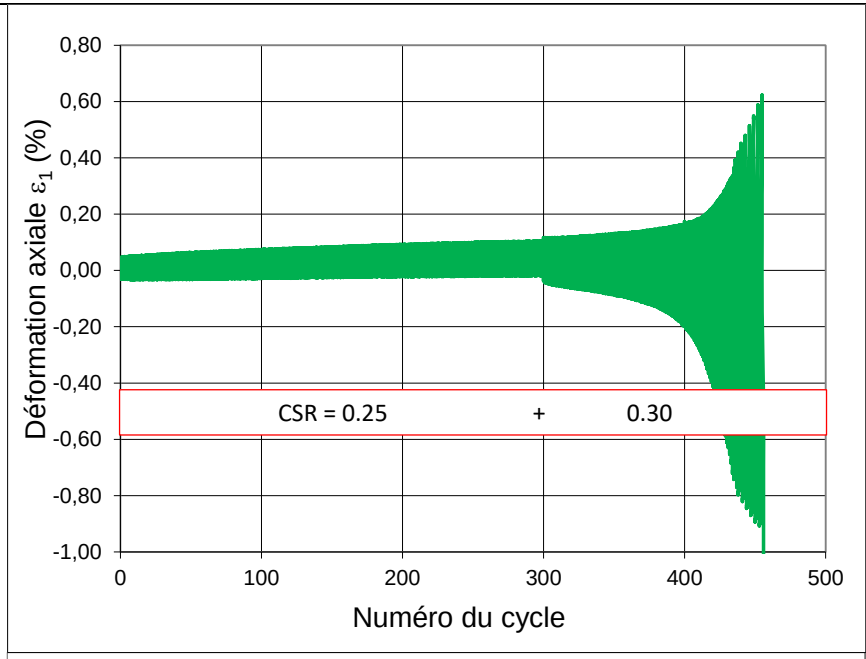

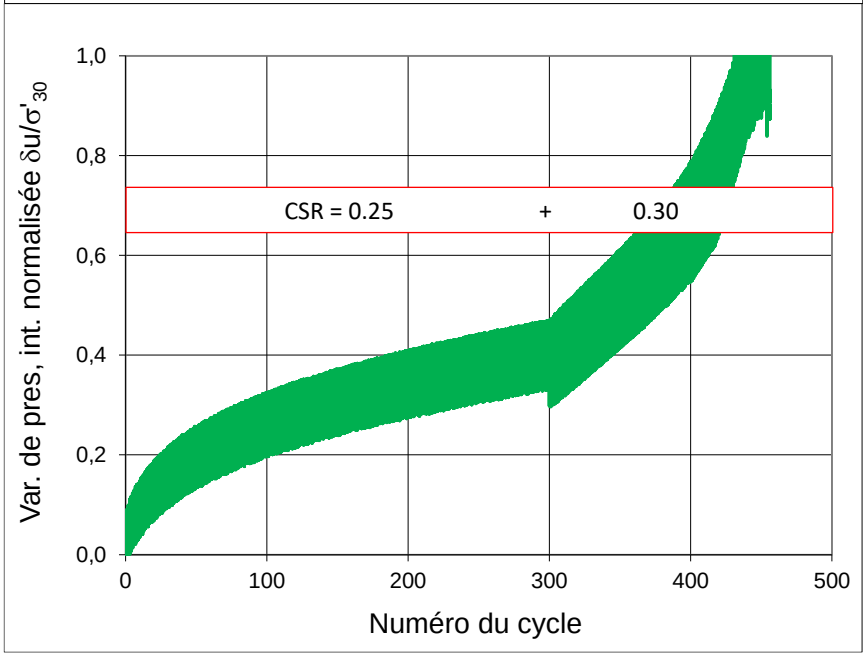

MS6.100_T3 (treated specimen), CSR=0.25-0.5, 0.1Hz, C=6.0%

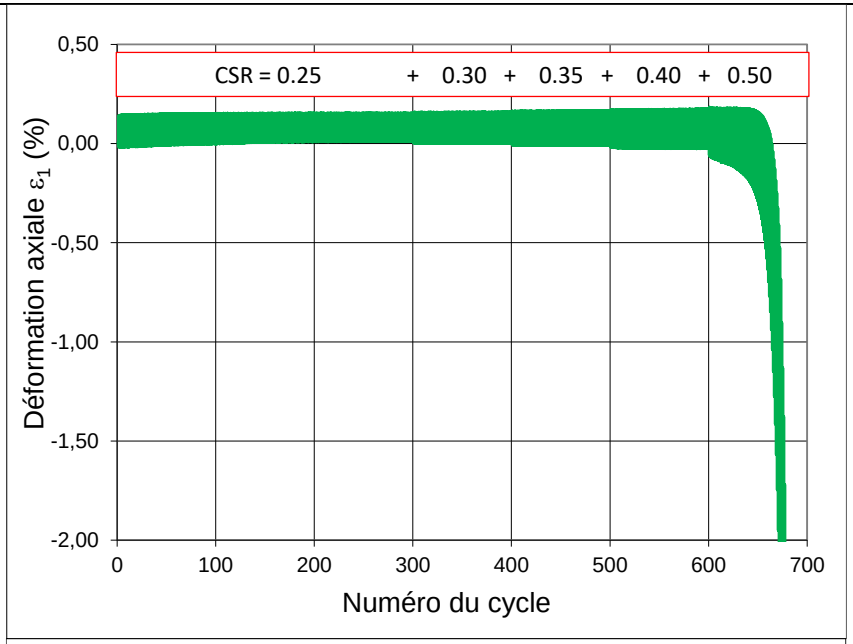

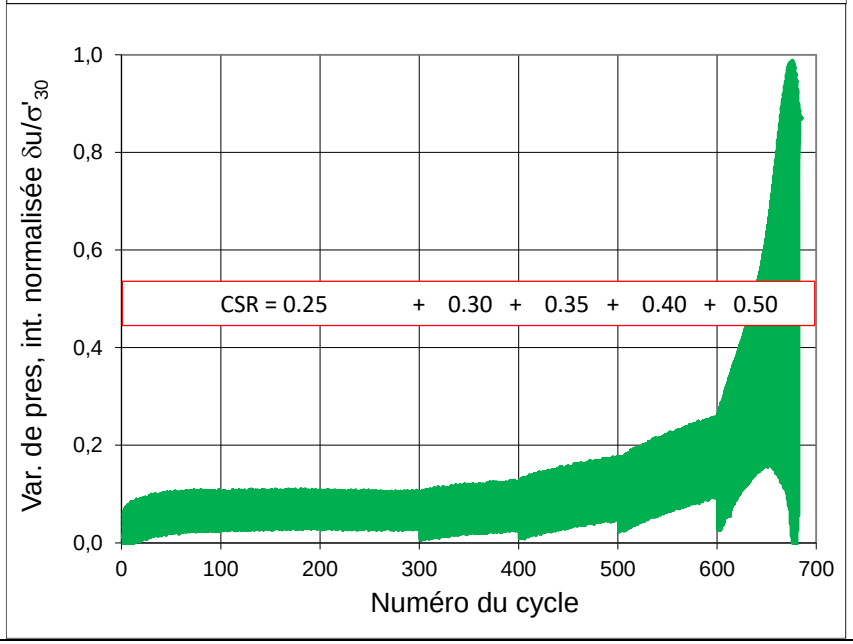

université PARIS-SACLAY
ÉCOLE DOCTORALE
Sciences mécaniques et énergétiques, matériaux et géosciences (SMEMAG)

Titre : Comportement mécanique des sols bio-cimentés

Mots clés : MICP, comportement monotone et cyclique, distribution granulométrique, teneur en $CaCO_3$

Résumé : La thèse présente une étude des propriétés mécaniques des sables traités par MICP (Précipitation Microbienne de Carbonate de Calcium), une méthode prometteuse à faible empreinte carbone. Les études précédentes étaient principalement basées sur des sables à grains très fins (< 1 mm), et étaient souvent qualitatives plutôt que quantitatives. De nombreux essais triaxiaux monotones et cycliques ont été effectués sur cinq mélanges de sables non traités et légèrement traités avec des diamètres de grains allant jusqu'à 5 mm. Les résultats des essais montrent que le traitement MICP améliore fortement la résistance des sols aux sollicitations tant monotones que cycliques, même lorsque les échantillons ne sont pas totalement cimentés, l'effet relatif de la densité et de la cimentation dépendant du pourcentage de grains fins (FC).

Dans les essais monotones et cycliques, la relation entre l'amélioration des propriétés mécaniques et la teneur en carbonate de calcium déposé est complexe, caractérisée par une teneur minimale en $CaCO_3$, qui augmente lorsque FC diminue, en dessous de laquelle son effet n'est pas visible. Au-dessus de la "valeur minimale", la résistance augmente linéairement avec la teneur en $CaCO_3$. Les observations au microscope confirment l'interaction complexe de plusieurs mécanismes qui peuvent expliquer l'effet du traitement MICP par le pontage des particules, l'augmentation de la rugosité de surface (revêtement) et de la densité (remplissage des pores). Des essais bio-physico-chimiques complémentaires ont aidé à interpréter les résultats.

Title : Mechanical behavior of bio-cemented soils

Keywords : MICP, monotonic and cyclic behavior, grain size distribution, $CaCO_3$ content

Abstract : The thesis presents a study of the mechanical properties of sands treated by MICP (Microbial-induced calcium carbonate precipitation), a promising bio-mediated methods with little carbon footprint. Previous studies were mainly based on poorly graded sands with very fine grains (< 1 mm) and were often qualitative rather than quantitative. Many monotonic and cyclic triaxial tests were done on five untreated and lightly treated sand mixtures with grain diameters up to 5 mm. Test results show that MICP treatment greatly enhances the resistance of the soils to both monotonic and cyclic solicitations, even when samples are not totally cemented, the relative effect of density and cementation depending on the percentage of fine grains (FC).

In both monotonic and cyclic tests, the relation between the enhancement of the mechanical properties and the deposited calcium carbonate content is complex, characterized by a minimum $CaCO_3$ content, which increases when FC decreases, below which its effect is not visible. Above the "minimum value", the resistance increases linearly with the $CaCO_3$ content. Microscope observations confirm the complex interplay of several mechanisms that can explain the effect of MICP treatment through the bridging of particles, surface roughness (coating) and density (pore-filling) increases. Additional bio-physico-chemical tests helped interpret the results.